



# UNIVERSITÀ DEGLI STUDI DI MILANO

CORSO DI DOTTORATO IN SCIENZE FARMACEUTICHE (XXXVI ciclo)

DIPARTIMENTO DI SCIENZE FARMACEUTICHE (DISFARM)

**Synthesis of pharmacologically active molecules through biocatalytic approaches: study of their stereochemistry and polymorphism by means of spectroscopic and crystallographic methods.**

SAMUELE CICERI

Matricola: R12966

TUTOR: Prof. FIORELLA MENEGHETTI

CO-TUTOR: Dr. PARIDE GRISENTI

COORDINATORE: Prof. GIULIO VISTOLI

A.A. 2022/2023





*I believe in the great discovery.  
I believe in the man who will make the discovery.  
I believe in the fear of the man who will make the discovery.*

*I believe in his face going white,  
His queasiness, his upper lip drenched in cold sweat.*

*I believe in the burning of his notes,  
burning them into ashes,  
burning them to the last scrap.*

*I believe in the scattering of numbers,  
scattering them without regret.*

*I believe in the man's haste,  
in the precision of his movements,  
in his free will.*

*I believe in the shattering of tablets,  
the pouring out of liquids,  
the extinguishing of rays.*

**“Discovery”** by Wislawa Szymborska



## **Keywords**

Atropisomerism

Conformational analysis

Crystal structure

Elagolix

Endometriosis

GnRH

Gonadotropin Releasing Hormone modulator

NMR spectroscopy

Uterine fibroids

## ABSTRACT

Elagolix is the first non-peptide orally active gonadotropin-releasing hormone (GnRH) antagonist, approved for the treatment of sex hormone-dependent diseases, such as endometriosis and uterine fibroids. This PhD project was focused on this drug, studying its conformational features, and improving the synthetic procedures found in the literature. Firstly, theoretical experiments revealed that this drug exists in solution as a mixture of two atropisomers (Chart 1), which belong to class 2 due to an estimated interconversion rotational barrier of 22.3 kcal/mol. This finding could help to face the great challenges in the drug discovery and development of this class of compounds, caused by the conformational instability. In addition, the deepen spectroscopic investigations performed on elagolix and its intermediates allowed for the complete assignment and interpretation of the  $^1\text{H}$ ,  $^{13}\text{C}$ , and  $^{15}\text{N}$  NMR signals, filling the existing gap in the literature.

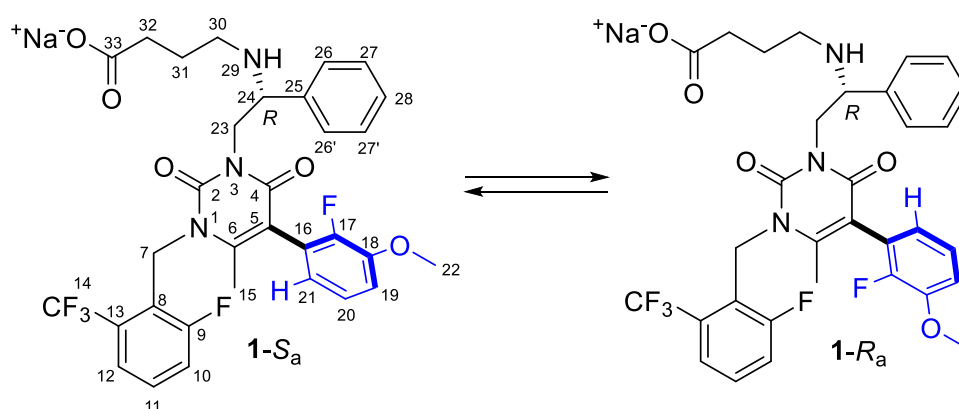


**Chart 1.** The two atropisomeric forms of elagolix sodium salt.

Because the individual atropisomers of a given molecule may differ considerably in their pharmacological properties, we designed and synthesized a new series of elagolix analogues, differently substituted at the 4- or 6-position of the uracil moiety, with the aim of studying the impact of these modifications on atropisomeric properties. Three of the newly obtained compounds have a higher rotational barrier than elagolix, allowing the separation and characterization of their single atropisomers by means of different analytical techniques.

Moreover, since our study on the already disclosed 21-bromoderivative of elagolix resulted in the identification of two thermally stable atropisomers, this

compound was selected for the development of a new enzymatic approach for the atropisomers separation.

For the new compounds and their single atropisomers, biological tests are currently underway on HEK-293 cells expressing the human GnRH receptor (*hGnRH1R*) to verify the good receptor affinity predicted by the molecular dynamics simulations.



# TABLE OF CONTENTS

---

|  |  |           |
|--|--|-----------|
| <b>Chapter 1</b>                                 |  |           |
| <b>Introduction</b>                              |  | <b>11</b> |
| 1.1  | Gonadotropin releasing hormone (GnRH)                  | 11        |
| 1.2  | Gonadotropin releasing hormone (GnRH) modulators       | 15        |
| 1.3  | Non-peptide GnRH modulators                            | 19        |
| 1.3.1  | Mechanism of action of non-peptide modulators on GnRHR | 22        |
| 1.4  | Atropisomerism   | 24        |
| 1.4.1  | Atropisomerism in drug discovery                       | 26        |
| <b>Chapter 2</b>                                 |  | <b>32</b> |
| <b>Aims and Outline of the Thesis</b>            |  |           |
| <b>Chapter 3</b>                                 |  | <b>34</b> |
| <b>Elagolix</b>                                  |  |           |
| 3.1  | Synthesis  | 34        |
| 3.2  | NMR spectroscopy                                       | 46        |
| 3.3  | HPLC analysis  | 52        |
| 3.4  | X-ray crystal structure                                | 53        |
| 3.5  | Conformational analysis                                | 55        |
| 3.6  | Conclusions  | 58        |
| <b>Chapter 4</b>                                 |  | <b>59</b> |
| <b>Elagolix analogues modified at 4-position</b> |  |           |
| 4.1  | Design   | 59        |
| 4.2  | Synthesis  | 60        |
| 4.3  | NMR spectroscopy                                       | 66        |
| 4.4  | HPLC analysis  | 75        |
| 4.5  | Evaluation of the rotational barriers                  | 76        |
| 4.6  | Crystallization trials                                 | 79        |
| 4.7  | Computational analysis                                 | 81        |
| 4.8  | Conclusions  | 83        |
| <b>Chapter 5</b>                                 |  | <b>85</b> |
| <b>Elagolix analogues modified at 6-position</b> |  |           |
| 5.1  | Design   | 85        |
| 5.2  | Synthesis  | 86        |
| 5.3  | Evaluation of the rotational barriers                  | 91        |
| 5.4  | Crystallization trials                                 | 93        |
| 5.5  | Biocatalytic approach                                  | 93        |
| 5.6  | Conclusions  | 96        |

|   |            |
|---|------------|
| <b>Chapter 6</b>                                  | <b>97</b>  |
| <b>Elagolix analogues modified at 21-position</b> |            |
| 6.1 Synthesis and analytical characterization     | 97         |
| 6.2 Biocatalytic approach                         | 100        |
| 6.3 Conclusions                                   | 103        |
| <b>Chapter 7</b>                                  | <b>104</b> |
| <b>Biological assays</b>                          |            |
| <b>Chapter 8</b>                                  | <b>107</b> |
| <b>Conclusions and Future perspectives</b>        |            |
| <b>Chapter 9</b>                                  | <b>109</b> |
| <b>Materials and Methods</b>                      |            |
| 9.1 Computational methods                         | 109        |
| 9.2 General chemistry                             | 114        |
| 9.3 Biological methods                            | 140        |
| 9.4 Crystallography                               | 141        |
| <b>References</b>                                 | <b>144</b> |
| <b>Appendix</b>                                   |            |
| List of Publications and Presentations            | 162        |
| Acknowledgements                                  | 166        |

## List of Abbreviations

---

AA: Amino acid

ACN: Acetonitrile

AD: Alzheimer's disease

ADME: Absorption, distribution, metabolism, and excretion

CAL-A: Lipase A from *Candida antarctica*

CAL-B: Lipase B from *Candida antarctica*

cAMP: Cyclic adenosine monophosphate

CCL: Lipase from *Candida rugosa*

CD: Circular dichroism

CLEA: Cross-linked enzyme aggregate

CNS: Central nervous system

COSY: Correlation Spectroscopy

CPCM: Conductor-like polarizable continuum model

*de*: Diastereomeric excess

DEAD: Diethyl azodicarboxylate

DFT: Density functional theory

DHPLC: Dynamic high performance liquid chromatography

DIPEA: *N,N*-Diisopropylethylamine

DMF: *N,N*-Dimethylformamide

DNMR: Dynamic nuclear magnetic resonance

DMSO: Dimethyl sulfoxide

EC<sub>50</sub>: Half maximal effective concentration

EMA: European Medicines Agency

EXSY: Exchange spectroscopy

FDA: Food and Drug Administration

FSH: Follicle stimulating hormone

GnRH: Gonadotropin-releasing hormone

GnRHR: Gonadotropin-releasing hormone receptor. Given the identification of two additional forms of GnRH, namely GnRH-II and GnRH-III, it becomes feasible to

label the first discovered GnRH and its receptor as GnRH-I and GnRH1R, respectively.

GnRHR-a (or GnRH-a): Gonadotropin-releasing hormone receptor agonist

GnRHR-ant (or GnRH-ant): Gonadotropin-releasing hormone receptor antagonist

GPCR: G protein-coupled receptors

Gs: Gradient selected

*h*GnRHR: Human gonadotropin-releasing hormone receptor

HMBC: Heteronuclear Multiple Bond Correlation

HPG axis: Hypothalamo-Pituitary-Gonadal axis

HPLC: High Performance Liquid Chromatography

HRMS: High Resolution Mass Spectrometry

HSQC: Heteronuclear Single Quantum Coherence

IC<sub>50</sub>: Half maximal inhibitory concentration

ICH: Idiopathic central hypogonadism

IP1: Inositol-1-phosphate

IP3: Inositol 1,4,5-Trisphosphate

*k*: rate constant for interconversion between atropisomers

K<sub>D</sub>: Equilibrium dissociation constant

K<sub>i</sub>: Inhibition constant

KRAS: Kirsten rat sarcoma viral oncogene homolog.

LH: Luteinizing hormone

LHRH: Luteinizing-Hormone-Releasing Hormone

LiSS: Ligand-induced select signaling theory

MAPK: Mitogen-activated protein kinase

MD: Molecular Dynamics

MM-GBSA: Molecular mechanics with generalised Born and surface area solvation

MsOH: Methanesulfonic acid

NMR: Nuclear Magnetic Resonance

NOESY: Nuclear Overhauser Effect Spectroscopy

OHSS: Ovarian hyperstimulation syndrome

ORTEP: Oak Ridge Thermal-Ellipsoid Plot Program

PCOS: Polycystic ovary syndrome

PFL: Lipase from *Pseudomonas fluorescens*  
P-gp: P-glycoprotein  
PI3K: Phosphoinositide 3-kinases  
*p*-TsOH: *para*-Toluenesulfonic acid  
Py: Pyridine  
QM: Quantum Mechanics  
RMSD: Root Mean Square Deviation  
SC-XRD: Single-crystal X-ray Diffraction  
SFC: Supercritical fluid chromatography  
 $t_{1/2}$ : half-life time  
TFA: Trifluoroacetic acid  
THF: Tetrahydrofuran  
URAT1: Urate transporter 1  
VT-NMR: Variable Temperature Nuclear Magnetic Resonance  
 $\Delta G$ : Ligand binding free energy  
 $\Delta G^\ddagger$ : Rotational barrier

# Chapter 1

## Introduction

---

### 1.1 GnRH

Gonadotropin-Releasing Hormone (GnRH), also known as Luteinizing-Hormone-Releasing Hormone (LHRH) [1], is a decapeptide (Figure 1) isolated and sequenced for the first time in 1971 by the Nobel Prize for Medicine Andrew Schally [2], crucial in the regulation of the so called hypothalamic-pituitary-gonadal (HPG) axis (Figure 2) [3,4].



**Figure 1.** Schematic representation of the GnRH peptide. Figure modified from Ref. [1].

GnRH, released in a pulsatile manner by a small number of neurons in the basal-medial hypothalamus and directly into the bloodstream *via* the hypophyseal system, exerts its effect as a central regulator of reproduction function [5]. It plays its role by activating the cell surface receptor located in the anterior pituitary to stimulate the release of gonadotropins luteinizing (LH) or follicle stimulating hormone (FSH). These two gonadotropins act on the reproductive organs (ovary or testis), where they participate in the regulation of folliculogenesis, spermatogenesis, and steroids biosynthesis (testosterone, estradiol and progesterone) [6]. The constant communication channel between the various levels of the HPG axis is vital for its normal functioning: the hypothalamus and the pituitary receive constant feedback from sex steroids (estrogens, progesterone or androgens), and polypeptide hormones (activins, inhibins, follistatins), produced by gonads, to regulate GnRH, LH, and FSH release [7]. Many mammals and women have been evaluated for the different regulatory effects that ovarian steroid have on GnRH secretion and pulsatility: progesterone exerts a suppressive action, while estradiol has both stimulatory effects and inhibitive effects depending on the stage of menstrual cycles [8]. Androgens, on

the other hand, only exert a negative regulatory effect on gonadotropin production [9]. GnRH may also regulate its own secretion *via* an ultra-short feedback loop on the hypothalamic neuronal cells [10]. Moreover, the activation of GnRH receptors (GnRHRs) in the pituitary requires a pulsatile GnRH stimulation. Indeed, a continuous exposure to GnRH results in desensitization to GnRH-stimulated secretion of gonadotropin. This is due to receptor down-regulation, internalization, and the reduced response of the gonadotrope cell [11–14]. The pulse frequency of GnRH in an adult male is approximately 120 minutes. In a female, the pattern can be more complex, as it varies during different stages of the reproductive cycle and the ovulatory phase [15]. Dysregulated GnRH pulse release is associated with several physiological and pathological conditions that lead to reproductive disorders [3].

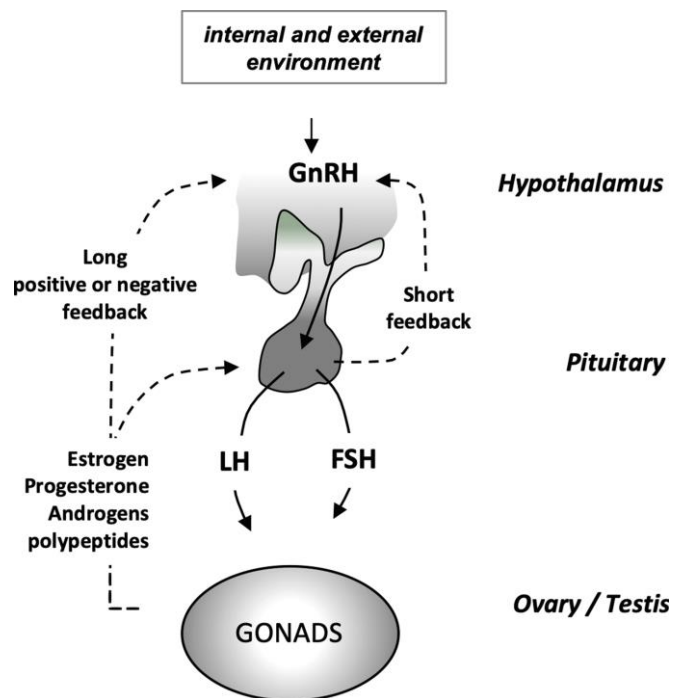


**Figure 2.** Schematic representation of the HPG axis [1].

The gonadal steroid also imprints sex phenotypes and sexual/reproductive behavior [16], as well as non-reproductive functions such as homeostasis and immunity [17]. The GnRH neuronal system responsible for peptide production is active in primates, including humans, during the late fetal and early neonatal periods. It becomes dormant during childhood and will be reactivated fully at puberty [18]. An impaired development and function in GnRH neuronal cells causes the idiopathic

central hypogonadism (ICH) [19]. It is a rare disease (1:8,000 males and 1:40,000 females) that can be acquired or congenital and may result from hypothalamic and pituitary lesions. This disease led to infertility by an insufficient GnRH stimulus resulting in low levels of male sex steroid (testosterone, estradiol), in the presence or low/normal levels of gonadotropins (LH and FSH). It is also can be associated with a normal or faulty sense of smell in normosmic ICH or Kallmann syndrome (KS), respectively.

Besides the first characterized GnRH, two other GnRH forms have been identified, and are known as GnRH-II and GnRH-III (Table 1) [20]. Due to this, it is possible to refer the first GnRH as GnRH-I.

**Table 1.** The amino acid sequences for GnRH isoforms.

|                 |   |
|-----------------|---|
| <b>GnRH-I</b>   | pGlu <sup>1</sup> -His <sup>2</sup> -Trp <sup>3</sup> -Ser <sup>4</sup> -Tyr <sup>5</sup> -Gly <sup>6</sup> -Leu <sup>7</sup> -Arg <sup>8</sup> -Pro <sup>9</sup> -Gly <sup>10</sup> -NH <sub>2</sub> |
| <b>GnRH-II</b>  | pGlu <sup>1</sup> -His <sup>2</sup> -Trp <sup>3</sup> -Ser <sup>4</sup> -His <sup>5</sup> -Gly <sup>6</sup> -Trp <sup>7</sup> -Tyr <sup>8</sup> -Pro <sup>9</sup> -Gly <sup>10</sup> -NH <sub>2</sub> |
| <b>GnRH-III</b> | pGlu <sup>1</sup> -His <sup>2</sup> -Trp <sup>3</sup> -Ser <sup>4</sup> -His <sup>5</sup> -Asp <sup>6</sup> -Trp <sup>7</sup> -Lys <sup>8</sup> -Pro <sup>9</sup> -Gly <sup>10</sup> -NH <sub>2</sub> |

Red indicates modified amino acids with respect to GnRH I. Highlighted in yellow the AA residues involved in receptor binding and activation, highlighted in green AA residues involved in receptor binding only.

Two rounds of genome duplication are thought to have evolved the three GnRH forms. All have the same AA sequences that are used for receptor activation and binding [21]. GnRH-II is found in vertebrates, and it is highly conserved across all species from fish to humans [22]. It shares 70% identity with GnRH-I, but differs in the His<sup>5</sup>, Tyr<sup>8</sup>, and Trp<sup>7</sup> residues (Table 1) [23]. GnRH-II is produced in certain nuclei in the central nervous systems (CNS), such as supraoptic, paraventricular, and suprachiasmatics nuclei acting as a neuromodulator for sexual behavior [22,24]. This isoform is also expressed in the mediobasal hippocampus and can interact with GnRH-I receptors (GnRH1R), but it is unlikely that it will be the primary regulator for gonadotropin in primates [22]. It has been hypothesized that the GnRH-I and GnRH-II neuronal populations may have a different but coordinated action in controlling fertility [25,26]. GnRH-II was also found in peripheral organs, such as the endometrium, placenta, and ovary in which GnRH-I and II have similar functions as autocrine/paracrine hormones in such structures: they regulate cell proliferation, and they mediate ovary and uterine hormonal secretion [27,28]. The “ligand-induced select signaling” theory (LISS), however, has been proposed because GnRH-II is more potent





Despite it was demonstrated the existence of a specific receptor for GnRH-II (GnRH2R) [45], the analysis of the gene encoding the human GnRH2R suggests that it is no functional [22,46]. Indeed, the effects exerted by GnRH-II or its analogues, as well as those mediated by GnRH-III [47,48], on the pituitary or peripheral tissues (e.g., antiproliferative/ antimotility effects on uterine endometrium and prostate), are mediated by the activation of GnRH1R [49].

At the same time, GnRH can have different effects depending on whether it acts on peripheral or pituitary receptors. This behavior can be explained considering that GnRH1R of extra-pituitary cells may adopt different conformations as a result of alternative post-translational processes [4]. GnRH analogs could bind these receptors differently, leading to different intracellular signaling pathways, and consequently, different biological effects [4]. Moreover, the intracellular signaling pathways of peripheral and pituitary GnRH1R are also different. GnRH1R in tumoral reproductive tissue has been found to be coupled to the  $G_{\alpha i}$  pathway, whose activation leads to a reduction of intracellular cAMP levels with the consequent activation of a signaling cascade, including MAPK, phosphatidylinositol-3-kinase (PI3K), and phosphotyrosine phosphatase [29]. This could explain the observed antitumor effects of GnRH analogues in cancer cell lines [50,51]. The LiSS theory could still be invoked to explain the difference in action between GnRH analogs and GnRH in peripheral tissues [29].

## 1.2 GnRH modulators

Historically, major advances in the pharmacology of GnRH came from the work of Knobil and colleagues [52] by demonstrating that continuous rather than pulsed administration of exogenous GnRH caused a decrease in response of pituitary gonadotrope cells, suggesting its use for both stimulation or inhibition of the HPG axis. The medical use of GnRH is, however, impaired by its short half-life (2-8 min) [53,54], mostly due to the prompt degradation of the bond between Gly<sup>6</sup> and Leu<sup>7</sup> by peptidases and cleared by glomerular filtration. For this reason, many efforts were done to synthesize GnRH analogues [1] (Table 2) endowed with better pharmacokinetic properties. There are two main types of GnRH analogues: agonists (GnRH-a) and antagonists (GnRH-ant) (Table 2).

**Table 2.** The amino acid sequences of GnRH analogues. Modified from Ref. [1].

| GnRH               | pGlu     | His   | Trp   | Ser | Tyr       | Gly                      | Leu | Arg                    | Pro | Gly—NH <sub>2</sub>    |
|--------------------|----------|-------|-------|-----|-----------|--------------------------|-----|------------------------|-----|------------------------|
| <b>Agonists</b>    |          |       |       |     |           |                          |     |                        |     |                        |
| Buserelin          | pGlu     | His   | Trp   | Ser | Tyr       | D-Ser (tBu)              | Leu | Arg                    | Pro | NHEt                   |
| Goserelin          | pGlu     | His   | Trp   | Ser | Tyr       | D-Ser (tBu)              | Leu | Arg                    | Pro | Azagly—NH <sub>2</sub> |
| Leuprolide         | pGlu     | His   | Trp   | Ser | Tyr       | D-Leu                    | Leu | Arg                    | Pro | NHEt                   |
| Triptorelin        | pGlu     | His   | Trp   | Ser | Tyr       | D-Trp                    | Leu | Arg                    | Pro | Gly—NH <sub>2</sub>    |
| Deslorelin         | pGlu     | His   | Trp   | Ser | Tyr       | D-Trp                    | Leu | Arg                    | Pro | NHEt                   |
| Nafarelin          | pGlu     | His   | Trp   | Ser | Tyr       | D-Nal                    | Leu | Arg                    | Pro | Gly—NH <sub>2</sub>    |
| Histrelin          | pGlu     | His   | Trp   | Ser | Tyr       | D-His (Bzl)              | Leu | Arg                    | Pro | NHEt                   |
| <b>Antagonists</b> |          |       |       |     |           |                          |     |                        |     |                        |
| Abarelix           | Ac-D-Ala | D-Cpa | D-Ala | Ser | Tyr       | D-Asp                    | Leu | Lys (iPr)              | Pro | D-Ala—NH <sub>2</sub>  |
| Cetrorelix         | Ac-D-Nal | D-Cpa | D-Pal | Ser | Tyr       | D-Cit                    | Leu | Arg                    | Pro | D-Ala—NH <sub>2</sub>  |
| Ramorelix          | Ac-D-Nal | D-Cpa | D-Trp | Ser | Tyr       | D-Ser (Rha)              | Leu | Arg                    | Pro | Azagly—NH <sub>2</sub> |
| Degarelix          | Ac-D-Nal | D-Cpa | D-Pal | Ser | Aph (Hor) | D-Aph (Cba)              | Leu | Lys (iPr)              | Pro | D-Ala—NH <sub>2</sub>  |
| Ganirelix          | Ac-D-Nal | D-Cpa | D-Pal | Ser | Tyr       | D-hArg (Et) <sub>2</sub> | Leu | hArg (Et) <sub>2</sub> | Pro | D-Ala—NH <sub>2</sub>  |

Abbreviations: *t*Bu: *tert*-butyl; Et: ethyl; AzaGly: aza-glycine; Bzl: 1-benzyl; Ac: acetyl; Cpa: chlorophenylalanine; Pal: 3-pyridylalanine; Cit: citrulline; Aph: 4-aminophenylalanine; Hor: L-hydroorotyl; Cba: carbamoyl; *i*Pr: isopropyl; Nal: 2-naphtylamine; hARg: homoarginine; D-Ser(Rha): O-(6-deoxy- $\alpha$ -L-mannopyranosyl)-D-serine. In grey background the modified residues with respect to mammalian GnRH.

GnRH-a mimic the action of the native GnRH, but they are designed to be more stable and potent. Indeed, they are also called “super agonists” since they are resistant to enzymatic breakdown, due to their lack of cleavage sites, resulting in a longer half-life and lower metabolic clearance compared to native GnRH [55]. To preserve their ability to interact with the GnRHRs, the N- and C- terminal sequences of these analogs were as close as possible to GnRH decapeptide (table 2) [56]. The modification of Gly<sup>6</sup>

to a AA of the D-series increases the plasma half-life when compared with GnRH. The removal of Gly<sup>10</sup> and the transformation of the N-terminus of Pro<sup>9</sup> in ethylamide, resulted in an increased affinity for GnRHRs [57]. GnRHR-a are characterized by high potency (up to 200 times the native GnRH), prolonged action and low toxicity. Due to their “superactivity”, GnRHR-a can cause a transient, intense stimulation of pituitary GnRH1R, with an increase in gonadotropin release, which is characterized by the flare-up effect (Figure 4). This response is then followed by GnRH1R desensitization, and reproductive axis shutdown, resulting in reversible castration [58].

GnRHR-ant were developed in response to the need for GnRH analogues that could block the HPG axis, without triggering unwanted flare-up responses (Figure 4). Since in their use the GnRH1R activation is not required, they had been modified extensively in the first 3 AA (the region required for receptor activation), and, as GnRHR-a, an AA of the “D series” was added in position 6 (Table 2) making them resistant to endopeptidases. As results, these compounds have a low AA similarity with GnRH [59–61]. GnRHR-ant binds human GnRH1R with high affinity ( $K_D$  values in the nM range), which may be 20 times greater than native GnRH [62]. GnRHR-ant block endogenous GnRH's effects on reproductive function, but exert GnRH-like antiproliferative activity on peripheral tumor cells [63–65]. This paradoxical action has yet to be explained but, nevertheless, a few hypotheses were put forward. One of them takes into consideration the molecular differences, due to post-translational modifications, between peripheral and central GnRHR [66,67]. One other possibility is that GnRHR could assume different conformations depending on the cell type where they are expressed, or the interacting ligand. This would activate different intracellular signaling pathway [29].

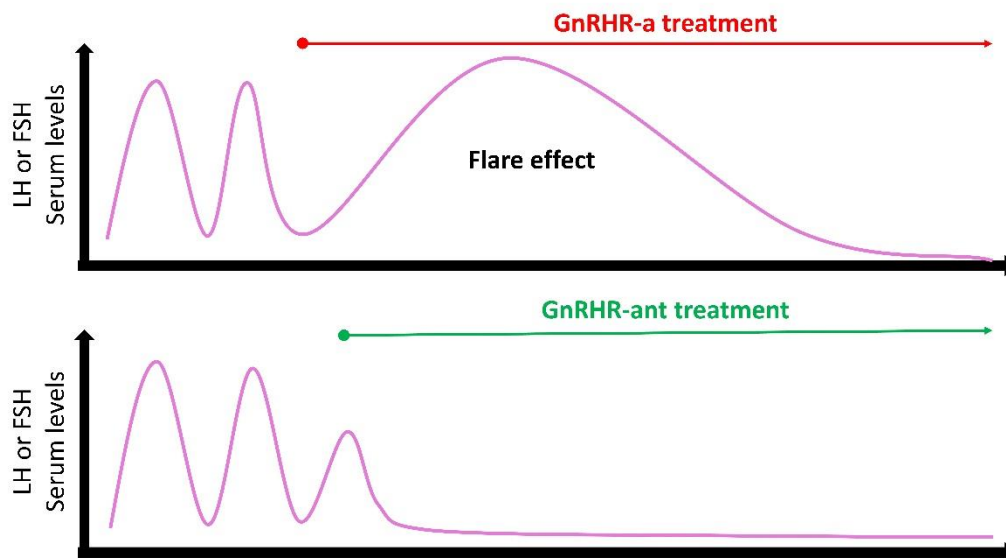


**Figure 4.** Schematic representation of the response, in terms of gonadotropin serum levels, to the administration of GnRHR-a or GnRHR-ant.

GnRH analogues can be used in various medical contexts, including:

- **Diseases of the Reproductive Axis and Organs:** GnRH analogues have been used to induce ovulation in women with reproductive defects due to inadequate GnRH secretion [68]. They are effective in conditions like polycystic ovary syndrome (PCOS), hyperandrogenic anovulation, and late-onset congenital adrenal hyperplasia [68,69]. They are particularly beneficial for patients with primary GnRH deficiency and hypothalamic amenorrhea.
- **Fertility Treatments:** GnRH analogues are used in assisted reproductive technologies to induce the development of multiple ovarian follicles [70,71], improving oocyte quality and reducing the risk of ovarian hyperstimulation syndrome (OHSS) [72–74].
- **Endometriosis:** These analogues are used for the medical treatment of endometriosis, where they suppress oestrogen support to endometrial tissue, reducing symptoms and progression [75,76].
- **Central Precocious Puberty:** GnRH analogues are used to delay the onset of puberty in children with central precocious puberty [77].
- **Gender Dysphoria:** In transgender individuals undergoing hormone therapy, GnRH analogues can suppress endogenous hormone production, facilitating a controlled transition [78].
- **Prostate Cancer:** GnRH analogues lower testosterone levels in men with advanced prostate cancer, slowing cancer growth [79].

- **Breast Cancer:** GnRH analogues can suppress ovarian function in premenopausal women with hormone receptor-positive breast cancer to prevent tumor growth [80].

- **Uterine Fibroids:** These analogues may be prescribed to shrink uterine fibroids and reduce associated symptoms [81].

In addition, GnRH analogues have been explored for various other conditions, such as preserving fertility in female patients undergoing chemotherapy [82–85], and potential use in neurological diseases, including Alzheimer's disease [86,87], spinal cord injuries [88], and multiple sclerosis [89].

Another important point is that several cancer types, including endometrial, ovarian, urinary bladder, and prostate carcinoma, demonstrate the presence of GnRH and its receptor within an autocrine system that regulates cell proliferation and metastasis [35]. Furthermore, breast and non-reproductive cancers, such as pancreatic cancer and glioblastoma, also exhibit the GnRH/GnRHR system. For this reason, GnRH analogues have been explored as carriers of chemotherapy due to elevated expression of GnRHR by cancer cells [90–92]. The approach involves attaching an anticancer drug with a GnRH-analog, increasing the drug's selectiveness for cells that express GnRHR while reducing peripheral toxicities. These bioconjugates, once bound to GnRHR are internalized by endocytosis. The anticancer drug is then released within the lysosomes.

### 1.3 Non-peptide GnRH modulators

Therapies involving peptide GnRH analogues usually require injections or depot preparations. Therefore, there has been an interest in developing agents targeting the GnRHR that are orally bioavailable [1]. Oral administration offers several advantages, including improved patient compliance and rapid, dose-dependent control of the functions of the HPG axis, which is challenging to achieve with non-customized systemic administration of peptide GnRH analogues [93,94].

In 1989, the journey to orally bioavailable GnRHR modulators began when it was discovered that orally administered ketoconazole displayed weak antagonistic activity towards GnRHR [95]. Since then, several non-peptide structures have been found to bind GnRH1R [94]. Notably, three compounds have recently entered clinical use: an

uracil-based analogue substituted at positions 1, 3, 5, and 6, with a stereocenter in the (*R*)-configuration (elagolix), a thieno[2,3-*b*]pyrimidine-2,4-one derivative (relugolix), and a 2,4-dioxo-1,2,3,4-tetrahydrothieno[3,4-*d*]pyrimidine-5-carboxylic acid derivative (linzagolix) (Figure 5).

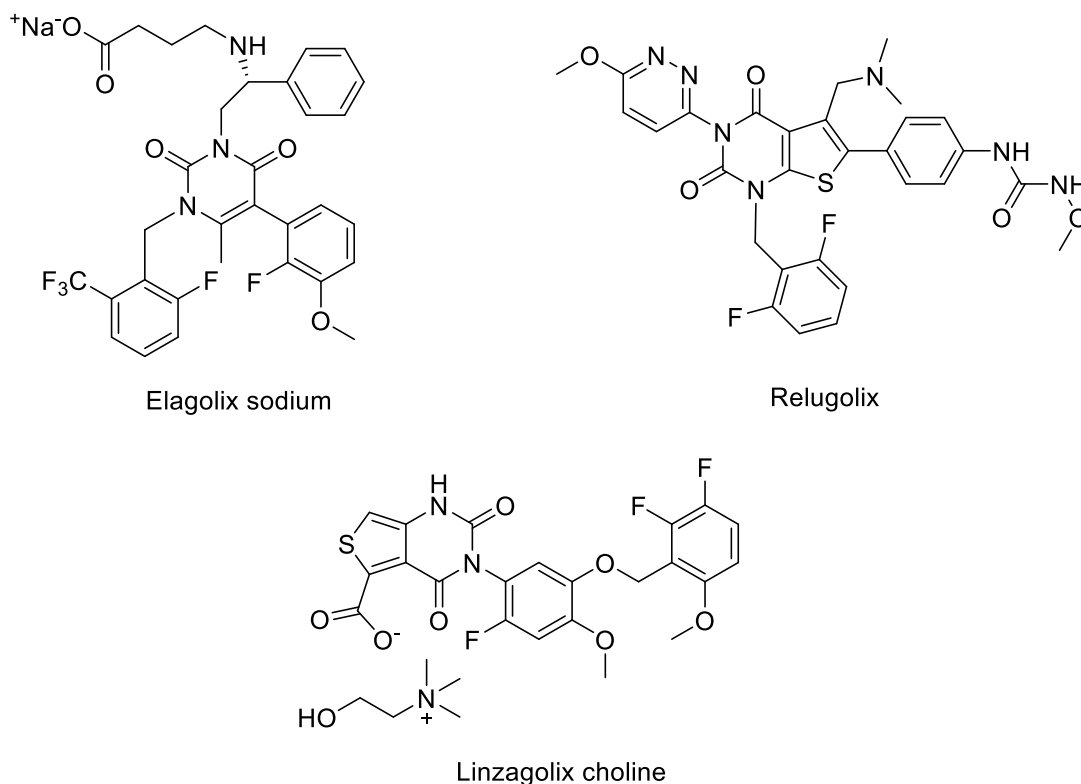


**Figure 5.** Chemical structures of clinically used non-peptide GnRHR-ants.

These three compounds bind specifically and competitively to the human pituitary GnRH1R leading to a stable and reversible inhibition of gonadotropin production displaying, at the same time, a faster onset/offset of therapeutic effects and a better safety profile than peptide GnRH analogues [96–98]. Elagolix has a very high affinity for GnRH1R ( $K_D=54$  pM) and inhibits GnRH *in vitro* by a  $K_i$  value in the low nanomolar range (1.5-2.8 nM) [99,100]. Relugolix binds GnRH1R in humans and monkeys with high affinity and has an estimated  $IC_{50}$  value of 0.12-0.15 nM for inhibiting GnRH-a binding [101,102]. Linzagolix is also a potent and select antagonist of *h*GnRH1R, with a  $K_i=27.4$  nM, capable of inhibiting GnRH-stimulated  $Ca^{2+}$  flow, with an  $IC_{50}$  value of 36.7 nM, comparable to the peptide GnRH-ant cetrorelix (Table 2) [98,103,104]. They are used to treat hormone-dependent diseases such as moderate to severe pain associated with endometriosis (elagolix) [105,106], prostate cancer

(relugolix) [107], and uterine fibroids, (elagolix, relugolix, and linzagolix) [104,108,109].

Endometriosis is a benign, chronic inflammatory disorder characterized by the presence and the growth of endometrial implants outside the uterine cavity. It is estimated to affect 10% of women of reproductive age [110,111]. Uterine fibroids are benign tumors that occur more frequently in women over 40 and those of African descent. They are often discovered by accident during a clinical examination or on imaging. If symptomatic they can cause abnormal bleeding, pelvic pain, bowel disorders, urinary urgency and frequency, low back discomfort, constipation and dyspareunia [112]. Prostate cancer stands as the most frequently identified cancer in men and ranks as the fifth primary cause of cancer-related fatalities among males. It usually develops slowly and may not cause noticeable symptoms for many years. In some cases, however, it can be aggressive and spread quickly. Common symptoms of prostate cancer may include urinary problems, blood in the urine or semen, erectile dysfunction, and pain and discomfort [113–115].

Currently, phase III clinical trials are ongoing for the treatment of endometriosis-associated pain with relugolix [116] and linzagolix [117].

Despite the undoubted benefits brought by these new drugs, some issues remain to be solved. For example, elagolix exhibits moderate oral bioavailability in human (about 50%) together with a short half-life time ( $t_{1/2} = 4\div 6\text{h}$ ) [100], making daily administration of several tablets necessary. Relugolix shows a low oral bioavailability in human (<10%), probably due to limited intestinal absorption as a P-glycoprotein (P-gp) substrate, and to a lesser extent first pass metabolism by cytochrome P450 (CYP)3A4 [102]. In addition, a case of skin toxicity associated with relugolix was recently reported [118]. Linzagolix showed appropriate half-life (15 $\div$ 18h) and oral bioavailability (86%) but, due to its high degree of plasma protein binding (>99%) [103], can cause several unwanted drug-drug interactions. Thus, the interest in developing non-peptide modulators that have better pharmacokinetics and pharmacodynamics properties is still high. Bayer researchers discovered in 2020 that spiroindolines are potent GnRHR-ant [119], which show, differently from elagolix, relugolix or linzagolix, similar *in vitro* and *in vivo* activity on both rat and human



GnRH1Rs. This will be beneficial to the optimization of drugs, using the rat model. More recently, a Chinese research group biologically evaluate some modification to the chemical structure of relugolix, to improve its pharmacokinetic profile and oral bioavailability [120]. A molecular-generative model named “LSMolGen” [121], which combines the existing knowledge of the *h*GnRH1R [43] with the structure of known active compounds, has been developed more recently for the design and development of new orally effective modulators. In 2022 [122], a discovery of notable significance for the further development of new *h*GnRH1R was documented, revealing the first non-peptide GnRH-a ( $EC_{50}=1.59 \mu M$ ) (Figure 6).

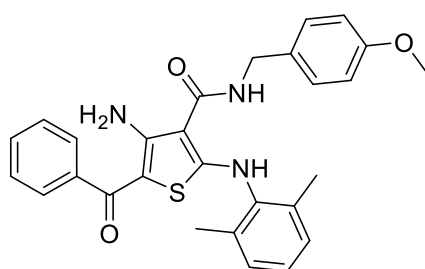


**Figure 6.** Chemical structures of the first example of non-peptide GnRHR-a.

### 1.3.1 Insights on the mechanism of action of non-peptide modulators on GnRHR

In an effort to understand the high specificity for the *h*GnRH1R displayed by non-peptide GnRH-ant, never reported for peptide GnRH analogues, the observed differences in selectivity between the human and dog [122] or rat [123] GnRH1R were deeply examined by mutagenesis experiments. The difference in selectivity between human and dog GnRH1R was attributed to Phe<sup>313</sup> residue, while the N-terminal region was responsible for the difference in selectivity observed between human and rat GnRH1R. These investigations showed also, for the first time, that non-peptide molecules do not overlap completely the binding site of peptide analogues. This result was further confirmed in the subsequent mapping of the *h*GnRH1R residues involved in the binding with peptide or non-peptide GnRHR-ant: the studied orthosteric non-peptide GnRH-ant occupies distinct GnRHR subregions, partially overlapping, of the larger binding site occupied by peptide GnRHR-ant [124] and was also identified the very first allosteric non-peptide GnRHR-ant interaction with the *h*GnRH1R [125]. Recently, the crystal structure of the *h*GnRH1R bound to elagolix was published (PDB

code: 7BR3) [43] thus allowing the identification of the ligand bind site and the structural determinants relevant for complex stabilization. The *hGnRH1R*/elagolix crystal structure was utilized, by the same authors, for docking simulations with relugolix and sufugolix (an analogue of linzagolix) resulted in conformational rearrangements in some parts of the binding area suggesting a plasticity within the orthosteric pocket when it comes different ligands (Figure 7). Moreover, recent studies using Molecular Dynamics (MD) simulations [126] showed that binding of non-peptide GnRHR-ant to *hGnRH1R* induces a conformational shift of transmembrane domain (TM) 6 outward, a well-known feature in the activation of class-A GPCRs.

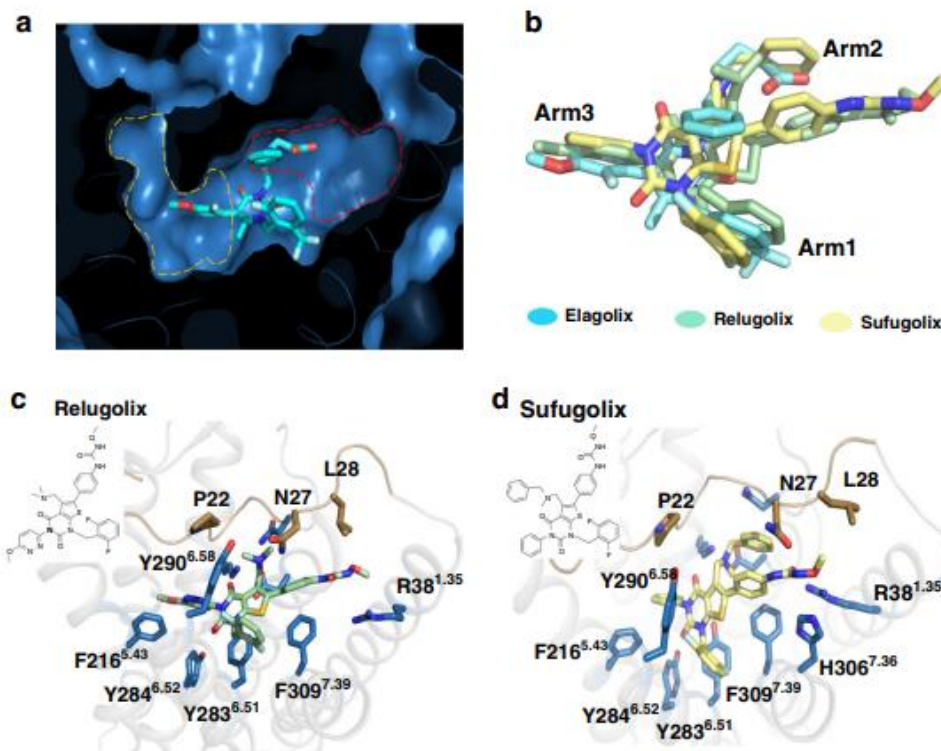


**Figure 7.** (a) Cutaway view of the elagolix binding pocket in GnRH1R. (b) Superposition of ligands conformations in *hGnRH1R*. Elagolix, relugolix, and sufugolix are shown in cyan, pale cyan, and pale-yellow sticks, respectively. (c) Relugolix and (d) sufugolix binding mode of *hGnRH1R*, key residues involved in potential interaction are represented as sky blue sticks. From Ref. [43]. License: [CC BY 4.0 Deed](https://creativecommons.org/licenses/by/4.0/).

## 1.4 Atropisomerism

The word “atropisomerism” was coined from the Greek “ατροπος”, meaning ‘not turning’, by the Nobel Prize Richard Kuhn in 1933 [127] to indicate a source of chirality resulting from hindered rotation about one or more single bonds. Since its discovery by Christie and Kenner in 1922 [128], who succeeded in resolving the atropisomers of 6,6'-dinitro-2,2'-diphenic acid (Figure 8), this type of conformational isomerism has been found in many biologically active compounds that have scaffolds such as biaryls, diaryl ethers, diaryl amines, benzamides and anilides [129,130].

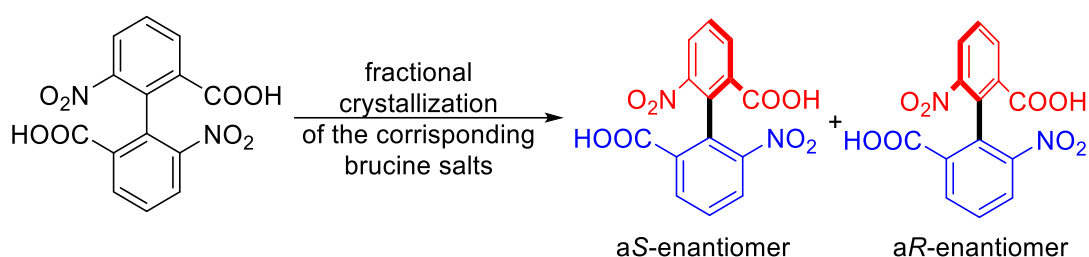


**Figure 8.** Example of atropisomers resolution.

Atropisomerism differs from other instances of chirality in that racemization can occur spontaneously *via* a time/temperature-dependent bond rotation rather than the process of bond breaking and bond making usually needed for the racemization [131]. This leads to a conformational instability that must be taken into account during drug discovery and development. The interconversion rate can be determined by both stereoelectronic and steric effects. Owing the temperature dependence of the interconversion of atropisomers, Oki refined the definition of atropisomers as those conformers that interconvert with a half-life of at least 1000 seconds at a given temperature [132], corresponding to an energy barrier of 22 kcal/mol at 300 K. Likewise, it should not be forgotten that atropisomers of the same molecules, being stereoisomers, can display profound differences in their pharmacological properties. For this reason, LaPlante and co-workers [133,134] conveniently classified them into three categories (Figure 9) based on their rotational energy barriers ( $\Delta G^\ddagger$ ).

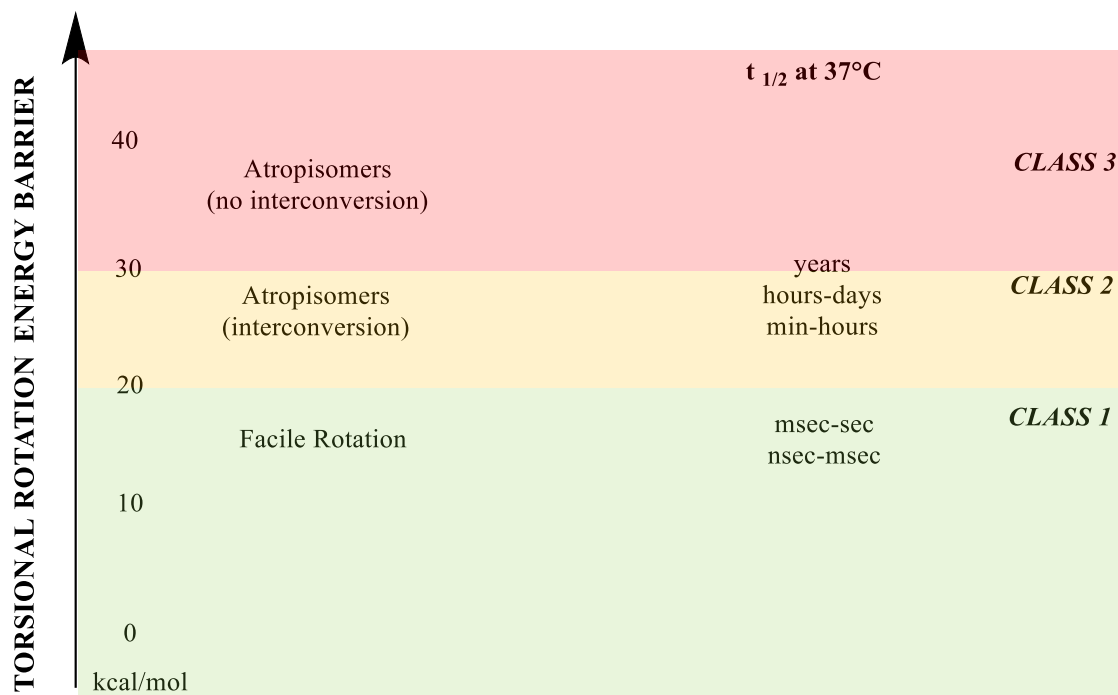


**Figure 9.** LaPlante's classification of atropisomers. Modified from Ref. [134].

Since class 3 atropisomers ( $\Delta G^\ddagger \geq 30$  kcal/mol) are stable for prolonged periods at physiological conditions, they are typically treated in a manner like point chiral molecules. Conversely, rapidly interconverting class 1 atropisomers ( $\Delta G^\ddagger \leq 20$  kcal/mol) can be considered as achiral molecules and are perhaps the most common manifestation of atropisomerism in medicinal chemistry. Class 2 ( $20$  kcal/mol  $\leq \Delta G^\ddagger \leq 30$  kcal/mol) atropisomers represent a conundrum in drug discovery as they interconverts on an intermediate time scale that can cause complications when characterizing the activities of each atropisomer at early stage development [131]. Moreover, since the  $t_{1/2}$  of interconversion between atropisomers (Figure 9) is a temperature dependent parameter, this value at human body temperature (37°C) is a crucial factor when considering atropisomers as potential drugs [135].

It has become clear that in many cases the majority of activity toward a desired target belongs to one atropisomer, while the other atropisomer contributes very little [136] and it has been recently demonstrated that various properties of an interconverting atropisomer can be modulated through the synthesis of atropisomer stable and pure analogues. Indeed, atropisomeric molecules have a rotational barrier that can allow the isolation of the individual conformers and this is important because the atropisomers can differ in their biological activity towards a target, in the off-target

selectivity and in their pharmacokinetic properties [131,137] as much as in cell uptake and therapeutic efficacy [138].

### 1.4.1 Atropisomerism in drug discovery

As mentioned before, the fact that the interconversion of atropisomers is a time- and temperature-dependent process, and that atropisomers of the same molecule can have different pharmacological properties can rise a range of analytical and synthetic challenges. In this regards, two small molecules recently approved by EMA and FDA can be mentioned: sotorasib and lesinurad.

Sotorasib [139] (Figure 10) is the first marketed single-atropisomer drug, recently approved by FDA (2021) and EMA (2022) as covalent inhibitor of KRAS<sup>G12C</sup> for the treatment of solid tumors.

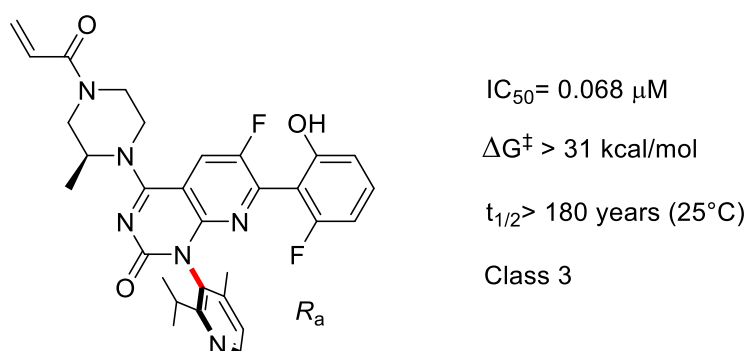


**Figure 10.** Chemical structure of sotorasib, the first marketed single-atropisomer drug. In red is indicated the axially chiral atropisomeric bond.

The development of this single-atropisomer drug gave rise to a range of analytical and synthetic challenges [140] since its chemical structure arose from a specific structural need: to provide a structural motif capable of accessing a "cryptic" pocket on the surface of the target protein, KRAS<sup>G12C</sup>. The research, aimed at maximizing the interaction with the "cryptic" pocket, led to the identification and synthesis of a potent precursor of sotorasib, which, however, NMR and HPLC analyses showed to be a mixture of class 2 atropisomers (Figure 11).

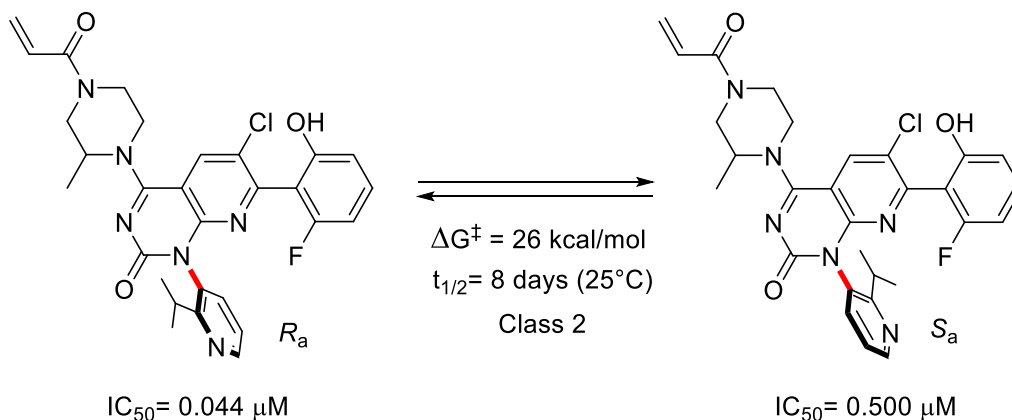


**Figure 11.** The two atropisomeric forms of the class 2 precursor of sotorasib.

It was anticipated that the moderate configurational stability of this compound (Figure 11) would pose significant regulatory challenges since its atropisomers, endowed with different pharmacological properties [139], interconvert each other during manufacture, distribution and *in-vivo* studies [140]. This potent precursor has been subjected further optimization in order to achieve the desired atropisomeric class 3 for the obtainment of the more active atropisomer, the *aR*-one, as a thermally stable species: sotorasib [140]. The research team involved in the sotorasib discovery had to evaluate the configurational stability of the atropisomers of all the synthesized compounds [140]. They used some of the available analytical techniques useful to characterize conformational dynamics that occurred at different time scales and with differing interconversion energy (Table 3) [141–143]. In this case, being the atropisomers of sotorasib diastereomers, NMR techniques proved one of the most versatile means of detecting and analyzing the obtained atropisomer mixtures [140].

**Table 3.** Useful techniques to analyze atropisomers interconversion. Data from Ref. [141–143].

| Technique            | Description   | Range of applicability                               |
|----------------------|---|--|
| Kinetic analysis     | The interconversion of a small amount of atropisomerically pure substance is followed by HPLC, NMR, or CD analysis carried out at different time intervals. | $\Delta G^\ddagger \geq 23 \text{ kcal/mol}$         |
| Dynamic HPLC (DHPLC) | The observed formation of plateaus, resulting from on-column interconversion, is compared with simulated ones.  | $\Delta G^\ddagger \approx 19 - 23 \text{ kcal/mol}$ |
| Dynamic NMR (DNMR)   | The observed coalescence of the NMR resonances is compared with that simulated by line-shape analysis.  | $\Delta G^\ddagger \leq 20 \text{ kcal/mol}$         |

|                              |   |  |
|------------------------------|---|--|
| Exchange spectroscopy (EXSY) | Using the intensities of the relevant peaks, it is possible to quantitatively calculate the rate constants ( <i>k</i> ) of interconversion. | $\Delta G^\ddagger \approx 20 - 23 \text{ kcal/mol}$ |
|------------------------------|---|--|

Lesinurad (Figure 12), instead, is a recent example of overlooked atropisomerism. It was approved by both FDA (2015) and EMA (2016) as an orally administered treatment for gout decreasing serum uric acid through inhibition of urate transporters in the kidney; the target is URAT1, a transporter known to be associated with uric acid reabsorption [144]. It was launched on the market believing it was an achiral molecule. Indeed, based on the structure (Figure 12), the triazole ring should rotate freely along the C–N bond. However, a few years later, a research group hypothesized that the thioacetic acid moiety and the bromine atom could hinder free rotation due to steric bulk [145]. This hypothesis was verified performing a chiral supercritical fluid chromatography (SFC) that led to the separation of the two enantio-atropisomers that constitute lesinurad (Figure 12).

Through the stability studies of (*S<sub>a</sub>*)/(*R<sub>a</sub>*)-lesinurad carried out in solid form, in solvent, and in plasma it was found that these two atropisomers are very stable and there was no interconversion between the two isomers under heat, in solutions, and in *in vivo* pharmacokinetic studies. Although the two atropisomers showed comparable data in most of the physicochemical properties, (*S<sub>a</sub>*)-lesinurad showed significant higher *in vitro* inhibition potency against hURAT1 than (*R<sub>a</sub>*)-lesinurad (Figure 12) [145]. Moreover, *in vitro* human recombinant CYP2C9 (the enzyme major responsible of lesinurad metabolism) stability study indicated that (*S<sub>a</sub>*)-atropisomer was more stable than (*aR*)-atropisomer. Considering the significant difference between the two isomers, it was speculated that the (*S<sub>a</sub>*)-lesinurad might offer a better hyperuricemia/gout therapy than (*R<sub>a</sub>*)-lesinurad or the racemate [145].

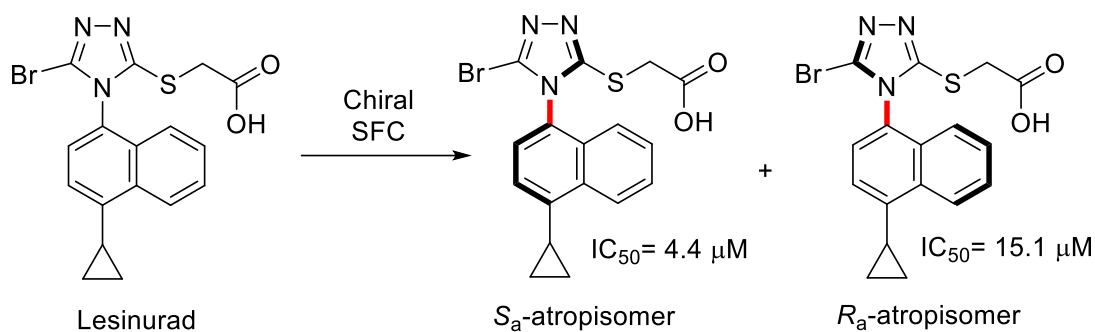


**Figure 12.** Lesinurad enantio-atropisomers.

These examples, as well as many others reported in the literature [131,136,137,146–149], make it clear how pursuing the development of single atropisomeric drugs, despite the practical challenges associated with their synthesis, purification, and analysis, is a viable strategy for achieving compounds with enhanced pharmacological characteristics, such as increased potency and selectivity, improved physicochemical properties like solubility and chemical stability, optimized pharmacokinetics/ADME, and enhanced toxicology/safety profiles. For this reason, the preparation of new atropisomeric scaffolds [141] and the development of atropisomeric modifications for known drugs [135] have gained significant attention in recent years.

In this context, the occurrence of atropisomerism in elagolix structure (Figure 5), was deeply investigated by our research group filling a gap in the characterization of this marketed drug [150].

1-(2,6-difluorobenzyl)-3-[(2*R*)-amino-2-phenethyl]-5-(2-fluoro-3-methoxyphenyl)-6-methyluracil (Figure 13) is a close analogue of elagolix that manifests a class 2 atropisomerism having a relatively short half-life of interconversion between the two atropisomers at 25°C ( $t_{1/2}$  = 35 and 114 min in chloroform and water, respectively) [151]. The two atropisomeric forms arise from the interaction of the *o*-fluorine of the 5-aryl group with the methyl group at the 6-position of the uracil moiety and the electronegative oxygen atom of the carbonyl functionality, which causes a slow rotation about the C-C bond.



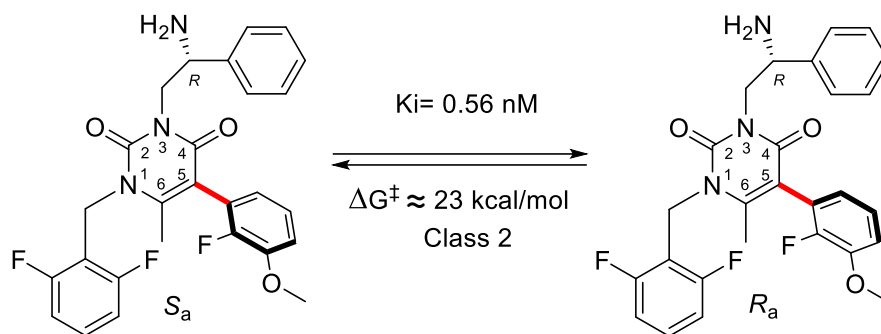


**Figure 13.** Atropisomeric forms of 1-(2,6-difluorobenzyl)-3-[(2*R*)-amino-2-phenethyl]-5-(2-fluoro-3-methoxyphenyl)-6-methyluracil. The rotation about the red bond is restricted by steric and electronic effects.

The proof of the existence of atropisomerism for this compound is given by its NMR and chiral HPLC analyses [151]. Given that they have only one conventional stereogenic center at the 3-side chain derived from *R*-phenylglycinol, the observation of two sets of signals implies that this compound is a mixture of two diastereo-atropisomers, as there is an additional element of asymmetry. It is also noteworthy that, the two atropisomers, despite being diastereoisomers, can only be separated in HPLC with the use of a chiral stationary phase.

As reported by the same authors in another paper [152], the moderate interconversion rate between atropisomers causes issues in the drug manufacturing and quality control processes, such as a low batch-to-batch reproducibility, and inconsistencies in the safety/efficacy evaluation of the drug. A valuable strategy in avoiding the obtention of class 2 atropisomers could be the elimination of the source of atropisomerism or the rigidification of the molecular structure [133]. These strategies have been already applied on some elagolix analogues. In order to avoid the atropisomerism, a different molecule has been prepared by deleting the 6-methyl group [152]; however, this compound exhibited a 10-fold lower affinity for the receptors (Figure 14), whereas an increase in steric hindrance, achieved by substituting the fluorine with the bulkier chlorine atom, led to the obtention of two stable atropisomers with a 600-fold potency difference in binding *hGnRH1R* (Figure 14), which evidenced the existence of a stereo-preference for receptor interactions [153].

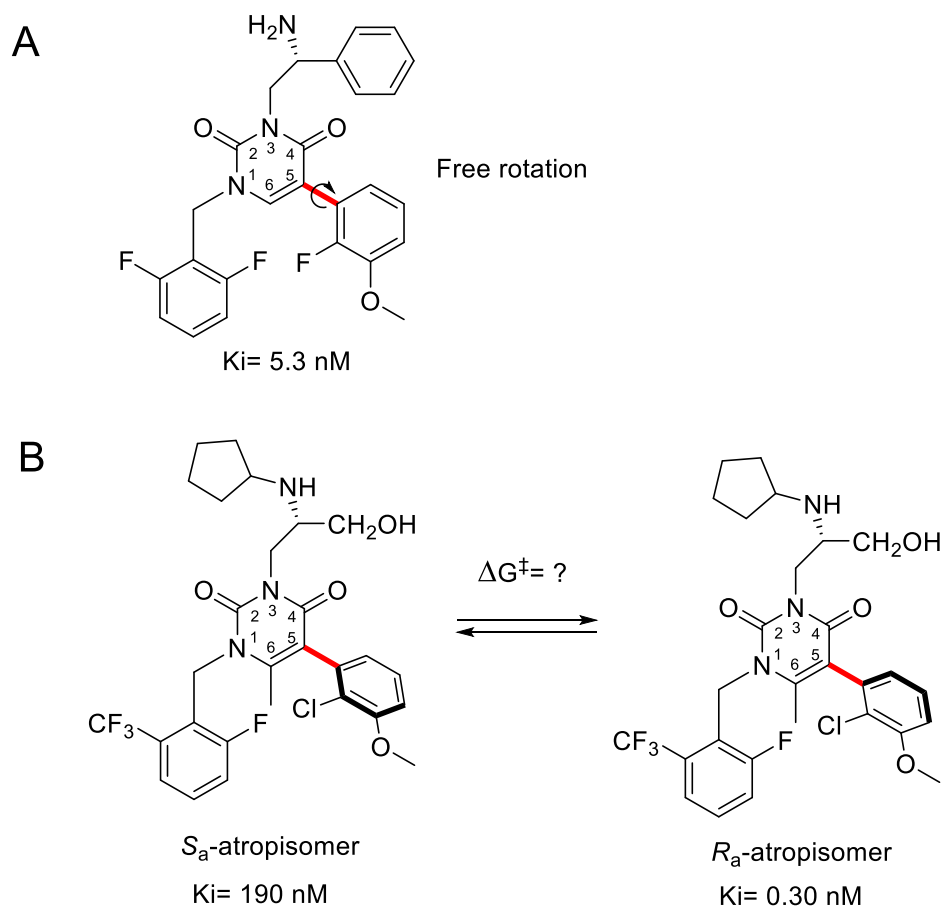


**Figure 14.** Elagolix analogues manifesting free rotation (A) or separable in two atropisomers (B). The last one has two stable atropisomers at room temperature (the rotational barrier is not disclosed); one of them is the favorite for the receptor interaction.

These results, as postulate by the authors of these studies [153], highlights that a thermally stable atropisomer may be a viable alternative for further development of non-peptide GnRHR-ant.

## Chapter 2

### Aims and Outline of the Thesis

---

Given the urgent demand for novel orally administered drugs to treat sex hormone-dependent diseases, with enhanced potency and improved pharmacokinetic profiles, the primary objective of this research project was to design, synthesize, characterize, and assess new modulators of the GnRHR.

To unveil new derivatives with improved pharmacological properties, the recently approved oral GnRHR-ant elagolix was selected as lead compound and three primary research objectives were defined:

1) To investigate the atropisomeric properties of elagolix and its intermediates to fill the literature gap.

2) To design, synthesize, characterize, and biologically assess new elagolix analogs featuring increased steric hindrance. A promising, but still unexplored, approach to achieve this goal could involve modification of the substituents at the 6- and 4- positions (referred to as **R** and **X** groups, respectively, Chart 2) of the uracil moiety.

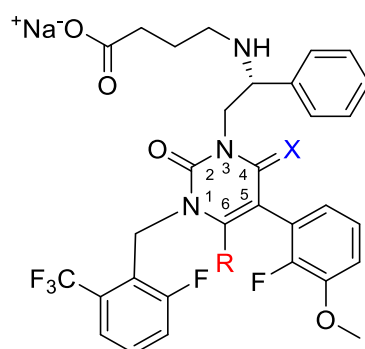


Chart 2.

3) To establish protocols for the enzymatic separation of the atropisomers of the new elagolix analogues.

The results obtained from these endeavors will contribute to a more profound understanding of the significance of atropisomerism and facilitate the identification of

prospective candidates for oral GnRHR-ant in the treatment of sex hormone-dependent diseases, with the potential to be developed as single atropisomers.

## Chapter 3

### Elagolix

---

Given the lack of existing data or references on elagolix atropisomerism, the research conducted in this section was primarily dedicated to determining whether elagolix exhibits atropisomerism and, if so, categorizing it within the relevant atropisomers classes (see section 1.4). To accomplish this objective, we embarked on the synthesis of elagolix, not only to address the gap in the literature regarding analytical information on elagolix, but also to establish an optimized synthetic route for obtaining a highly pure elagolix sodium salt sample, suitable for biological assays by a way potentially useful for developing the new elagolix analogs.

The obtained results were published in Ref. [150].

#### 3.1 Synthesis of elagolix

The synthesis of elagolix (**1**) was initially carried out according to a modified literature procedure [96,154] (Figure 15). The variations to the published experimental protocol included:

- 1) the use of *tert*-butyl acetoacetate instead of the dangerous, toxic and unstable reagent, "diketene";
- 2) the identification of different reaction conditions to obtain intermediate **18** in higher yields.
- 3) the use of Lewatit CNP80, a weakly acidic resin, in the ion-exchange step instead of Dowex MSC, a strong acidic resin that failed in our tests.

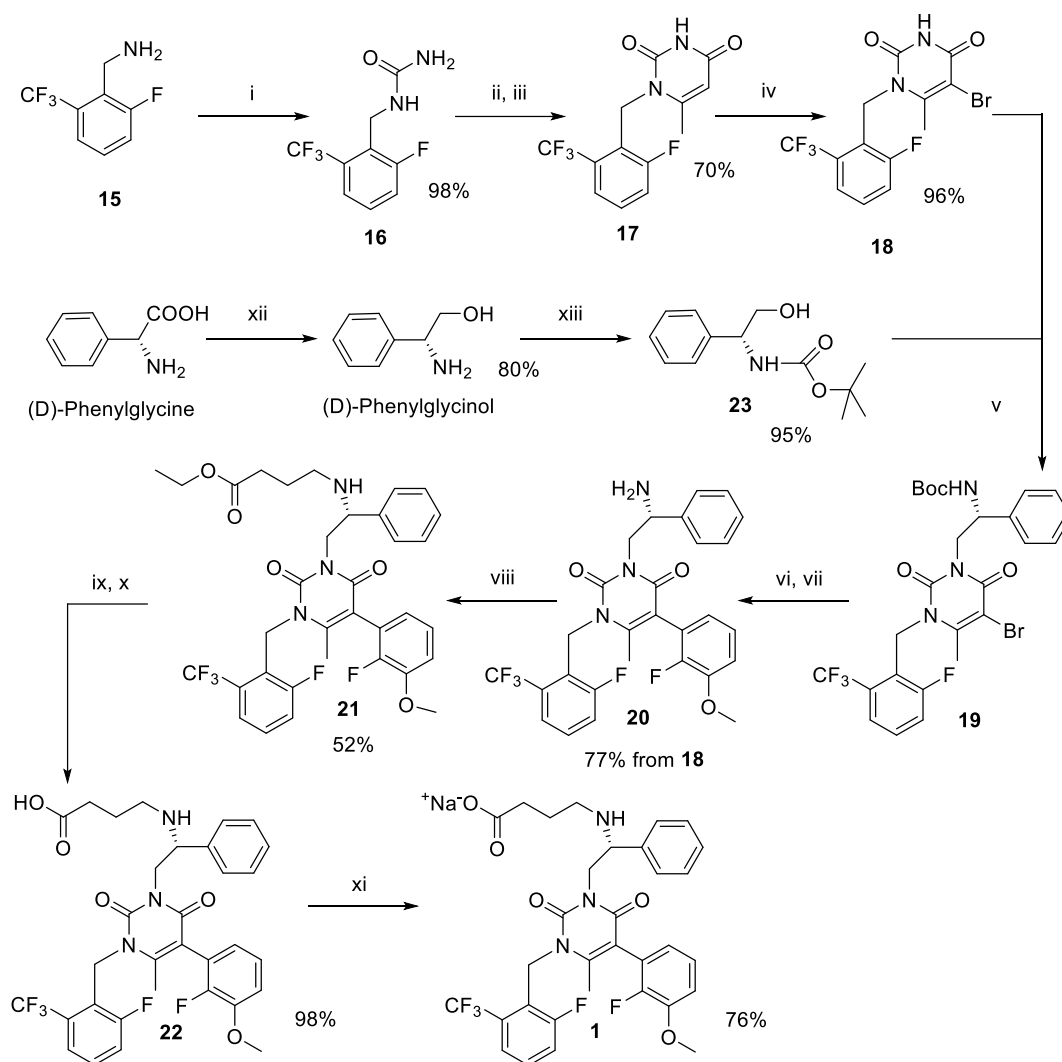


**Figure 15.** First synthetic approach followed for the synthesis of elagolix (**1**). Reagents and conditions: (i) urea, HCl, H<sub>2</sub>O, reflux; (ii) *tert*-butyl acetoacetate, toluene, reflux, Dean-Stark apparatus; (iii) *p*-TsOH·H<sub>2</sub>O, reflux; (iv) Br<sub>2</sub>, acetic acid, rt; (v) di-*tert*-butyl azadicarboxylate, PPh<sub>3</sub>, THF, nitrogen atmosphere, rt; (vi) 2-fluoro-3-methoxyphenylboronic acid, Pd(PPh<sub>3</sub>)<sub>4</sub>, Na<sub>2</sub>CO<sub>3</sub>, H<sub>2</sub>O, dioxane, under argon atmosphere, reflux; (vii) TFA, CH<sub>2</sub>Cl<sub>2</sub>, rt; (viii) ethyl 4-bromobutyrate, DIPEA, ACN, 80 °C; (ix) NaOH, H<sub>2</sub>O, THF, 50°C; (x) citric acid, rt; (xi) ion-exchange resin Lewatit CNP80; (xii) NaBH<sub>4</sub>/I<sub>2</sub>, THF, reflux; (xiii) (Boc)<sub>2</sub>O, TEA, THF, rt.

Starting from 2-fluoro-6-(trifluoromethyl)benzylamine **15**, the corresponding urea analogue **16** was obtained in 98% yield after reaction with urea at reflux under acidic conditions. The next step was the formation of the 5-methyl uracil derivative compound **17**. As reported in the literature [96,154], this conversion is carried out by means of diketene, a highly reactive and flammable chemical that poses a high risk of explosion and development of poisonous gases [155,156]. We focused our attention on replacing this reagent by a safer alternative. Since the use of the less reactive and

dangerous diketene acetone adduct led, in contrast to what is reported in a 2018 patent for the preparation of **1** [157], to an unwanted isomer of **17** (Figure 16), the use of  $\beta$ -keto ester could be a viable option [158]: similar to diketenes, acetoacetates also undergo a reaction with monosubstituted ureas, resulting in the formation of 3-substituted derivatives known as 1-acetoacetylureas. Under acidic conditions, this intermediate undergoes cyclization, ultimately yielding 6-methyl-1-substituted uracil. Using ethyl acetoacetate, under reflux, and employing a Dean-Stark apparatus to remove the formed water, the desired product **17** was obtained along with its unwanted isomer in a relative ratio of 1:0.6 (Figure 16). The best result was obtained using a different  $\beta$ -keto ester, *tert*-butyl acetoacetate, reported in a 2009 patent [159], that led to the formation of **17** in 70% yield (Figure 16).

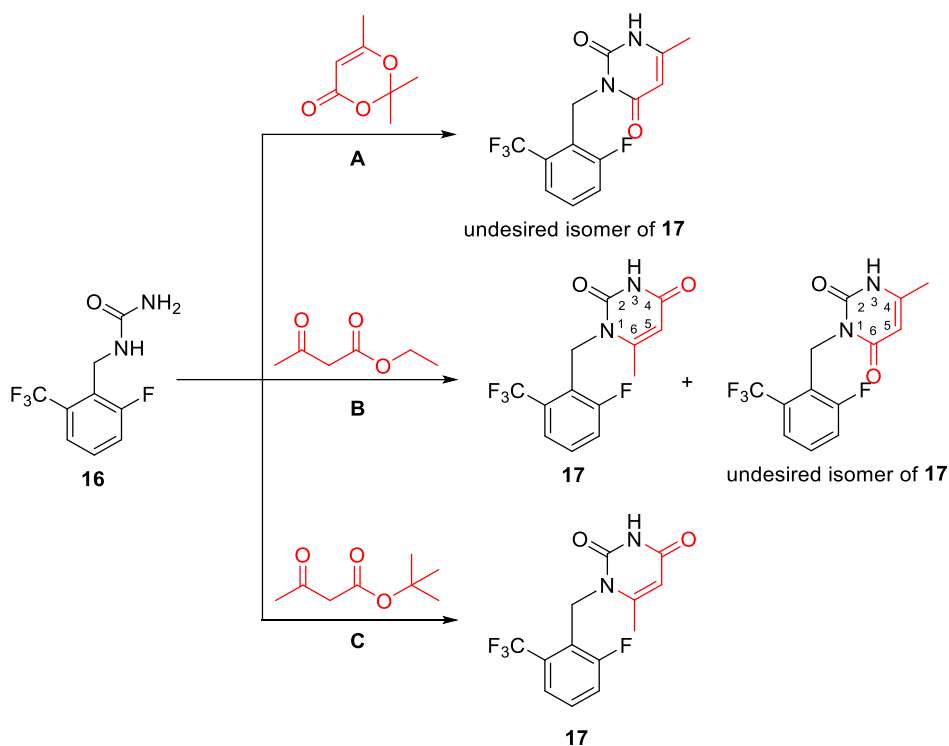


**Figure 16.** Reaction of **16** with (A) diketene-acetone adduct, (B) ethyl acetoacetate, and (C) *tert*-butyl acetoacetate.

The structure of compound **17** was verified through NOESY experiments. This 2D-NMR technique is employed to identify the spatial proximity of specific protons within the analysed molecule, even if they are not directly bonded [160]. The observation of a cross-peak between the methyl group at the 6-position of the uracil

moiety and the benzyl protons confirms their spatial proximity (Figure 17). In the case of the undesired isomer of **17**, this cross peak is not present.

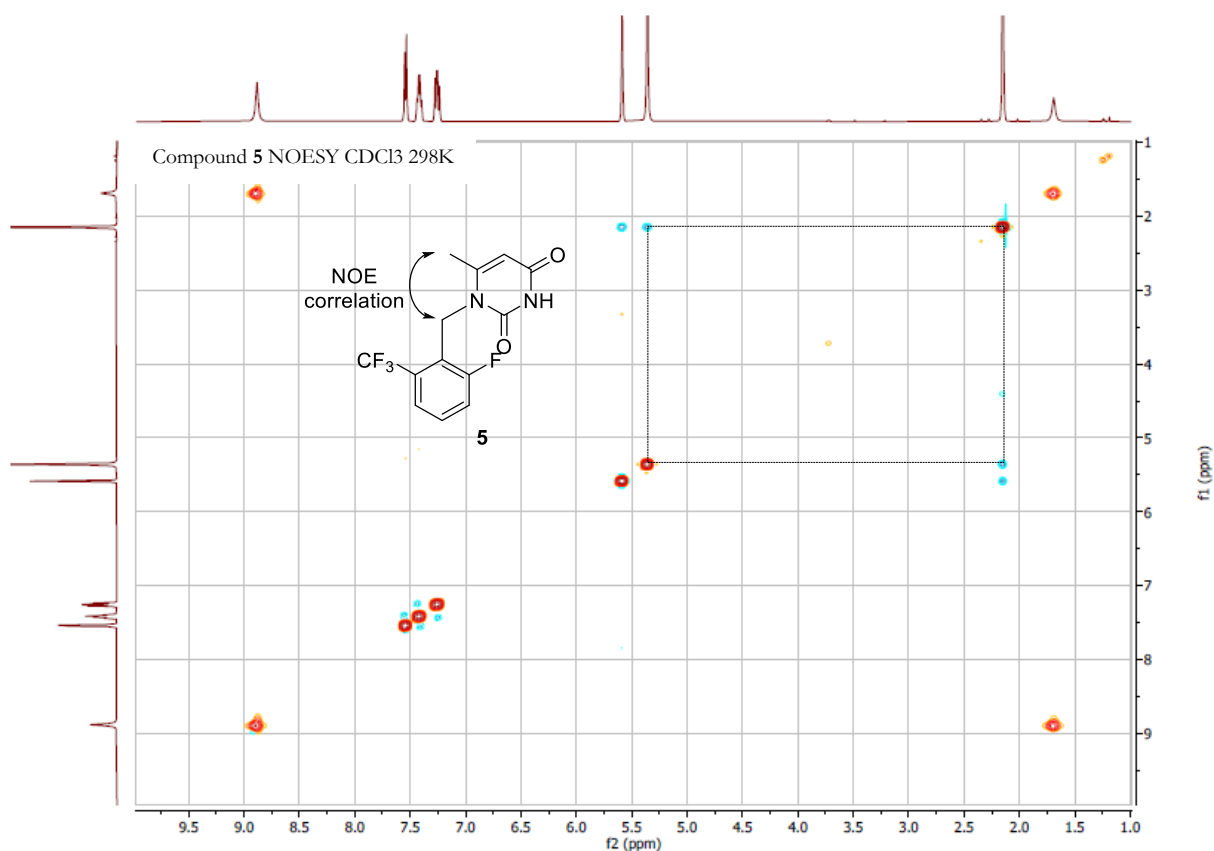
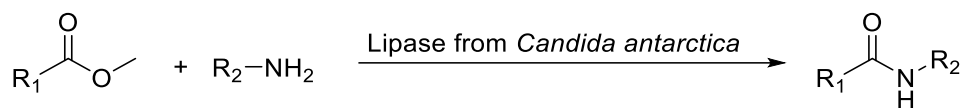


**Figure 17.** NOESY NMR experiment of compound **17**.

Since ethyl acetoacetate is cheaper than *tert*-butyl acetoacetate, we try the use of hydrolases, already used to catalyse aminolysis and Biginelli reactions [161–163] (Figure 18), to increase the regioselectivity of the reaction between ethyl acetoacetate and the urea analogue **16**.



Aminolysis



Biginelli reaction

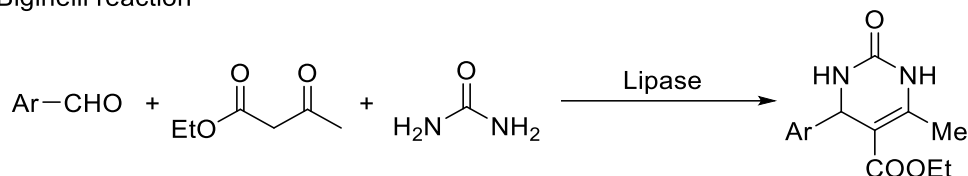


**Figure 18.** Aminolysis and Biginelli reaction catalyzed by hydrolases.

We tested different commercially available enzymes (namely, protease from *Aspergillus sojae* type XIX, *Pseudomonas fluorescens* lipase, lipase A from *Candida antarctica* Immobead 150, lipase B from *Candida antarctica* Novozymes, and lipase from *Candida rugosa*) in various solvents (*tert*-BuOH, DMF, DMSO, THF, 1,4-dioxane) at room temperature. Unfortunately, the high polar solvents needed to dissolve the urea analogue denatured enzymes. So, the use of *tert*-butyl acetoacetate remained the best approach in this synthetic step. Following the method described in the literature [96,154], bromination at the 5-position of the uracil moiety was carried out using 2 equivalents of bromine in glacial acetic acid. In our experiments, this reaction conditions gave **18** in low yield (43%) due to the formation of by-products. To optimize this synthetic step, we initially explored the use of 1.2 equivalents of *N*-bromosuccinimide (NBS) in THF. In this case, we were able to obtain quantitatively the desired product **18**, but its purification was only possible with a chromatographic process (72% isolated yield). Therefore, optimization of the reaction with bromine in acetic acid, the only one that can avoid chromatographic purification, was pursued. The most favourable conditions identified, which also proved to be effective on 10g scale, involved slowly addition of a solution of 1.1 M solution of bromine (1.1 eq) in glacial acetic acid to a 0.25 M solution of **17** in glacial acetic acid. At the end of reaction, the excess of bromine was removed from the solution by nitrogen bubbling, resulting in an almost colourless solution. This acetic acid solution was concentrated under reduced pressure, yielding a light-yellow solid. The solid was then suspended in *tert*-butyl-methyl ether, stirred for 30 minutes, filtered, and dried, ultimately providing the desired intermediate **18** in high yield (96%). The next reaction was a Mitsunobu reaction which led to the formation of a new C-N bond starting from **18** and **23**. The

main drawback of this kind of reaction is the formation of by-products, such as triphenylphosphine oxide and *tert*-butyl hydrazine dicarboxylate (Figure 19).

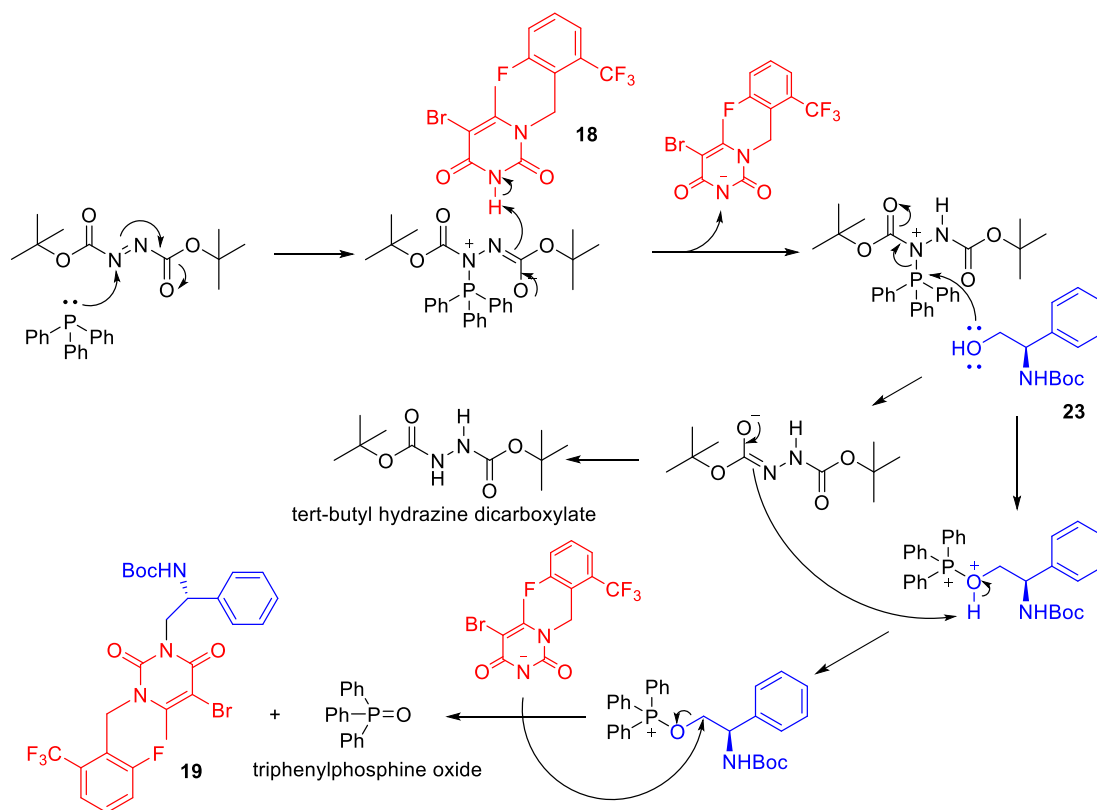


**Figure 19.** Mechanism of the Mitsunobu reaction between **18** and (*R*)-*N*-Boc-phenylglycinol.

Triphenylphosphine oxide can be easily removed by chromatographic purification on silica gel. However, *tert*-butyl hydrazine dicarboxylate co-eluted with the desired product **19** during this process. Our attempts to remove this associated by-product through a second round of chromatographic purification on silica gel proved unsuccessful. Considering that even in the reported literature procedure [96,154], intermediate **19** was utilized in its crude form in the next step, we opted to proceed in the same way. The subsequent Suzuki coupling reaction resulted in the formation of the *N*-Boc derivative of compound **20**, a product with greater polarity than the starting material, allowing successful purification through silica gel chromatography (achieving an overall yield of 77% from **18**). Significantly, this purification step also effectively eliminated the *tert*-butyl hydrazine dicarboxylate formed during the Mitsunobu reaction. The Boc protective group was removed by treatment with a 1:1 mixture of CH<sub>2</sub>Cl<sub>2</sub> and trifluoroacetic acid (TFA) at room temperature (95 % yield). The obtained free amine **20** underwent *N*-alkylation with ethyl 4-bromobutyrate in

acetonitrile, utilizing di-isopropyl ethyl amine (DIPEA) as base. After a chromatographic purification, which was necessary to separate the dialkylation product and unreacted ethyl 4-bromobutyrate, we obtained the desired intermediate **21** in 52% yield. Subsequent hydrolysis of the ethyl ester group with a sodium hydroxide THF/H<sub>2</sub>O solution, followed by acidification with citric acid and extraction with ethyl acetate, furnished the corresponding carboxylic acid **22** in almost quantitative yield (98%). The transformation of elagolix (**22**) into its sodium salt (**1**) was initially carried out using the same method reported in the literature [96,154]. This was achieved by using the Dowex Marathon<sup>TM</sup> MSC strong ion exchange resin, which had been activated employing a 1M NaCl aqueous solution. Thus, compound **22** was dissolved into a 1:1 mixture of MeOH/H<sub>2</sub>O, passed through a ion exchange resin column, by elution with water. The eluted fractions, displaying an acidic pH (pH= 4), were analysed by NMR spectroscopy: this showed that the carboxylic acids remained unchanged. For this reason, we switched to a weaker cation-exchange resin, specifically Lewatit CNP80. This resin was activated in its sodium form using 1M NaOH in a glass column until a basic pH was detected in the output flow. After activation, the resin was washed multiple times with distilled water to reach a neutral pH. Compound **22** was loaded and eluted as previously described. We collected the fractions based on their pH values, starting when the eluates reached a basic pH (around 8-9) and stopping when the pH value returned to 7. Freeze-drying of the collected eluates furnished **1** in 76% yield. This initial synthetic approach allowed us to generate the first batch of **1** (2 g) with 20% overall yield. However, to address some issues, it was necessary to make further improvements. Above all, the HPLC purity of **1** was not satisfactory (85.9%: Figure 20) and this hindered the ability to perform biological and physicochemical analyses.

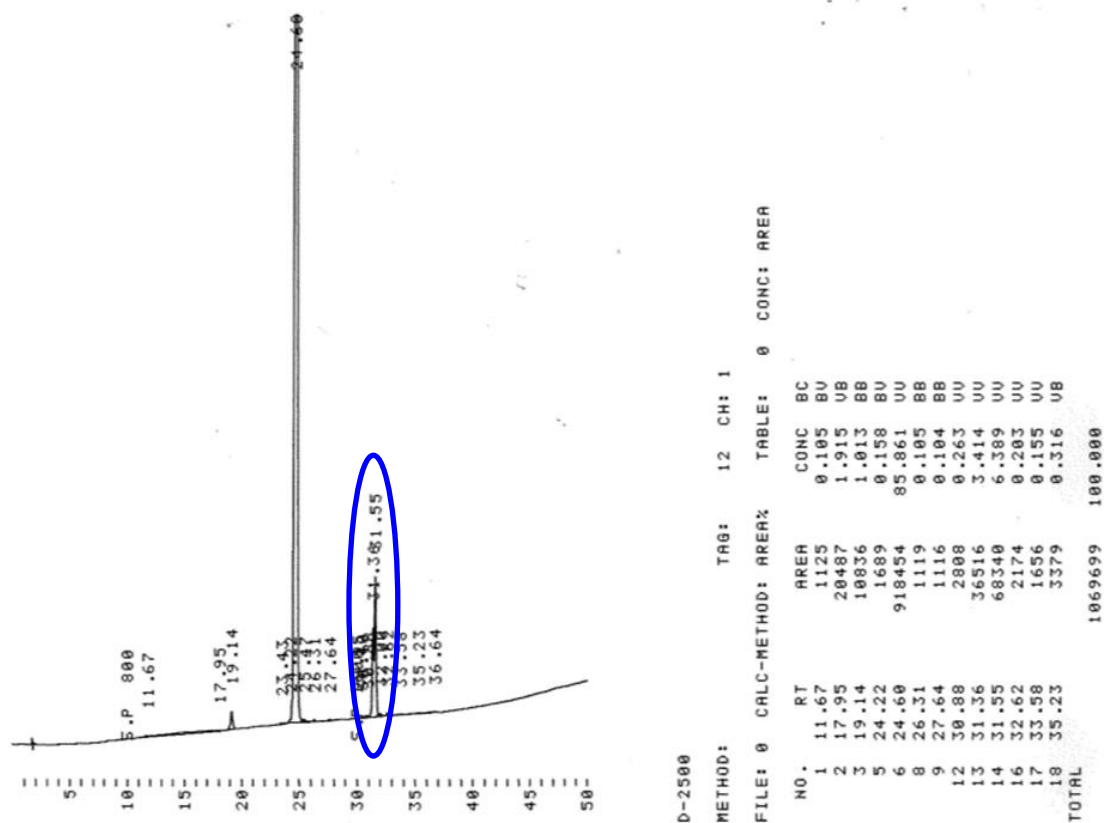


**Figure 20.** HPLC analysis of the first obtained sample of **1**.

Furthermore, in consideration of the synthesis of elagolix analogues, it would be advantageous to establish a more direct synthetic pathway that avoids the generation of the observed impurities, indicated in blue in Figure 20. To address this, we isolated these impurities through chromatographic purification and carried out their NMR characterization. These analyses revealed that these two peaks corresponded to the lactam derivative **24** (constituted by a mixture of two diastereo-atropisomers), as showed in Figure 21.

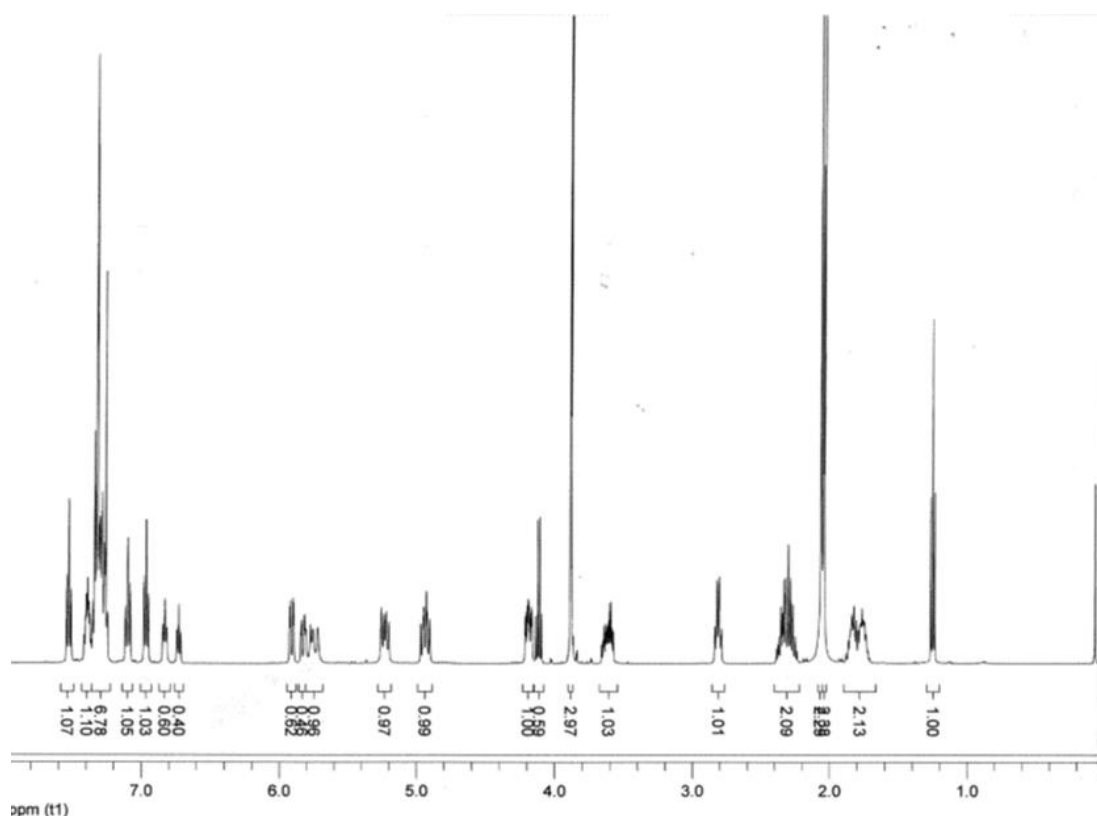


**Figure 21.**  $^1\text{H}$  NMR analysis (500 MHz,  $\text{CDCl}_3$ ) of the isolated lactam derivative **24**.

It is likely that the acidic conditions, involving citric acid, employed for the isolation of compound **22** catalyse the cyclization process between the carboxylic and amine groups, resulting in the formation of the lactam **24**, as illustrated in Figure 22.

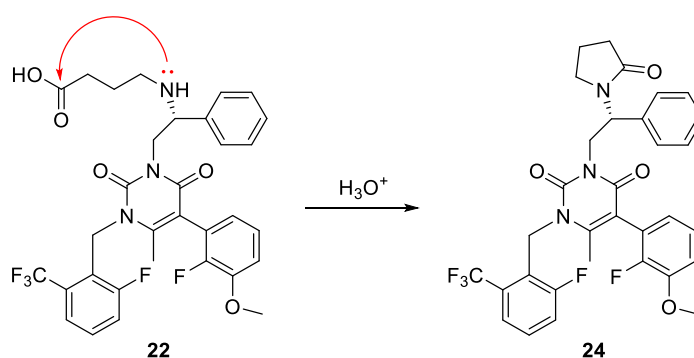


**Figure 22.** Schematic representation of the reaction yielding to the lactam derivative **24**.

Furthermore, we observed that storing compound **22** in a dichloromethane or acetonitrile solution, at room temperature, leads to a gradual rise in the amount of compound **24** over time.

The chromatographic purifications, the ion-exchange resin and the problems arising from the formation of the lactam impurity **24** were all overcome carrying out a

combination of the methods described in two patents [157,159]. In particular we preferred to retain the use of intermediate **18** in the synthesis of **1**, instead of its iodo-analog described in the 2009 patent [159], to avoid the use of the highly toxic and expensive reagent iodine monochloride.

It was possible to avoid the formation of the impurity **24** by hydrolyzing the ethyl ester **21** in an aqueous-methanolic NaOH solution, followed by the extraction of the formed **1** directly from the basic aqueous solution by means of methyl isobutyl ketone. The compound **1** was then isolated by adding dropwise the methyl isobutyl ketone solution to heptane under vigorously stirring. The obtained white precipitate was collected by suction and dried. Following this procedure, by HPLC and NMR analysis of **1**, the formation of lactam **24** was not observed, and the ion exchange resin was also no longer required.

Regarding chromatographic purifications, we eliminated them by reordering the sequence of the synthetic steps and their corresponding work-up.

Following the experimental protocol outlined in the 2018 patent [157], the Suzuki reaction was directly conducted on intermediate **18**. We employed bis(tri-*tert*-butylphosphine)-palladium(0) as the catalyst, as depicted in Figure 23.

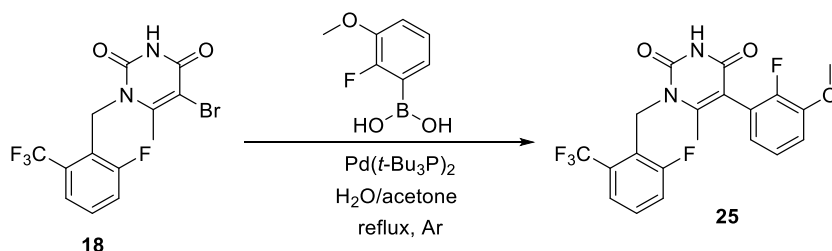


**Figure 23.** Suzuki reaction reported in the 2018 patent [157].

The catalyst was generated in situ by utilizing two air-stable compounds: Pd(OAc)<sub>2</sub>, serving as the source of palladium, and [(*t*-Bu)<sub>3</sub>PH]BF<sub>4</sub>, which acted as the source of the ligand [(*t*-Bu)<sub>3</sub>P]. The primary benefits of these experimental conditions included the reduced catalyst amount (0.5% molar, as opposed to the 10% of previously used tetrakis(triphenylphosphine)-palladium(0)) and the possibility of easily recovering product **25** by precipitating it through the addition of acetic acid to the reaction mixture. The incorporation of the *N*-Boc-(*R*)-phenylglycinol moiety was achieved by substituting the Mitsunobu reaction with a nucleophilic substitution, disclosed in the 2009 patent [159], between intermediate **25** and (*R*)-2-((*tert*-

butoxycarbonyl)amino)-2-phenylethyl methanesulfonate (**26**) (Figure 24). This reaction successfully afforded the desired compound **27** in 81% yield. Furthermore, we explored the utilization of iodine as an alternative leaving group, obtaining compound **27** in 86% molar yield (Figure 24). Regrettably, the synthesis of the necessary reagent *tert*-butyl-(*R*)-(2-iodo-1-phenylethyl)carbamate (**28**), achieved through the reaction of **23** with iodine in the presence of triphenylphosphine, necessitated a chromatographic purification step for the removal of the generated triphenylphosphine oxide, step not required employing the mesylate derivative **26**.

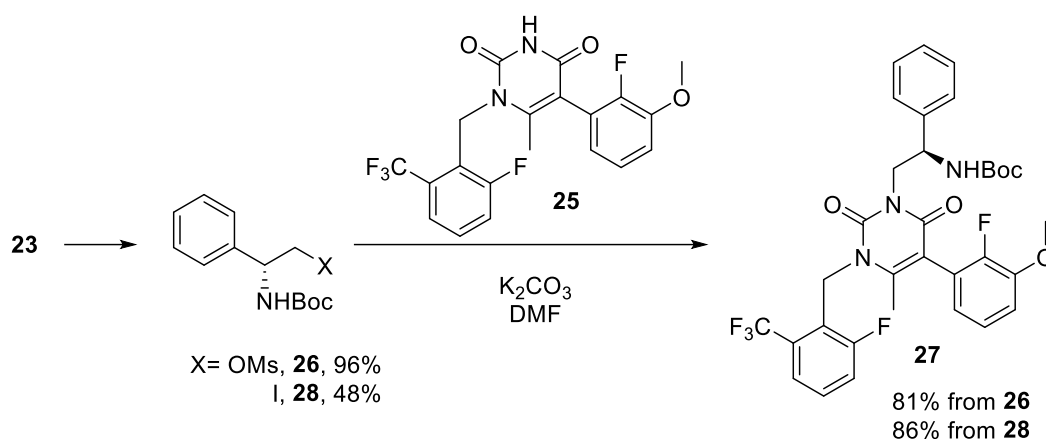


**Figure 24.** Synthesis of **27** through nucleophilic substitution.

Rather than isolating compound **27**, we opted to deprotect it *in situ* using methanesulfonic acid and purify the obtained free amine **20** with a sequence of acid-base work-up involving an aqueous phosphoric acid solution and subsequently an aqueous potassium carbonate solution. This process afforded **20** as a white foam in 81% yield and high HPLC purity (97.7%). Subsequently, compound **20** was condensed with ethyl-4-bromobutyrate in dimethylformamide (DMF), employing *N,N*-diisopropylethylamine (DIPEA) as a base, to obtain **21**. Similarly, to the previous synthetic attempt, this reaction resulted in a complex mixture with the formation of several by-products (Figure 25). We examined the acid-base extraction procedures outlined in the 2009 patent [159], involving an aqueous phosphoric acid solution and then an aqueous potassium carbonate solution, and confirmed, through a TLC analysis, that this treatment effectively purified product **21** (Figure 25).

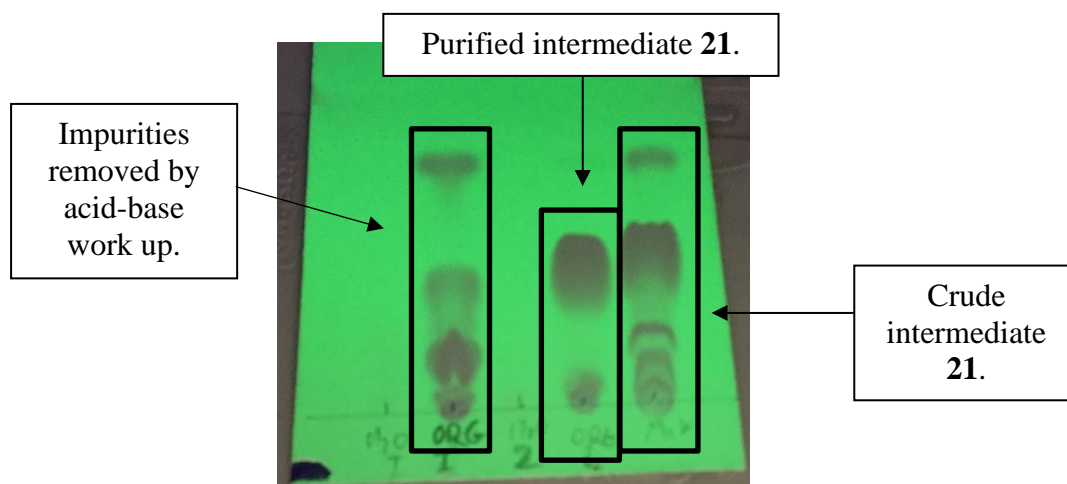


**Figure 25.** TLC analysis of intermediate **21** after and before the series of acid-base work-up.

Intermediate **21** was successfully further purified by means of a filtration over a silica gel pad, eluting with a 1:1 mixture of hexane and ethyl acetate. This procedure resulted in the isolation of **21** in 50% yield and high HPLC purity (98.8%).

All the previous reported improvements enabled us to achieve **1** in 21% overall yields and with the HPLC purity ( $\geq 99.9\%$ ) required for the biological tests and for the physico-chemical characterization. Moreover, the improved synthetic pathway (Figure 26) is also suitable, as reported in sections 4.2, 5.2, and 6.1, for the synthesis of new analogues.

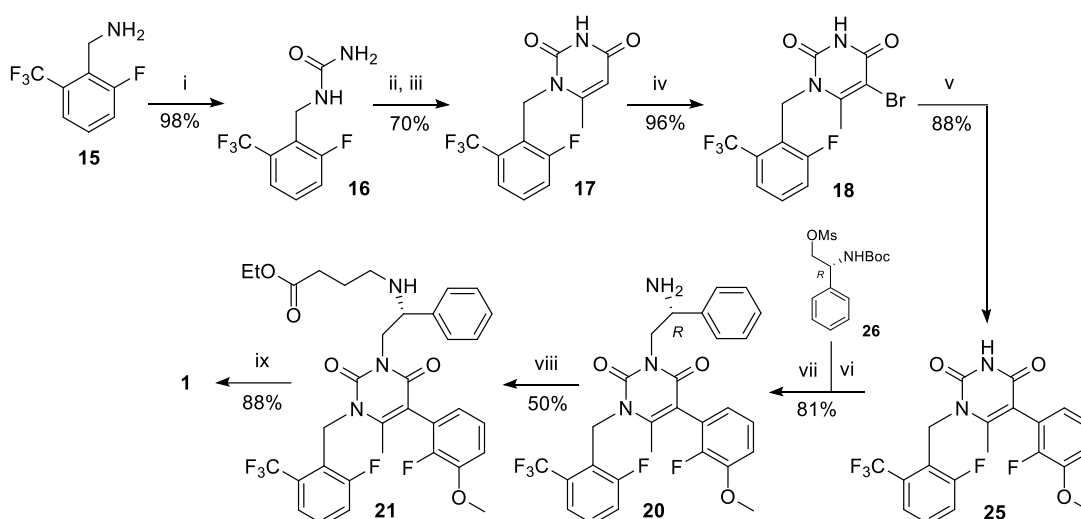


**Figure 26.** Improved synthetic approach to the synthesis of **1**. Reagents and conditions: (i) urea, HCl, H<sub>2</sub>O, reflux; (ii) *tert*-butyl acetoacetate, toluene, reflux, Dean-Stark apparatus; (iii) *p*-TsOH·H<sub>2</sub>O, reflux; (iv) Br<sub>2</sub>, acetic acid, rt; (v) 2-fluoro-3-methoxyphenylboronic acid, Pd(OAc)<sub>2</sub>, [(*t*-Bu)<sub>3</sub>PH]BF<sub>4</sub>, KOH, H<sub>2</sub>O, acetone, under argon atmosphere, reflux; (vi) K<sub>2</sub>CO<sub>3</sub>, DMF, 55 °C; (vii) MsOH, 60 °C; (viii) ethyl 4-bromobutyrate, DIPEA, DMF, 60 °C; (ix) NaOH, H<sub>2</sub>O, ethanol, rt.





spectra, as well as gradient selected (gs)-COSY and NOESY experiments. In cases where assignments were ambiguous, gs-HSQC and gs-HMBC spectra were employed as definitive and unequivocal tools for specific assignments, particularly for quaternary carbons. For attributing  $^{13}\text{C}$  NMR resonances, the analysis of  $^nJ_{13\text{C}-19\text{F}}$  couplings [165] was found useful in some cases, despite the increased spectrum complexity introduced.

**Table 4.**  $^1\text{H}$  NMR chemical shifts (ppm)<sup>a</sup> and coupling constants (Hz)<sup>b</sup> of **17**, **18**, **25**, **20**, **21**, and **1**.

| $^1\text{H}$ | <b>17</b>                           | <b>18</b>                                | <b>25</b>                           | <b>20</b>  | <b>21</b>   | <b>1</b>                                     |
|--------------|-------------------------------------|--|-------------------------------------|--|---|--|
| 1            | /                                   | /  | /                                   | /  | /   | /  |
| 2            | /                                   | /  | /                                   | /  | /   | /  |
| 3            | 8.97 (brs)                          | Exchanged with<br>$\text{CD}_3\text{OD}$ | 8.52 (brs)                          | /  | /   | /  |
| 4            | /                                   | /  | /                                   | /  | /   | /  |
| 5            | 5.59 (s)                            | /  | /                                   | /  | /   | /  |
| 6            | /                                   | /  | /                                   | /  | /   | /  |
| 7            | 5.36 (s)                            | 5.38 (s)                                 | 5.47 (s)                            | 5.50 (m)   | 5.47 (m)  | 5.43 (m)                                     |
| 8            | /                                   | /  | /                                   | /  | /   | /  |
| 9            | /                                   | /  | /                                   | /  | /   | /  |
| 10           | 7.25 (dd, $J = 12.3$<br>and 8.5 Hz) | 7.20 (dd, $J = 11.7$<br>and 8.3 Hz)      | 7.28 (dd, $J = 11.8$<br>and 8.3 Hz) | 7.26 (m,<br>overlapped with<br>28)   | 7.29 (m,<br>overlapped with<br>28)  | 7.44 (m)                                     |
| 11           | 7.42 (m)                            | 7.37 (m)                                 | 7.42 (m)                            | 7.41 (m,<br>overlapped with<br>26 and 26')   | 7.41 (m)  | 7.53 (td, $J = 8.1, 5.0$<br>Hz)              |
| 12           | 7.54 (d, $J = 7.9$ Hz)              | 7.48 (d, $J = 7.8$ Hz)                   | 7.54 (d, $J = 7.9$ Hz)              | 7.55 (d, $J = 7.9$ Hz)   | 7.54 (d, $J = 7.9$ Hz)  | 7.62 (d, $J = 7.9$ Hz)                       |
| 13           | /                                   | /  | /                                   | /  | /   | /  |
| 14           | /                                   | /  | /                                   | /  | /   | /  |
| 15           | 2.15 (s)                            | 2.35 (s)                                 | 2.05 (s)                            | 2.07 (s)   | 2.07 and 2.06 *   | 2.085 (s) and 2.076<br>(s) *                 |
| 16           | /                                   | /  | /                                   | /  | /   | /  |
| 17           | /                                   | /  | /                                   | /  | /   | /  |
| 18           | /                                   | /  | /                                   | /  | /   | /  |
| 19           | /                                   | /  | 6.97 (m)                            | 6.97 (td, $J = 8.2$ and<br>1.3 Hz)   | 6.97 (tt, $J = 8.1$ and<br>1.6 Hz)  | 7.10 (nd,<br>overlapped with<br>20)          |
| 20           | /                                   | /  | 7.10 (dd, $J = 9.0$<br>and 7.9 Hz)  | 7.11 (tdd, $J = 8.0,$<br>2.8, and 1.3 Hz)  | 7.11 (tdd, $J = 8.0,$<br>4.6, and 1.3 Hz)   | 7.11 and 7.14 (nd,<br>overlapped with<br>19) |
| 21           | /                                   | /  | 6.81 (m)                            | 6.85 (td, $J = 6.2$ and<br>1.5 Hz) and 6.78<br>(td, $J = 6.2$ and 1.4<br>Hz)*                | 6.83 (ddd, $J = 7.7,$<br>6.0, and 1.6 Hz)<br>and 6.76 (ddd, $J =$<br>7.7, 6.0, and 1.6<br>Hz) * | 6.76 (m) and 6.61<br>(m) *                   |
| 22           | /                                   | /  | 3.88 (s)                            | 3.89 (s)   | 3.889 (s) and 3.886<br>(s) *  | 3.883 (s) and 3.880<br>(s) *                 |
| 23           | /                                   | /  | /                                   | 4.29 (m o ddd, $J =$<br>16.2, 13.1, 9.8 Hz,<br>$\text{H}_a$ ) and 4.11 (m,<br>$\text{H}_b$ ) | 4.28 (m, $\text{H}_a$ ) and<br>4.04(m, $\text{H}_b$ )   | 4.26–4.07 (m)                                |

|                                 |   |   |   |                                    |  |  |
|---------------------------------|---|---|---|------------------------------------|--|--|
| 24                              | / | / | / | 4.42 (dd, $J = 9.8$<br>and 4.5 Hz) | 4.12 (m)   | 4.11 (nd)  |
| 25                              | / | / | / | /                                  | /  | /  |
| 26 and 26'                      | / | / | / | 7.41 (m,<br>overlapped with<br>11) | 7.37 (m)   | 7.29 (nd,<br>overlapped with<br>28)                        |
| 27 and 27'                      | / | / | / | 7.32 (m)                           | 7.30 (m,<br>overlapped with<br>10)                         | 7.27 (nd,<br>overlapped with<br>26 and 26')                |
| 28                              | / | / | / | 7.27 (m,<br>overlapped with<br>10) | 7.24 (m)   | 7.22 (m)   |
| 29                              | / | / | / | 2.13                               | 1.63 (brs)   | /  |
| 30                              | / | / | / | /                                  | 2.46 (m, H <sub>a</sub> ) and<br>2.38 (m, H <sub>b</sub> ) | 2.40 (m)   |
| 31                              | / | / | / | /                                  | 1.68 (m)   | 1.75 (m, H <sub>a</sub> ) and<br>1.68 (m, H <sub>b</sub> ) |
| 32                              | / | / | / | /                                  | 2.29 (m)   | 2.09 (m,<br>overlapped with<br>15)                         |
| 33                              | / | / | / | /                                  | /  | /  |
| CH <sub>2</sub> CH <sub>3</sub> | / | / | / | /                                  | 4.084 (q, $J = 7.1$ Hz,<br>and 4.082 (q, $J =$<br>7.1Hz) * | /  |
| CH <sub>2</sub> CH <sub>3</sub> | / | / | / | /                                  | 1.21 (t, $J = 7.1$ Hz)                                     | /  |

nd =  $J(\text{H,H})$  were not determined due to the overlapping. <sup>a</sup> Assignments from <sup>1</sup>H-<sup>1</sup>H COSY, HSQC, and HMBC data in CDCl<sub>3</sub> (**17**, **25**, **20**, and **21**), CD<sub>3</sub>OD (**1**), and CDCl<sub>3</sub>/CD<sub>3</sub>OD 9:1 mixture (**18**) at 298K. <sup>b</sup> Coupling constants were obtained by direct inspection of the spectra. Experimental error in the measured <sup>1</sup>H-<sup>1</sup>H couplings was  $\pm 0.5$  Hz. \* The two signals are due to the presence of two atropisomers.

**Table 5.** <sup>13</sup>C NMR chemical shifts (ppm) <sup>a</sup> and <sup>13</sup>C-<sup>19</sup>F coupling constants (Hz) <sup>b</sup> data of **17**, **18**, **25**, **20**, **21**, and **1**.

| <sup>13</sup> C | <b>17</b>                    | <b>18</b>                    | <b>25</b>                    | <b>20</b>                    | <b>21</b>                    | <b>1</b>  |
|-----------------|------------------------------|------------------------------|------------------------------|------------------------------|------------------------------|---|
| 1               | /                            | /                            | /                            | /                            | /                            | /   |
| 2               | 151.7                        | 150.8                        | 151.0                        | 152.3                        | 152.3 and 152.2 *            | 153.3 and 153.2 *   |
| 3               | /                            | /                            | /                            | /                            | /                            | /   |
| 4               | 162.4                        | 159.6                        | 161.2                        | 161.8 and 161.6 *            | 161.7 and 161.6 *            | 163.5 and 163.3 *   |
| 5               | 102.5                        | 99.2                         | 108.8                        | 108.3 and 108.2 *            | 108.3 and 108.2 *            | 109.3 and 109.2 *   |
| 6               | 153.6                        | 151.6                        | 151.9                        | 149.9 and 149.8 *            | 149.7 and 149.6 *            | 152.6 and 152.5 *   |
| 7               | 41.1 (m)                     | 42.5 (m)                     | 41.8 (m)                     | 42.7 (brs)                   | 42.7 (brs)                   | 44.1 (brs)  |
| 8               | 121.8 (d, $J = 11.6$<br>Hz)  | 121.2 (d, $J = 11.3$<br>Hz)  | 121.8 (d, $J = 11.1$<br>Hz)  | 122.0 (d, $J = 11.4$<br>Hz)  | 122.1 (d, $J = 11.3$<br>Hz)  | 123.6 (overlapped<br>with 12 and 16)                            |
| 9               | 161.4 (d, $J = 250.0$<br>Hz) | 161.1 (d, $J = 249.6$<br>Hz) | 161.4 (d, $J = 250.0$<br>Hz) | 161.3 (d, $J = 249.5$<br>Hz) | 161.3 (d, $J = 250.0$<br>Hz) | 162.8 (d, $J = 248.0$<br>Hz)                                    |
| 10              | 120.9 (d, $J = 24.0$<br>Hz)  | 120.9 (d, $J = 24.0$<br>Hz)  | 121.0 (d, $J = 24.4$<br>Hz)  | 120.9 (d, $J = 24.1$<br>Hz)  | 120.9 (d, $J = 24.4$<br>Hz)  | 122.15 (d, $J = 24.3$<br>Hz) and 122.19 (d,<br>$J = 24.3$ Hz) * |
| 11              | 129.5 (d, $J = 10.0$<br>Hz)  | 129.6 (d, $J = 9.7$<br>Hz)   | 129.5 (d, $J = 9.8$<br>Hz)   | 129.3 (d, $J = 9.8$<br>Hz)   | 129.3 (d, $J = 9.6$<br>Hz)   | 130.9 and 130.8 *   |
| 12              | 122.6 (m)                    | 122.5 (m)                    | 122.6 (m)                    | 122.6 (m)                    | 122.5 (m)                    | 123.7 (overlapped<br>with 8 and 16)                             |

|                                 |   |                                    |                                    |  |   |                                    |
|---------------------------------|---|------------------------------------|------------------------------------|--|---|------------------------------------|
| 13                              | 129.6 (dd, $J = 30.0$ and 3.6 Hz; partially hidden by 11) | 129.3 (dd, $J = 30.9$ and 3.7 Hz)  | 129.6 (dd, $J = 30.9$ and 4.0 Hz)  | 129.5 (dd, $J = 31.0$ and 3.1, partially overlapped with 11) | 129.3 (dd, $J = 30.2$ and 3.0 Hz)                       | 130.6 (dd, $J = 31.1$ and 3.3 Hz)  |
| 14                              | 123.4 (dd, $J = 273.6$ and 4.0 Hz)                        | 123.3 (dd, $J = 274.3$ and 4.2 Hz) | 123.5 (dd, $J = 273.8$ and 3.9 Hz) | 123.5 (dd, $J = 273.6$ and 3.8 Hz)                           | 123.5 (dd, $J = 271.1$ and 3.7 Hz)                      | 125.1 (dd, $J = 273.3$ and 3.8 Hz) |
| 15                              | 20.1  | 20.1                               | 17.9                               | 17.8   | 17.8  | 18.1                               |
| 16                              | /   | /                                  | 121.5 (d, $J = 13.6$ Hz)           | 122.3 (d, $J = 13.7$ Hz) and 122.2 (d, $J = 13.7$ Hz) *      | 122.37 (d, $J = 13.8$ Hz) and 122.35 (d, $J = 13.8$ Hz) | 123.8 (overlapped with 8 and 12)   |
| 17                              | /   | /                                  | 149.9 (d, $J = 246.4$ Hz)          | 150.2 (d, $J = 246.3$ Hz) and 150.1 (d, $J = 246.3$ Hz) *    | 150.23 (d, $J = 245.5$ ) and 150.17 (d, $J = 245.5$ )   | 151.8 (d, $J = 245.4$ Hz)          |
| 18                              | /   | /                                  | 148.0 (d, $J = 11.0$ Hz)           | 148.0 (d, $J = 11.0$ Hz)                                     | 148.0 (d, $J = 11.0$ Hz)                                | 149.5 (d, $J = 11.2$ Hz)           |
| 19                              | /   | /                                  | 113.5                              | 113.3  | 113.2   | 114.8                              |
| 20                              | /   | /                                  | 123.8                              | 123.8 (overlapped with 21)                                   | 123.80 (s) and 123.76 (s) *                             | 125.1 (s) and 125.0 (s) *          |
| 21                              | /   | /                                  | 123.9 (d, $J = 4.6$ Hz)            | 123.9 and 123.8 (overlapped with 20) *                       | 123.92 (s) and 123.85 (s) *                             | 125.0 and 124.9 *                  |
| 22                              | /   | /                                  | 56.3                               | 56.2   | 56.2  | 56.8                               |
| 23                              | /   | /                                  | /                                  | 49.10 and 49.14 *  | 47.7 and 47.6 *   | 48.1 and 47.9 *                    |
| 24                              | /   | /                                  | /                                  | 54.1 and 54.2 *  | 60.9 and 60.8 *   | 62.2 and 62.0 *                    |
| 25                              | /   | /                                  | /                                  | 143.7 and 143.6 *  | 141.92 (s) and 141.89 (s) *                             | 142.1 and 141.9 *                  |
| 26 and 26'                      | /   | /                                  | /                                  | 126.4 and 126.3 *  | 127.2 and 127.1 (overlapped with 28) *                  | 128.7                              |
| 27 and 27'                      | /   | /                                  | /                                  | 128.5 and 128.4 *  | 128.4 and 128.3 *                                       | 129.4                              |
| 28                              | /   | /                                  | /                                  | 127.3 and 127.2 *  | 127.2 (overlapped with 26 and 26')                      | 128.5                              |
| 29                              | /   | /                                  | /                                  | /  | /   | /                                  |
| 30                              | /   | /                                  | /                                  | /  | 46.51 (s) and 46.47 (s) *                               | 48.7                               |
| 31                              | /   | /                                  | /                                  | /  | 25.4  | 27.86 (s) and 27.83 (s) *          |
| 32                              | /   | /                                  | /                                  | /  | 32.0  | 37.03 (s) and 37.00 (s) *          |
| 33                              | /   | /                                  | /                                  | /  | 173.7   | 182.3                              |
| CH <sub>2</sub> CH <sub>3</sub> | /   | /                                  | /                                  | /  | 60.1  | /                                  |
| CH <sub>2</sub> CH <sub>3</sub> | /   | /                                  | /                                  | /  | 14.2  | /                                  |

<sup>a</sup> Assignments from HSQC and HMBC data in CDCl<sub>3</sub> (**17**, **25**, **20**, and **21**), CD<sub>3</sub>OD (**1**), and CDCl<sub>3</sub>/CD<sub>3</sub>OD 9:1 mixture (**18**) at 298K. <sup>b</sup> Coupling constants were obtained by direct inspection of the spectra. Experimental error in the measured <sup>1</sup>H-<sup>1</sup>H coupling constants was  $\pm 0.5$  Hz. \* The two signals are due to the presence of two atropisomers.

**Table 6.**  $^{15}\text{N}$  NMR chemical shifts (ppm) <sup>a</sup> of **17**, **18**, **25**, **20**, **21**, and **1**.

| $^{15}\text{N}$ | <b>17</b>          | <b>18</b>          | <b>25</b>          | <b>20</b> | <b>21</b> | <b>1</b> |
|-----------------|--------------------|--------------------|--------------------|-----------|-----------|----------|
| 1               | 136.7              | 137.9              | 134.3              | 134.3     | 135.5     | 137.1    |
| 3               | 154.3 <sup>b</sup> | 153.4 <sup>b</sup> | 151.9 <sup>b</sup> | 160.1     | 161.3     | 160.5    |
| 29              | /                  | /                  | /                  | 31.2      | 43.6      | 46.3     |

<sup>a</sup> Assignments from  $^1\text{H}$ - $^{15}\text{N}$  HMBC data in  $\text{CDCl}_3$  (**17**, **25**, **20**, and **21**),  $\text{CD}_3\text{OD}$  (**1**), and  $\text{CDCl}_3/\text{CD}_3\text{OD}$  9:1 mixture (**18**) at 298K using nitromethane as external reference (neat nitromethane = 381.7 ppm as reported in Ref. [166]). <sup>b</sup> Assignments from  $^1\text{H}$ - $^{15}\text{N}$  HSQC data in  $\text{CDCl}_3$  (**17** and **25**), and  $\text{CDCl}_3 + 3\%$  of  $\text{DMSO-d}_6$  (**18**) at 298K using ammonia as external reference (ammonia = 0.0 ppm as reported in Ref. [166]).

The assignment of proton resonances for compounds **17**, **18**, and **25** relied on general knowledge of chemical shift dispersion, coupled with the proton–proton coupling patterns and the COSY experiment for aromatic protons. Additionally, H-10 displayed an additional coupling constant ( $J_{\text{H-19F}} = 12.3$  Hz) due to the presence of fluorine at the 9-position. The correctness of the structural features of **17** was confirmed through a NOESY experiment, which distinguished between two isomers that could form under the employed reaction conditions (see section 3.1). This distinction was established by observing a cross peak between the H-15 (2.15 ppm) and the H-7 (5.36 ppm) signals in the NOESY spectrum of **17** (Figure 17) that was absent in the isomer's spectrum. Beginning with compound **20**, derived from **25** through the introduction of the (*R*)-phenylamino ethyl moiety at the 3-position of the uracil core, multiple resonances for the H-21 proton were observed (6.85 and 6.78 ppm, 6.83 and 6.76 ppm, and 6.76 and 6.61 ppm for **20**, **21**, and **1**, respectively). These signals exhibited a 1:1.07, 1:1.04, and 1:1.13 ratio (Figure 28), indicating that compounds **20**, **21**, and **1** are a mixture of two diastereo-atropisomers. The same phenomenon was also observed, though less conspicuous (distance between the two signals  $\leq 0.01$  ppm), for H-15 and H-22 signals of **21** and **1**. Furthermore, the non 1:1 ratio between the two signal sets suggests that one atropisomer is favoured over the other in solution.

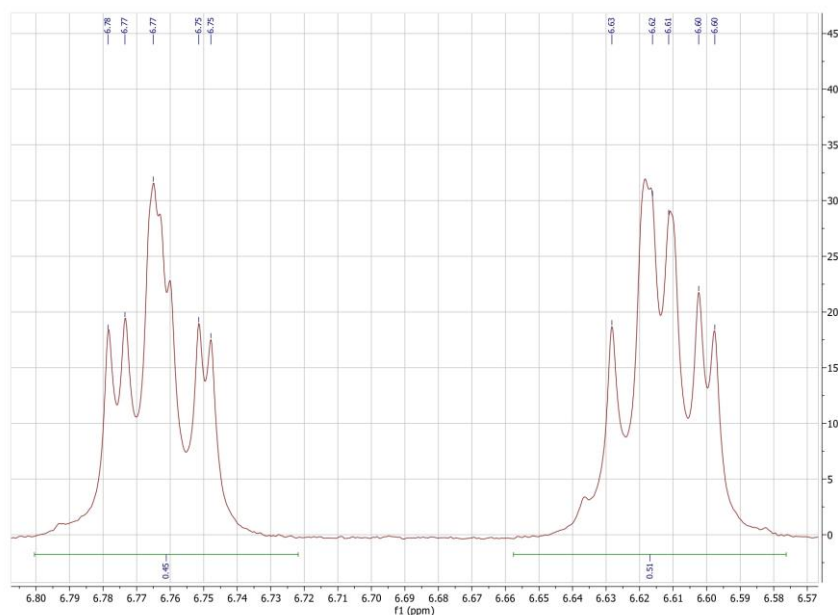


**Figure 28.** The observed two sets of signals for H-21 in the  $^1\text{H}$  NMR spectrum (500 MHz,  $\text{CD}_3\text{OD}$ ) of **1**.

NOESY experiments on **1** dissolved in  $\text{CD}_3\text{OD}$  indicated the proximity of H-15 (2.085 and 2.076 ppm) to H-21 (6.76 and 6.61 ppm) and H-7 (5.43 ppm), of H-19 (7.10 ppm) to H-22 (3.883 and 3.880 ppm), and of H-30 (2.40 ppm) to H-23 (4.26 - 4.07 ppm), H-24 (4.11 ppm), and H-26/H-26' (7.29 ppm) in both atropisomers. The assignment of  $^{13}\text{C}$  NMR resonances of CH,  $\text{CH}_2$ , and  $\text{CH}_3$  groups was corroborated using the gs-HSQC experiment. Quaternary carbon atoms were definitively assigned through the  $^1\text{H}$ - $^{13}\text{C}$  gs-HMBC experiment. In some cases, the  $^nJ_{13\text{C}-19\text{F}}$  couplings [165] were very useful for additional structural confirmation.

Due to atropisomerism, the  $^{13}\text{C}$  NMR spectra of compounds **20**, **21**, and **1** exhibited closely adjacent singlets for certain carbon atoms (Table 5). Also in this case, the intensity of  $^{13}\text{C}$  signals, although not quantitative, indicated a ratio between atropisomers other than 1:1.

To further support the proposed structures of the studied compounds,  $^1\text{H}$ - $^{15}\text{N}$  HMBC experiments were conducted. Resonances for N-1 and N-3 were assigned for all compounds, and N-29 was assigned for **20**, **21**, and **1**. The chemical shift of N-1 remained nearly constant from intermediate **17** to **1**. However, the chemical shift of N-3 changed from 154.3 (**17**), 153.4 (**18**), and 151.9 (**25**) ppm to 160.1 (**20**), 161.3 (**21**),

and 160.5 (**1**) ppm, reflecting the *N*-alkylation of this nitrogen [165]. A similar trend was observed for N-29, with a shift from 31.2 ppm for **20** (primary amine) to 43.6 and 46.3 for **21** and **1** (secondary amine), respectively. For all compounds,  $^1\text{H}$ - $^{15}\text{N}$  gs-HMBC spectra exhibited cross peaks of H-15 and H-7 with N-1. In the case of N-3 and N-29 for **20**, **21**, and **1**, cross peaks of H-24/N-3, H-23/N-29, H-24/N-29, and H-31/N-29 were also observed.

### 3.3 HPLC analysis

In addition to the NMR analysis discussed in Section 3.2, the presence of atropisomerism in elagolix was also confirmed by HPLC techniques. Indeed, the HPLC analysis of compound **1**, performed as reported in the literature [148] on a non-chiral reverse stationary phase (RP), revealed only one chromatographic peak, although rather broadened and irregular (Figure 29A). In contrast, when **1** was subjected to HPLC analysis on a chiral stationary phase (cellulose tris(3,5-dimethylphenylcarbamate)), two distinct peaks became evident (Figure 29B), corresponding to its two diastereo-atropisomers.

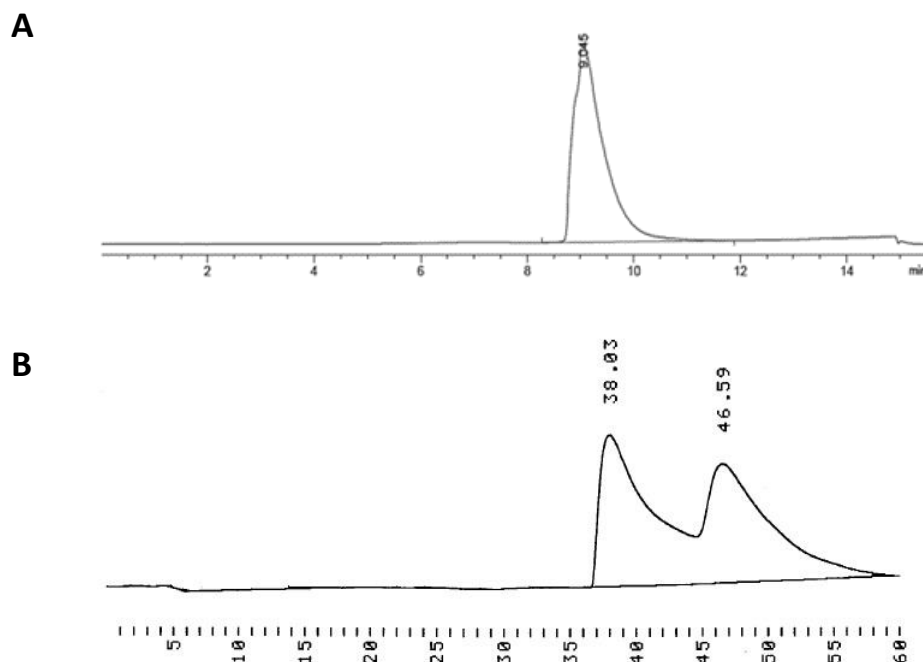


**Figure 29.** HPLC chromatogram of compound **1** on (A) a reverse stationary phase and (B) a chiral stationary phase.

The inability of a RP-HPLC analysis in showing the atropisomers of **1**, even though they are diastereoisomers, is intriguing. However, this observation is in line with the findings disclosed for its analogues reported in section 1.4.1 [151,153]. We also try to isolate the atropisomers of **1** by preparative chiral HPLC at room temperature, but without success.

In addition, given that compound **25** is the first intermediate carrying the biaryl system implicated in atropisomerism, we chose to analyze it using chiral HPLC. As depicted in Figure 30, two discernible peaks confirm the presence of two enantio-atropisomers in this compound.

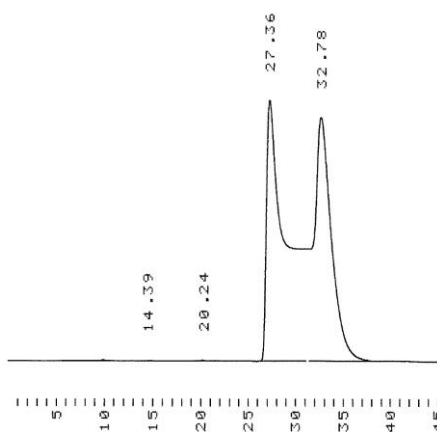


**Figure 30.** Chiral HPLC chromatogram of compound **25**.

The observed peak shape (Figure 30), characterizing on-column interconversion processes, signifies the presence of dynamic interconversion within the timeframe of the analysis [167,168].

### 3.4 X-ray crystal structure

Since Single-crystal X-ray diffraction (SC-XRD) provides precise details about the arrangement of atoms within a crystal lattice, crucial for understanding the properties and behavior of compounds, we tested the possibility of obtaining single crystals of compounds **25**, **20**, **21**, and **1**. We succeeded in this aim with compound **25**, the first synthetic intermediate bearing the crucial biaryl system of **1**, through the gradual evaporation of a methanol/water 95:5 solution over a week's time. With the other compounds, using alone or in a mixture, methanol, ethanol, 2-propanol, acetonitrile, acetone, dichloromethane, tetrahydrofuran, water, toluene, hexane,



heptane, cyclohexane, and methyl isobutyl ketone, glassy residues were obtained. This first result, which agrees with the lack of crystalline elagolix in the literature, suggests that the presence of rapid equilibrium between atropisomers (diastereomers for **20**, **21**, and **1**) could impair crystal formation [169]. The obtained crystallographic data of compound **25** were deposited to the Cambridge Crystallographic Data Center under accession number CCDC 2248213 and the refined structure, inspected using ORTEP-3 [170], is reported in Figure 31. Crystallographic data and refinement details are given in Section 9.4.

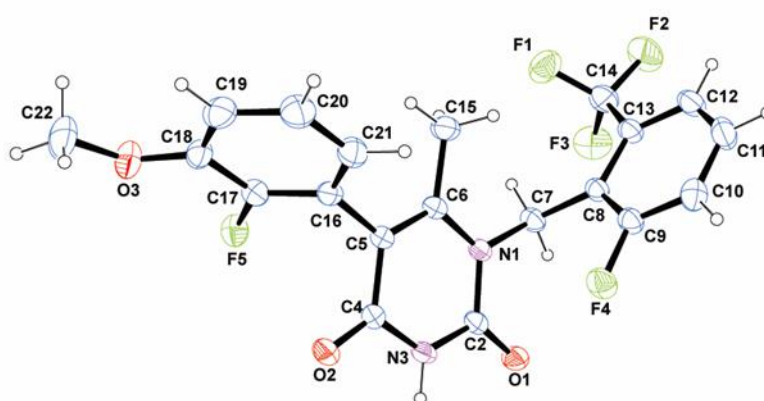


**Figure 31.** ORTEP [170] diagram of compound **25** with an arbitrary atom-numbering scheme. Thermal ellipsoids were depicted at the 40% probability level.

The obtained crystal is constituted by a racemate of the two enantio-atropisomers and the angles between the best mean plane calculated for the heterocyclic component and these two aromatic components are  $87.4(1)^\circ$  and  $67.2(1)^\circ$ . The dihydropyrimidine was near-planar, with a maximum deviation  $0.021(1)$  Å. Its conformation is defined by the dihedral angle  $C2-N1-C7-C8 - 105.3(1)^\circ$ ;  $N1-C7-C8-C13 - 144.7(3)^\circ$ ; and  $C4-C5-C16-C21 - 110.4(3)^\circ$ . These data showed that the 2-fluoro-3-methoxy phenyl ring lay in an orthogonal orientation to the uracil ring indicating a steric repulsion between the methyl, the carbonyl oxygen and fluorine, being the source of atropisomerism in this molecule.

The crystal packing, shown in Figure 32, was consolidated by strong dimeric H-bonds involving  $N3-H \cdots O1^I$  ( $I$  at  $1-x, -y, -z$ ); the donor-acceptor ( $D \cdots A$ ) distance is  $2.87(1)$  Å, the hydrogen and the acceptor ( $D-H \cdots A$ ) are at  $2.063(2)$  Å, and the angle is  $155.2(5)^\circ$ . These H-bonds give rise to the formation of molecular chains along the a

axis. Parallel  $\pi$ - $\pi$  stacking interactions between (trifluoromethyl)benzyl moieties were present and further contributed to the crystal packing: the distance between the centroids was 3.20(6) Å, while the angle between the centroid-centroid vector and the plane normal was 3.62(4)°. Loose CH $\cdots$ O and CH $\cdots$ F contacts contributed to the stabilization of the crystal structure; these non-traditional H-bonds were established between C12-H $\cdots$ O2<sup>II</sup>, D $\cdots$ A = 3.26(8) Å, D-H $\cdots$ A = 2.63(1) Å, angle = 124.3(9)° (<sup>II</sup> at 1 + x, y, z), C11-H $\cdots$ F4<sup>III</sup>, D $\cdots$ A = 3.42(8) Å, D-H $\cdots$ A = 2.54(1) Å, angle = 163.5(9)° (<sup>III</sup> at  $\frac{1}{2}$  + x,  $\frac{1}{2}$  - y, z) and C19-H $\cdots$ F5<sup>IV</sup>, D $\cdots$ A = 3.37(8) Å, D-H $\cdots$ A = 2.48(1) Å, angle = 160.3(9)° (<sup>IV</sup> at x,  $\frac{1}{2}$  + y,  $\frac{1}{2}$  - z). The Van der Waals interactions between the aromatic rings of adjacent molecules favored a two-dimensional-sheet structure, in which the molecules in the two layers are inclined as shown in Figure 32.

The crystallization conditions of methanol + 5% of water may have facilitated the solubilization and formation of a dense network of interactions that allowed for the orderly arrangement of molecules in a crystal.

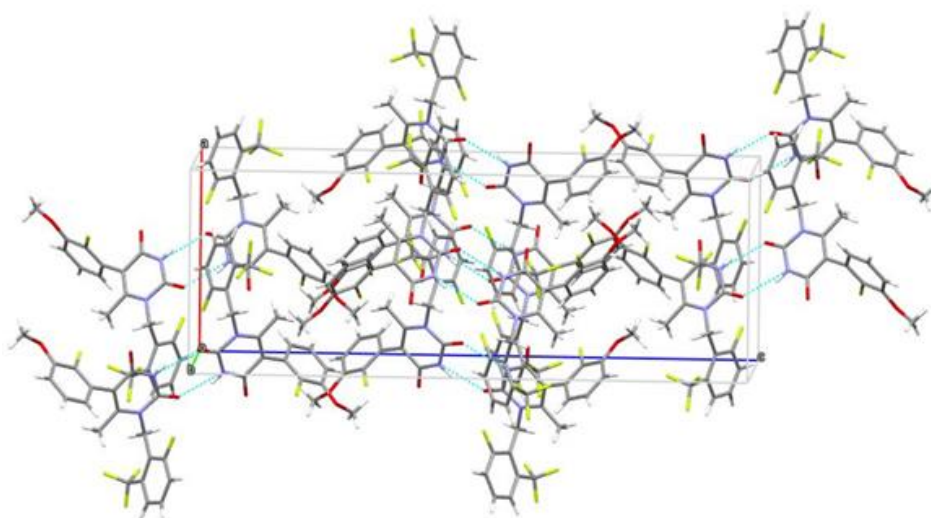


**Figure 32.** Graphical representation of the crystal packing along a axis, showing the H-bonds as dotted blue lines.

### 3.5 Conformational analysis

The observation that the <sup>1</sup>H NMR spectrum of **1**, obtained in both CD<sub>3</sub>OD and D<sub>2</sub>O, displayed a slightly unequal ratio between the two atropisomers (0.88:1.00 and 0.84:1.00 in CD<sub>3</sub>OD and D<sub>2</sub>O, respectively), prompted us to conduct a conformational analysis, using computational tools under the same NMR experimental conditions, thanks to a collaboration with Prof. G. Grazioso and Dr. E.M.A. Fassi at the

Department of Pharmaceutical Sciences, University of Milan. In summary, we simplified the structure of **1** by shortening the side chain carrying the carboxylate moiety (Figure 33) to reduce the number of dihedral angles to be examined. Subsequently, we performed the conformational analysis employing the DFT/B3LYP-D3/6-31G(\*\*) level of theory [171,172] within the Jaguar module of Maestro (release 2021-2, Schrödinger, LLC, New York, NY, USA). More details are reported in Section 9.1.2. Specifically, we focused on the critical  $\tau_5$  dihedral angle, responsible for generating the atropisomerism phenomenon, while scanning it in the lowest energy conformer of the simplified structure of **1**. We concurrently optimized the conformers at the DFT/B3LYP-D3/6-31G(\*\*) level of theory, incorporating the CPCM water solvent model [173]. The results obtained (Figure 34) indicated the presence of four distinct energy-minimum conformers (**1A**, **1B**, **1C**, **1D**). We further improved the precision of these findings by geometrically optimizing their geometries at the same level of theory. These outcomes revealed that **1B** converged into the lowest energy **1A** ( $R_a$  atropisomer of **1**), while **1C** and **1D** ( $S_a$  atropisomer of **1**) represented two other relative minimum energy conformers (Table 7). Additionally, single-point calculations utilizing the CPCM methanol solvent model (the solvent used in the NMR experiments) exhibited results consistent with those observed using the CPCM water solvent model.

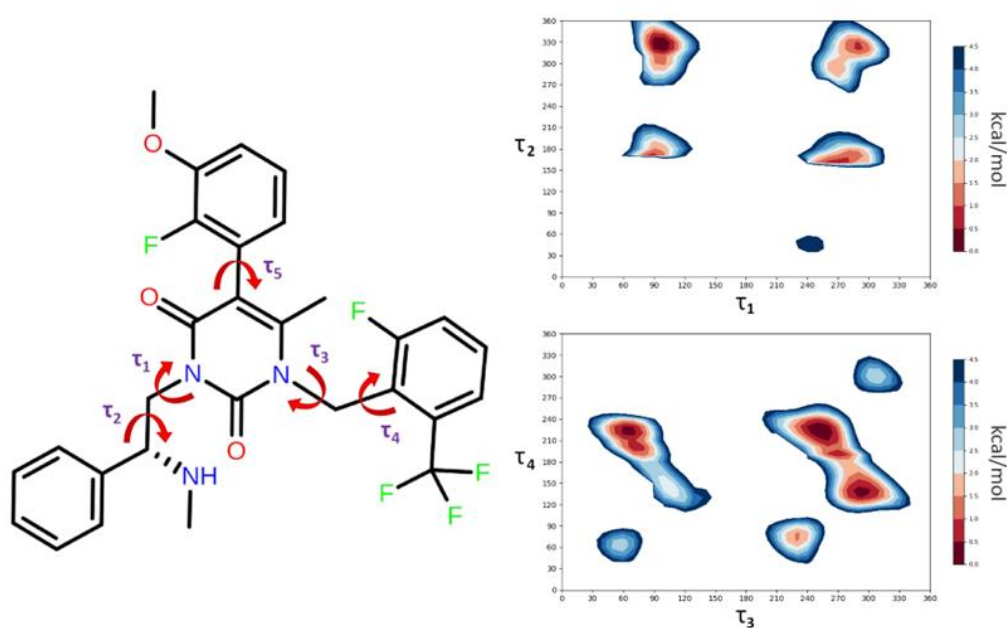


**Figure 33.** Simplified structure of **1**. The red arrows indicate the investigated torsional angles. On the right, the scan plots of the  $\tau_1$ – $\tau_4$  torsional angles are reported.

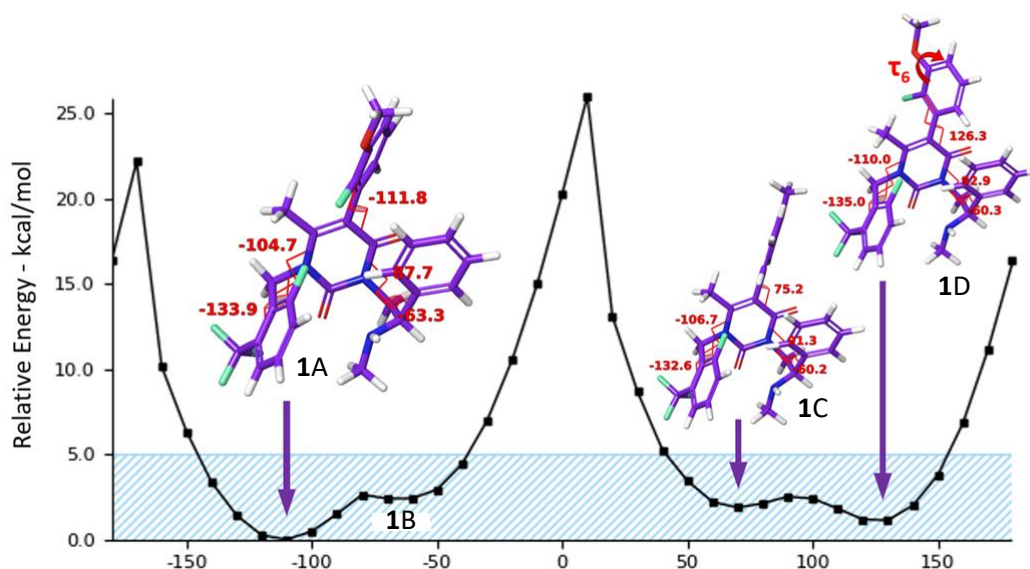


**Figure 34.** This coordinate scan plot illustrates the variation of the  $\tau_5$  torsional angle, along with the low-energy conformers derived from the data presented in Table 7.

**Table 7.** Geometrical features, relative energies and equilibrium percentages after geometry optimization of the most populated conformations of a simplified structure of **1**.

| Entry | $\tau_1$ | $\tau_2$ | $\tau_3$ | $\tau_4$ | $\tau_5$ | Water $\Delta E$<br>(kcal/mol) | Water (%) |
|-------|----------|----------|----------|----------|----------|--------------------------------|-----------|
| 1A    | 87.7°    | -63.3°   | -104.7°  | -133.9°  | -111.8°  | 0.00                           | 83.6      |
| 1C    | 91.3°    | -60.2°   | -106.7°  | -132.6°  | 75.2°    | 2.07                           | 2.6       |
| 1D    | 92.9°    | -60.3°   | -110.0°  | -135.0°  | 126.3°   | 1.06                           | 13.8      |

Thus, since the conformational study showed that, under the NMR experimental condition, the major conformer is **1A**, corresponding to **1-aR** atropisomer, we can conclude that the diagnostic H-21 (6.61 ppm), H-22 (3.880 ppm), and H-15 (2.076 ppm)  $^1\text{H}$  NMR resonances can be assigned to the most abundant atropisomer **1-R<sub>a</sub>**, while the H-21 (6.76 ppm), H-22 (3.883 ppm), and H-15 (2.085 ppm) signals to the least abundant atropisomer **1-S<sub>a</sub>**. Additionally, by examining the data presented in the energy profile of **1** (Figure 34), we can approximate its  $\Delta G^\ddagger$  to be around 22.3 kcal/mol. This outcome agrees with what has been reported in the literature ( $\Delta G^\ddagger \approx 23$  kcal/mol) for the elagolix analogue belonging to class 2 [151], discussed in the Section 1.4.1.

### 3.6 Conclusions

In summary, we successfully conducted an efficient synthesis of elagolix sodium salt (**1**) with a focus on enhancing reaction yields and purity. Moreover, this optimized synthetic pathway, as will be discussed in Chapter 4, has demonstrated its utility in the synthesis of selected analogues of **1**.

The analytical characterization of the obtained samples of **1** and of its synthetic intermediates also allowed us to fill a significant gap in the literature regarding NMR and HPLC data confirming, at the same time, that **1** exists in solution as a mixture of two diastereo-atropisomers. As observed in the SC-XRD structure of **25**, which represents the first synthetic intermediate featuring the crucial biaryl system of **1**, this phenomenon can be attributed to steric repulsion between the *ortho*-fluorine, the carbonyl oxygen, and the methyl group at the 4- and 6-positions of the uracil moiety, respectively.

Furthermore, the agreement of the NMR outcomes with the conformations located through the computational study provided insights into the stereochemical profile of the two atropisomers, **1-*R*<sub>a</sub>** and **1-*S*<sub>a</sub>**, present in solution. Finally, the estimated rotational barrier of approximately 22.3 kcal/mol confirmed that **1** belongs to the challenging atropisomeric class 2.

## Chapter 4

### Elagolix analogues modified at 4-position

---

The confirmation that elagolix (**1**) falls under the category of atropisomeric molecules, particularly class 2 (as discussed in Chapter 3), prompt us to embark on the development of new elagolix analogues. Our aim was to design analogues that do not exhibit atropisomerism of class 2. To circumvent this challenge, we have designed analogues featuring increased steric hindrance, in a manner akin to the approach taken in the development of the recently approved single-atropisomer drug sotorasib (see Section 1.4.1). A viable, not yet explored, way to achieve this goal could be the modification of the substituents at the 4- or 6-position of the uracil moiety. This modification could lead to the identification of new analogues that may remain stable as single atropisomers while also exhibiting robust pharmacological activity and/or improved pharmacokinetic properties.

In parallel, literature research for analogues of elagolix with unknown atropisomeric and biological characteristics were carried out. In this context, an elagolix derivative bearing a bromine atom at the 21-position is described as intermediate of the tritium-labelled **1**.

#### 4.1 Design

The evaluation of synthetically feasible modification at the 4-position were carried out in collaboration with Prof. G. Grazioso and Dr. E.M.A. Fassi at the Department of Pharmaceutical Sciences, University of Milan. The conformational space of a simplified system mimicking the phenyl-uracyl moiety of elagolix was explored, by scanning the dihedral angle responsible for generating the atropisomers (Figure 35) at the B3LYP/6-31g(d,p) level of quantum mechanics (QM) calculations, then refined using higher-level QM calculations (B3LYP/aug-cc-PVTZ). These calculations revealed that the rotational energy barrier ( $\Delta G^\ddagger$ ) faced by the *ortho*-fluorine atom, when it approaches the oxygen atom at the 4-position ( $F \rightleftharpoons CO$ ), was approximately 3 kcal/mol higher than that calculated for the isomerization involving proximity to the

methyl group ( $F \rightleftharpoons \text{Met}$ ). This difference primarily arose from the repulsion exerted by the two lone pairs of the oxygen atoms in contrast to the three lone pairs on fluorine. Conversely, the methyl group at the 6-position of the uracil ring presented less resistance to atropisomer conversion, as the steric clash was only offered by one of the hydrogen atoms in the methyl group. We hypothesized that a bulkier atom than the carbonyl oxygen could further impede the free rotation of the dihedral angle responsible for atropisomer interconversion. To test this hypothesis, we computationally investigated a phenyl-thiouracil simplified system (Figure 34).

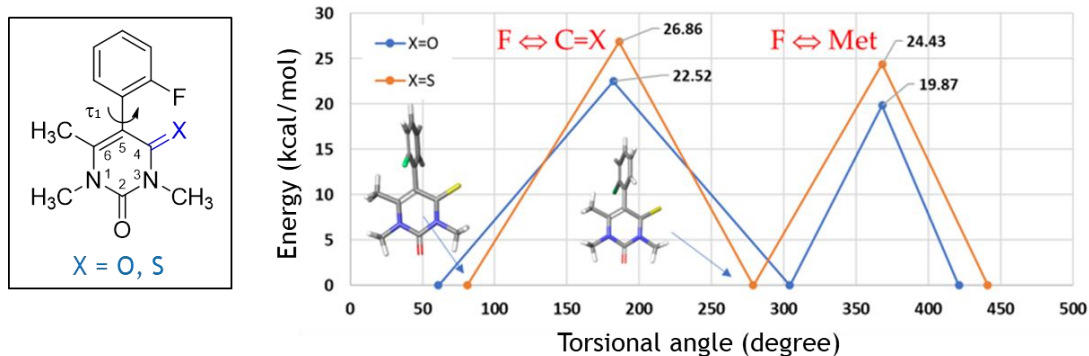


**Figure 35.** Chemical structure of the simplified system investigated by QM calculations (on the left) and potential energy profile attained scanning the  $\tau_1$  dihedral angle (on the right).

The results showed that this replacement could increase the two transition states of about 4 kcal/mol, significantly slowing down the atropisomers interconversion by the presence of the sulfur atom in the uracil moiety, potentially enabling their separation and analysis as individual atropisomers at room temperature (around +25°C).

## 4.2 Synthesis

Based on the results obtained from the preliminary QM study (see Section 4.1), we started the synthesis of the first elagolix analogue, compound **2**, in which the oxygen atom at the 4-position of the uracil moiety was replaced by the bulkier sulfur atom (Figure 36).

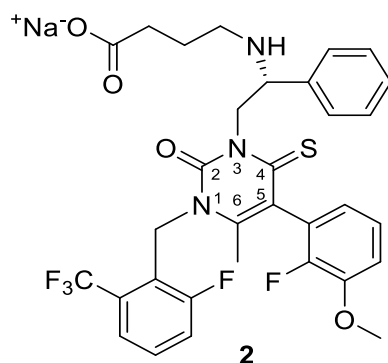


**Figure 36.** Elagolix analogue **2**.

We planned the use of Lawesson's reagent, a mild and cheap thionating agent [174] already mentioned in the literature for the conversion of 6-methyl uracil into 6-methyl 4-thiouracil (Figure 37) [175].

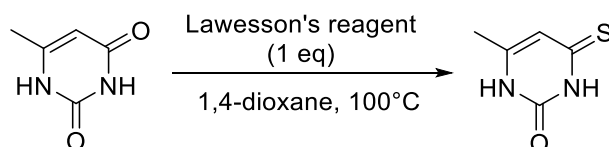


**Figure 37.** Literature reported conversion of methyl uracil in methyl thiouracil. Ref. [175].

The first attempt to synthesize compound **2** was carried out starting from **1** which was refluxed with 1 equivalent of Lawesson's reagent in 1,4-dioxane at 100°C. Instead of the desired **2**, as proved by NMR characterization, we observed the formation of its thiolactam derivative **29** (Figure 38).

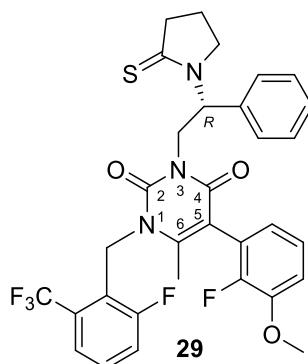


**Figure 38.** Compound **29** obtained using Lawesson's reagent on **1**.

Indeed, we observed the shift of the  $^{13}\text{C}$  NMR resonance of the carboxylic carbon of **1** from 182 to 203 ppm of compound **29**, indicating the presence of a thiolactam carbon [165]. Therefore, we worked in parallel on both *N*-Boc protected and deprotected synthetic elagolix intermediate **20** (Figure 39). Unfortunately, with 1



equivalent of Lawesson's reagent in 1,4-dioxane at 100°C, we obtained in both cases a complex mixture of products. So, we decided to carry out this reaction on intermediate **25**, which lack the carboxylic and amine groups (Figure 39). In this way, we obtained **30** in 29% yield, after chromatographic purification.

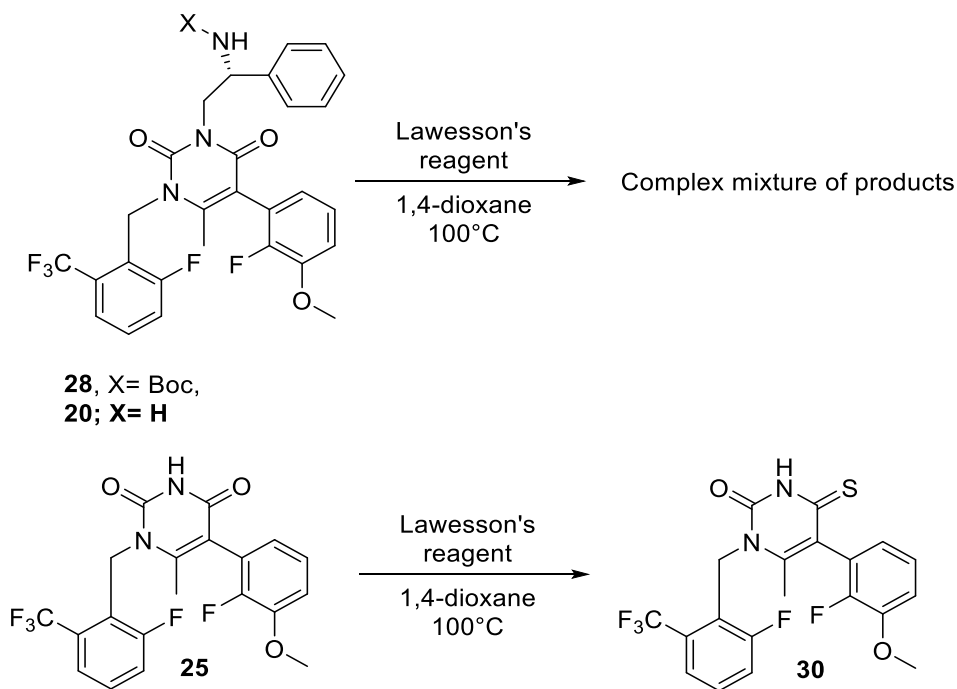


**Figure 39.** Reactions performed with the Lawesson's reagent.

The correct structure of **30** was confirmed by NMR characterization, in particular the shift of the  $^{13}\text{C}$  resonance of the carbon at the 4-position of the uracil moiety from 163 to 188 ppm for compounds **25** and **30**, respectively, indicated the replacement of the oxygen with sulfur at this position [176]. Moreover, the chiral HPLC (see Section 4.4) showed the presence of two atropisomers. Unfortunately, the stability of the two atropisomers cannot be studied due to the lability of **30**. Indeed, this intermediate, if stored in solution in presence of light and air, come back to **25** with evolution of the typical hydrogen sulfide smell. For this reason, we modified the synthetic procedure reacting the rapidly isolated **30** with *N*-Boc-D-phenylglycinol mesylate **26**, using the same conditions used for elagolix. The product was recovered, in 97% yield from **25**, after chromatographic purification. Surprisingly, the NMR characterization showed that **26** reacted with the sulfur atom of **30**, instead of the nitrogen, yielding compound **31** (Figure 40).

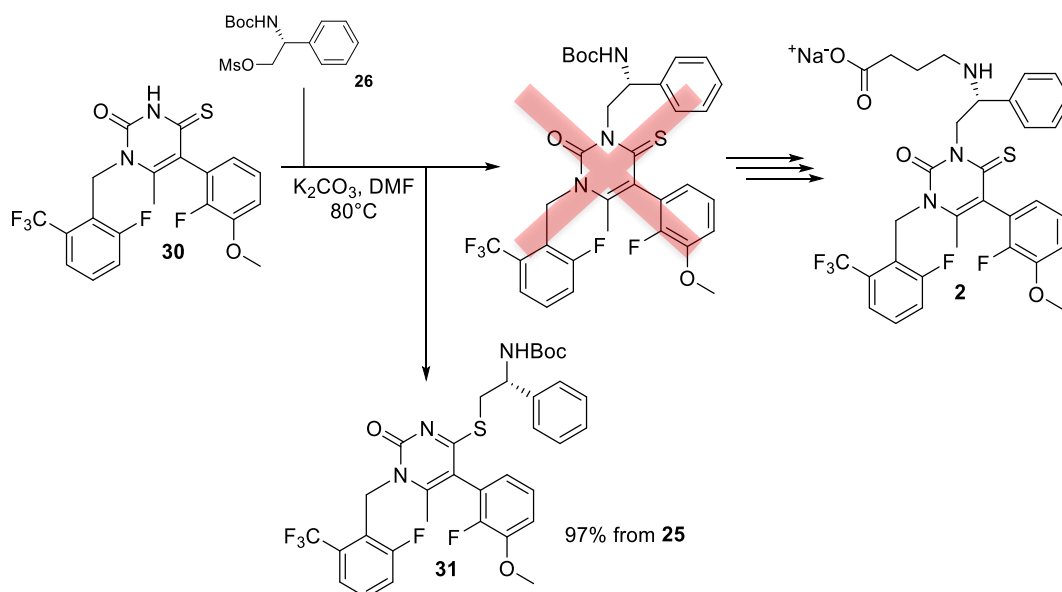


**Figure 40.** Formation of compound **31**.

This outcome can be rationalized considering the tautomerism of the 4-thio uracil moiety (Figure 41) [177] and the higher nucleophilicity of sulfur respect to nitrogen [178]. Since the equilibrium between the tautomeric forms of 4-thio uracil moiety can be influenced by acids and bases, we carried out this reaction under neutral reaction conditions employing diethyl azodicarboxylate (DEAD) and PPh<sub>3</sub>, obtaining also in this case quantitatively compound **31**.

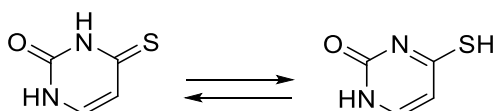


**Figure 41.** Tautomeric forms of 4-thio uracil.

The N-Boc protective group of **31** was removed to yield the free amine **32** in 96% yield (Figure 42). This free amine was subsequently subjected to *N*-alkylation using ethyl 4-bromobutyrate, resulting in the simultaneous formation of two different ethyl ester derivatives, namely compounds **33** and **35**. The presence of these two distinct products was elucidated through time-course NMR analysis of a sample of compound **32** dissolved in Py-d<sub>5</sub> at various time intervals (see Section 4.3). The evolution of the <sup>1</sup>H and <sup>13</sup>C spectra was indicative of an intramolecular nucleophilic substitution by the free amine on the carbon bearing the sulfur atom, ultimately leading to the creation of compound **34** (Figure 42).

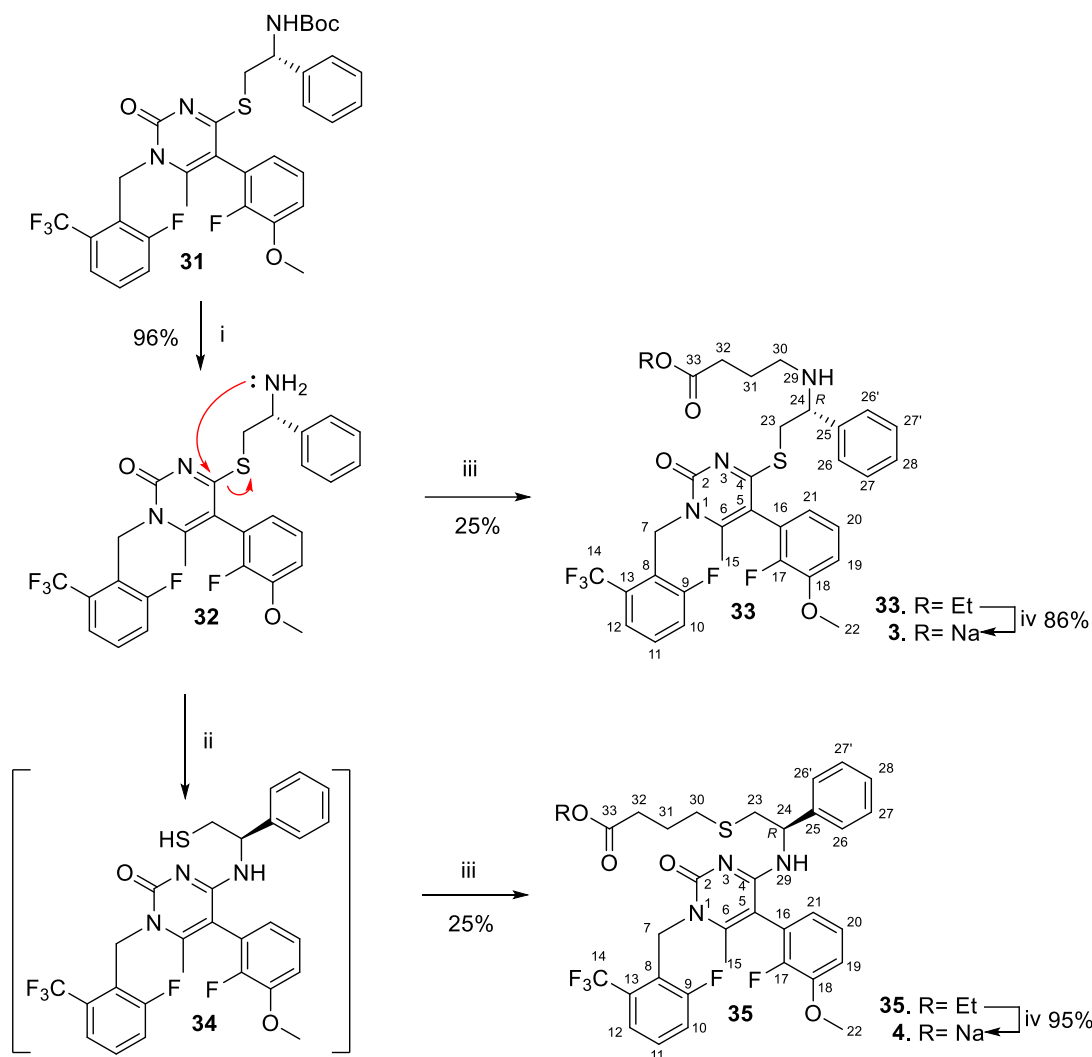


**Figure 42.** Synthesis of **3** and **4** from **31**. Reagents and conditions: (i) TFA, CH<sub>2</sub>Cl<sub>2</sub>; (ii) intramolecular nucleophilic substitution; (iii) ethyl 4-bromobutyrate, DIPEA, DMF, 80°C; (iv) NaOH, H<sub>2</sub>O, ethanol.

A similar behavior was previously observed in 1991 with 4-methyl-thiouracils in the presence of benzylamine or morpholine [179]. Furthermore, it was discovered that the ratio between compounds **33** and **35** in the crude reaction mixture was influenced by the stoichiometry of the reaction. Specifically, when 1 equivalent of both ethyl 4-bromobutyrate and *N,N*-diisopropylethylamine (DIPEA) were employed, compound **35** was nearly exclusively obtained. However, when 3 equivalents of ethyl 4-bromobutyrate and 1 equivalent of DIPEA were used, compounds **33** and **35** were obtained in approximately a 1:1 ratio. It was interesting to find that the thin layer chromatography (TLC) analysis of **33** and **35** revealed the existence of two sets of atropisomers (Figure 43), a pair for each analogue, which can be separated using achiral chromatography.

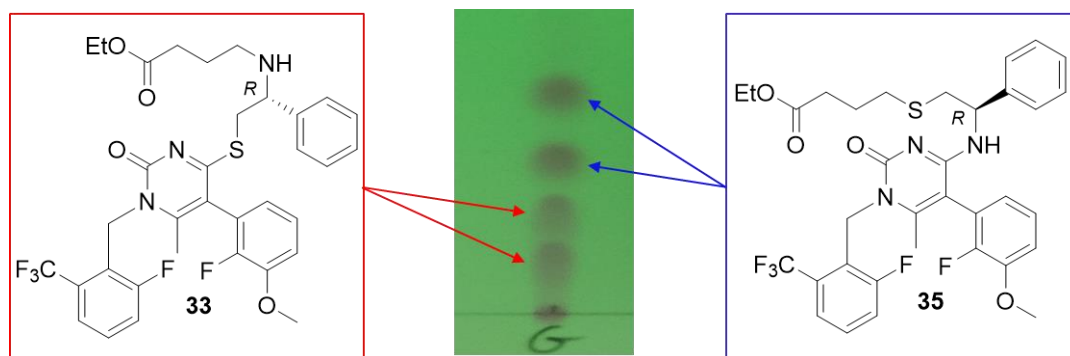


**Figure 43.** TLC analysis on silica gel (eluant: hexane/AcOEt 1:1) of the reaction mixture obtained reacting **32** with 3 equivalents of 4-ethyl bromobutylate.

This is a noteworthy result since the atropisomers of elagolix (**1**) and its intermediate cannot be separated.

The final compounds **3** and **4** were obtained in 86% and 95% yields, respectively, through the hydrolysis of their corresponding ethyl esters, **33** and **35**, employing a 1:1 mixture of 2M aqueous NaOH and ethanol (Figure 42). In contrast to their precursors, it was not feasible to separate the atropisomers of **3** and **4** using a column chromatography on silica gel. However, due to the relatively short hydrolysis time (approximately 30 minutes), the individual atropisomers of **3** and **4** can be obtained starting from atropisomerically pure **33** and **35**.

### 4.3 NMR spectroscopy

A comprehensive NMR analysis was conducted on compounds **3** and **4**, along with their respective esters **33** and **35**, as well as the common precursors **30-32**, to verify their chemical structures and investigate the intramolecular nucleophilic substitution mechanism as depicted in Figure 42. Indeed, for these compounds, except for compound **30**, we could not obtain suitable crystals for SC-XRD analysis to unambiguously verify their chemical structure. NMR spectra of compounds **3** and **4** were recorded in deuterated methanol (CD<sub>3</sub>OD) for better comparability with the reported signals of elagolix (**1**) (refer to Section 3.2), while the spectra of intermediates **30-33** and **35** were recorded in deuterated chloroform (CDCl<sub>3</sub>), at 298 K. The study of the interconversion of **32** into **34** was conducted in deuterated pyridine (Py-d<sub>6</sub>) to achieve improved spectral resolution. Tables 8–10 summarize the unambiguous assignments of all <sup>1</sup>H and <sup>13</sup>C signals, which were established analogously to those in Section 3.2. The atom numbering is reported in Figure 42. Similar to **1** and its precursors (refer to Section 3.2), the presence of duplicated NMR signals in the recorded 1D and 2D NMR spectra of compounds **30-35**, **3**, and **4** was due to the concurrent presence of a stereogenic center and a chiral axis, rendering these compounds mixtures of atropo-diastereomers.

**Table 8.** NMR chemical shifts (ppm) and coupling constants (Hz) of compounds **25**, **30**, and **31**.

| Atom | 25 <sup>a</sup>             |                      | 30 <sup>b</sup>      |                      | 31 <sup>b</sup>                   |  |
|------|-----------------------------|----------------------|----------------------|----------------------|-----------------------------------|--|
|      | <sup>1</sup> H              | <sup>13</sup> C      | <sup>1</sup> H       | <sup>13</sup> C      | <sup>1</sup> H                    | <sup>13</sup> C                            |
| 1    | /                           | /                    | /                    | /                    | /                                 | /  |
| 2    | /                           | 151.0                | /                    | 148.5                | /                                 | 152.9 and 152.8 *                          |
| 3    | 8.52 (brs)                  | /                    | 9.77 (brs)           | /                    | /                                 | /  |
| 4    | /                           | 161.2                | /                    | 187.8                | /                                 | 177.0 and 176.9 *                          |
| 5    | /                           | 108.8                | /                    | 118.5                | /                                 | 110.8                                      |
| 6    | /                           | 151.9                | /                    | 148.8                | /                                 | 154.4 (two singlets very close together) * |
| 7    | 5.47 (s)                    | 41.8 (m)             | 5.46 (m)             | 42.4 (m)             | 5.55 (m)                          | 43.07 (brs)                                |
| 8    | /                           | 121.8 (d, J = 11.1)  | /                    | 120.3 (d, J = 4.2)   | /                                 | 121.9 (brd, J = 11.1, overlapped with 16)  |
| 9    | /                           | 161.4 (d, J = 250.0) | /                    | 161.5 (d, J = 250.0) | /                                 | 161.3 (d, J = 250.7)                       |
| 10   | 7.28 (dd, J = 11.8 and 8.3) | 121.0 (d, J = 24.4)  | 7.55 (d, J = 7.8 Hz) | 122.8 (m)            | 7.22 (overlapped with 28)         | 120.7 (d, J = 24.0)                        |
| 11   | 7.42 (m)                    | 129.5 (d, J = 9.8)   | 7.45 (m)             | 129.9 (d, J = 9.5)   | 7.38 (overlapped with 26 and 26') | 129.3 (d, J = 9.8)                         |
| 12   | 7.54 (d, J = 7.9)           | 122.6 (m)            | 7.29 (m)             | 121.2 (d, J = 23.8)  | 7.53 (d, J = 7.8)                 | 122.5 (m)                                  |

|                                  |                              |                                 |                        |                         |   |   |
|----------------------------------|------------------------------|---------------------------------|------------------------|-------------------------|---|---|
| 13                               | /                            | 129.6 (dd, $J = 30.9$ and 4.0)  | /                      | 126.8 (m)               | /   | 129.8 (brd, $J = 30.0$ )                              |
| 14                               | /                            | 123.5 (dd, $J = 273.8$ and 3.9) | /                      | 123.6 (d, $J = 274.8$ ) | /   | 125.7 (dd, $J = 273.6$ and 3.6)                       |
| 15                               | 2.05 (s)                     | 17.9                            | 1.99 (s, 3H)           | 18.6                    | 2.04 (s) and 2.03 (s) *                           | 17.7  |
| 16                               | /                            | 121.5 (d, $J = 13.6$ )          | /                      | 124.8 (d, $J = 13.8$ )  | /   | 121.9 (d, $J = 13.6$ , overlapped with 8)             |
| 17                               | /                            | 149.9 (d, $J = 246.4$ )         | /                      | 150.0 (d, $J = 245.5$ ) | /   | 150.2 (d, $J = 248.4$ ) and 150.1 (d, $J = 248.4$ ) * |
| 18                               | /                            | 148.0 (d, $J = 11.0$ )          | /                      | 148.1 (d, $J = 10.9$ )  | /   | 148.2 (d, $J = 10.8$ ).                               |
| 19                               | 6.97 (m)                     | 113.5                           | 6.79 (t, $J = 6.9$ )   | 123.8                   | 7.04 (m)  | 114.3   |
| 20                               | 7.10 (dd, $J = 9.0$ and 7.9) | 123.8                           | 7.12 (t, $J = 8.0$ )   | 124.2 (d, $J = 4.5$ )   | 7.13 (m)  | 124.3 (m)   |
| 21                               | 6.81 (m)                     | 123.9 (d, $J = 4.6$ )           | 6.99 (t, $J = 8.1$ Hz) | 113.6                   | 6.77 (m)  | 123.9   |
| 22                               | 3.88 (s)                     | 56.3                            | 3.89 (s)               | 56.3                    | 3.91 (s)  | 56.3  |
| 23                               | /                            | /                               | /                      | /                       | 3.80 – 3.15 (m, H <sub>a</sub> + H <sub>b</sub> ) | 36.2 and 36.0 *                                       |
| 24                               | /                            | /                               | /                      | /                       | 4.83 (m)  | 55.4 and 55.0 *                                       |
| 25                               | /                            | /                               | /                      | /                       | /   | 141.6   |
| 26 and 26'                       | /                            | /                               | /                      | /                       | 7.39 (overlapped with 11)                         | 126.3   |
| 27 and 27'                       | /                            | /                               | /                      | /                       | 7.29 (m)  | 128.5   |
| 28                               | /                            | /                               | /                      | /                       | 7.22 (overlapped with 10)                         | 127.5   |
| 29                               | /                            | /                               | /                      | /                       | 5.75 (d, partially overlapped with 7)             | /   |
| C(CH <sub>3</sub> ) <sub>3</sub> | /                            | /                               | /                      | /                       | /   | 79.2  |
| C(CH <sub>3</sub> ) <sub>3</sub> | /                            | /                               | /                      | /                       | 1.38 (s)  | 28.3  |

nd =  $J$  were not determined due to the overlapping. <sup>a</sup> Assignments according to Section 3.2 in CD<sub>3</sub>OD at 298 K. <sup>b</sup> Assignments from <sup>1</sup>H–<sup>1</sup>H COSY, HSQC, and HMBC data in CD<sub>3</sub>OD at 298K. Coupling constants were obtained by direct inspection of the spectra. Experimental error in the measured <sup>1</sup>H–<sup>1</sup>H coupling constants was  $\pm 0.5$  Hz. \* The two signals are due to the presence of two atropisomers.

**Table 9.** NMR chemical shifts (ppm) and coupling constants (Hz) of compounds **32**, **33**, and **35**.

| Atom | 32 <sup>a</sup>               |   | 33 <sup>b</sup>               |                         | 35 <sup>b</sup>                                |                            |
|------|-------------------------------|---|-------------------------------|-------------------------|--|----------------------------|
|      | <sup>1</sup> H                | <sup>13</sup> C                                       | <sup>1</sup> H                | <sup>13</sup> C         | <sup>1</sup> H                                 | <sup>13</sup> C            |
| 1    | /                             | /   | /                             | /                       | /  | /                          |
| 2    | /                             | 154.9   | /                             | 154.7                   | /  | 157.01 and 156.97 *        |
| 3    | /                             | /   | /                             | /                       | /  | /                          |
| 4    | /                             | 177.2   | /                             | 176.7                   | /  | 161.0 and 160.9 *          |
| 5    | /                             | 111.2   | /                             | 110.9                   | /  | 100.9 and 100.8 *          |
| 6    | /                             | 154.5   | /                             | 152.4                   | /  | 152.2                      |
| 7    | 5.63 (m)                      | 44.1  | 5.56 (s)                      | 42.98 and 42.95 *       | 5.55 (m)                                       | 42.4 (brs)                 |
| 8    | /                             | 123.6   | /                             | 122.1 (d, $J = 12.3$ )  | /  | 123.2 (overlapped with 21) |
| 9    | /                             | 162.1 (d, $J = 248.8$ )                               | /                             | 161.3 (d, $J = 249.3$ ) | /  | 161.4 (d, $J = 250.8$ )    |
| 10   | 7.22 (nd, overlapped with Py) | 121.40 (d, $J = 24.0$ ) and 121.38 (d, $J = 24.0$ ) * | 7.23 (nd, overlapped with 28) | 120.8 (d, $J = 24.0$ )  | 7.19 (nd, overlapped with 20, 26, 26', and 28) | 120.8 (d, $J = 24.0$ )     |

|                                 |  |   |   |   |  |  |
|---------------------------------|--|---|---|---|--|--|
| 11                              | 7.32 (m)                                     | 130.2 (d, J = 9.7)                      | 7.38 (m)                                    | 129.3 and 129.2 *                               | 7.34 (m)   | 128.78 (d, J=9.5) and 128.76 (d, J=9.5) *      |
| 12                              | 7.51 (d, J=7.8)                              | 123.2                                   | 7.52 (d, J= 7.8)                            | 122.46 and 122.42 *                             | 7.48 (d, J = 7.8)  | 122.2 (m)                                      |
| 13                              | /  | 127.8 (d, J= 30.8)                      | /   | 129.7 (dd, J= 30.8 and 3.3)                     | /  | 129.5 (dd, J= 30.9 and 3.8)                    |
| 14                              | /  | 124.8                                   | /   | 123.6 (dd, J= 273.0 and 3.3)                    | /  | 123.6 (d, J= 274.2 and 3.6)                    |
| 15                              | 2.17 (s)                                     | 18.2 and 18.0 *                         | 2.01 (s)                                    | 17.6  | 1.94 (s)   | 17.5   |
| 16                              | /  | 123.8                                   | /   | 122.1 (d, J= 13.7)                              | /  | 121.4 (d, J= 14.0)                             |
| 17                              | /  | 151.1 (d, J= 253.0)                     | /   | 150.12 (d, J= 247.0) and 150.08 (d, J= 247.0) * | /  | 150.28(d, J= 247.3) and 150.25 (d, J= 247.3) * |
| 18                              | /  | 149.1 (d, J= 10.9)                      | /   | 148.1 (d, J= 11.0)                              | /  | 148.72 (d, J= 11.0) and 148.68 (d, J= 11.0)    |
| 19                              | 7.14 (tt, J = 8.2, 2.1).                     | 115.2                                   | 7.03 (m)                                    | 114.2 and 114.1 *                               | 7.06 (tt, J = 8.1 and 1.8)   | 114.1  |
| 20                              | 7.22 (n.d, overlapped with Py)               | 125.5                                   | 7.12 (m).                                   | 124.30 and 124.26 *                             | 7.20 (nd, overlapped with 10, 26, 26', and 28)                         | 125.07 (t, J= 5.6)                             |
| 21                              | 7.02 (m)                                     | 124.6                                   | 6.78 (m)                                    | 123.8   | 6.89 (ddd, J= 7.6, 6.0, and 1.6) and 6.81(ddd, J= 7.6, 6.0, and 1.6) * | 123.4 and 123.2 *                              |
| 22                              | 3.80 (s) and 3.79 (s) *                      | 56.6 (brs)                              | 3.91 (s) and 3.92 (s) *                     | 56.26 and 56.22 *                               | 3.93 (s)   | 56.3   |
| 23                              | 3.84 (ddd, J= 12.9, 8.0, 4.7) and 3.46 (m) * | 40.8 (brs)                              | 3.54 – 3.41 (m, Ha) and 3.35 – 3.20 (m, Hb) | 37.9  | 3.04 – 2.86 (m)  | 38.24 and 38.22 *                              |
| 24                              | 4.43 (ddd, J= 12.8, 8.6, 4.6)                | 55.9 (two singlets very close together) | 3.90 (nd, overlapped with 22)               | 61.6 and 61.4 *                                 | 5.75 (dt, J = 9.7, 5.4) and 5.69 (dt, J = 8.2, 6.1) *                  | 52.1   |
| 25                              | /  | 145.6                                   | /   | 142.3 (m)                                       | /  | 140.5 and 140.4 *                              |
| 26 and 26'                      | 7.60 (nd, overlapped with Py)                | 127.5                                   | 7.34 (nd, partially overlapped with 11)     | 127.31 and 127.25 *                             | 7.21(nd, overlapped with 10, 20, and 28)                               | 127.41 and 127.36 *                            |
| 27 and 27'                      | 7.29 (nd, overlapped with 11 and 19)         | 129.2                                   | 7.28 (m)                                    | 128.38 and 128.36 *                             | 7.27 (m)   | 128.51   |
| 28                              | 7.22 (n.d, overlapped with Py)               | 127.9                                   | 7.22 (nd, partially overlapped with 10)     | 127.4 and 127.3 *                               | 7.17 (nd, overlapped with 10, 20, 26, and 26')                         | 126.4 and 126.3 *                              |
| 29                              | /  | /                                       | /   | /   | 5.39 (d, J= 8.4) and 5.32 (d, J= 8.1) *                                | /  |
| 30                              | /  | /                                       | 2.56 – 2.37 (m)                             | 46.6  | 2.36 – 2.25 (m)  | 32.1 and 31.8 *                                |
| 31                              | /  | /                                       | 1.72 (m)                                    | 25.24   | 1.74 (dp, J= 22.4 and 7.5).  | 24.7 and 24.6 *                                |
| 32                              | /  | /                                       | 2.37 – 2.21 (m)                             | 32.1  | 2.28 (m)   | 32.91 and 32.88 *                              |
| 33                              | /  | /                                       | /   | 173.7   | /  | 172.98 and 172.96 *                            |
| CH <sub>2</sub> CH <sub>3</sub> | /  | /                                       | 4.07 (q, J=7.1, two overlapped quartet) *   | 60.2  | 4.10 (q, J=7.1, two overlapped quartet) *                              | 60.4 and 60.3 *                                |

|                                 |   |   |  |      |  |      |
|---------------------------------|---|---|--|------|--|------|
| CH <sub>2</sub> CH <sub>3</sub> | / | / | 1.20 (t, J=7.1, two overlapped triplet)<br>* | 14.2 | 1.24 (t, J=7.1, two overlapped triplet)<br>* | 14.2 |
|---------------------------------|---|---|--|------|--|------|

nd = *J* were not determined due to the overlapping. <sup>a</sup> Assignments from <sup>1</sup>H-<sup>1</sup>H COSY, HSQC, and HMBC data in Py-d<sub>5</sub> at 298K. <sup>b</sup> Assignments from <sup>1</sup>H-<sup>1</sup>H COSY, HSQC, and HMBC data in CD<sub>3</sub>OD at 298K. Coupling constants were obtained by direct inspection of the spectra. Experimental error in the measured <sup>1</sup>H-<sup>1</sup>H coupling constants was ±0.5 Hz. \* The two signals are due to the presence of two atropisomers.

**Table 10.** NMR chemical shifts (ppm) and coupling constants (Hz) of compounds **1**, **3** and **4**.

| Atom | 1 <sup>a</sup>                         |  | 3 <sup>b</sup>   |  | 4 <sup>b</sup>                              |   |
|------|--|--|--|--|---|---|
|      | <sup>1</sup> H                         | <sup>13</sup> C  | <sup>1</sup> H   | <sup>13</sup> C                                | <sup>1</sup> H                              | <sup>13</sup> C                                 |
| 1    | /                                      | /  | /  | /  | /   | /   |
| 2    | /                                      | 153.3 and 153.2 *  | /  | 157.0  | /   | 154.22 and 154.16 *                             |
| 3    | /                                      | /  | /  | /  | /   | /   |
| 4    | /                                      | 163.5 and 163.3 *  | /  | 178.47 and 178.42 *                            | /   | 159.5   |
| 5    | /                                      | 109.3 and 109.2 *  | /  | 113.3  | /   | 103.7 and 103.5 *                               |
| 6    | /                                      | 152.6 and 152.5 *  | /  | 155.3  | /   | 152.8   |
| 7    | 5.43 (m)                               | 44.1 (brs)   | AB System<br>5.59 (d, J= 16.7, H <sub>b</sub> ), 5.53 (d, J= 16.7, H <sub>a</sub> ). | 44.6 (brs)                                     | 5.48 (nd, overlapped with 24)               | 43.9 (m)  |
| 8    | /                                      | 123.6 (overlapped with 12 and 16)                                      | /  | 123.3 (d, J= 12.2)                             | /   | 124.2 (d, J= 12.4)                              |
| 9    | /                                      | 162.8 (d, J=248.0)<br>122.15 (d, J= 24.3 Hz) and 122.19 (d, J= 24.3) * | /  | 162.7 (d, J=248.0)                             | /   | 162.8 (d, J=248.6)                              |
| 10   | 7.44 (m)                               | 130.9 and 130.8 *  | 7.40 (m)   | 122.0 and 121.8 *                              | 7.36 (m)                                    | 122.0 and 121.9 *                               |
| 11   | 7.53 (td, J= 8.1, 5.0)                 | 123.7 (overlapped with 8 and 16)                                       | 7.53 (td, J= 8.0, 5.0)   | 130.96 and 130.88 *                            | 7.48 (m)                                    | 130.6 and 130.5 *                               |
| 12   | 7.62 (d, J= 7.9)                       | 130.6 (dd, J= 31.1 and 3.3)  | 7.63 (d, J= 7.9)   | 123.8 (m)                                      | 7.58 (d, J= 7.9)                            | 123.6 (m)                                       |
| 13   | /                                      | 125.1 (dd, J= 273.3 and 3.8)   | /  | 131.2 (dd, J= 31.0 and 3.8)                    | /   | 130.8 (dd, J= 31.0 and 3.8)                     |
| 14   | /                                      | 18.1   | /  | 125.1 (dd, J= 273.1 and 3.6)                   | /   | 125.2 (dd, J= 273.7 and 3.8)                    |
| 15   | 2.085 (s) and 2.076 (s) *              | 123.8 (overlapped with 8 and 12)                                       | 2.12 (s)   | 18.0   | 2.06 (s)                                    | 17.8  |
| 16   | /                                      | 151.8 (d, J= 245.4)  | /  | 123.1 (d, J= 13.6)                             | /   | 122.2 (d, J= 13.8) and 122.3 (d, J= 13.8)       |
| 17   | /                                      | 149.5 (d, J= 11.2)   | /  | 151.49 (d, J= 246.5) and 151.46(d, J= 245.8) * | /   | 151.79 (d, J= 246.5) and 151.81 (d, J= 246.1) * |
| 18   | /                                      | 114.8  | /  | 149.7 (d, J= 11.0)                             | /   | 150.2 (d, J= 10.8) and 150.4 (d, J= 11.2) *     |
| 19   | 7.10 (nd, overlapped with 20)          | 125.1 (s) and 125.0 (s) *  | 7.19 (nd, overlapped with 20)  | 115.9  | 7.26 (nd, overlapped with 26, 27, 26', 27') | 115.9   |
| 20   | 7.11 and 7.14 (nd, overlapped with 19) | 125.84 and 125.80 *  | 7.18 (nd, overlapped with 19)  | 7.32 (m) and 7.30 (m) *                        | 124.81                                      |   |



|            |   |                   |   |                     |   |                   |
|------------|---|-------------------|---|---------------------|---|-------------------|
| 21         | 6.76 (m) and 6.61 (m) *                                 | 125.0 and 124.9 * | 6.78 (m)  | 124.86 and 124.80 * | 6.92 (m) and 6.87 (m) *                   | 124.8 and 124.2 * |
| 22         | 3.883 (s) and 3.880 (s) *                               | 56.8              | 3.90 (s)  | 56.9 and 56.8 *     | 3.95 (s) and 3.94 (s) *                   | 56.92 and 56.89 * |
| 23         | 4.26–4.07 (m)   | 48.1 and 47.9 *   | 3.50 – 3.43 (m, H <sub>a</sub> ) and 3.41 – 3.34 (m, H <sub>b</sub> ) | 37.9 and 37.8 *     | 3.04–2.84 (m)                             | 39.2 and 39.1 *   |
| 24         | 4.11 (nd)   | 62.2 and 62.0 *   | 3.90 (nd, overlapped with 22)   | 63.0 and 62.9 *     | 5.47 (nd, overlapped with 7)              | 54.3              |
| 25         | /   | 142.1 and 141.9 * | /   | 142.7               | /   | 142.6 and 142.7 * |
| 26 and 26' | 7.29 (nd, overlapped with 27 and 27')                   | 128.9             | 7.34 (m)  | 128.7               | 7.25 (nd, overlapped with 19, 27 and 27') | 127.4 and 127.5 * |
| 27 and 27' | 7.27 (nd, overlapped with 26 and 26')                   | 129.4             | 7.28 (m)  | 129.5               | 7.26 (nd, overlapped with 19, 26 and 26') | 129.3 and 129.4 * |
| 28         | 7.22 (m)  | 128.5             | 7.22 (m)  | 128.6               | 7.20 (m)                                  | 128.2 and 128.3 * |
| 29         | /   | /                 | /   | /                   | /   | /                 |
| 30         | 2.40 (m)  | 48.7              | 2.44 (m)  | 48.6                | 2.40–2.29 (m) and 2.32–2.23 (m) *         | 37.3              |
| 31         | 1.75 (m, H <sub>a</sub> ) and 1.68 (m, H <sub>b</sub> ) | 27.86 and 27.83 * | 1.72 (m)  | 27.4                | 1.75–1.63 (m)                             | 27.6 and 27.5 *   |
| 32         | 2.09 (m, overlapped with 15)                            | 37.03 and 37.00 * | 2.11 (m)  | 37.02 and 36.98 *   | 2.20–2.12 (m)                             | 37.4              |
| 33         | /   | 182.3             | /   | 182.2               | /   | 181.1             |

nd =  $J(\text{H,H})$  were not determined due to the overlapping. <sup>a</sup> Assignments according to section 3.2 in CD<sub>3</sub>OD at 298 K. <sup>b</sup> Assignments from <sup>1</sup>H–<sup>1</sup>H COSY, HSQC, and HMBC data in CD<sub>3</sub>OD at 298K. Coupling constants were obtained by direct inspection of the spectra. Experimental error in the measured <sup>1</sup>H–<sup>1</sup>H coupling constants was ±0.5 Hz. \* The two signals are due to the presence of two atropisomers.

To confirm the regioselective substitution of the oxygen at the 4-position of the uracil moiety with sulfur in compound **30**, a comparison was made with the reported chemical shifts for **25** (refer to Section 3.2). This analysis proved valuable, as even though the <sup>1</sup>H NMR spectra of compounds **25** and **30** exhibited remarkable similarity, the chemical shift of C-4 increased from 161.2 ppm in compound **25** to 187.8 ppm in compound **30**, while the chemical shift of C-2 remained nearly unchanged. This analytical result aligns with literature findings [176] for 4-thio analogs of pyrimidine bases. Similarly to **1** (as discussed in Section 3.2), the incorporation of the (*R*)-phenylamino ethyl moiety in compound **31** led to the observation of two distinct resonances for certain signals, indicating the presence of a mixture of two atropisomers, now diastereoisomers following the introduction of a stereogenic center. Moreover, despite the absence of a cross-peak between H-23 (3.80–3.15 ppm) and C-4 (117.0 and 176.9 ppm) in the HMBC spectra, possibly due to the broad nature of H-

23 resonances, the chemical shift observed for H-23 aligns with that of a methylene group in the  $\alpha$ -position of a sulfur atom and in the  $\beta$ -position to a phenyl group. This spectroscopic result suggests that the nucleophilic attack on the activated form of (*R*)-phenylglycinol was carried out by the sulfur atom, unlike the synthesis of **1**, where the nucleophilic attack was performed by the nitrogen at the 3-position of the uracil moiety. This outcome can be explained, as discussed in Section 4.2, by considering the higher nucleophilicity of the sulfur atom respect to the nitrogen one displayed in 4-thio uracil moieties [178]. Compound **32**, obtained through deprotection of the Boc-protected amine **31** using trifluoroacetic acid, exhibited instability when stored in various solvents, including DMSO- $d_6$ ,  $CDCl_3$ , and  $Py-d_5$ . Over time, a shift in the NMR spectra was observed. To gain better resolution of the NMR resonances and comprehend the transformation of compound **32**, we monitored its spectral evolution in  $Py-d_5$ . This revealed that compound **32**, initially identifiable at time zero (as indicated in Table 9), undergoes a rearrangement reaction to yield compound **34** (Figure 44).

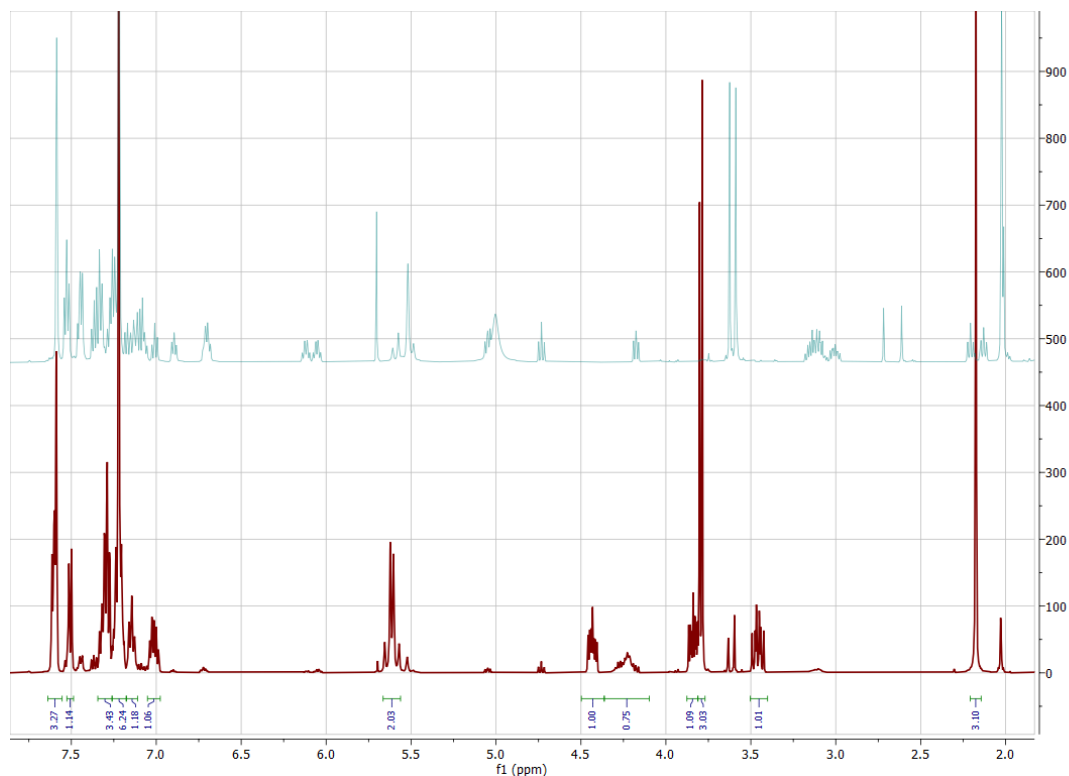


**Figure 44.** Superimposed  $^1H$  NMR spectra of **32** at time zero (in red) and after 72 hours in  $Py-d_5$  solution (completely converted in **34**, in blue).

During this process, the H-23 protons became shielded (the two multiplets at 3.84 and 3.46 ppm at time zero transformed into a multiplet at 3.20 - 2.95 ppm), while the H-24 proton became deshielded (the multiplet at 4.43 ppm split into two quartets at 6.12 and 6.06 ppm). Additionally, two triplets at 2.21 and 2.13 ppm, and two signals at 7.28 and 7.25 ppm corresponding to the SH and NH protons, respectively, emerged. The  $^{13}\text{C}$  NMR spectra also displayed the shift of C-23, C-24, and C-4 carbon resonances from 40.8, 55.9, and 177.2 ppm to 30.8, 56.2, and 142.4 ppm. These  $^1\text{H}$  and  $^{13}\text{C}$  NMR data support the occurrence of an intramolecular nucleophilic attack of N-29 on C-4 of **32**, resulting in the formation of compound **34**. A similar reactivity had been reported previously with 4-methyl-thiouracils in the presence of benzylamine or morpholine [179]. Furthermore, the observed cross-peak in the HMBC spectrum at time zero between C-4 (177.2 ppm) and H-23 protons (3.84 and 3.46 ppm) provides further confirmation that the nucleophilic attack on the (*R*)-phenylamino ethyl moiety by **30** was carried out by the sulfur atom at the 4-position of the uracil moiety.

The identification and assignment of the correct bonding sequence of positional isomers **33** and **35**, both originating from the nucleophilic attack of **32** (which, as previously mentioned, is actually a mixture of **32** and **34** in solution) on ethyl 4-bromobutyrate, was determined by analysing the chemical shift values of the C-4, C-23, C-24, and C-30 carbons. In the case of **33**, the carbon atoms exhibited chemical shift values of 176.7, 37.9, 61.6, 61.4, and 46.6 ppm for C-4, C-23, C-24, and C-30, respectively, indicating that the sulfur atom is positioned between C-4 and C-23, while the nitrogen is between C-24 and C-30. Conversely, in compound **35**, the chemical shift values of 161.0, 160.9 (C-4), 38.24, 38.22 (C-23), 52.1 (C-24), and 32.1, 31.8 (C-30) ppm indicated a reversal in the positions of the nitrogen atom and sulfur with respect to **33**. Differences in the resonance of H-23, H-24, and H-30 protons between **33** and **35**, as well as the presence of distinct cross-peaks in the HMBC experiments, further corroborated the differentiation in atom connectivity between the two compounds. It is worth noting that the atropo-diastereomeric ratio at equilibrium (25°C,  $\text{CDCl}_3$ , 10 mg/mL) is not precisely 1:1 but slightly skewed toward one atropisomer over the other (0.52:0.48 for **35** and 0.55:0.45 for **33**). The ability to separate the atropisomers of **33** and **35** through column chromatography on silica gel

facilitated the acquisition of their individual  $^1\text{H}$  NMR spectra (Figures 45 and 46) and the monitoring of their interconversion over time in  $\text{CDCl}_3$  (refer to Section 4.4).

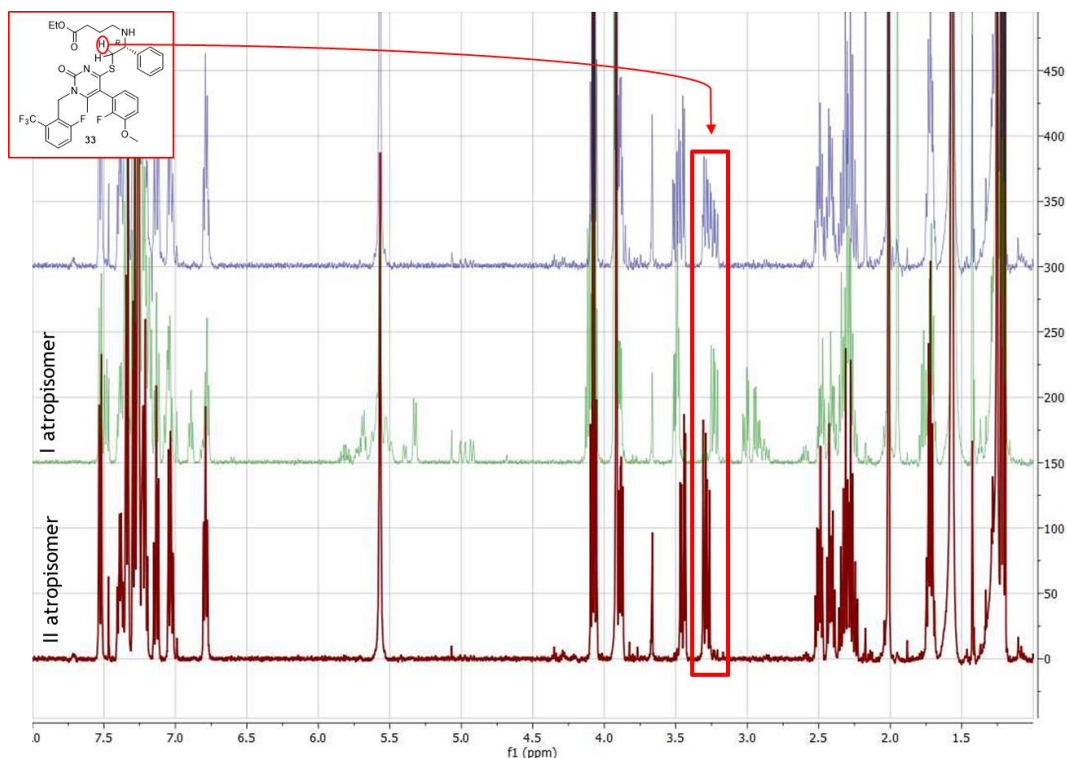


**Figure 45.** Superimposed spectra of the atropisomeric mixture (blue), purified I atropisomer (green), and purified II atropisomer of **33**. I and II refers to the order of elution.

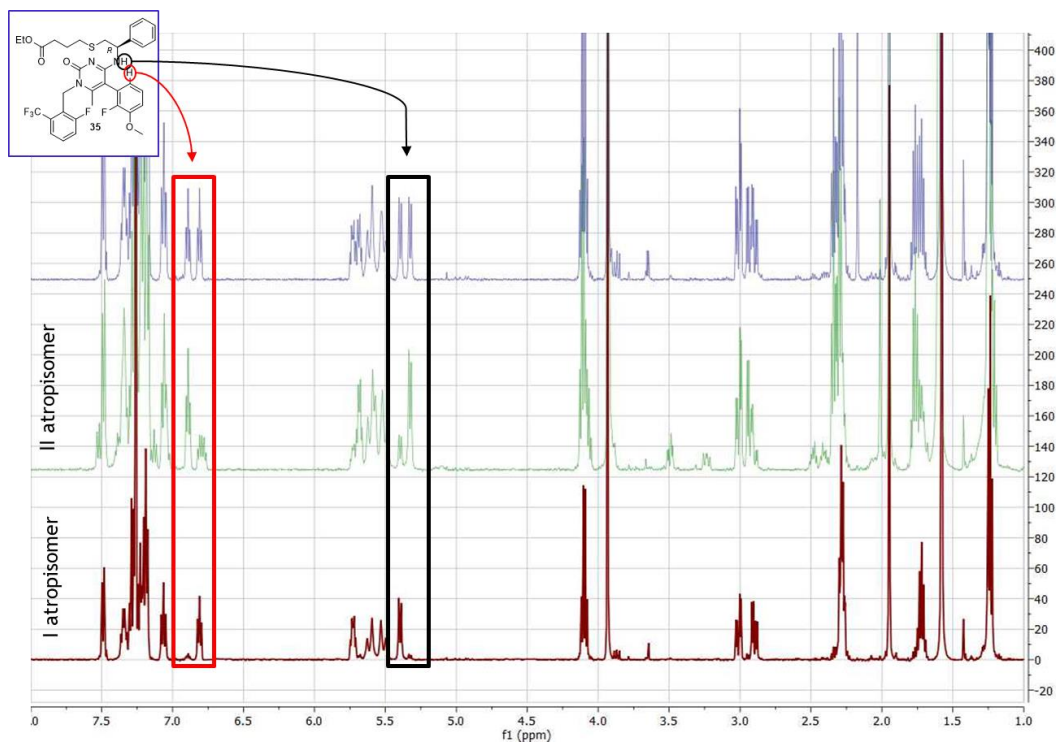


**Figure 46.** Superimposed spectra of the atropisomeric mixture (blue), purified II atropisomer (green), and purified I atropisomer of **35**. I and II refers to the order of elution.

Notable differences among the  $^1\text{H}$  and  $^{13}\text{C}$  resonances of elagolix (**1**), **3**, and **4** (as outlined in Table 10) primarily involve C-4, C-5, C-6, C-21, C-23, C-24, C-30, H-21, H-23, H-24, and H-30 atoms. These differences are largely influenced by the heteroatom directly connected to C-4, which is oxygen in **1**, sulfur in **3**, and nitrogen in **4**. Additionally, the  $^1\text{H}$ - $^{13}\text{C}$  HMBC analysis confirms the presence of sulfur between C-4 and C-23 in compound **3** and of nitrogen between C-4 and C-24 in **4**. Notably, while the atropisomeric ratio in **1** and **4** is distinguishable in the  $^1\text{H}$  NMR spectra due to a well-resolved duplicated H-21 resonance, this distinction is less apparent in **3**, where the H-21 resonances of both atropisomers (at 6.78 ppm) and other  $^1\text{H}$  NMR resonances are nearly superimposed.

The NOESY experiments conducted on **3** and **4** did not provide useful information for predicting the conformation of the atropisomers but further affirmed the structures established for **3** and **4**. In particular, cross-peaks were identified in both compounds, including H-7/H-15, H-19/H-22, H-20/H-21, H-23/H-24, H-24/(H-26 and H-26'), H-30/H-31, H-31/H-32, and H-30/H-32. Moreover, in the NOESY spectrum of **3**, the cross-peak H-24/H-30 was observed.

## 4.4 HPLC analysis

The HPLC analysis conducted on compounds **3** and **4**, similar to **1** (see Section 3.3), using a non-chiral reverse stationary phase (RP-C18), did not yield separation of the diastereo-atropisomers. However, when HPLC analysis was performed using a chiral stationary phase based on cellulose tris(3,5-dimethylphenylcarbamate), it clearly revealed two distinct peaks corresponding to the two atropo-diastereomers. These peaks are well defined for compound **4**, but there is some partial overlapping in **3** (Figure 47).

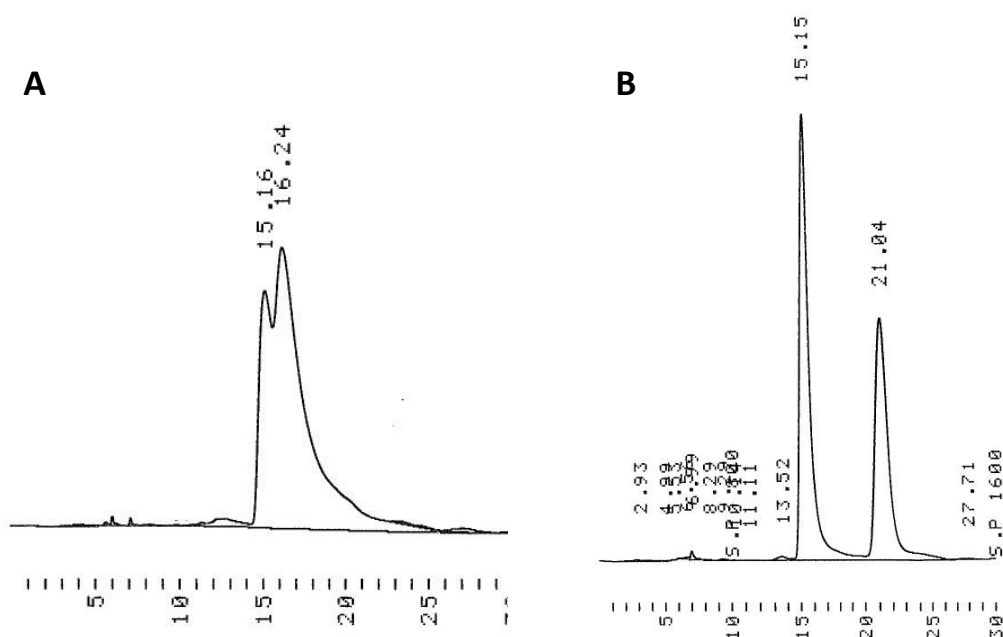


**Figure 47.** Chiral HPLC analysis of **3** (A) and **4** (B).

The HPLC chromatograms of **3** and **4** showed a difference in atropisomeric distribution, which was consistent with the NMR results.

The chiral HPLC analysis (Figure 48) of the first intermediate bearing the sulfur atom at the 4-position of the uracil moiety, compound **30**, on a cellulose tris(3,5-dimethylphenylcarbamate) based column exhibited two peaks corresponding to its two enantio-atropisomers.

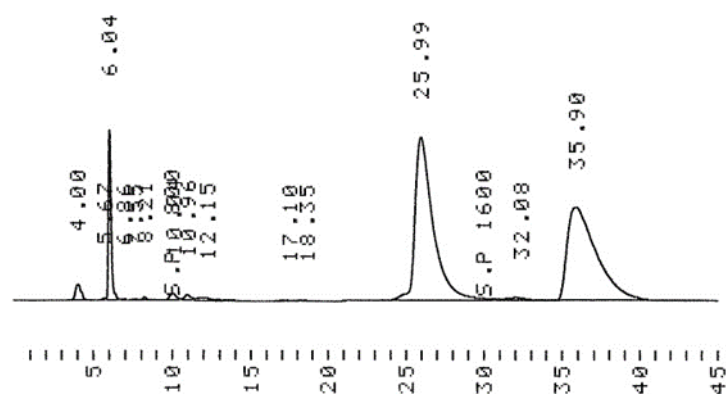


Figure 48. Chiral HPLC analysis of **30**.

When comparing this chiral HPLC analysis with that of intermediate **25** (see Section 3.3), obtained under the same experimental conditions, it is immediately visible that the plateau between the two chromatographic peak that did not reach baseline, is not present. This shows that, in the case compound **30**, the "on-column conversion" didn't occur, confirming that the substitution of the oxygen at the 4-position of the uracil moiety with sulfur was effective in increasing the rotational barrier.

## 4.5 Evaluation of the rotational barriers

An essential parameter for characterizing the atropisomeric properties of a molecule is its rotational barrier ( $\Delta G^\ddagger$ ). The literature [143] provides several experimental methods for estimating this value. Since the atropisomers of **33** and **35** can be readily separated through column chromatography on silica gel, we opted to monitor the re-equilibration of their atropisomers in solution at a fixed temperature after their separation by NMR spectroscopy. Consequently, a kinetic study was conducted by tracking the variation, over time, of the NMR spectra of solutions ( $\text{CDCl}_3$ , 10 mg/mL) of atropisomerically enriched samples of **33** and **35**, stored at 25°C. Specifically, changes in the integrals of the H-21 proton (6.89 and 6.81 ppm, see Figure 46), corresponding to the two atropisomers of **35**, or the H-22 (3.91 and 3.92 ppm) and H<sub>a</sub>-23 (3.32-3.26 and 3.26-3.20) protons (as shown in Figure 45) for compound **33** were monitored. These integral values were used to quantify the amounts of each rotamer in solution and were plotted as  $\ln[de(t)/de(0)]$  versus time (t) (Figure 49). Here,  $de(t)$  represents the diastereomeric excess ( $de$ ) at time t, while  $de(0)$

represents the *de* at time 0. The slope of the linear regression yields to  $2k$ , where  $k$  is the rate constant for a first-order interconversion [142,143,151,180]. Subsequently, the  $\Delta G^\ddagger$  can be calculated using the Eyring equation,  $\Delta G^\ddagger$  (kJ/mol) =  $0.01914 \times T \times [10.319 + \log(T/k)]$ , with the half-life given by  $t_{1/2} = 0.693/2k$  [142,143,151,180]. Accordingly, under these experimental conditions, at 25°C (298 K), the estimated values for  $k$ ,  $\Delta G^\ddagger$ , and  $t_{1/2}$  for the interconversion between the atropo-diastereomers of **33** and **35** were found to be  $2.01 \times 10^{-6} \text{ s}^{-1}$  and  $5.64 \times 10^{-6} \text{ s}^{-1}$ , 25.2 and 24.6 kcal/mol, and 48 and 17 hours, respectively. The extrapolated  $t_{1/2}$  for **33** and **35**, under physiological conditions (37°C), are 9 and 3 hours, respectively.

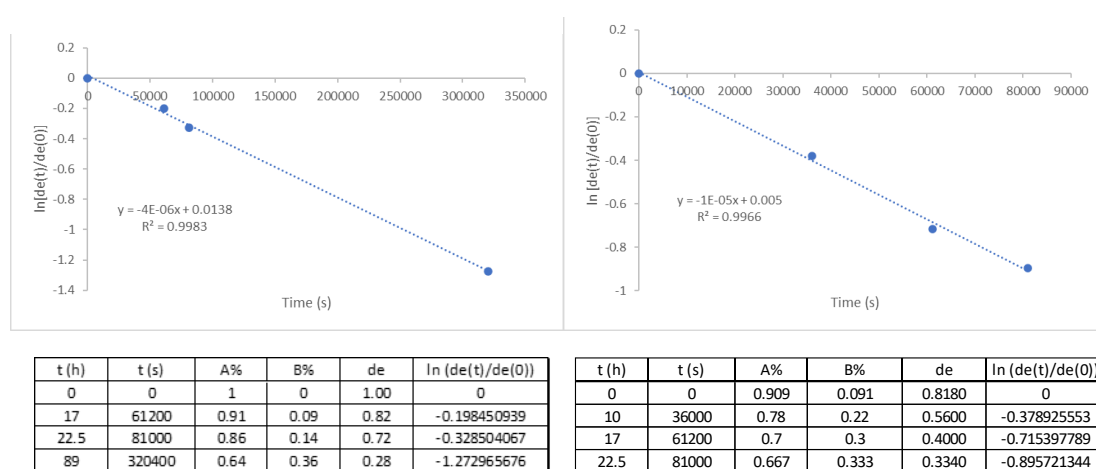


**Figure 49.** Plot of the logarithm of the relative *de* value  $\{\ln[de(t)/de(0)]\}$  over time (seconds) for interconversion of the atropisomers of **33** (left) and **35** (right) at 25° C in  $\text{CDCl}_3$ . A% and B% indicate the percentage of the two atropisomers.

The estimated  $\Delta G^\ddagger$  value for **33** (25.2 kcal/mol), which bears a sulfur atom at the 4-position of the uracil moiety, is consistent with the calculated value in Section 4.1. Interestingly, compound **35**, with a nitrogen atom at the 4-position of the uracil moiety, possesses a rotational barrier (24.6 kcal/mol) not significantly lower than that of **33**, probably because the bulky benzylamine group is directly bonded to C-4, bringing the phenyl group closer to the 5-aryl ring.

The  $\Delta G^\ddagger$  (24.1 kcal/mol) and  $t_{1/2}$  (8 and 1.5 hours at 25 and 37°C, respectively) values for **4** were estimated in a similar manner (as shown in Figure 50), starting from a diastereo-atropisomerically enriched sample. The H-21 resonances of its two atropisomers (6.92 and 6.87 ppm) were used to monitor the interconversion. Equilibrium (0.58:0.42 atropisomeric ratio) was reached in  $\text{CD}_3\text{OD}$  (10 mg/mL) at



25°C after 43 hours. The data from the initial 2 hours were used to determine the initial rate of interconversion. Under these experimental conditions, the estimated  $\Delta G^\ddagger$  value for **4** was found to be 0.5 kcal/mol lower than that of **35** in  $\text{CDCl}_3$  at the same temperature, suggesting that the rate of conformational interconversion may be solvent-dependent.

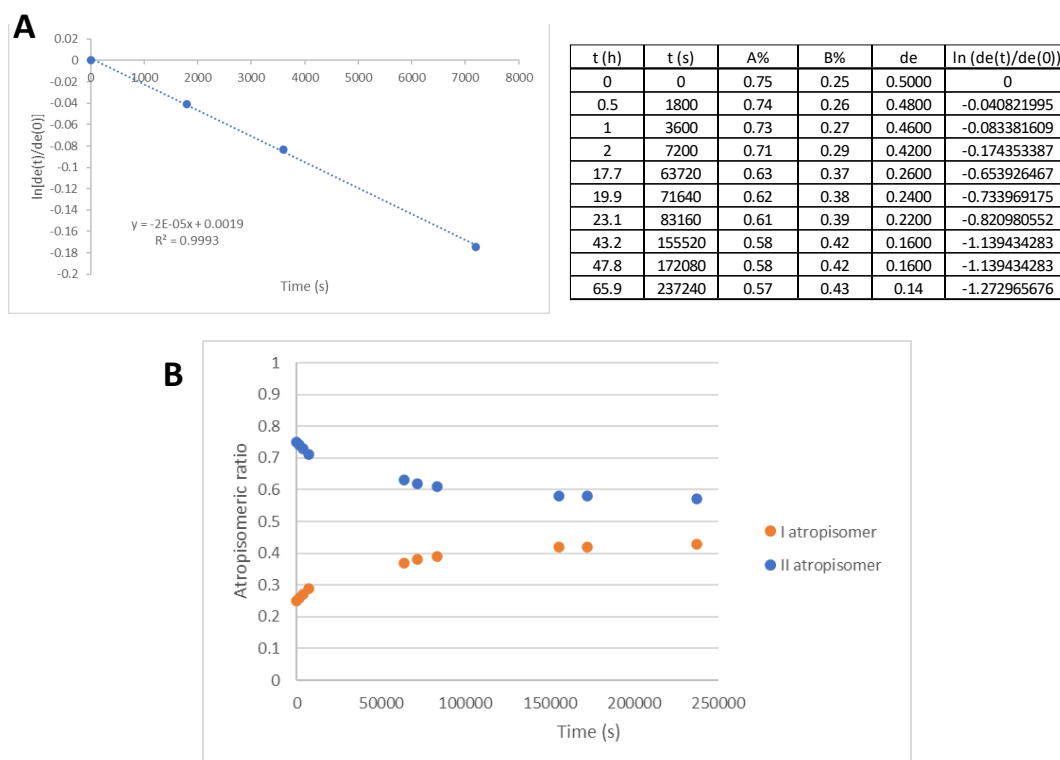


**Figure 50.** (A) Plot of the logarithm of the relative de value  $\{\ln[de(t)/de(0)]\}$  over time (seconds) for interconversion of the atropisomers of **4** at 25°C in  $\text{CD}_3\text{OD}$ . Data of the first 2h were used to determine the initial rate of interconversion. A% and B% indicate the percentage of the two atropisomers. (B) Ratio between the atropisomers of **4** over time.

Unfortunately, these calculations cannot be applied to compound **3** due to the overlapping of the signals of its two diastereo-atropisomers, both in  $^1\text{H}$  NMR (as discussed in Section 4.3) and HPLC analysis (as detailed in Section 4.4).

## 4.6 Crystallization trials

As for **25** (Section 3.4), the first intermediate in which the biaryl system responsible for atropisomerism of **1** is present, we were able to obtain single crystals of its sulfur derivative **30**, by the slow evaporation of a methanol/water 95:5 solution after 1 week. Crystallographic data and refinement details are given in Section 9.4. Compound **30** crystallized in the triclinic space group P-1 with four independent molecules in the asymmetric unit (Figure 51A). The overall conformation of the molecule is shown in as an ORTEP diagram [170], indicating the arbitrary atom-numbering scheme used in the following discussion (Figure 51B).

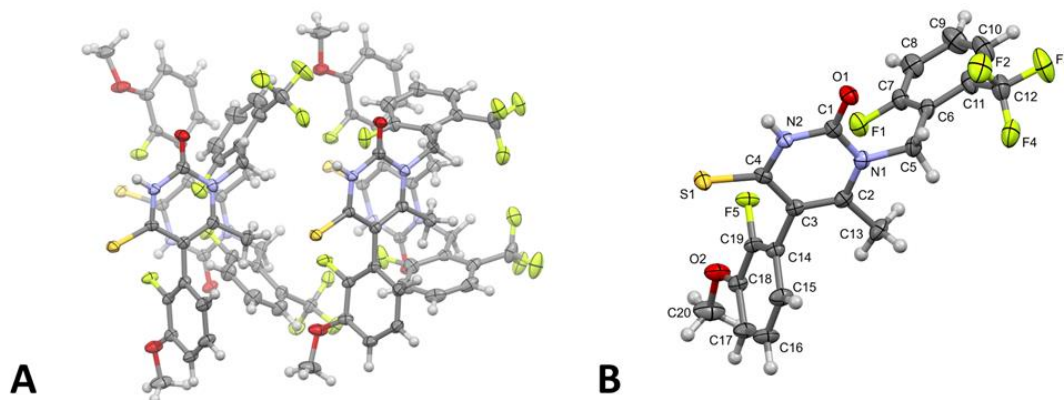


**Figure 51.** (A) Thermal ellipsoid diagram of the asymmetric unit in an arbitrary view. Displacement ellipsoids are drawn at the 40% probability level. (B) Thermal ellipsoid diagram of one of the molecules of the asymmetric unit, with the arbitrary atom-numbering scheme.

The overlay of the four independent molecules is shown in Figure 52, which evidenced the conformation differences, mainly attributable to the distal trifluoro-substituted phenyl ring.

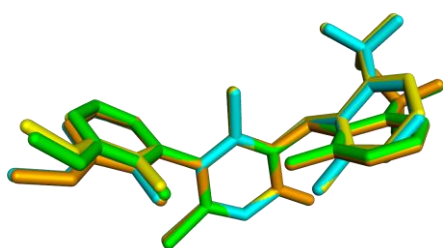


**Figure 52.** Superimposition of the four molecules of the asymmetric unit, represented as differently colored sticks.

The single-crystal X-Ray analysis of **30**, unambiguously confirmed that the use of Lawesson's reagent on **25**, regioselectively introduce the sulfur atom at the 4-position of the uracil moiety. The crystal structure of **30** showed that the 2-fluoro-3-methoxy phenyl ring is orthogonally orientated with respect to the uracil ring, indicating the presence of steric hindrance between the *ortho*-fluorine, the methyl and the sulfur at the 6- and 4-positions, respectively as source of atropisomerism. The crystal structure also showed that this compound, in the solid form, is in the thione tautomeric form.

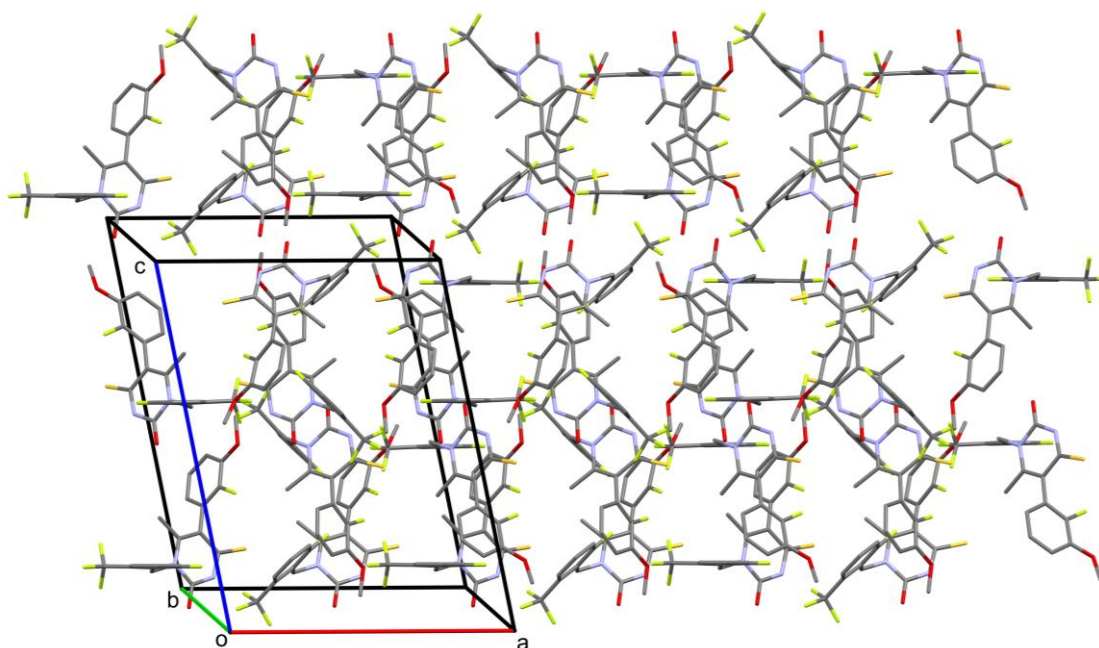


**Figure 53.** Crystal packing viewed along the *b* axis.

In the crystals, the main intermolecular contacts

- strong N-H $\cdots$ S H-bonds forming molecular pairs,
- weak C $\pi$ -H $\cdots$ F and C $\pi$ -H $\cdots$ O H-bonds,
- weak offset C $\pi$ -H- $\pi$  interactions, as depicted in Figure 53.

The crystal packing is also characterized empty spaces in the unit cell, constituted by large central voids among the four independent molecules, occupied by disordered solvent molecules (Figure 54). In this case, the voids are big enough to fit a spherical probe of 1.3 Å radius and occupy 3.7% of the unit cell volume, corresponding to 145.62 Å<sup>3</sup>.

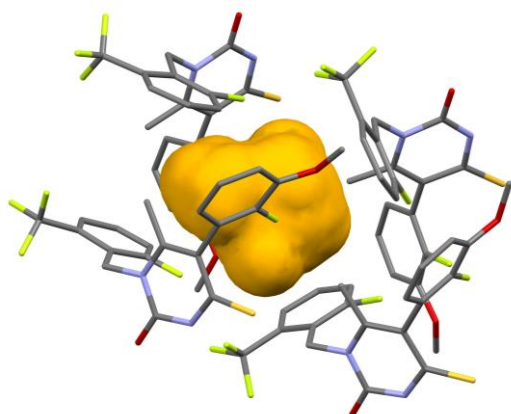


**Figure 54.** Graphical representation of the central void, occupied by disordered solvent molecules. Voids are defined as empty spaces in the unit cell, big enough to fit a spherical probe of a given radius (in this case, 1.3 Å). In the present structure, voids occupy 3.7% of the unit cell volume, corresponding to 145.62 Å<sup>3</sup>.

In the meantime, since we were able to separate the two atropisomers of **33** and **35** by chromatography over silica gel, various crystallization attempts were conducted to acquire single crystals suitable for SC-XRD analysis, with the goal of definitively determining the absolute configuration of the two atropisomers. Despite using different solvents (dichloromethane, chloroform, methanol, ethanol, 2-propanol, acetonitrile, water) on the free amine or salt forms (hydrochloride, acetate, and (1*S*)-(+)-3-bromocamphor-10-sulfonate) of **33** and **35** atropisomers, suitable crystals have not been obtained to date. As documented in the literature [169], this difficulty can be attributed to the relatively short interconversion times between the atropisomers.

## 4.7 Computational analysis

In collaboration with Professor G. Grazioso and Dr. E.M.A. Fassi at the Department of Pharmaceutical Sciences, University of Milan, and leveraging the recently published crystal structure of the hGnRH1R/1 complex [43], we conducted molecular dynamics (MD) simulations to investigate the potential binding of the unexpected products **3** and **4** to hGnRH1R. Specifically, the complex with the membrane underwent two independent 200 ns MD simulations. Subsequently, MM-GBSA analysis was carried out to compute the predicted  $\Delta G$  values (as shown in Table 11), taking into consideration the 50 ns of the simulation during which the ligand exhibited the highest stability based on the C $\alpha$  atoms RMSD plot. To validate the docking protocol, we re-docked **1** into the active site of the hGnRH1R protein,



modulators characterized by high potency and potentially improved pharmacokinetic profiles compared to those already available on the market.

## 4.8 Conclusions

In conclusion, in the effort to obtain new analogues of **1** endowed with a higher rotational barrier, we proceeded to replace the oxygen atom at the 4-position of the uracil moiety with a bulkier sulfur. This substitution was suggested by QM studies, which calculated for these derivatives an increased hindrance to the rotation for the biaryl system with respect to **1**. Contrary to our expectation, this replacement led to the obtainment of two new compounds at once: a thio-uracil (**3**) and a cytosine (**4**), as confirmed by SC-X-ray diffraction. Of note, the atropisomers of their corresponding ethyl esters, compounds **33** and **35**, respectively, were easily isolated by column chromatography on silica gel, allowing us to study them as single atropisomers. In this way, we were able to understand their kinetic of interconversion in solution using time-lapse NMR analyses and the Eyring equation. Thus, in a 10 mg/mL solution in CDCl<sub>3</sub> at 25°C, the  $\Delta G^\ddagger$  and half-life ( $t_{1/2}$ ) values for interconversion between the diastereo-atropisomers of **33** and **35** were estimated to be 25.2 and 24.6 kcal/mol, and 48 and 17 h, respectively. Despite their interconversion barriers did not reach the stability values characterizing the class 3 atropisomers ( $\Delta G^\ddagger > 30$  kcal/mol), their intermediate/hemi-stability allowed their separation and analysis as single entities. Then, MD simulations were carried out to estimate the thermodynamics and kinetics values associated with the drug–target recognition. The  $\Delta G$  values calculated using the crystal structure of *h*GnRH1R [15] and the unexpected products **3** and **4** showed better values (-98.3 and -102.2 kcal/mol, respectively) compared to that of elagolix (-97.3 kcal/mol). Therefore, if the biological tests will confirm these predictions, the scaffolds of **3** and **4** could be subjected to further optimization to obtain even more stable atropisomers belonging to class 3. In addition, the MD simulations of **3** and **4** evidenced different binding poses with respect to **1**, suggesting possible biological implications (see in Section 1.3.1). As part of our future research efforts, since good crystals of the atropisomers of compounds **33**, **35**, **3**, and **4** could not be obtained, we are evaluating the possibility to assign their absolute configuration combining NMR or chiroptical spectroscopy with DFT simulations. Additionally, the <sup>19</sup>F NMR spectra of these

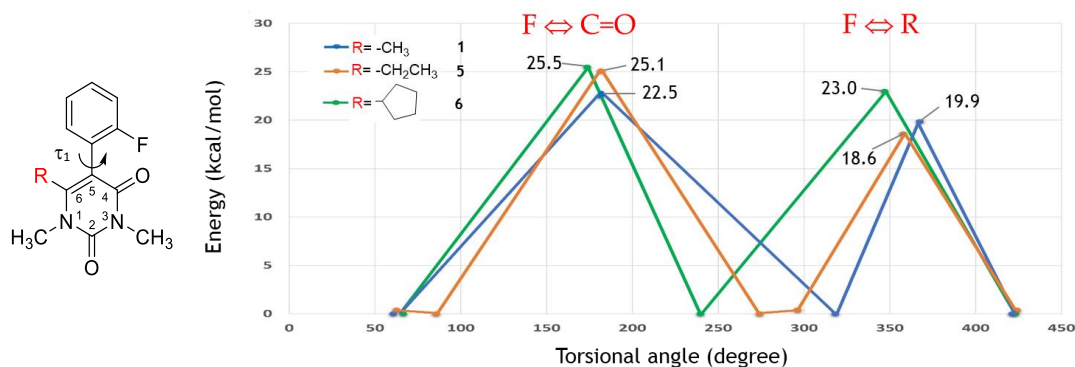
compounds, which we expect to be much simpler than  $^1\text{H}$  and  $^{13}\text{C}$  ones, will be acquired and studied.

## Chapter 5

# Elagolix analogues modified at 6-position

### 5.1 Design

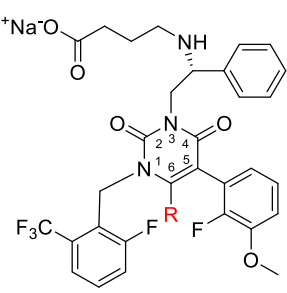
The evaluation of the viable modifications at the 6-position was carried out in collaboration with Prof. G. Grazioso and Dr. E.M.A. Fassi at the Department of Pharmaceutical Sciences, University of Milan. The conformational space of a simplified system mimicking the phenyl-uracyl moiety of **1** was explored by scanning the dihedral angle responsible for generating the atropisomers (Figure 56) at the B3LYP/6-31g(d,p) level of quantum mechanics (QM) calculations, then refined using higher-level QM calculations (B3LYP/aug-cc-PVTZ). We hypothesized that a bulkier group than methyl one could further increase the energetic barrier for atropisomer interconversion. To test this hypothesis, we computationally investigated a phenyl 6-ethyl and 6-cyclopentyl uracil simplified system (Figure 56).

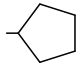


**Figure 56.** Chemical structure of the simplified system investigated by QM calculations (on the left) and potential energy profile attained scanning the  $\tau_1$  dihedral angle (on the right).

The results showed that this replacement could increase both the two transition states, through inductive effects within the uracil ring. In particular, moving from the methyl of **1** to the cyclopentyl of **6**, the rotational barriers could increase of about 3 kcal/mol, significantly slowing down the atropisomers interconversion. Moreover, MD simulations were carried out, as described in section 4.6, on different possible analogues differently substituted at the 6-position of the uracil moiety, to have an idea of the impact of this position on the binding affinity to the *hGnRH1R* (Table 12).



**Table 12.** Calculated binding free energy values ( $\Delta G$ ) of the compounds during MD simulations.

| Compound  | R   | $\Delta G$<br>(kcal/mol) | $\Delta\Delta G$<br>(kcal/mol) |
|-----------|---|--------------------------|--------------------------------|
| <b>1</b>  | -CH <sub>3</sub>  | -97.3 (2.0)              | 0                              |
| <b>5</b>  | -CH <sub>2</sub> CH <sub>3</sub>  | -85.9 (6.9)              | +11.4                          |
| <b>6</b>  |  | -90.7 (3.3)              | +6.6                           |
| <b>7</b>  | -CH <sub>2</sub> OCH <sub>3</sub>   | -89.9 (6.2)              | +7.4                           |
| <b>8</b>  | -CH <sub>2</sub> Cl   | -96.0 (5.2)              | +1.3                           |
| <b>9</b>  | -CH <sub>2</sub> F  | -90.8 (4.2)              | +6.5                           |
| <b>10</b> | -CF <sub>3</sub>  | -88.2 (4.2)              | +9.1                           |

(MD) simulations (200 ns) and the binding affinity ( $\Delta G$ ) was estimated using the MM-GBSA function implemented in Maestro (Schrödinger). In brackets the standard deviation.

The results from MD simulations (Table 12) revealed that the planned analogues, distinguished by the inclusion of a bulky substituent capable of influencing the molecule's atropisomeric properties, displayed, with the exception of compound **8**, potentially reduced yet still favourable receptor affinities compared to elagolix (**1**). This may be attributed to restricted space in the binding site for this molecular segment. However, this hypothesis requires validation through biological assays. Additionally, our quest extends beyond receptor affinity; we are also looking for a candidate with a potentially better pharmacodynamic profile than **1**.

## 5.2 Synthesis

We successfully synthesized three compounds, namely **5**, **6**, and **7**, from the planned compounds outlined in Table 12 (Section 5.1). These compounds are characterized by the presence of substituents bulkier than methyl, at the 6-position of the uracil moiety.

In the synthesis of compound **1** (Section 3.1), the 6-methyl uracil core was obtained using *tert*-butyl acetoacetate as starting material. Similarly, we planned to obtain the suitable 6-ethyl, 6-cyclopentyl, and 6-methylmethoxy uracil cores employing the appropriate  $\beta$ -keto esters **36**, **37**, and **38**, as illustrated in Figure 57.

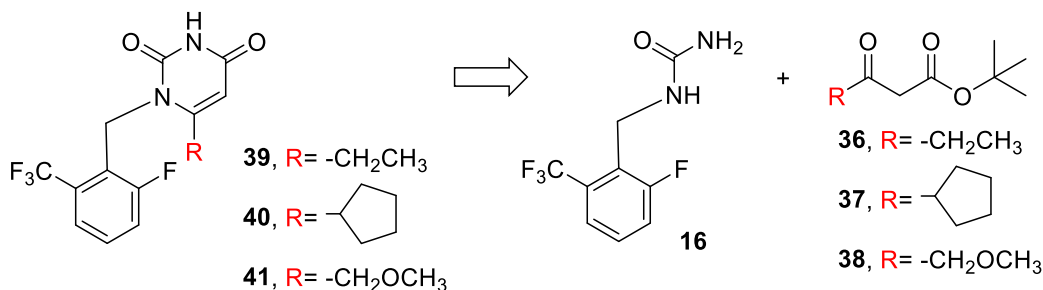


**Figure 57.** Formation of the suitable uracil moiety necessary for the synthesis of **5**, **6**, and **7**.

Compounds **36**, **37**, **38** were easily obtained from Meldrum's acid **42**, an economical and versatile starting material for generating  $\beta$ -ketoesters, in combination with the appropriate acyl chloride [181] (Figure 58).

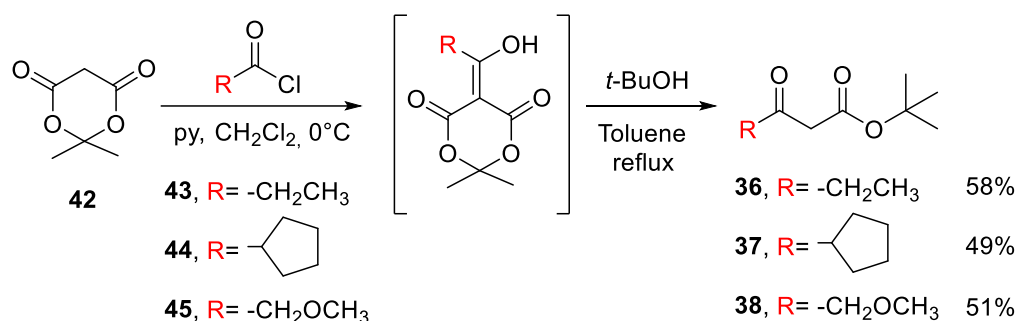


**Figure 58.** Synthesis of **36**, **37**, **38** from Meldrum's acid (**42**) and the suitable acyl chloride.

We synthesized Meldrum's acid **42** in our laboratory starting from cheap raw materials: malonic acid, acetic anhydride, and acetone in 56% yield (Figure 59). Moreover, unlike acyl chlorides **43** and **45**, **44** is not commercially available. Thus, in parallel, we performed the synthesis of the suitable acyl chloride **44** (87% yield), by reaction of cyclopentanecarboxylic acid (**46**) and thionyl chloride (Figure 59).

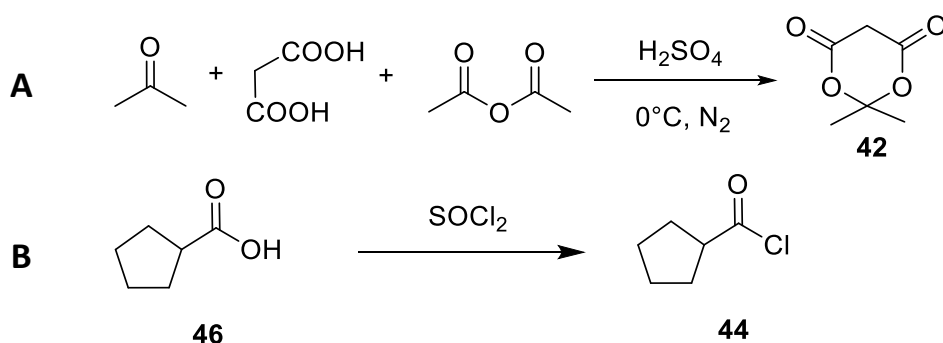


**Figure 59.** (A) Synthesis of Meldrum's acid (**42**) and (B) cyclopentanecarbonyl chloride **44**.

The following step involved the formation of the  $\beta$ -ketoesters **36-38**, required to obtain the uracil ring bearing the ethyl, cyclopentyl, and methoxymethyl group at the

6-position. The reaction between compounds **43-45** and **42** gave the corresponding Meldrum's acids derivative, suitably functionalized, which were subjected to alcoholysis to give **36-38** in 49-58% yields, after chromatographic purification (Figure 58).

Then, the uracil derivatives **39-41** were obtained by reacting **36-38** with compound **16** under the conditions previously described for **1** (Figure 60). At the end of the reaction, **39** was recovered by precipitation from 2-propanol in 61% yield, whereas **41** was isolated by chromatographic purification in 87% yield. Regarding the synthesis of compound **40**, TLC analysis indicated the presence of two products, which were separated through chromatographic purification on silica gel. The first compound to elute was the undesired isomer of **40** ( $R_f = 0.59$ ), followed by the desired **40** ( $R_f = 0.32$ ), as confirmed by NMR experiments. The latter was isolated with a 49% yield. These results imply that the hindrance caused by the R group significantly influences the regiochemistry of uracil core formation.

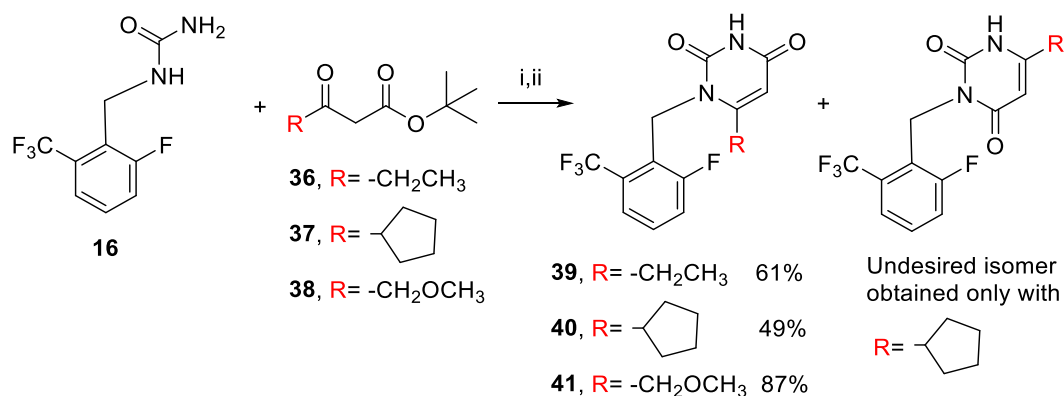


**Figure 60.** Synthesis of compound **20**. Reagents and conditions: (i) Toluene, reflux, Dean-Stark apparatus; (ii) *p*-TsOH, reflux.

As above reported, the isomers of **40** were identified by means of NOESY experiments: the NMR spectra of the desired **40** showed a cross peak between the proton in position 1' of the cyclopentyl group at the 6-position of the uracil moiety and the benzyl protons (Figure 61).

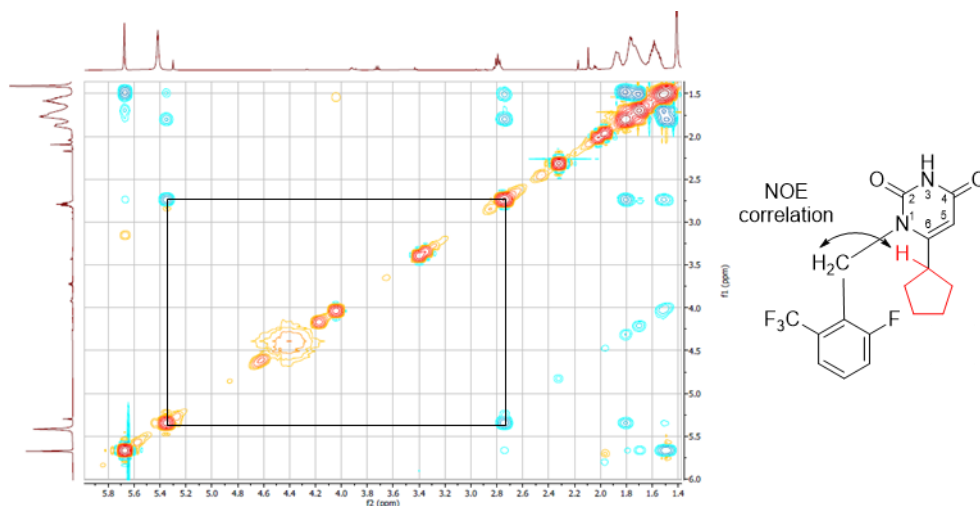


**Figure 61.** NOESY experiment of compound **40**.

The purified compounds **39**, **40**, and **41** were converted in the 5-bromine derivatives **47**, **48**, and **49** in 83, 77, and 58% yield, respectively, by treatment with bromine in acetic acid. Following the improved synthetic approach used for the synthesis of **1** (Figure 26, Section 3.1), we performed the Suzuki reaction directly on compounds **47-49** (Figure 62). Unfortunately, the observed conversion rate in the coupling products **50-52** was very low (5-10% yield). The catalytic system used is probably not suitable for substrates that have a higher steric hindrance at the 6-position than the methyl group.

We decided, therefore, to perform the Suzuki coupling under the experimental conditions described in the first published synthetic pathway for **1** [96,154]. This procedure was already tested in our laboratory (Figure 15, Section 3.1).

First, compounds **47-49** were *N*-alkylated with *N*-Boc-D-phenylglycynol through a Mitsunobu reaction employing diethyl azodicarboxylate (DEAD) and triphenylphosphine (PPh<sub>3</sub>), obtaining **53**, **54**, and **55** in 99, 94, and 91% yield, respectively, after silica gel chromatographic purification. Then, compounds **53-55** were coupled with 2-fluoro-3-methoxyphenylboronic acid through a Suzuki reaction using 10% mol of tetrakis(triphenylphosphine)palladium (Pd(PPh<sub>3</sub>)<sub>4</sub>) as catalyst, affording compound **56**, **57**, and **58** in 92, 94, and 95% yield, respectively, after chromatographic purification over silica gel (Figure 62). This process involved two rounds of chromatographic purification but yielded compounds **56-58** from **47-49** in high yields. We also attempted to utilize the "in-situ" generated Pd(*t*-Bu<sub>3</sub>P)<sub>2</sub> catalyst,

which was successfully employed in the optimized synthesis of **1** (as depicted in Figure 26, Section 3.1), on compounds **53-55**.

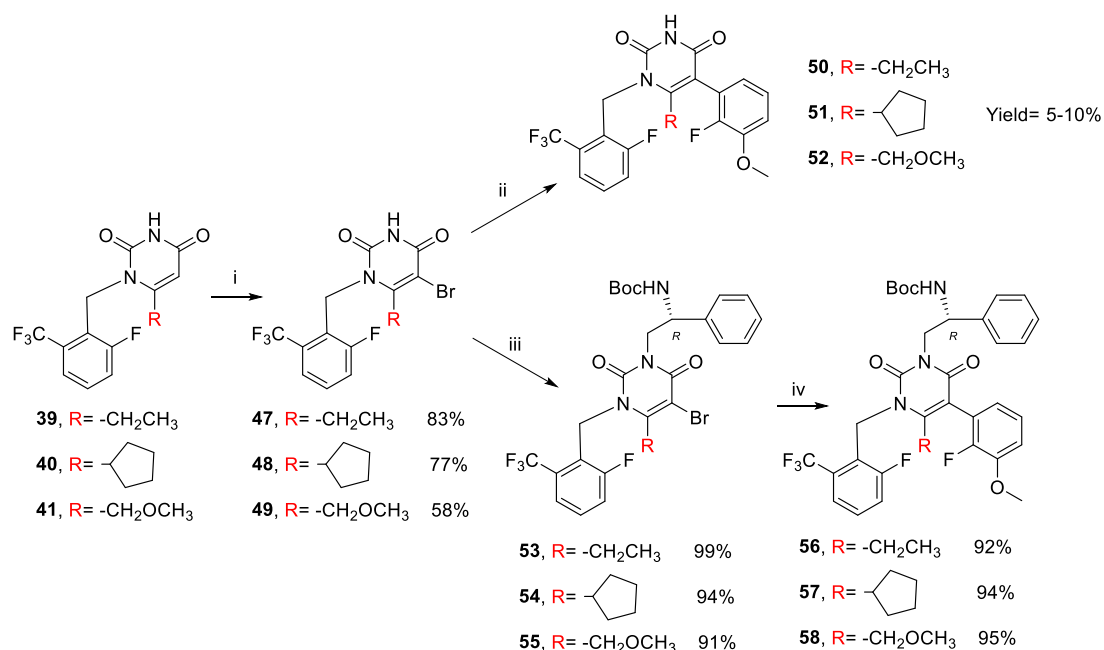


**Figure 62.** Synthesis of compounds **56-58** from **39-41**. Reagents and conditions: (i) Br<sub>2</sub>, AcOH, rt; (ii) 2-fluoro-3-methoxyphenylboronic acid, Pd(OAc)<sub>2</sub>, [(t-Bu)<sub>3</sub>PH]BF<sub>4</sub>, KOH, H<sub>2</sub>O, acetone, under argon atmosphere, reflux; (iii) *N*-Boc-D-phenylglycinol, DEAD, PPh<sub>3</sub>, THF, rt; (iv) 2-fluoro-3-methoxyphenylboronic acid, Pd(PPh<sub>3</sub>)<sub>4</sub>, Na<sub>2</sub>CO<sub>3</sub>, H<sub>2</sub>O, dioxane, under argon atmosphere, reflux.

As compounds **56-58** are the first intermediates containing the biaryl system, source of atropisomerism, we conducted a semi-preparative HPLC separation of their atropisomers. This separation utilized a chiral stationary phase derived from cellulose tris(3,5-dimethylphenylcarbamate), aiming to gain insights into their racemization kinetics.

We accomplished the synthesis of **5-7** (Figure 63) removing the Boc protecting group of **56-58** by treatment with trifluoroacetic acid in dichloromethane and the obtained amines **59-61** (97, 89, and 95 % yield, respectively) were alkylated with ethyl-4-bromobutyrate affording the intermediates **62-64** in 43, 49, and 34% yield, respectively, after purification by silica gel chromatography. The silica gel chromatographic purification was preferred to the acid-base extraction already tested by us for the purification of **21** (see Section 3.1) since the acid-base extraction was not very effective on removing the impurities. This behavior was probably due to the different polarity of these compounds, if compared to **21**. Finally, compounds **5-7** were obtained by hydrolysis of the ethyl ester moieties of **62-64** with an aqueous/ethanolic

solution of sodium hydroxide, followed by extraction with methyl isobutyl ketone and precipitation from *n*-heptane (65, 65, and 60% yield, respectively). The overall yield of **5-7** starting from the common elagolix intermediate **16** and the suitable  $\beta$ -keto esters **36-38** was 13, 9, and 8%, respectively.

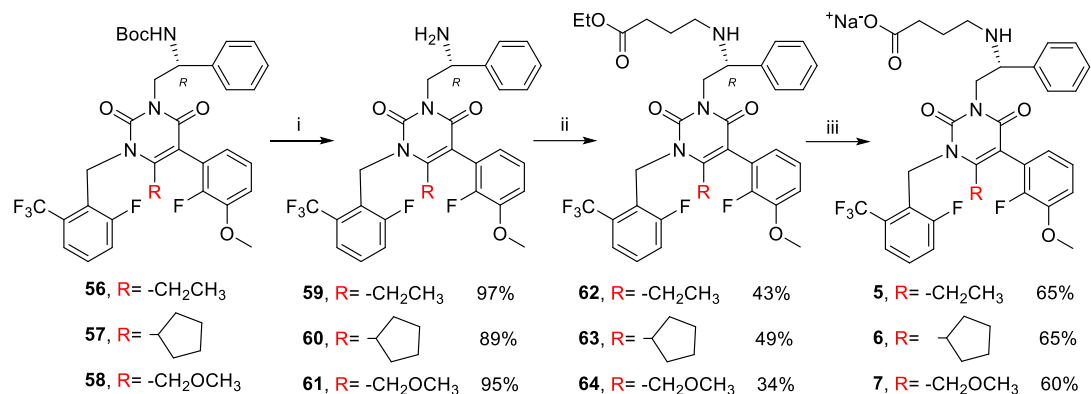


**Figure 63.** Synthesis of **6-7** from **56-58**. Reagents and conditions: (i) TFA, CH<sub>2</sub>Cl<sub>2</sub>, rt; (ii) ethyl 4-bromobutyrate, DIPEA, DMF, 60 °C; (iii) NaOH, H<sub>2</sub>O, ethanol, rt.

Unfortunately, the synthesis of the other planned analogues of **1** (Table 12) as well as a more hindered 6-*tert*-butyl analogue of **1**, are at the moment unsuccessful, but different approaches are under investigation.

### 5.3 Evaluation of the rotational barriers

To investigate the kinetics of the interconversion of the synthesized compounds **5-7**, we employed chiral HPLC. This approach was necessary because the atropisomers of these compounds, along with their synthetic intermediates, could not be separated using achiral methods. Specifically, for an initial understanding of the atropisomer interconversion during the synthesis of **5-7**, we separated small quantities (2 mg) of each atropisomer of **56-58** by preparative chiral HPLC. These compounds represent the first intermediates bearing the crucial biaryl system. Subsequently, we analyzed them over time, stored in the elution mixture (hexane/2-propanol 8:2) at 25 °C, using the same chiral HPLC system. While the atropisomers of **56** and **58** achieved equilibriums within a few hours, those of compound **57** exhibited greater stability. In Figure 64 are reported the chiral HPLC chromatograms of the isolated second atropisomer of **57** analyzed immediately after its separation, and after 42 hours; in Figure 65 is reported the diastereomeric excess of the II atropisomer over time.

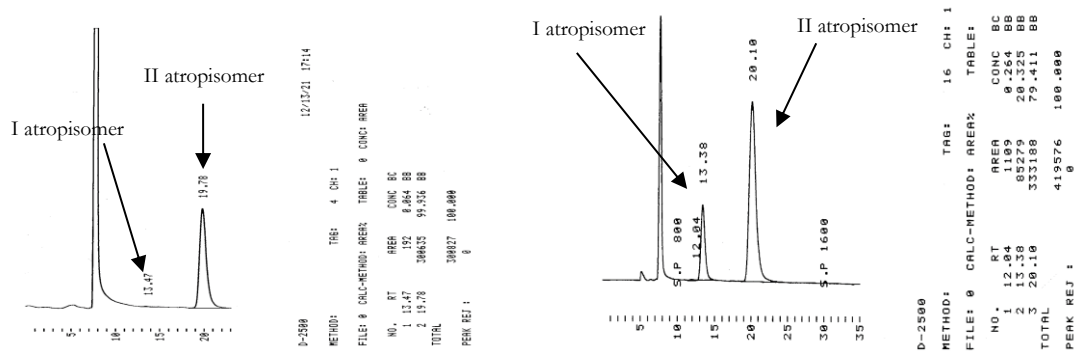
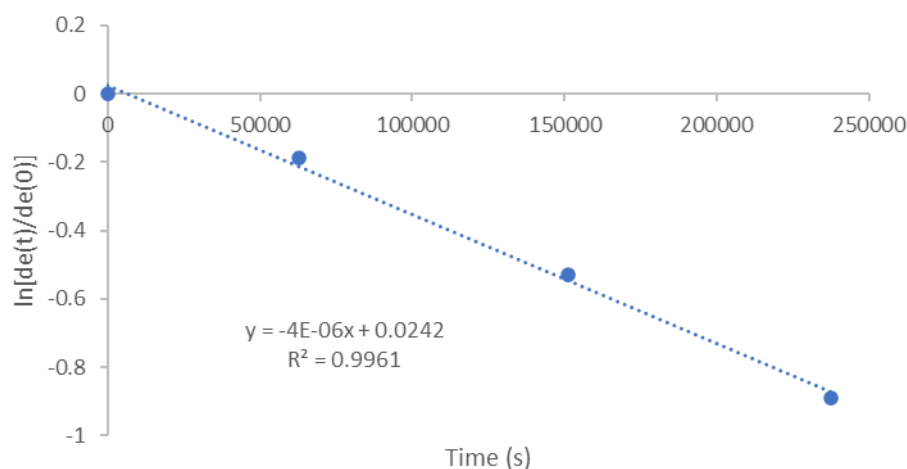


**Figure 64.** HPLC analysis on chiral stationary phase of the II atropisomer of compound **57** immediately after its separation (left) and after 42 hours (right) of storage in a hexane/2-propanol 8:2 mixture.



| t (h) | t (s)  | A%    | B%    | de     | $\ln[de(t)/de(0)]$ |
|-------|--------|-------|-------|--------|--------------------|
| 0     | 0      | 0.999 | 0.001 | 0.9980 | 0                  |
| 17.5  | 63000  | 0.913 | 0.087 | 0.8260 | -0.189158503       |
| 42    | 151200 | 0.794 | 0.206 | 0.5880 | -0.529026328       |
| 66    | 237600 | 0.705 | 0.295 | 0.4100 | -0.889596117       |
| 211   | 759600 | 0.58  | 0.42  | 0.1600 | -1.830579461       |

**Figure 65.** Plot of the logarithm of the relative *de* value  $\{\ln[de(t)/de(0)]\}$  over time (seconds) for interconversion of the II atropisomer of **57** at 25°C in a hexane/2-propanol 8:2 mixture. A% and B% indicate the percent HPLC area of the two atropisomers.

Using the same mathematical tools disclosed in Section 4.5, under these experimental conditions, at 25°C (298 K), the estimated values for  $k$ ,  $\Delta G^\ddagger$ , and  $t_{1/2}$  for the interconversion between the diastereo-atropisomers of **57** was found to be  $2.18 \times 10^{-6} \text{ s}^{-1}$ , 25.2 kcal/mol, and 44 hours, respectively. This result was confirmed analyzing the atropisomers interconversion of **6** with estimated values for  $k$ ,  $\Delta G^\ddagger$ , and  $t_{1/2}$  of  $1.57 \times 10^{-6} \text{ s}^{-1}$ , 25.4 kcal/mol, and 61 hours, respectively. The extrapolated  $t_{1/2}$  of **6** under physiological conditions (37°C) is 10 hours.

This experimental confirmation substantiates that the presence of a bulkier group, such as cyclopentyl, at the 6-position of the uracil moiety results in the formation of two separable and characterizable atropisomers.

## 5.4 Crystallization trials

Following the separation of the two atropisomers of **57**, **60**, **63**, and **6** by preparative chiral HPLC, various crystallization attempts were conducted to acquire single crystals suitable for SC-XRD analysis, with the goal of definitively determining the absolute configuration of the two atropisomers. Despite using different solvents (dichloromethane, chloroform, methanol, ethanol, 2-propanol, acetonitrile, water) on **57**, **60**, **63**, and **6** such as, or on the salt forms (hydrochloride, acetate, and (1*S*)-(+)-3-bromocamphor-10-sulfonate) of **60** and **63** atropisomers, suitable crystals have not been obtained to date. As documented in the literature [169], this difficulty can be attributed to the relatively short interconversion times between the atropisomers.

## 5.5 Biocatalytic approach

At this stage, having in our hands a synthetic route for the synthesis of racemic **6**, the compound that display the highest atropisomeric stability among **5-7**, we directed our efforts toward the challenging task of separating atropisomers. An effective strategy for enantiomer resolution, bypassing the need for costly and time-consuming preparative HPLC on chiral stationary phases or diastereomeric salt crystallizations, involves the use of enzymes [182,183]. It's worth noting that despite the diastereomeric nature of the two atropisomers of **57** and **6**, their separation in HPLC necessitates the use of a chiral stationary phase.

Among the different classes of enzymes, hydrolases (lipases, esterases, proteases, and amidases) has gained growing interest in organic synthesis as they do not need cofactors for their catalytic action, accept a broad range of substrates and, many of them, are commercially available and stable in organic solvents [184,185]. In literature [186] are reported different examples of kinetic resolution of atropisomers catalyzed by enzymes. In particular, an example of a successful resolution of atropisomers on an industrial scale by means of a hydrolase is described in a granted European patent [187] for the production on kilogram scale of PH-797804, which is the atropisomer



(a*S*) endowed with > 100-fold more potency in p38 MAP kinase inhibition than the other one (a*R*) [188]. Starting from a racemic mixture of the suitable methyl-ester intermediate ((±)-PHA-797102), the separation of the two atropisomers was accomplished by means of the commercially available protease Savinase® (Figure 66).

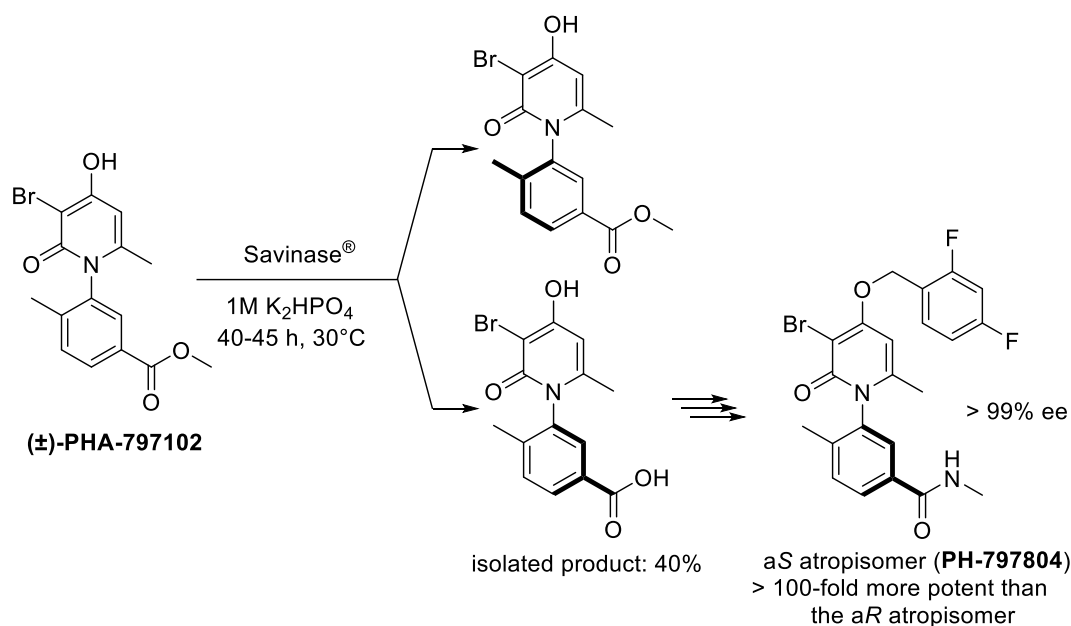


**Figure 66.** Enzymatic hydrolytic resolution of atropisomers described in Ref. [187].

For these reasons, having in our hands the racemic mixtures of the ethyl ester **63** (Figure 63) and the corresponding carboxylate **6** (Figure 63) together with the HPLC analytical methods for monitoring the conversion rate and the optical purity excess, we tested the resolution of **63** using different proteases (Savinase CLEA®, Alcalase CLEA®, protease XIX, protease from bovine pancreas, and protease from *Bacillus licheniformis*), lipases (lipases A and B from *Candida antarctica*, lipase from *Candida rugosa*, and lipase from *Pseudomonas fluorescens*), and esterase from hog liver, under hydrolytic conditions. Among the enzymes tested, lipase B from *Candida antarctica* was the sole enzyme that exhibited activity toward **63**. By conducting the enzyme-catalyzed hydrolysis in di-isopropyl ether saturated with water, we obtained a sample of **63** that was slightly diastereo-atropisomerically enriched (15% *de*) by halting the reaction at 66% conversion (after 20 hours). Due to this not satisfying result, we planned to test if the enzyme-catalyzed *N*-acylation of the free amine intermediate **60** can led to better results. Unexpectedly, during the synthesis of **65**, the *N*-acetyl

derivative of **60**, which is essential as a standard for establishing the analytical methods needed to monitor the conversion and *de* of enzymatic reactions, we discovered that the atropisomers of **65** can be readily separated using silica gel chromatography (see Figure 67).

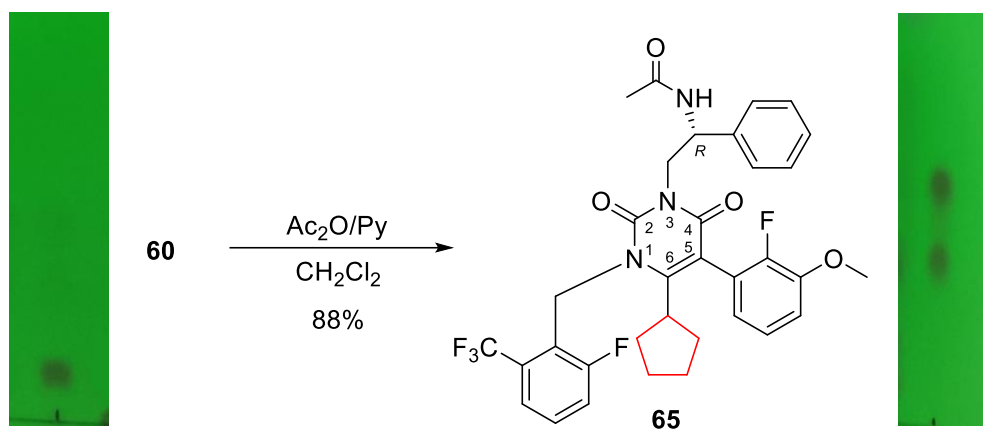


**Figure 67.** Transformation of **60** in its *N*-acetyl derivative **65**, easily separable in its single atropisomers by chromatographic purification over silica gel (eluant: n-hexane/AcOEt 1:1). The TLC analysis of **60** and **65** are reported on the left and the right, respectively.

This method eliminates the necessity for enzymatic, chiral HPLC, or crystallization techniques in separating the atropisomers.

## 5.6 Conclusions

In summary, our search of analogues of **1** with enhanced rotational barriers, led us to substitute the methyl group at the 6-position of the uracil moiety with more sterically hindered substituents. This substitution, supported by QM and MD studies, had the potential to enhance the hindrance to the rotation of the biaryl system in **1**, without significantly compromising its receptor binding affinity. The ability to perform the planned modification was facilitated by the insights gained from our improved synthesis of **1**, where the use of  $\beta$ -keto esters instead of the diketene paved the way for such replacements. Indeed, employing the suitable  $\beta$ -keto esters, synthesized in-house from the readily available Meldrum's acid, led to the obtainment of analogues **5-7**. Among them, the 6-cyclopentyl analogue (**6**) exhibited a longer interconversion time between atropisomers than elagolix, with an experimentally determined  $\Delta G^\ddagger$  of approximately 25.4 kcal/mol. This feature will allow us to perform biological assays on each individual atropisomer. Moreover, derivatizing the free amine intermediate **60** as *N*-acetyl derivative **65**, the atropisomers can be easily separated, in high amounts, by purification on silica gel column chromatography. As part of our future research efforts, since good crystals of the atropisomers of compounds **57**, **60**, **63**, **65** and **6** could not be obtained, we are evaluating the possibility to assign their absolute configuration combining NMR or chiroptical spectroscopy with DFT simulations. Additionally, to experimentally evaluate the rotational barrier between the fast-interconverting atropisomers of compounds **5** and **7**, Dynamic NMR and Dynamic HPLC techniques will be considered. Finally, to further characterize compounds **5-7**, their  $^{19}\text{F}$  NMR spectra will be acquired and studied.

## Chapter 6

### Elagolix analogues modified at 21-position

After establishing the atropisomeric nature of compound **1** and striving to identify analogs with elevated rotational barriers, we explored existing literature to ascertain if compounds, structurally similar to **1**, sharing both unknown atropisomeric and biological traits were documented. In this pursuit, we isolated and synthesized derivative **14**, featuring a bromine atom at the 21-position (Figure 68) described as an intermediate for tritium-labeled **1** in 2021 [189], with the aim of investigating its potential atropisomeric properties.

#### 6.1 Synthesis and analytical characterization

The synthesis of compound **14** was carried out as reported in the literature (Figure 68) [189] starting from compound **20**, an intermediate of the synthesis of **1**, thus available in our lab (Section 3.1).

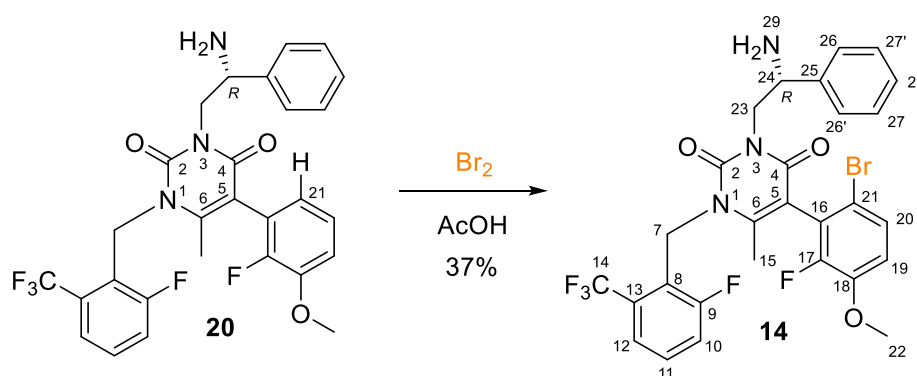
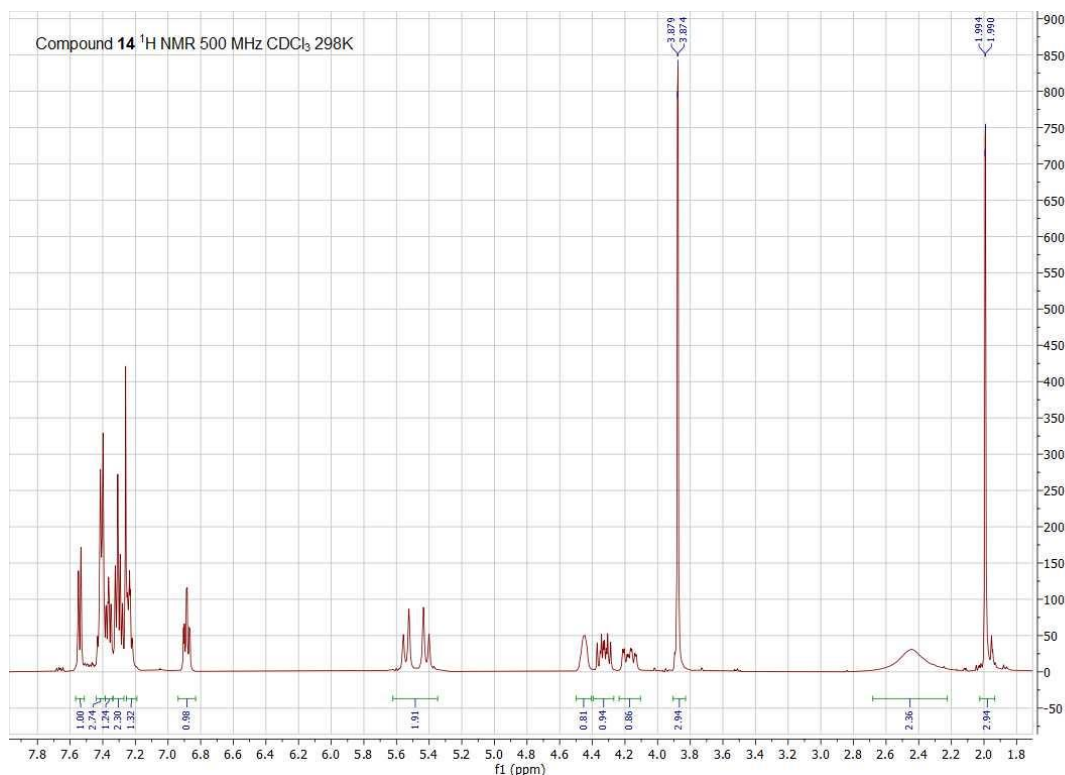


Figure 68. Synthesis of compound **14**.

The obtained compound **14** was characterized through NMR and chiral HPLC techniques to identify the possible presence of atropisomerism, not addressed in the literature reference [189]. The high-resolution  $^1\text{H}$  NMR analysis displayed two set of signals, although quite superimposed, for the H-15 (1.994 and 1.990 ppm) and H-22 (3.879 and 3.874 ppm) protons (Figure 69).



**Figure 69.**  $^1\text{H}$  NMR of compound **14**.

The same pattern was observed for some  $^{13}\text{C}$  resonances. To confirm the obtained chemical structure, the assignment of all the  $^1\text{H}$  and  $^{13}\text{C}$  resonances was carried out (Table 13).

**Table 13.**  $^1\text{H}$  and  $^{13}\text{C}$  NMR chemical shifts (ppm) <sup>a</sup> and coupling constants (Hz) <sup>b</sup> data of **14**.

| Atom           | $^1\text{H}$  | $^{13}\text{C}$                                       |
|----------------|---|---|
| 1              | /   | /   |
| 2              | /   | 152.3 (brs)   |
| 3              | /   | /   |
| 4              | /   | 160.8 and 160.7 *                                     |
| 5              | /   | 108.4   |
| 6              | /   | 150.60 and 160.56 *                                   |
| AB Spin System |   |   |
| 7              | 5.54 (d, $J=17.3$ Hz, $\text{H}_b$ ) and 5.42 (d, $J=17.4$ Hz, $\text{H}_a$ ) | 42.8 (brs)  |
| 8              | /   | 122.0 (dd, $J=11.2$ and 4.8 Hz)                       |
| 9              | /   | 161.34 (d, $J=249.8$ Hz)                              |
| 10             | 7.26 (nd, overlapped with 27 and 27', 28, and $\text{CDCl}_3$ )               | 121.0 (d, $J=24.1$ Hz)                                |
| 11             | 7.41 (nd, overlapped with 26 and 26')   | 129.4 (d, $J=9.6$ Hz)                                 |
| 12             | 7.54 (d, $J=7.8$ Hz)  | 122.6 (m)   |
| 13             | /   | 129.2 (dd, $J=31.3$ and 3.8 Hz)                       |
| 14             | /   | 123.5 (dd, $J=274.3$ and 3.6 Hz)                      |
| 15             | 1.993 (s) and 1.991 (s) *   | 17.53   |
| 16             | /   | 123.96 (d, $J=16.7$ Hz) and 123.93 (d, $J=16.7$ Hz) * |

|            |  |  |
|------------|--|--|
| 17         | /  | 150.80 (d, $J=248.9$ Hz) and<br>150.77 (d, $J=248.9$ Hz) * |
| 18         | /  | 122.00 (d, $J=4.7$ Hz) and 121.91<br>(d, $J=4.8$ Hz) *     |
| 19         | 6.88 (td, $J=8.7, 2.8$ Hz)   | 114.5 (brs)  |
| 20         | 7.36 (ddd, $J=8.4, 6.2, 1.8$ Hz)                                   | 127.59 and 127.56 *  |
| 21         | /  | 116.12   |
| 22         | 3.88 (s) and 3.87 (s) *  | 56.4   |
| 23         | 4.39 – 4.27 (H <sub>b</sub> ) and 4.24 – 4.11<br>(H <sub>a</sub> ) | 48.9 and 48.8 *  |
| 24         | 4.45 (m)   | 54.2 and 54.0 *  |
| 25         | /  | 142.4 (brs)  |
| 26 and 26' | 7.41 (nd, overlapped with 11)                                      | 126.6 and 126.5 *  |
| 27 and 27' | 7.31 (nd, overlapped with 12)                                      | 128.5 (brs)  |
| 28         | 7.24 (m)   | 127.43 and 127.41 *  |
| 29         | 2.44 (brs)   | /  |

nd =  $J(H,H)$  were not determined due to the overlapping. <sup>a</sup> Assignments from  $^1H-^1H$  COSY, HSQC, and HMBC data in  $CDCl_3$  at 298K. Coupling constants were obtained by direct inspection of the spectra. Experimental error in the measured  $^1H-^1H$  coupling constants was  $\pm 0.5$  Hz. \* The two signals are due to the presence of two atropisomers.

This preliminar indication of the presence of atropisomerism was further confirmed carrying out a chiral HPLC analysis employing an amylose tris (3,5-dimethylphenylcarbamate) based stationary phase: two compounds, in a 1:1 ratio, are well detectable (Figure 70).

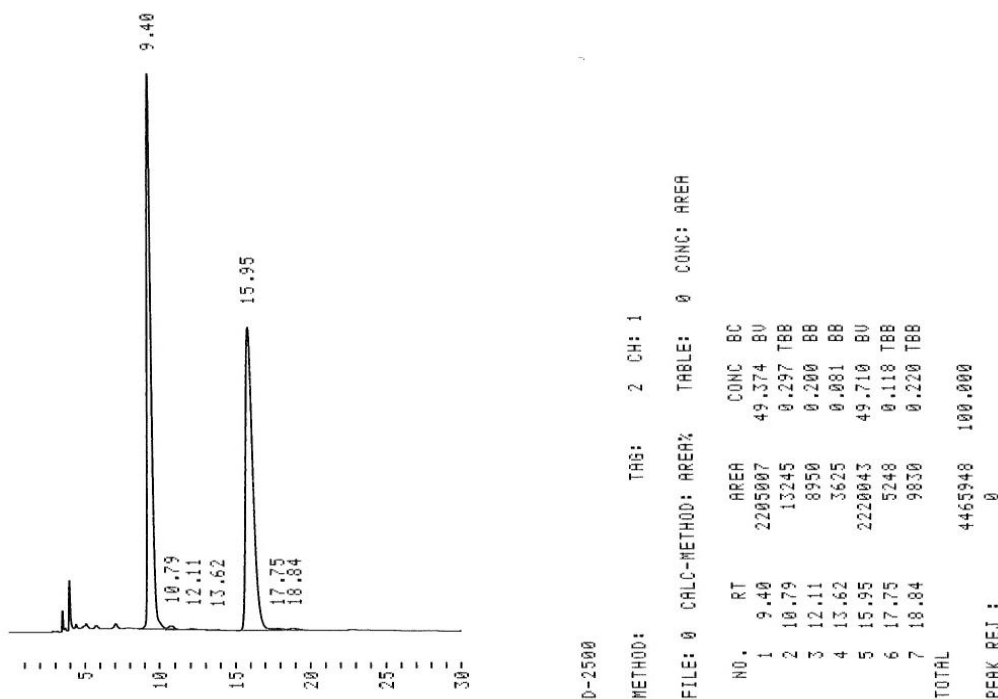


**Figure 70.** HPLC analysis of **14** on an amylose tris (3,5-dimethylphenylcarbamate) based stationary phase.

After establishing that compound **14** comprises two atropisomers, we conducted their separation using preparative HPLC to assess their thermal stability (Figure 71).

During a one-month duration at 25°C and 24 hours under reflux (82°C) in 2-propanol, no interconversion was observed for either isomer. Additionally, no interconversion took place even at 150°C in DMSO after 24 hours. As a result, the extrapolated energy barrier was determined to be higher than 36 kcal/mol [135].

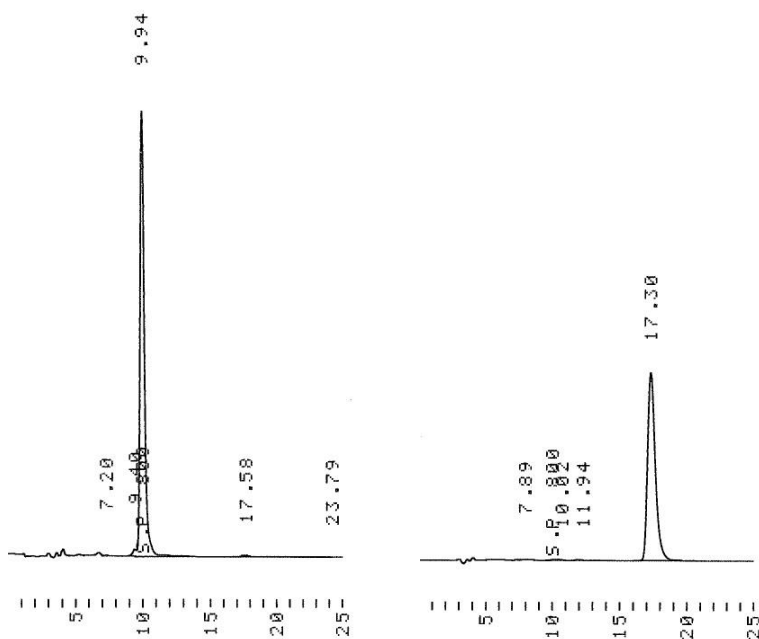


**Figure 71.** Chiral HPLC analyses of the two separated atropisomers of **14**.

Currently, our objective is to investigate whether thermally stable atropisomers are more readily crystallizable than hemistable ones. Additionally, we aim to assign the absolute configuration through single-crystal X-ray diffraction (SC-XRD). To achieve this, we are conducting crystallization trials as outlined in Sections 4.6 and 5.4.

Furthermore, these two isolated atropisomers will undergo biological testing to determine their activity and assess whether there is a variation in potency between the two isomers.

## 6.2 Biocatalytic approach

Since we have found that the individual atropisomers of **14** cannot be separated by achiral methods as compounds **3** and **4**, even after derivatization which had proven

effective on the free amine intermediate of **6**, a separation catalyzed by an enzyme could be a viable alternative to the long and expensive processes that characterize preparative HPLC, as already discussed in Section 5.5. In particular, compound **14** meets our need for highly stable atropisomers to apply this approach to their separation. Additionally, literature reports an example of successful enzyme-catalyzed atropisomer resolution of binaphthyl amine through *N*-acylation, as illustrated in Figure 72.

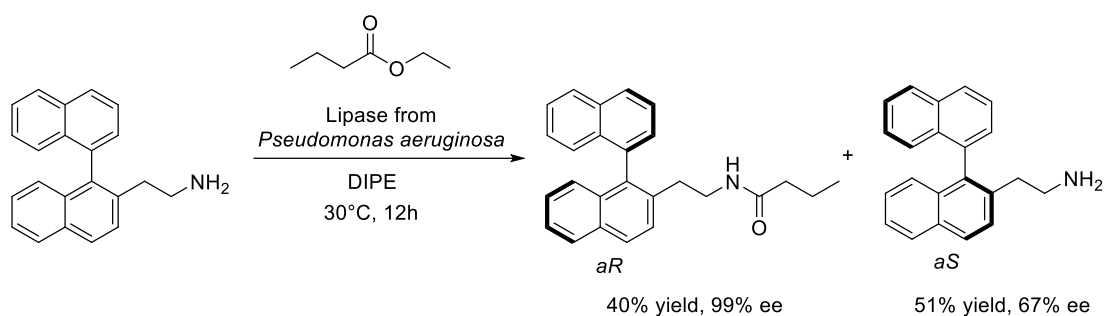


**Figure 72.** Literature example of enzyme-catalyzed resolution of binaphthyl amine.

In this context, we are exploring the potential utilization of the high stereoselectivity offered by biocatalysts for the separation of the atropisomers of compound **14** (Figure 73). In particular, the lipase- (lipases A and B from *Candida antarctica*, lipase from *Candida rugosa*, and lipase from *Pseudomonas fluorescens*) or protease- (Alcalase, Subtilisin, and protease from *Bacillus licheniformis*) catalyzed *N*-acylation of **14** (Table 14) or hydrolysis or alcoholysis of the *N*-acyl derivatives of **14** (Table 15) are under evaluation. For the time being the best preliminary result was obtained employing the lipase B from *Candida antarctica* in ethyl acetate: a diastereo-atropisomerically enriched sample of **14** (34% *de*) was obtained stopping the reaction at 77% conversion (Table 14). Despite the not satisfactory results achieved so far, the enzymes have demonstrated some ability to differentiate between the two atropisomers of **14**. Consequently, the research will continue, aiming to enhance diastereo-atroposelection by exploring alternative reaction conditions such as solvents, acyl donors, temperatures, concentration, and more.



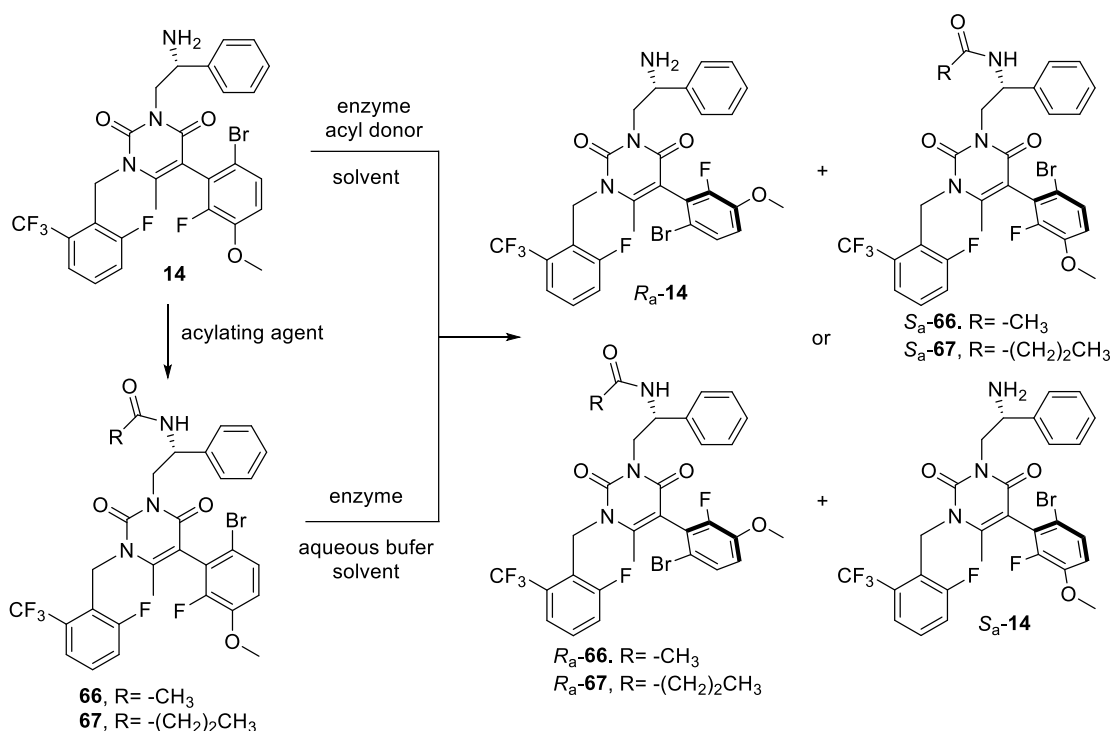


**Figure 73.** Schematic representation of the enzymatic separation of the atropisomers of compound **14** under evaluation. The outcome of the enzymatic reaction is a mixture of the free amine of one atropisomer and the amide derivative of the other.

**Table 14.** Enzyme-catalyze *N*-acylation of **14**.

| Entry | Solvent        | Enzyme                                      | Acyl donor  | Time (h) | T(°C) | de <b>14</b> <sup>a</sup> | de <b>66</b> <sup>a</sup> | de <b>67</b> <sup>a</sup> | Conv% <sup>a</sup> | E <sup>b</sup> |
|-------|----------------|---|---|----------|-------|---------------------------|---------------------------|---------------------------|--------------------|----------------|
| 1     | DIPE           | CAL B                                       | PrCO <sub>2</sub> CH <sub>2</sub> CF <sub>3</sub> | 24       | rt    | 0                         | /                         | /                         | 0                  | /              |
| 2     | Toluene        | CAL A                                       | PrCO <sub>2</sub> CH <sub>2</sub> CF <sub>3</sub> | 48       | rt    | 4                         | /                         | 9                         | 30                 | 1              |
| 3     | Amylic alcohol | Protease from <i>Bacillus licheniformis</i> | PrCO <sub>2</sub> CH <sub>2</sub> CF <sub>3</sub> | 24       | 45    | 0                         | /                         | 0                         | 15                 | 0              |
| 4     | AcOEt          | CAL B                                       | AcOEt   | 72       | rt    | 0.34                      | 0.10                      | /                         | 77                 | 2              |
| 5     | AcOEt          | CAL A                                       | AcOEt   | 72       | rt    | 0                         | /                         | /                         | 0                  | /              |
| 6     | AcOEt          | CRL   | AcOEt   | 72       | rt    | 0                         | /                         | /                         | 0                  | /              |
| 7     | AcOEt          | PFL   | AcOEt   | 72       | rt    | 0                         | /                         | /                         | 0                  | /              |
| 8     | PrCOOBu        | CAL B                                       | PrCOOBu   | 168      | rt    | 0.06                      | /                         | 0.08                      | 43                 | 1              |
| 9     | PrCOOBu        | CAL A                                       | PrCOOBu   | 168      | rt    | 0.09                      | /                         | 0.06                      | 60                 | 1              |
| 10    | PrCOOBu        | CRL   | PrCOOBu   | 168      | rt    | 0.22                      | /                         | 0.24                      | 48                 | 2              |
| 11    | PrCOOBu        | PFL   | PrCOOBu   | 168      | rt    | 0.17                      | /                         | 0.26                      | 40                 | 2              |

<sup>a</sup> Determined by chiral HPLC; <sup>b</sup> E = ln[1 - conv(1 + de(product))] / ln[1 - conv(1 - de(product))].

**Table 15.** Enzyme-catalyze hydrolysis or alcoholysis of **66** or **67**.

| Entry | Substrate | Enzyme        | Solvent <sup>a</sup> | Time (h) | T(°C) | de <b>14</b> <sup>b</sup> | de <b>66</b> <sup>b</sup> | de <b>67</b> <sup>b</sup> | Conv% <sup>b</sup> | E <sup>c</sup> |
|-------|-----------|---------------|----------------------|----------|-------|---------------------------|---------------------------|---------------------------|--------------------|----------------|
| 1     | <b>79</b> | CAL B         | pH 9/TBME            | 168      | 47    | /                         | /                         | 0                         | trace              | /              |
| 2     | <b>79</b> | CAL A         | pH 9/TBME            | 168      | 47    | /                         | /                         | 0                         | trace              | /              |
| 3     | <b>79</b> | CRL           | pH 9/TBME            | 168      | 47    | /                         | /                         | 0                         | 0                  | /              |
| 4     | <b>79</b> | PFL           | pH 9/TBME            | 168      | 47    | /                         | /                         | 0                         | 0                  | /              |
| 5     | <b>79</b> | Savinase CLEA | pH 9/TBME            | 168      | 47    | /                         | /                         | 0                         | 0                  | /              |

|    |    |                                |            |     |    |   |   |   |   |   |
|----|----|--------------------------------|------------|-----|----|---|---|---|---|---|
| 6  | 79 | Alcalase CLEA<br>Protease from | pH 9/TBME  | 168 | 47 | / | / | 0 | 0 | / |
| 7  | 79 | Bacillu<br>licheniformis       | pH 9/TBME  | 168 | 47 | / | / | 0 | 0 | / |
| 8  | 78 | CAL B                          | pH 7.5/THF | 24  | rt | / | 0 | / | 0 | / |
| 9  | 79 | CAL B                          | pH 7.5/THF | 24  | rt | / | / | 0 | 0 | / |
| 10 | 79 | CAL A                          | pH 7.5/THF | 24  | rt | / | / | 0 | 0 | / |
| 11 | 79 | Alcalase CLEA                  | pH 7.5/THF | 24  | rt | / | / | 0 | 0 | / |
| 12 | 78 | CAL B                          | pH 7.5/THF | 47  | rt | / | 0 | / | 0 | / |
| 13 | 79 | CAL B                          | pH 7.5/THF | 47  | rt | / | / | 0 | 0 | / |
| 14 | 79 | CAL A                          | pH 7.5/THF | 47  | rt | / | / | 0 | 0 | / |
| 15 | 79 | Alcalase CLEA                  | pH 7.5/THF | 47  | rt | / | / | 0 | 0 | / |
| 16 | 78 | CAL B                          | i-PrOH     | 168 | /  | / | 0 | / | 0 | / |
| 17 | 79 | CAL B                          | i-PrOH     | 168 | /  | / | / | 0 | 0 | / |
| 18 | 79 | CAL A                          | i-PrOH     | 168 | /  | / | / | 0 | 0 | / |
| 19 | 79 | Alcalase CLEA                  | i-PrOH     | 168 | /  | / | / | 0 | 0 | / |

<sup>a</sup>The indicated pH refers to the phosphate buffer utilized; <sup>b</sup>Determined by chiral HPLC;

<sup>c</sup> $E = \ln[1 - \text{conv}(1 + de(\text{product}))] / \ln[1 - \text{conv}(1 - de(\text{product}))]$ .

### 6.3 Conclusions

Concerning the modification at the 21-position of **1**, it can be asserted that it is suitable for achieving atropisomers with high thermal stability. Notably, compound **14**, a derivative used in the literature to synthesize a tritium-labeled derivative of **1** featuring a bulky bromine at the 21-position, still has unknown atropisomeric and biological characteristics. We disclosed that **14** comprised two distinct and thermally stable atropisomers ( $\Delta G^\ddagger > 36$  kcal/mol), isolable through preparative chiral HPLC, which will undergo biological assessments to determine whether they exhibit distinct pharmaceutical activities. Additionally, crystallization and biocatalytic experiments are underway to determine the absolute configuration and explore more efficient methods for producing significant amounts of the two atropisomers.

## Chapter 7

### Biological assays

---

The biological evaluation of the synthesized compounds is currently underway thanks to a collaborative effort with Prof. M. Bonomi, Dr. V. Vezzoli of Istituto Auxologico Italiano, and Prof. Roberto Maggi at the Department of Pharmaceutical Sciences, University of Milan.

To set up the experimental conditions for testing the activity of compounds **3-7** and **14**, we performed preliminary experiments using **1**, the reference GnRH1R-ant prepared by us as described in Section 3.1.

The cDNA of *hGnRH1R* (UniProt accession P30968) wild type, generously provided by Prof. L. Casarini and Dr. S. Sperduti at the Unit of Endocrinology, University of Modena and Reggio Emilia, was sub-cloned into pcDNA3.1 (+) expression vector with a HA signal and expressed in HEK293T cells.

The modulation of the *hGnRH1R* response by the modulators was assessed by quantifying and comparing the accumulation of inositol monophosphate (IP) in cells. This comparison involves cells treated solely with the GnRH peptide versus those pre-treated with GnRHR modulators followed by treatment with the GnRH peptide.

GnRH1R, likely other G-protein-coupled receptors (GPCRs), is a transmembrane protein pivotal in extracellular stimulus signal transduction. This receptor forms intricate assemblies with intracellular proteins, regulating diverse signaling pathways. Specifically, the activation of Gq-coupled receptors is indicated by the production of inositol 1,4,5-triphosphate (IP3). However, due to IP3 short half-life, is much more convenient monitoring inositol monophosphate (IP1), a downstream metabolite of IP3 (Figure 74) [190]. Thus, monitoring GnRH1R activity by IP accumulation is a functional assay. Functional assays allow compounds that modulate GPCR function, such as agonists and allosteric modulators, to be differentiated from antagonists within

a cell context. When conducting primary screening campaigns, functional assays are usually preferred over binding assays [190].

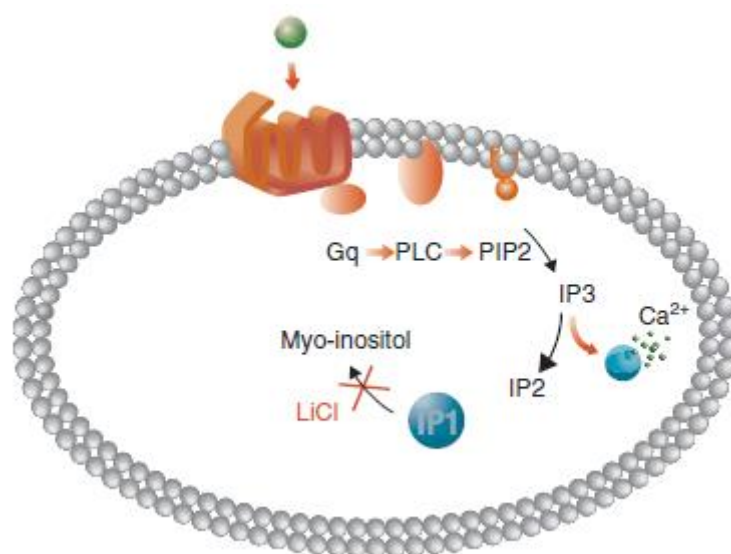


**Figure 74.** Downstream metabolites triggered by Gq-coupled receptors activation. LiCl inhibits IP1 degradation. Image taken from Ref. [190].

IP accumulation was determined using the commercially available Cisbio IP1 assay kit after cell lysis. In Figure 75 are reported the data obtained from **1**

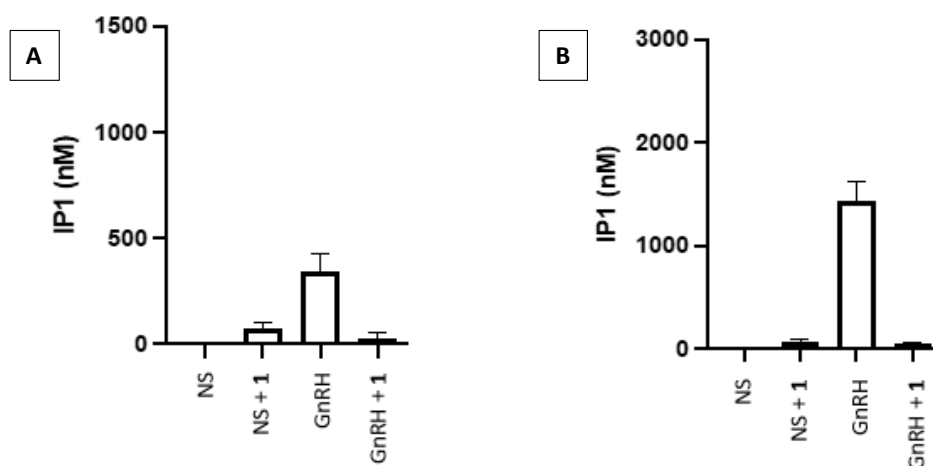


**Figure 75.** Antagonist (**1**, 10<sup>-4</sup>M) response of *h*GnRH1R stimulated by 10<sup>-6</sup>M (A) and 10<sup>-4</sup>M (B) GnRH agonist determined by IP assays. NS= not stimulated. Data were represented as the mean ± SEM from three independent experiments.

The obtained data for **1** (Figure 75) agreed with that reported in the literature [43]: at 10<sup>-4</sup> M concentration, **1** is able to suppress *h*GnRH1R functionality.

As soon as we improve the efficiency of transfection and the homogeneity in the expression between the cells, we will analyze the new compounds either as an atropisomeric mix or as individual atropisomers.

## Chapter 8

### Conclusions and future perspectives

---

In conclusion, our investigations successfully confirmed the presence of atropisomerism of **1**, the first approved oral GnRHR-ant. In order to characterize this phenomenon, it was necessary to perform an improved synthesis of **1** and a comprehensive analysis of its conformational characteristics using spectroscopic, analytical, and theoretical methods that contributed to bring out new insights for the identification and characterization of atropisomers of **1**. The data allowed to categorize them within the challenging atropisomeric class two, according to LaPlante's classification [133].

On the same time, to obtain a high pure sample of **1** for the setup of the biological assays, we improved the synthetic route by exploring innovative strategies to enhance the purity and the reaction yields of the product and its intermediates. Additionally, we developed a novel chiral HPLC method, able to discriminate the atropisomers, and to monitor the chemical and optical purity of **1** and its synthetic intermediates. We also conducted a thorough assignment of the  $^1\text{H}$ ,  $^{13}\text{C}$ , and  $^{15}\text{N}$  NMR signals; these NMR data, supported by the conformational analysis experiments, enabled the determination of the stereochemical profile of the two atropisomers of **1**, detectable in solution.

This optimized synthetic pathway demonstrated its applicability in synthesizing selected analogues, designed with the aid of molecular modelling techniques. In particular, the modification of the substituents at the 4-, 6-, or 21-position led to the enhancement of the rotational barriers with respect to **1**. Four new derivatives exhibited a rotational barrier higher than **1**, enabling the separation and the examination of the individual atropisomers, by means of different analytical techniques. The atropisomers of **3**, **4**, and **6** displayed a slow interconversion rate at room temperature, with an experimentally evaluated  $\Delta G^\ddagger$  of 24-25 kcal/mol. Atropisomers of **14** exhibited markedly increased stability compared to the previous compounds, as evidenced by an extrapolated  $\Delta G^\ddagger$  exceeding 36 kcal/mol.

Remarkably, molecular dynamics simulations conducted on the new designed compounds revealed a good receptor affinity, particularly for **3** and **4**, also greater than **1**.

To investigate this aspect, biological tests on HEK-293 cells expressing *hGnRH1R*, utilizing the IP-One ELISA kit, were set up for **1**, the reference compound. Further assays will subsequently be conducted on the newly developed analogues, and the individual atropisomers, in order to provide insights into their distinct biological properties.

Overall, these findings could have a crucial role in elucidating the structural determinants that govern the spatial arrangement of substituents within compound **1** and its analogues. This knowledge, along with the biological assays being carried out, is instrumental for the future development of single atropisomer drugs, with improved pharmacological properties.

The modifications carried out at the 4-, or 6-, or 21-position of the elagolix scaffold could also be combined to develop improved derivatives.

Given the increasing interest in novel orally active small molecules as modulators of GnRHR, this approach could be followed to limit the therapeutic use of peptide modulators having a less-than-optimal pharmacokinetic profiles.

## Chapter 9

### Materials and methods

---

#### 9.1 Computational methods

The computational studies were performed in collaboration with Prof. Giovanni Grazioso and Dr. Enrico Mario Alessandro Fassi at the Department of Pharmaceutical Sciences, University of Milan in Italy.

##### 9.1.1 QM investigations

The conformational space of the simplified systems reported in Sections 4.1 and 5.1 were analyzed by scanning the dihedral angle,  $\tau_1$ , responsible for the generation of the atropisomers. In particular, the energy of the conformations generated by rotating by  $10^\circ$  the  $\tau_1$  dihedral angle were calculated at B3LYP/6-31g(d,p) level of QM calculations. The attained plot led us to retrieve the rough geometry of the energy minima and the ones of transition states to be further refined by QM calculations at higher level of theory (B3LYP/aug-cc-PVTZ). Vibrational frequencies were computed at this level of theory to confirm whether the structures correspond to a minimum or a transition state.

The calculated harmonic frequencies (first 5, for sake of simplicity) for the simplified systems of compounds **1**, **2**, **5**, and **6** are reported below. The 1<sup>st</sup> and 2<sup>nd</sup> transition states are associated with the interaction between the *ortho*-fluorine and the substituents at the 4- and 6-positions of the uracil moiety, respectively.

| Compound <b>1</b> |                                  |                      |                                  |                      |
|-------------------|----------------------------------|----------------------|----------------------------------|----------------------|
| Entry             | 1 <sup>st</sup> Transition state |                      | 2 <sup>nd</sup> Transition state |                      |
|                   | vibrational frequencies          | infrared intensities | vibrational frequencies          | infrared intensities |
| 1                 | -58.41                           | 0.0636               | -79.37                           | 1.5455               |
| 2                 | 53.71                            | 0.3085               | 51.14                            | 0.4191               |
| 3                 | 71.84                            | 0.7145               | 60.58                            | 0.3790               |
| 4                 | 82.87                            | 0.0516               | 88.19                            | 4.1981               |
| 5                 | 106.10                           | 8.5107               | 106.60                           | 2.8610               |



| Compound 2 |                                  |                      |                                  |                      |
|------------|----------------------------------|----------------------|----------------------------------|----------------------|
| Entry      | 1 <sup>st</sup> Transition state |                      | 2 <sup>nd</sup> Transition state |                      |
|            | vibrational frequencies          | infrared intensities | vibrational frequencies          | infrared intensities |
| 1          | -47.37                           | 0.1455               | -68.54                           | 1.2551               |
| 2          | 57.22                            | 0.6733               | 55.63                            | 0.4867               |
| 3          | 69.30                            | 1.5364               | 60.46                            | 0.9882               |
| 4          | 104.07                           | 7.7431               | 96.98                            | 9.4343               |
| 5          | 135.85                           | 1.1211               | 126.41                           | 1.3432               |

| Compound 5 |                                  |                      |                                  |                      |
|------------|----------------------------------|----------------------|----------------------------------|----------------------|
| Entry      | 1 <sup>st</sup> Transition state |                      | 2 <sup>nd</sup> Transition state |                      |
|            | vibrational frequencies          | infrared intensities | vibrational frequencies          | infrared intensities |
| 1          | -63.48                           | 0.0573               | -65.19                           | 1.0053               |
| 2          | 47.87                            | 0.3639               | 50.29                            | 0.1666               |
| 3          | 58.57                            | 0.0523               | 62.77                            | 0.7982               |
| 4          | 69.52                            | 0.0344               | 83.23                            | 0.9765               |
| 5          | 101.95                           | 5.0034               | 94.35                            | 2.0043               |

| Compound 6 |                                  |                      |                                  |                      |
|------------|----------------------------------|----------------------|----------------------------------|----------------------|
| Entry      | 1 <sup>st</sup> Transition state |                      | 2 <sup>nd</sup> Transition state |                      |
|            | vibrational frequencies          | infrared intensities | vibrational frequencies          | infrared intensities |
| 1          | -48.61                           | 0.0280               | -56.78                           | 0.5114               |
| 2          | 49.89                            | 0.0147               | 46.66                            | 0.0500               |
| 3          | 52.88                            | 0.2569               | 56.33                            | 0.3727               |
| 4          | 68.23                            | 0.0596               | 77.55                            | 0.2534               |
| 5          | 75.64                            | 0.3871               | 86.32                            | 0.3572               |

## 9.1.2 Conformational analysis of 1

These studies were performed using the tools available in Maestro (release 2021-2, Schrödinger, LLC, New York, NY, USA). The simplified structure of **1** (Section 3.5) was created by means of the “Build” tool; the potential energy of the conformers, resulting from the different combination of the  $\tau_1$ – $\tau_4$  values, was calculated with the “Coordinate scan” tool of Macromodel, using the OPLS4 force field and choosing the proper couple of torsional angles to be scanned in the calculations. The plots were obtained by the “plot coordinate scan” tool of Macromodel, focusing the displayed energy values from 0 to 5 kcal/mol. Then, all the energy minima identified by

Macromodel, or manually constructed rotating the dihedral angles indicated, were optimized by using Jaguar, at the DFT/B3LYP-D3/6-31G(\*\*) level of theory [171,172]. In the table reported below, the geometrical features, relative energy values and equilibrium percentages of the predicted conformations in the gas phase, as resulting after geometry optimization are indicated:

| Conformers | $\tau_1$ (°) | $\tau_2$ (°) | $\tau_3$ (°) | $\tau_4$ (°) | Gas Phase $\Delta E$<br>(kcal/mol) | Gas Phase (%) |
|------------|--------------|--------------|--------------|--------------|------------------------------------|---------------|
| 1          | -81.6        | -48.5        | -132.0       | 49.1         | 4.35                               | 0.0           |
| 2          | -70.0        | 147.8        | -130.0       | 49.7         | 6.84                               | 0.0           |
| 3          | 96.0         | -54.0        | -125.0       | 70.0         | 0.67                               | 20.5          |
| 4          | 111.8        | 134.3        | -133.0       | 52.5         | 4.60                               | 0.0           |
| 5          | -80.5        | -47.0        | -61.3        | -52.4        | 4.67                               | 0.0           |
| 6          | -69.4        | 150.3        | -55.0        | -55.5        | 7.09                               | 0.0           |
| 7          | 113.0        | 136.0        | -60.5        | -55.6        | 5.01                               | 0.0           |
| 8          | 93.2         | -62.1        | -64.1        | -55.6        | 1.90                               | 2.6           |
| 9          | 94.5         | -53.6        | 61.3         | -142.6       | 2.26                               | 1.4           |
| 10         | 118.5        | 147.4        | 59.4         | -140.8       | 4.86                               | 0.0           |
| 11         | -74.0        | -40.3        | 67.8         | -141.2       | 4.78                               | 0.0           |
| 12         | -69.1        | 148.9        | 60.5         | -142.9       | 3.69                               | 0.1           |
| 13         | 92.6         | -61.9        | -110.0       | -134.5       | 0.00                               | 63.9          |
| 14         | 113.6        | 146.5        | -77.5        | 147.4        | 3.98                               | 0.1           |
| 15         | -85.9        | -51.6        | -115.4       | -136.4       | 3.58                               | 0.2           |
| 16         | -70.9        | 148.7        | -75.9        | 146.3        | 5.33                               | 0.0           |
| 17         | -81.0        | -46.4        | -75.4        | 142.8        | 3.64                               | 0.1           |
| 18         | -71.1        | 148.9        | -75.2        | 147.0        | 5.40                               | 0.0           |
| 19         | 92.7         | -55.0        | -76.1        | 139.9        | 1.09                               | 10.1          |
| 20         | 113.9        | 146.9        | -77.6        | 147.5        | 3.93                               | 0.1           |
| 21         | -86.3        | -49.9        | 56.0         | 53.0         | 4.53                               | 0.0           |
| 22         | -70.1        | 145.9        | 51.1         | 55.2         | 3.67                               | 0.1           |
| 23         | 93.5         | -53.5        | 49.9         | 53.8         | 2.77                               | 0.6           |
| 24         | 114.2        | 142.7        | 51.3         | 53.6         | 5.32                               | 0.0           |

The relative energies and equilibrium percentages of the optimized conformations endowed with  $\Delta E < 5$  kcal/mol in the gas phase, in water and methanol solvent models are reported below:

| Conformers | Water $\Delta E$<br>(kcal/mol) | Water (%) | Methanol $\Delta E$<br>(kcal/mol) | Methanol (%) |
|------------|--------------------------------|-----------|-----------------------------------|--------------|
| 1          | 4.65                           | 0.0       | 4.68                              | 0.0          |
| 3          | 0.84                           | 18.4      | 0.73                              | 21.2         |
| 4          | 4.74                           | 0.0       | 4.72                              | 0.0          |
| 5          | 7.88                           | 0.0       | n.c.                              | n.c.         |
| 8          | 2.54                           | 1.0       | 2.52                              | 1.0          |

|    |      |      |      |      |
|----|------|------|------|------|
| 9  | 2.66 | 0.9  | 2.64 | 0.8  |
| 10 | 5.68 | 0.0  | n.c. | n.c. |
| 11 | 5.42 | 0.0  | n.c. | n.c. |
| 12 | 4.61 | 0.0  | 4.58 | 0.0  |
| 13 | 0.00 | 75.6 | 0.00 | 73.0 |
| 15 | 4.22 | 0.1  | 4.20 | 0.1  |
| 17 | 4.45 | 0.0  | 4.43 | 0.0  |
| 19 | 1.93 | 2.9  | 1.92 | 2.9  |
| 20 | 4.30 | 0.1  | 4.28 | 0.1  |
| 21 | 4.59 | 0.0  | 4.58 | 0.0  |
| 22 | 4.27 | 0.1  | 4.32 | 0.0  |
| 23 | 2.75 | 0.7  | 2.74 | 0.7  |

n.c. = not calculated.

The lowest energy conformer (13, highlighted in yellow), of the simplified structure of **1**, was used to investigate the  $\tau_5$  torsion angle, by an increment of  $10^\circ$  (from  $-180^\circ$  to  $+180^\circ$ ). The obtained conformers were contextually optimized at DFT/B3LYP-D3/6-31G(\*\*) level of theory, using the CPCM water solvent model (Table 7, Section 3.5). Single point calculations using the CPCM methanol solvent displayed results similar to those observed using the CPCM water solvent model.

### 9.1.3 Preparation of the computational complex model

The complex of the *h*GnRH1R with **1** was retrieved from the Protein Data Bank, with accession code 7BR3 [43]. The mutated residue Lys<sup>128</sup> was changed to proline in order to restore the wild-type protein. The missing loops Gln<sup>65</sup>–Ser<sup>74</sup>, Thr<sup>144</sup>–Asn<sup>152</sup> and Leu<sup>183</sup>–Val<sup>192</sup> were built by homology modelling using the SWISS-MODEL workspace web-tool [191,192]. The structure of the human oxytocin receptor (PDB entry 6TPK) was used as a template, due to its good structural similarity with GnRH1R (58% sequence identity) [193]. After alignment, an RMSD value of 2.8 Å was obtained considering the backbone atoms, calculated using the Protein Structure Alignment tool, implemented in the Maestro Schrödinger suite (release 2021–2, Schrödinger, LLC, New York, USA). The resulting model was then optimized and minimized using the Protein Preparation Wizard tool of Maestro software, applying the default parameters. This tool allowed us to: (1) complete the complex structure by adding the missing hydrogens and creating the disulfide bonds, (2) check the protonation state of the residues at pH 7.0, (3) remove the atomic clashes, and (4) assign the OPLS4 force field [194].

### 9.1.4 Docking and Molecular Dynamics (MD) procedure

The energy minimized 3D molecular structure of compounds **3-10** were prepared for docking using the LigPrep tool of Maestro. The docking grid was centered on **1** placed in the active site. The docking calculations were performed using Glide software [195] implemented in Maestro, applying the extra-precision (XP) mode, in order to achieve the most favorable binding mode of this compounds on the active site. The docking protocol was validated through re-docking of **1**. The System Builder tool of Maestro was used to: (1) immerse the protein-ligand complexes into an orthorhombic box of TIP3P water molecules [196], (2) set up the POPC membrane model, which was placed on the hydrophobic residues of the *hGnRH1R* seven canonical transmembrane helices (3) place the proper number of counter-ions to neutralize the system. Then, the Desmond algorithm implemented in Maestro was used to energy minimize the systems and to perform 200 ns-long MD simulations. Two independent MD replicas were accomplished for each compound, also the *hGnRH1R/1* complex was simulated in order to obtain a reference value. The Simulation Interactions Diagram tool of Maestro was used to evaluate the ligand stability in the active site by considering the C $\alpha$  atoms RMSD vs. time plots. Finally, 50 ns of MD trajectories in which the ligands displayed the highest stability were considered for the calculations of the binding free energy values, which were accomplished by the Prime algorithm [197] available on the Maestro platform, by adopting the MM-GBSA algorithm [198].

## 9.2 General chemistry

All reagents and solvents were purchased from Sigma-Aldrich. TLC analyses were performed on silica gel 60 F254 plates, precoated with a fluorescent indicator; spots were detected by UV lamp 254 nm, or by a 0.3% *w/v* ninhydrin solution in *n*-butanol/acetic acid (100:3) and heating at 110 °C.

Lipase B from *Candida antarctica* (CAL-B, Novozym® 435,  $\geq 10000$  U/g), lipase A from *Candida antarctica* (CAL-A, Immobead 150, 1620 U/g), lipase from *Candida rugosa* (CCL, 6.54 U/mg), lipase from *Pseudomonas fluorescens* (PFL, 40.2 U/mg), lipase from *Aspergillus niger* (194 U/mg), lipase from porcine pancreas (PPL, 23.9 U/mg), lipase F-AP15 from *Rhizopus orizae* (165 U/mg), esterase from hog liver (9.2 U/mg), protease XIX (0.43 U/mg), protease from bovine pancreas (7.3 U/mg), and protease from *Bacillus licheniformis* (10.7 U/mg) were purchased from Sigma-Aldrich (Merck Life Science S.r.l., Milano, Italy).

The proteases Alcalase CLEA (946 U/g) and Savinase CLEA (50 KNPU/g) were purchased from CLEA Technologies (CLEA Technologies, Delft, The Netherlands).

Optical rotation values were registered on an Anton Paar instrument (Mod MCP 100; Anton Paar Strasse 10, 8054 Graz, Austria) at 589 nm and 25 °C.

Mass spectrometry analyses were performed at the Mass Spectrometry facility of the Unitech COSPECT at the University of Milan (Italy). High-resolution mass spectra (HRMS) were recorded on Q-ToF Synapt G2-Si using an electrospray ionization source; acquisition parameters were set as follows: Capillary voltage 0.5-3.0 kV, Sampling cone 30-80, Source heater temperature 120°C, Desolvation temperature 150°C, Desolvation gas flow rate 600 L/h, Acquisition range: 50–1200 *m/z*, Lock-mass compound: leucine enkephalin. The samples were dissolved in MS-grade methanol and analyzed by direct infusion. Data acquisition and analysis were accomplished with MassLynx v4.2 software.

HPLC analyses were conducted using two different HPLC units:

- For chiral HPLC analysis: a Merck-Hitachi, equipped with a UV detector model L-4250, pump system model L-6200 and a chromato-integrator model D-2500. The column employed in the analyses were a Phenomenex Lux Cellulose-1 250 × 4.6 mm (3  $\mu$ m) and a Daicel Chiralpak AD-H 250 × 4.6 mm

(5  $\mu\text{m}$ ). The elution was in isocratic mode with the indicated column, eluant and flow. All the samples were measured at  $\lambda = 254 \text{ nm}$ .

- For RP-HPLC analysis: Agilent 1100 system equipped with a Zorbax SB-C18 column (150 mm  $\times$  3.0 mm, 3.5  $\mu\text{m}$ ) or with a Supelco Discovery C18 (250 mm  $\times$  4.6 mm, 5.0  $\mu\text{m}$ ).

All the samples were detected at  $\lambda = 254 \text{ nm}$  and 25  $^{\circ}\text{C}$ .

NMR spectra were recorded on a Bruker AVANCE 500 spectrometer equipped with a 5 mm broadband inverse (BBI) detection probe with field z-gradient operating at 500.13, 125.76, and 50.69 MHz for  $^1\text{H}$ ,  $^{13}\text{C}$ , and  $^{15}\text{N}$ , respectively. The spectra were recorded, as made explicit in the experimental part, in chloroform-d ( $\text{CDCl}_3$ ), or in methanol-d<sub>4</sub> ( $\text{CD}_3\text{OD}$ ), or  $\text{CDCl}_3/\text{CD}_3\text{OD}$  9:1 mixture, or in pyridine-d<sub>5</sub> ( $\text{Py-d}_5$ ), or in dimethylsulfoxide-d<sub>6</sub> ( $\text{DMSO-d}_6$ ) or in deuterium oxide ( $\text{D}_2\text{O}$ ). All the used deuterated solvents are isotopic enrichment 99.9 atom % D. Chemical shifts ( $\delta$ ) of the  $^1\text{H}$  NMR and  $^{13}\text{C}$  NMR spectra are reported in ppm using the signal for residual solvent proton resonance as the internal standard ( $^1\text{H}$  NMR:  $\text{CDCl}_3$  7.26,  $\text{CD}_3\text{OD}$  3.31,  $\text{Py-d}_5$  7.22 (higher field signal),  $\text{DMSO-d}_6$  2.50, and  $\text{D}_2\text{O}$  4.79 ppm;  $^{13}\text{C}$  NMR:  $\text{CDCl}_3$  77.0 (central line),  $\text{CD}_3\text{OD}$  49.00 (central line),  $\text{Py-d}_5$  123.9 (higher field signal), and  $\text{DMSO-d}_6$  39.52. The  $^{13}\text{C}$  NMR spectra recorded in  $\text{D}_2\text{O}$  were referenced to external TSP-d<sub>4</sub> (3-(trimethylsilyl)propionic-2,2,3,3-d<sub>4</sub> acid sodium salt) at 0.00 ppm. For  $^{15}\text{N}$  nuclei, in the  $g\text{s-}^1\text{H-}^{15}\text{N}$  HMBC experiment, nitromethane was used as the external reference ( $^{15}\text{N}$  at 381.7 ppm [166]) whereas, in the  $g\text{s-}^1\text{H-}^{15}\text{N}$  HSQC experiment, ammonia ( $^{15}\text{N}$  at 0.0 ppm [166]) was used. The pulse widths were 8.00  $\mu\text{s}$  ( $90^{\circ}$ ) for  $^1\text{H}$ , 13.00  $\mu\text{s}$  ( $90^{\circ}$ ) for  $^{13}\text{C}$ , and 27.50  $\mu\text{s}$  ( $90^{\circ}$ ) for  $^{15}\text{N}$ . Data were collected and processed by XWIN-NMR software (version 3.5, Bruker, Billerica, MA, USA) running on a PC with Microsoft Windows 7. The samples (20 mg) were dissolved in the appropriate solvent (0.75 mL) in a 5 mm NMR tube. The acquisition parameters for 1D were as follows:  $^1\text{H}$  spectral width of 5000 Hz and 32 K data points providing a digital resolution of ca. 0.153 Hz per point, relaxation delay 20 s, “zg” pulse sequence of the Bruker library was used;  $^{13}\text{C}$  spectral width of 29,499 Hz, and 32 K data points providing a digital resolution of ca. 0.900 Hz per point, relaxation delay 2 s, “zgpg” pulse sequence of the Bruker library was used. The experimental error in the measured  $^1\text{H-}^1\text{H}$  coupling constants was  $\pm 0.5 \text{ Hz}$ . The splitting pattern abbreviations were as

follows: s, singlet; d, doublet; t, triplet; q, quartet; m, multiplet; and br, broad signal. Except for NOESY, standard Bruker microprograms using gradient selection (gs) were applied for two-dimensional experiments. Gs-COSY-45 (“cosygpqf” pulse sequence of the Bruker’s library) and phase-sensitive NOESY (“noesyph” pulse sequence of the Bruker’s library) experiments were acquired with 512  $t_1$  increments, 2048  $t_2$  points, and a spectral width of 10.0 ppm. The NOESY experiments were performed on samples degassed under a flush of argon in a screwcap sample tube. There were no significant differences in the results obtained at different mixing times (0.5–1.5 s). The acquisition data for gs-HSQC (“hsqcetgp” pulse sequence of the Bruker’s library) and gs-HMBC (“hmbcgpplndqf” pulse sequence of the Bruker’s library) experiments were acquired with 512  $t_1$  increments, 2048  $t_2$  points, and a spectral width of 10.0 ppm for  $^1\text{H}$  and 240 ppm for  $^{13}\text{C}$ . Delay values were optimized to 140 Hz for  $^1\text{J}_{13\text{C},1\text{H}}$  and 8.0 Hz for  $^n\text{J}_{13\text{C},1\text{H}}$ . The gs- $^1\text{H}$ - $^{15}\text{N}$  HMBC (“hmbcgpndqf” pulse sequence of the Bruker’s library) and HSQC (“hsqcetgpsi” pulse sequence of the Bruker’s library) experiments, were performed with 256  $t_1$  increments, 1024  $t_2$  points, and a spectral width of 10.0 ppm for  $^1\text{H}$  and 600 ppm for  $^{15}\text{N}$  setting an acquisition time of 0.5 s, a relaxation delay of 2 s, a  $^1\text{J}_{15\text{N},1\text{H}}$  value of 90.0 Hz, and a  $^n\text{J}_{15\text{N},1\text{H}}$  value of 4.5 Hz. This last parameter was set after several attempts between 1 and 11 Hz. The total experimental time for  $^1\text{H}$ - $^{15}\text{N}$  gs-HMBC analyses was about 12 h.

The NMR spectra are available in the Supplementary Materials of this Thesis.

## 9.2.1. Synthesis of elagolix (1)

### 9.2.1.1 1-(2-fluoro-6-(trifluoromethyl)benzyl) urea (16)

Compound **16** was synthesized as reported in literature [96]: to a mixture of **15** (9.4 g; 48.7 mmol) and urea (11.7 g; 195 mmol) in water (19 mL), 37% aqueous hydrochloric acid (5.7 mL; 68.18 mmol) was added. The reaction mixture was refluxed for 6 hours. There was the formation of a white solid during the reaction progress. The reaction progress was monitored by TLC analysis ( $\text{CH}_2\text{Cl}_2/\text{MeOH}$  9:1). At the disappearing of the starting material, the reaction mixture was cooled to 0-5°C and stirred at this temperature for about 30 minutes. The obtained white solid was filtered by suction, washed with water (10 mL) cooled at 0-5°C and dried (60°C, 2 mmHg, 8h). 11.32 g of product were obtained (98% yield).  $R_f = 0.60$ .  $^1\text{H}$  NMR (500 MHz, DMSO)  $\delta$  7.61–7.56 (m, 3H), 6.15 (t,  $J = 5.3$  Hz, 1H), 5.47 (s, 2H), 4.36 (d,  $J = 5.0$

Hz, 2H). The other physico-chemical properties were in agreement with the reported ones [96,199].

#### **9.2.1.2 1-(2-fluoro-6-(trifluoromethyl)benzyl)-6-methylpyrimidine-2,4(1H,3H)-dione (17)**

Compound **17** was synthesized as reported in literature [159]: a suspension of **16** (17.7 g; 75.1 mmol) in toluene (900 mL) was refluxed under stirring and anhydrous atmosphere with a Dean Stark apparatus. The first 25 mL of distilled toluene were discarded. Maintaining the reflux, *tert*-butyl acetoacetate (36 mL; 217.1 mmol) was slowly added. The reaction mixture was refluxed for 4 hours. The reaction progress was monitored by TLC analysis (CH<sub>2</sub>Cl<sub>2</sub>/MeOH 9:1) until starting material disappearance. *p*-TsOH monohydrate (19.4 g; 112.7 mmol) was added portionwise. The reaction mixture was refluxed for 1 hour removing through the Dean-Stark apparatus the water formed during the reaction. The reaction progress was monitored by TLC analysis (hexane/ethyl acetate 1:1). At the end of the reaction, the reaction mixture was concentrated under reduced pressure (30 mmHg; 50°C) to oil residue. Isopropanol (20 mL) was added and removed under reduced pressure (30 mmHg; 50°C) in order to remove traces of toluene. Isopropanol (200 mL) was added to the residue and the resulting mixture was kept at room temperature under stirring overnight. The obtained white precipitate was filtered by suction, washed with isopropanol (20 mL) and dried (60°C; 2 mmHg; 8 hours) affording 15.79 g (52.25 mmol; 70%). R<sub>f</sub> = 0.27 (hexane/ethyl acetate 1:1). The full assignment of <sup>1</sup>H, <sup>13</sup>C, and <sup>15</sup>N NMR signals is given in Section 3.2. The other physico-chemical properties were in agreement with those reported [96,159].

#### **9.2.1.3 5-bromo-1-(2-fluoro-6-(trifluoromethyl)benzyl)-6-methylpyrimidine-2,4(1H,3H)-dione (18)**

Compound **18** was synthesized improving a literature procedure [96]: A solution of bromine (2 mL; 38.5 mmol) in glacial acetic acid (36 mL) was slowly added (in about 20 min) to a solution of **17** (10.58 g; 35 mmol) in glacial acetic acid (140 mL) under vigorous stirring. The reaction progress was monitored by TLC analysis (hexane/ethyl acetate 7:3) until starting material disappearance (2h). The excess of bromine was removed bubbling nitrogen through the reaction mixture until almost complete disappearance of its colour. The reaction mixture was concentrated at



reduced pressure (60 °C, 30 mmHg), affording a yellow residue which was suspended in *tert*-butyl methyl ether (25 mL). The suspension was stirred at room temperature for 2 h, filtered by suction and washed with *tert*-butyl methyl ether (5 mL). The solid was dried (60 °C, 2 mmHg, 8 h) affording **6** (12.86 g, 33.7 mmol; 96%).  $R_f = 0.69$  (hexane/ethyl acetate 1:1). The full assignment of  $^1\text{H}$ ,  $^{13}\text{C}$ , and  $^{15}\text{N}$  NMR signals is given in Section 3.2. The other physico-chemical properties were in agreement with those reported [96].

#### 9.2.1.4 5-(2-fluoro-3-methoxyphenyl)-1-(2-fluoro-6-(trifluoromethyl)benzyl)-6-methylpyrimidine-2,4(1H,3H)-dione (**25**)

Compound **25** was synthesized improving a literature procedure [157]: an aqueous solution (10 mL) of KOH (4.64 g; 82.70 mmol) was added to a mixture of **18** (7.7 g; 20.20 mmol) and 2-fluoro-3-methoxy-phenyl boronic acid (4.12 g; 24.24 mmol) in acetone (30 mL) and water (20 mL). The obtained solution was degassed (bubbling argon for about 30 min) and tri-*tert*-butyl-phosphonium tetrafluoroborate (62 mg; 0.21 mmol) was added. After 20 min at 45 °C, Pd(OAc)<sub>2</sub> (23 mg; 0.10 mmol) was added. The reaction mixture was refluxed under argon atmosphere and stirred while the reaction progress was monitored by TLC analysis (hexane/ethyl acetate 1:1) until disappearance of the starting material (24 h). The reaction mixture was cooled to 55 °C and glacial acetic acid (3.5 mL) was added and further stirred for 30 min. A white precipitate formed. The reaction mixture was cooled to room temperature and stirred at this temperature for 2 h. The white precipitate was filtered by suction and washed with water (15 mL) and then with methanol (30 mL). The solid was dried (60 °C; 2 mmHg; 8 h) affording 7.38 g (86% yield).  $R_f = 0.36$  (hexane/ethyl acetate 1:1). The full assignment of  $^1\text{H}$ ,  $^{13}\text{C}$ , and  $^{15}\text{N}$  NMR signals is given in Section 3.2. RP-HPLC analysis (Supelco Discovery C18, elution in gradient mode: Mobile phase: A = water with 0.05% trifluoroacetic acid; B = acetonitrile with 0.05% trifluoroacetic acid. Gradient: 95%A/5%B to 5%A/95%B over 50 min, then 5%A/95%B to 1%A/99%B over 0.1 min, then hold 1%A/99% for 0.8 min and back to 95%A/5% over 0.2 min, hold such gradient for 4 min. Flow rate 2.0 mL/min):  $t_R = 25.1$  min. HPLC on chiral stationary phase (Phenomenex Lux Cellulose-1, elution in isocratic mode: hexane/IPA 1:1. Flow rate 0.5 mL/min):  $t_R$  (**I** atropisomer) = 27.4 min,  $t_R$  (**II** atropisomer) = 32.8

min. The other physico-chemical properties were in agreement with those reported [157,159].

#### 9.2.1.5 (*R*)-2-((*tert*-butoxycarbonyl)amino)-2-phenylethyl methanesulfonate (**26**)

Compound **26** was synthesized as reported in literature [200,201]: to a solution of *N*-Boc-D-phenylglycinol (**23**, 6.62 g; 27.92 mmol) in CH<sub>2</sub>Cl<sub>2</sub> (32 mL) triethylamine (7.82 mL; 56.1 mmol) was added, under stirring and in inert atmosphere (N<sub>2</sub>). The solution was cooled at 0°C and MsCl (2.6 mL; 33.5 mmol) was added dropwise. The reaction progress was monitored by TLC (CH<sub>2</sub>Cl<sub>2</sub>/MeOH 95:5) until starting material disappearance (1h). The reaction mixture was washed with brine (40 mL) and water (40 mL). The organic phase was dried under sodium sulfate and the solvent evaporated at reduced pressure. The residue was dried (2mmHg, 25°C, 2h) affording a white solid (8.78 g; 26.8 mmol; 96%). R<sub>f</sub> = 0.80. <sup>1</sup>H NMR (500 MHz, CDCl<sub>3</sub>) δ 7.40 – 7.34 (m, 2H), 7.34 – 7.29 (m, 3H), 5.18 (d, *J* = 8.2 Hz, 1H), 5.02 (s, 1H), 4.52 – 4.32 (m, 2H), 2.88 (s, 3H), 1.43 (s, 9H). The physico-chemical properties were in agreement with the reported one [200,201].

#### 9.2.1.6 (*R*)-3-(amino(phenyl)methyl)-5-(2-fluoro-3-methoxyphenyl)-1-(2-fluoro-6-(trifluoromethyl)benzyl)-6-methylpyrimidine 2,4(1H,3H)-dione (**20**)

Compound **20** was synthesized as reported in literature [159]: to a mixture of **25** (7.31 g; 17.2 mmol) and **26** (8.78 g; 27.84 mmol) in anhydrous DMF (44 mL), K<sub>2</sub>CO<sub>3</sub> (5.94 g; 42.96 mmol) was added. The reaction mixture was kept under stirring, in inert atmosphere at 55°C, monitoring the reaction progress by TLC (hexane/ethyl acetate 7:3) until disappearance of **12** (5h). To the reaction mixture, cooled at room temperature, ethyl acetate (58.4 mL) and water (68 mL) were added. The mixture was stirred, and the phases separated. The aqueous phase was discharged while the organic phase was washed with water (36 mL). Methanesulfonic acid (3.36 mL; 51.84 mmol) was added to the organic phase and the obtained mixture was kept at 60°C. The reaction progress was monitored by TLC (hexane/ethyl acetate 7:3) until disappearance of the starting material (2h). To the reaction mixture, cooled at room temperature, an aqueous solution of potassium carbonate (11.85 g in 62 mL) was slowly added. The mixture was stirred, and the phases separated. The aqueous phase was discharged while to the organic phase an aqueous solution of phosphoric acid (10 g 85% phosphoric acid in 104 mL) was added. The mixture was stirred, and the phases

separated. The organic phase was discharged while the aqueous phase was washed with ethyl acetate (2 x 72 mL). To the aqueous phase, an aqueous solution of potassium carbonate (16.1 g in 62 mL) and ethyl acetate (91.2 mL) were carefully added. The phases were separated, and the organic phase was dried under sodium sulfate and the solvent evaporated at reduced pressure affording a white foam (7.53 g; 13.8 mmol; 81%).  $R_f$  0.17 (hexane/ethyl acetate/triethylamine 1:1:0.1).  $[\alpha]_D^{25} + 15.1$  (c 1,  $\text{CHCl}_3$ ). The full assignment of  $^1\text{H}$ ,  $^{13}\text{C}$ , and  $^{15}\text{N}$  NMR signals is given in Section 3.2. The other physico-chemical properties were in agreement with those reported [159,202].

**9.2.1.7 Ethyl (R)-4-(((5-(2-fluoro-3-methoxyphenyl)-3-(2-fluoro-6-(trifluoromethyl)benzyl)-4-methyl-2,6-dioxo-3,6-dihydropyrimidin-1(2H)-yl)(phenyl)methyl)amino)butanoate (21)**

Compound **21** was synthesized as reported in literature [159]: to a solution of **20** (7.53 g; 13.8 mmol) in anhydrous DMF (4.3 mL), diisopropylamine (2.92 mL; 16.76 mmol) and ethyl 4-bromobutyrate (2.16 mL; 15.1 mmol) were added. The mixture was kept at 60°C. The reaction progress was monitored by TLC (hexane/ethyl acetate/triethylamine 1:1:0.1) until disappearance of the starting material (**6h**). To the cooled reaction mixture, ethyl acetate (37.6 mL) and water (37.6 mL) were added. The mixture was stirred, and the phases separated. The aqueous phase was discharged while the organic phase was washed with water (37.6 mL). To the organic phase, phosphoric acid (3.98 g of 85% phosphoric acid in 42.4 mL) was added. After separation of the phases, the organic phase was treated with an aqueous solution of phosphoric acid (940 mg of 85% phosphoric acid in 7.6 mL). The collected aqueous phases were washed with ethyl acetate (9.6 mL) and an aqueous solution of potassium carbonate (8.62 g in 10.4 mL) and ethyl acetate (37.6 mL) were added. The mixture was stirred, and the phases separated. The aqueous phase was discharged while the organic phase was evaporated at reduced pressure affording a solid residue (5.1 g). The solid residue dissolved in ethyl acetate (1.88 mL) was purified by silica gel column chromatography. Elution with hexane/ethyl acetate 1:1 afforded, after evaporation of the solvents, the desired product **21** as white foam (4.56 g; 6.92 mmol; 50%).  $R_f = 0.44$  (hexane/ethyl acetate/triethylamine 1:1:0.1).  $[\alpha]_D^{25} - 5.7$  (c 1,  $\text{CHCl}_3$ ). The full assignment of  $^1\text{H}$ ,  $^{13}\text{C}$ , and  $^{15}\text{N}$  NMR signals is given in Section 3.2. The other physico-chemical properties were in agreement with the reported one [159,202].

**9.2.1.8 Elagolix sodium salt (1)**

Compound **1** was synthesized as reported in literature [159]: to a solution of **21** (4.56 g; 6.92 mmol) in ethanol/water (21.2 mL:18.8 mL), kept under stirring, at room temperature, NaOH (588 mg; 14.68 mmol) was added. The reaction progress was monitored by TLC (hexane/ethyl acetate 1:1 and CH<sub>2</sub>Cl<sub>2</sub>/MeOH 95:5) until disappearance of the starting material (7h). Ethanol was removed at reduced pressure (40°C; 30mmHg) and to the aqueous mixture methyl isobutylketone (MIBK) (32.4 mL) was added. The mixture was kept at 55°C (1h), under vigorous stirring. The warm phases were separated. The organic phase containing only a little amount of the desired product, together with a mixture of byproducts, was discarded. To the aqueous phase MIBK (32.4 mL) and an aqueous solution of 48% NaOH m/v (8.81 g) were added. The obtained emulsion required a carefully separation (overnight at room temperature). The separated aqueous phase was extracted with MIBK (2 x 32.4 mL). The collected organic phases were concentrated (about 20.25 mL) at 50°C and at reduced pressure (30 mmHg). The mixture was filtered (0.2 μm filter) and the filtrate was added dropwise to heptane (45.6 mL), under vigorous stirring. After 2 h the precipitate was recovered by suction, washed with heptane (5.2 mL) and dried (24h at 2mmHg; 90°C), affording **1** (4.02 g; 6.15 mmol; 88%). R<sub>f</sub>=0.74 (CHCl<sub>3</sub>/MeOH/H<sub>2</sub>O 12.5:4:0.5). [α]<sub>D</sub><sup>25</sup> + 12.2 (c 1, MeOH). RP-HPLC analysis (Zorbax SB-C18, elution in gradient mode in agreement with Ref. [28]): t<sub>R</sub> = 9.0 min. HPLC on chiral stationary phase (Phenomenex Lux Cellulose-1, elution in isocratic mode: hexane/IPA 6:4 + 0.1% TFA. Flow rate 0.3 mL/min): t<sub>R</sub> (**I** atropisomer) = 38.0 min, t<sub>R</sub> (**II** atropisomer) = 46.6 min. The full assignment of <sup>1</sup>H, <sup>13</sup>C, and <sup>15</sup>N NMR signals is given in Section 3.2. The other physico-chemical properties were in agreement with those reported [96,159].

## 9.2.2 Modifications at the 4-position

### 9.2.2.1 5-(2-fluoro-3-methoxyphenyl)-1-(2-fluoro-6-(trifluoromethyl)benzyl)-6-methyl-4-thioxo-3,4-dihydropyrimidin-2(1H)-one (**30**)

To a suspension of compound **25** (0.5 g; 1.17 mmol) in anhydrous 1,4-dioxane (6 mL), Lawesson's reagent (0.47 g; 1.17 mmol) was added. The obtained mixture was heated under stirring and inert atmosphere at 100°C for two hours. The reaction progress was monitored by TLC until disappearance of the starting material. The reaction mixture was concentrated under reduced pressure affording an oily residue

that was purified by means of a silica pad: by elution with a mixture of hexane/ethyl acetate 6:4 compound **5** was obtained, which was used immediately in the next step without further purification. For analytical purposes a sample (200 mg) was purified by silica gel column chromatography. Elution with hexane/ethyl acetate 8:2 afforded pure **30** that was stored at 4°C under nitrogen atmosphere in an amber glass vial.  $R_f = 0.63$  (Hexane/AcOEt 6:4). HRMS (ESI)  $m/z$ : Calcd. for  $C_{20}H_{15}N_2O_2NaSF_5$   $[M + Na]^+$  465.0672; Found 465.0674. The full assignment of  $^1H$  and  $^{13}C$  NMR signals is given in Section 4.3. HPLC on chiral stationary phase (Phenomenex Lux Cellulose-1, elution in isocratic mode: hexane/IPA 6:4. Flow rate 0.75 mL/min):  $t_R$  (I atropisomer) = 25.99 min,  $t_R$  (II atropisomer) = 35.90 min.  $R_f = 0.57$  (hexane/ethyl acetate 1:1).

#### **9.2.2.2 tert-butyl (R)-(2-((5-(2-fluoro-3-methoxyphenyl)-1-(2-fluoro-6-(trifluoromethyl)benzyl)-6-methyl-2-oxo-1,2-dihydropyrimidin-4-yl)thio)-1-phenylethyl)carbamate (31)**

To a solution of compound **30** dissolved in anhydrous dimethylformamide (10.0 mL), **26** (450 mg; 1.43 mmol) and potassium carbonate (323 mg; 2.34 mmol) were added. The reaction mixture was stirred at 80°C monitoring the reaction progress by TLC (hexane/ ethyl acetate 6:4) until starting material disappearance (4h). Water (50 mL) was added to the reaction mixture and the product was extracted with ethyl acetate (3 x 10 mL). The collected organic phases were washed with brine, dried over sodium sulfate and filtered. The solvent was removed under reduce pressure affording a yellow oily residue. Purification by silica gel column chromatography (hexane/ethyl acetate 7:3 as eluant) afforded pure compound **31** (752 mg, 1.14 mmol, 97% from **25**) as white foam.  $R_f = 0.45$  (Hexane/AcOEt 6:4). HRMS (ESI)  $m/z$ : Calcd. for  $C_{33}H_{32}N_3O_4NaSF_5$   $[M + Na]^+$  684.1931; Found 684.1933. The full assignment of  $^1H$  and  $^{13}C$  NMR signals is given in Section 4.3. HPLC on chiral stationary phase (Phenomenex Lux Cellulose-1, elution in isocratic mode: hexane/IPA 8:2. Flow rate 0.75 mL/min):  $t_R$  (I atropisomer) = 14.04 min,  $t_R$  (II atropisomer) = 15.30 min.  $R_f = 0.51$  (hexane/ethyl acetate 1:1).

#### **9.2.2.3 (R)-4-((2-amino-2-phenylethyl)thio)-5-(2-fluoro-3-methoxyphenyl)-1-(2-fluoro-6-(trifluoromethyl)benzyl)-6-methylpyrimidin-2(1H)-one (32)**

Compound **31** (700 mg, 1.06 mmol) was dissolved in a mixture of dichloromethane and trifluoroacetic acid 1:1 (5 mL) and stirred at room temperature. The reaction progress was monitored by TLC until starting material disappearance

(1h). The solvent was removed under reduced pressure to oily residue. To the residue dichloromethane (5 mL) was added and the resulting organic solution was washed with a saturated aqueous solution of sodium bicarbonate (5 mL) and with water (5 mL), dried over sodium sulfate, and filtered. The removal of the solvent under reduced pressure afforded pure **32** (570 mg, 1.02 mmol, 96%) as a white foam.  $R_f = 0.38$  ( $\text{CHCl}_3/\text{MeOH}/\text{H}_2\text{O}$  12.5:4:0.5). HRMS (ESI)  $m/z$ : Calcd. for  $\text{C}_{28}\text{H}_{24}\text{N}_3\text{O}_2\text{NaSF}_5$  [ $\text{M} + \text{Na}$ ] $^+$  584.1407; Found 584.1411. Calcd. for  $\text{C}_{28}\text{H}_{25}\text{N}_3\text{O}_2\text{SF}_5$  [ $\text{M} + \text{H}$ ] $^+$  562.1588; Found 562.1589. The full assignment of  $^1\text{H}$  and  $^{13}\text{C}$  NMR signals is given in Section 4.3.

**9.2.2.4 Ethyl (R)-4-((2-((5-(2-fluoro-3-methoxyphenyl)-1-(2-fluoro-6-(trifluoromethyl)benzyl)-6-methyl-2-oxo-1,2-dihydropyrimidin-4-yl)thio)-1-phenylethyl)amino)butanoate (33) and ethyl (R)-4-((2-((5-(2-fluoro-3-methoxyphenyl)-1-(2-fluoro-6-(trifluoromethyl)benzyl)-6-methyl-2-oxo-1,2-dihydropyrimidin-4-yl)amino)-2-phenylethyl)thio)butanoate (35)**

To a solution of compound **32** (550 mg, 0.98 mmol) in anhydrous dimethyl formamide (5 mL), *N,N*-diisopropylethylamine (0.19 mL, 1.1 mmol) and ethyl 4-bromobutyrate (0.42 mL, 3.0 mmol) were added. The reaction mixture was stirred at 60°C and the reaction progress was monitored by TLC until starting material disappearance (10 hours). The reaction mixture was poured into water (50 mL) and the obtained aqueous phase was extracted with dichloromethane (3 x 10 mL). The collected organic phases were washed with brine, dried over sodium sulfate and filtered. The removal of the solvent under reduced pressure gave an oily residue (572 mg) composed by a mixture of **33** and **35** and unidentified by-products. Purification by silica gel column chromatography (ratio substrate/silica gel 1:100; hexane/ethyl acetate 1:1 as eluant) gave:

**33-I atropisomer** (80 mg, 0.12 mmol, 12%).  $R_f = 0.22$  (Hexane/AcOEt 1:1). HRMS (ESI)  $m/z$ : Calcd. for  $\text{C}_{34}\text{H}_{34}\text{N}_3\text{O}_4\text{NaSF}_5$  [ $\text{M} + \text{Na}$ ] $^+$  698.2088; Found 698.2083. Calcd. for  $\text{C}_{34}\text{H}_{35}\text{N}_3\text{O}_4\text{SF}_5$  [ $\text{M} + \text{H}$ ] $^+$  676.2268; Found 676.2267. HPLC on chiral stationary phase (CHIRALPAK AD-H, elution in isocratic mode: hexane/IPA 7:3 + 0.1%  $\text{Et}_2\text{NH}$ . Flow rate 1.0 mL/min):  $t_R = 13.35$  min.

**33-II atropisomer** (86 mg, 0.13 mmol, 13%).  $R_f = 0.11$  (Hexane/AcOEt 1:1).

HRMS (ESI)  $m/z$ : Calcd. for  $C_{34}H_{34}N_3O_4NaSF_5$   $[M + Na]^+$  698.2088; Found 698.2083. Calcd. for  $C_{34}H_{35}N_3O_4SF_5$   $[M + H]^+$  676.2268; Found 676.2267. HPLC on chiral stationary phase (CHIRALPAK AD-H, elution in isocratic mode: hexane/IPA 7:3 + 0.1%  $Et_2NH$ . Flow rate 1.0 mL/min):  $t_R$  = 23.55 min.

**35-I atropisomer** (90 mg, 0.13 mmol, 13%).  $R_f$  = 0.42 (Hexane/AcOEt 1:1). HRMS (ESI)  $m/z$ : Calcd. for  $C_{34}H_{34}N_3O_4NaSF_5$   $[M + Na]^+$  698.2088; Found 698.2086. Calcd. for  $C_{34}H_{35}N_3O_4SF_5$   $[M + H]^+$  676.2268; Found 676.2266. HPLC on chiral stationary phase (CHIRALPAK AD-H, elution in isocratic mode: hexane/IPA 7:3 + 0.1%  $Et_2NH$ . Flow rate 1.0 mL/min):  $t_R$  = 12.55 min.

**35-II atropisomer** (79 mg, 0.12 mmol, 12%).  $R_f$  = 0.30 (Hexane/AcOEt 1:1). HRMS (ESI)  $m/z$ : Calcd. for  $C_{34}H_{34}N_3O_4NaSF_5$   $[M + Na]^+$  698.2088; Found 698.2086. Calcd. for  $C_{34}H_{35}N_3O_4SF_5$   $[M + H]^+$  676.2268; Found 676.2266. HPLC on chiral stationary phase (CHIRALPAK AD-H, elution in isocratic mode: hexane/IPA 7:3 + 0.1%  $Et_2NH$ . Flow rate 1.0 mL/min):  $t_R$  = 19.92 min.

The atropisomers of **33** and **35** were identified by NMR, see Section 4.3.

#### 9.2.2.5 Sodium (*R*)-4-((2-((5-(2-fluoro-3-methoxyphenyl)-1-(2-fluoro-6-(trifluoromethyl)benzyl)-6-methyl-2-oxo-1,2-dihydropyrimidin-4-yl)thio)-1-phenylethyl)amino)butanoate (**3**)

A suspension of **33** (50 mg, 0.07 mmol, atropo-diastereomeric mixture) in a 1:1 mixture of 2M aqueous sodium hydroxide and ethanol (1 mL) was stirred at room temperature. The reaction progress was monitored by TLC analysis until starting material disappearance (30 minutes). At this point a clear solution was obtained. Ethanol was removed under nitrogen flow and the resulting aqueous solution was extracted with ethyl acetate (3 x 0.5 mL). The collected organic phases were washed with water (0.5 mL), dried over sodium sulfate, and filtered. The removal of the solvent under reduced pressure afforded **3** (43 mg, 0.06 mmol, 86%) as a white solid.  $R_f$  = 0.66 ( $CHCl_3/MeOH/H_2O$  12.5:4:0.5). HRMS (ESI)  $m/z$ : Calcd. for  $C_{32}H_{31}N_3O_4F_5S$   $[M - Na + 2 H]^+$  648.1955; Found 648.1959. Calcd. for  $C_{32}H_{30}N_3O_4F_5NaS$   $[M + H]^+$  670.1775; Found 670.1774. The full assignment of  $^1H$  and  $^{13}C$  NMR signals is given in Section 4.3. HPLC on chiral stationary phase (Phenomenex Lux Cellulose-1, elution in isocratic mode: hexane/IPA 6:4 + 0.1% TFA. Flow rate 0.5 mL/min):  $t_R$  (I

atropisomer) = 15.16 min,  $t_R$  (II atropisomer) = 16.24 min, peaks not resolved; (CHIRALPAK AD-H, elution in isocratic mode: hexane/IPA 7:3 + 0.1% TFA. Flow rate 1.0 mL/min):  $t_R$  = 10.00 min (single broad peak). In the same way, a single atropisomer of **1** can be obtained starting from the corresponding single atropisomer of **8**.  $R_f$  = 0.66 (CHCl<sub>3</sub>/MeOH/H<sub>2</sub>O 12.5:4.0:0.5).

#### 9.2.2.6 Sodium (R)-4-((2-((5-(2-fluoro-3-methoxyphenyl)-1-(2-fluoro-6-(trifluoromethyl)benzyl)-6-methyl-2-oxo-1,2-dihydropyrimidin-4-yl)amino)-2-phenylethyl)thio)butanoate (**4**)

Compound **4** (47 mg, 0.07 mmol, 95%, white solid) was obtained starting from **35** (50 mg, 0.07 mmol, atropo-diastereomeric mixture) following the experimental procedure reported in Section 9.2.2.5.  $R_f$  = 0.85 (CHCl<sub>3</sub>/MeOH/H<sub>2</sub>O 12.5:4:0.5). HRMS (ESI)  $m/z$ : Calcd. for C<sub>32</sub>H<sub>31</sub>N<sub>3</sub>O<sub>4</sub>F<sub>5</sub>S [M - Na + 2 H]<sup>+</sup> 648.1955; Found 648.1958. Calcd. for C<sub>32</sub>H<sub>30</sub>N<sub>3</sub>O<sub>4</sub>F<sub>5</sub>NaS [M + H]<sup>+</sup> 670.1775; Found 670.1776. The full assignment of <sup>1</sup>H and <sup>13</sup>C NMR signals is given in Section 4.3. HPLC on chiral stationary phase (Phenomenex Lux Cellulose-1, elution in isocratic mode: hexane/IPA 6:4 + 0.1% TFA. Flow rate 0.5 mL/min):  $t_R$  (I atropisomer) = 15.15 min,  $t_R$  (II atropisomer) = 21.04 min; (CHIRALPAK AD-H, elution in isocratic mode: hexane/IPA 7:3 + 0.1% TFA. Flow rate 1.0 mL/min):  $t_R$  (I atropisomer) = 12.36 min,  $t_R$  (II atropisomer) = 15.63 min. In the same way, a single atropisomer of **4** can be obtained starting from the corresponding single atropisomer of **35**.  $R_f$  = 0.84 (CHCl<sub>3</sub>/MeOH/H<sub>2</sub>O 12.5:4.0:0.5).

## 9.2.3 Modifications at the 6-position

### 9.2.3.1 Synthesis of Meldrum's acid (**42**)

Compound **42** was synthesized as reported in literature [203]: to a mixture of malonic acid (20 g; 149 mmol) and acetic anhydride (21.4 mL; 193.7 mmol), sulfuric acid 98% (77 mL) was added under inert atmosphere at 0°C. The resultant mixture was stirred at 0°C for one hour. Acetone (15.3 mL) was added, and the reaction mixture was stirred at 0°C overnight. The formation of a precipitate was observed. The precipitate was recovered by suction, washed with iced water (3 x 100 mL), and dried (2 mmHg; 60°C; 24h) to give the desired product **42** (12.12 g; 84.1 mmol; 56% yield).

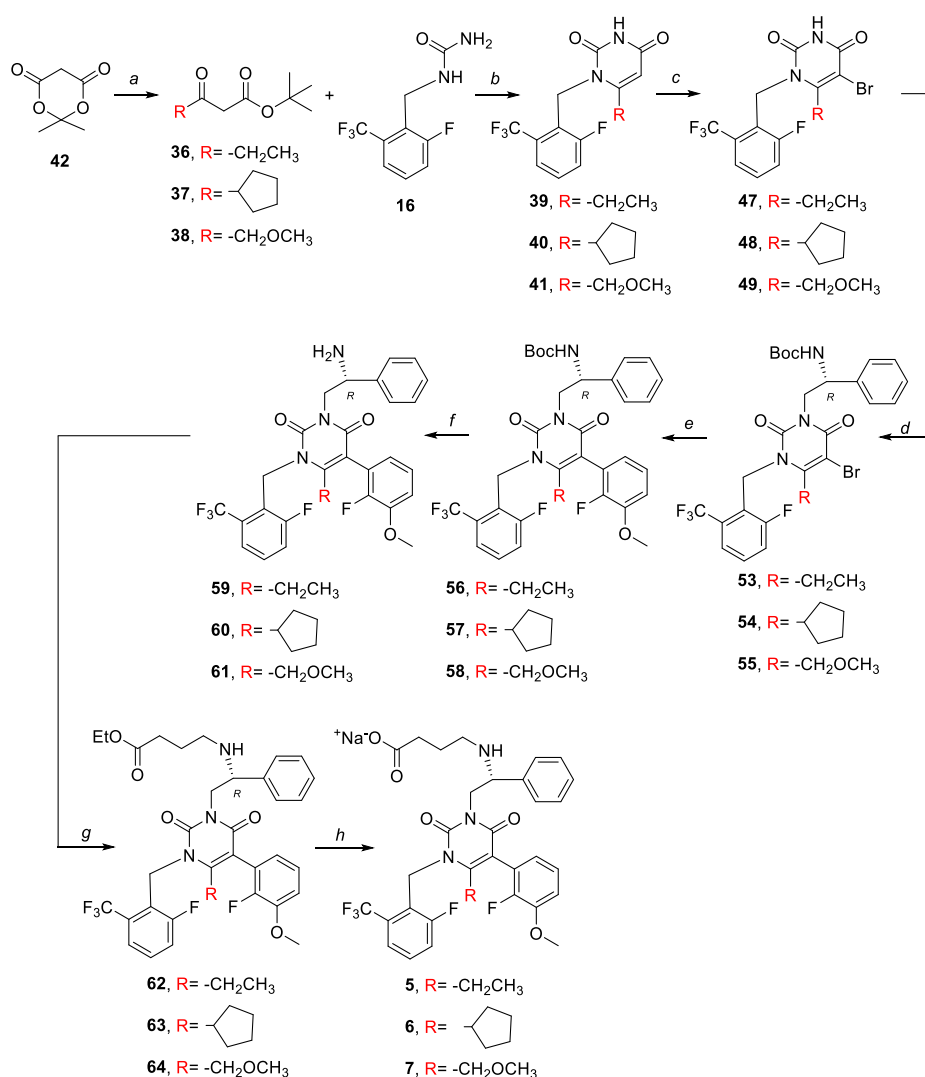


The physico-chemical properties were in agreement with the reported one [203].  $^1\text{H}$  NMR (500 MHz,  $\text{CDCl}_3$ )  $\delta$  3.62 (s, 2H), 1.79 (s, 6H).

### 9.2.3.2 Synthesis of cyclopentanecarbonyl chloride (44)

Compound **44** was synthesized as reported in literature [204]: to cyclopentanecarboxylic acid (4.8 mL; 44.6 mmol), thionyl chloride (4.6 mL; 63.4 mmol) was added dropwise under inert atmosphere and refluxed until the gas evolution stopped. The excess of thionyl chloride was removed under reduce pressure yielding the desired product **44** as a slightly yellow liquid (6.8 g; 51.3 mmol; 87%) which was used in the next step without further purifications. The physico-chemical properties were in agreement with the reported one [204].

### 9.2.3.3 Synthesis of 5-7 (General Scheme)



### General procedure for the synthesis of $\beta$ -keto esters (*a*)

To a solution of **42** (5.0 g; 34.7 mmol) in dichloromethane (225 mL), pyridine (7.4 mL), and the suitable acyl chloride (49.7 mmol) were sequentially added under inert atmosphere at 0°C until the starting material disappeared (1h), monitoring the reaction progress by TLC (hexane/ethyl acetate 8:2). The reaction mixture was washed with 1 M aqueous solution of hydrochloric acid (225 mL), and with brine (225 mL). After drying over sodium sulfate, filtration, and removal of the solvent under reduced pressure, was obtained an oily residue that was dissolved in a mixture of *tert*-butanol (13.3 mL) and toluene (135 mL). The reaction mixture was refluxed, and reaction progress was monitored by TLC analysis (hexane/ethyl acetate 6:4) until the starting material disappeared (4 h). The mixture was then concentrated under reduced pressure to an oily residue and purified by silica gel column chromatography eluting with hexane/ethyl acetate (9:1).

*Tert-butyl 3-oxopentanoate* (**36**). Starting acyl chloride: propionyl chloride (**43**). Colourless oil. Yield: 58%. The physico-chemical properties were in agreement with the reported one [205].

*Tert-butyl 3-cyclopentyl-3-oxopropanoate* (**37**). Starting acyl chloride: cyclopentanecarbonyl chloride (**44**). Yellowish oil. Yield: 49%. The physico-chemical properties were in agreement with the reported one [206].

*Tert-butyl 4-methoxy-3-oxobutanoate* (**38**). Starting acyl chloride: methoxyacetyl chloride (**45**). Colourless oil. Yield: 51%. The physico-chemical properties were in agreement with the reported one [207].

### General procedure for the synthesis of 6-alkyl uracil derivatives (*b*)

A suspension of **16** (3.9 mmol) in toluene (130 mL) was refluxed under stirring and anhydrous atmosphere with a Dean-Stark apparatus. The first 25 mL of distilled toluene were discarded. Maintaining the reflux, the suitable  $\beta$ -keto ester (11.78 mmol) was slowly added. The reaction mixture was refluxed monitoring the reaction progress by TLC analysis (CH<sub>2</sub>Cl<sub>2</sub>/MeOH 95:5) until starting material disappearance (4h). *p*-TsOH monohydrate (1.05 g; 5.5 mmol) was added in portions to avoid excessive boiling. The reaction mixture was refluxed for 1 hour removing through the Dean-

Stark apparatus the water that was going to form during the reaction. The reaction progress was monitored by TLC analysis (CH<sub>2</sub>Cl<sub>2</sub>/MeOH 95:5). At the end of the reaction, the reaction mixture was concentrated under reduced pressure (30 mmHg; 50°C).

*6-Ethyl-1-(2-fluoro-6-(trifluoromethyl)benzyl)pyrimidine-2,4(1H,3H)-dione (39)*. Starting compound: *tert*-butyl 3-oxopentanoate (**36**). The crude was purified by precipitation from 2-propanol (40 mL). The obtained white solid was recovered by suction, washed with 2-propanol (3 x 5 mL), and dried (2 mmHg, 25°C, 8h). White solid. Yield: 61%. R<sub>f</sub> = 0.74 (CH<sub>2</sub>Cl<sub>2</sub>/MeOH 95:5). <sup>1</sup>H NMR (500 MHz, DMSO-d<sub>6</sub>) δ 11.26 (s, 1H), 7.65 (d, *J* = 7.6 Hz, 1H), 7.56 (m, 1H), 7.52 (m, 1H), 5.47 (s, 1H), 5.23 (s, 2H), 2.50 (q, *J* = 7.3 Hz, 2H), 1.08 (t, *J* = 7.3 Hz, 3H).

*6-Cyclopentyl-1-(2-fluoro-6-(trifluoromethyl)benzyl)pyrimidine-2,4(1H,3H)-dione (40)*. Starting compound: *tert*-butyl 3-cyclopentyl-3-oxopropanoate (**37**). The crude was purified by silica gel column chromatography by elution with hexane/ethyl acetate (6:4). The undesired isomer eluted first (Yield: 48%. R<sub>f</sub> = 0.59 (*n*-hexane/AcOEt 1:1)) followed by the desired one. White solid. Yield: 49%. R<sub>f</sub> = 0.32 (*n*-hexane/AcOEt 1:1). <sup>1</sup>H NMR (500 MHz, CDCl<sub>3</sub>) δ 8.23 (s, 1H), 7.54 (d, *J* = 7.9 Hz, 1H), 7.41 (td, *J* = 8.0, 4.9 Hz, 1H), 7.28 – 7.18 (m, 1H), 5.68 (s, 1H), 5.42 (s, 2H), 2.79 (p, *J* = 7.7 Hz, 1H), 1.95 – 1.50 (m, 8H).

*1-(2-fluoro-6-(trifluoromethyl)benzyl)-6-(methoxymethyl)pyrimidine-2,4(1H,3H)-dione (41)*. Starting compound: *tert*-butyl 4-methoxy-3-oxobutanoate (**38**). The crude was purified by silica gel column chromatography by elution with hexane/ethyl acetate (6:4). White solid. Yield: 87%. R<sub>f</sub> = 0.63 (CH<sub>2</sub>Cl<sub>2</sub>/MeOH 95:5). <sup>1</sup>H NMR (500 MHz, CDCl<sub>3</sub>) δ 9.10 (brs, 1H), 7.53 (d, *J* = 7.9 Hz, 1H), 7.40 (td, *J* = 8.0, 5.1 Hz, 1H), 7.27 – 7.19 (m, 1H), 5.82 (s, 1H), 5.35 (s, 2H), 4.16 (s, 2H), 3.35 (s, 3H).

#### **General procedure for bromination reaction (c)**

To a solution of the suitable 6-alkyl uracil derivative (1.54 mmol) in acetic acid (8.0 mL), bromine (95 μL; 1.85 mmol) was added at 0°C. The mixture was stirred at room temperature until the starting material disappeared, monitoring reaction progress by TLC analysis (hexane/ethyl acetate 1:1). The mixture was then concentrated under

reduced pressure affording a solid residue. The residue was washed with *tert*-butyl methyl ether (3 x 2 mL) in order to remove excess bromine, obtaining the desired product.

*5-bromo-6-ethyl-1-(2-fluoro-6-(trifluoromethyl)benzyl)pyrimidine-2,4(1H,3H)-dione* (**47**). Starting material: 6-ethyl-1-(2-fluoro-6-(trifluoromethyl)benzyl)pyrimidine-2,4(1H,3H)-dione (**39**). White solid. Yield: 83%.  $R_f = 0.82$  (hexane/ethyl acetate 1:1).  $^1\text{H NMR}$  (500 MHz,  $\text{CDCl}_3$ )  $\delta$  8.45 (s, 1H), 7.56 (d,  $J = 7.9$  Hz, 1H), 7.44 (td,  $J = 8.1, 5.0$  Hz, 1H), 7.26 (m, 1H), 5.46 (s, 2H), 2.76 (q,  $J = 7.6$  Hz, 2H), 1.18 (t,  $J = 7.5$  Hz, 3H).

*5-bromo-6-cyclopentyl-1-(2-fluoro-6-(trifluoromethyl)benzyl)pyrimidine-2,4(1H,3H)-dione* (**48**). Starting material: 6-cyclopentyl-1-(2-fluoro-6-(trifluoromethyl)benzyl)pyrimidine-2,4(1H,3H)-dione (**40**). White solid. Yield: 77%.  $R_f = 0.85$  (hexane/ethyl acetate 1:1).  $^1\text{H NMR}$  (500 MHz,  $\text{CDCl}_3$ )  $\delta$  8.53 (brs,  $J = 70.9$  Hz, 1H), 7.57 (d,  $J = 7.8$  Hz, 1H), 7.44 (td,  $J = 8.1, 5.0$  Hz, 1H), 7.32 – 7.22 (m, 1H), 5.55 (brs, 2H), 3.22 (m, 1H), 2.23 – 1.98 (m, 2H), 1.98 – 1.82 (m, 2H), 1.80 – 1.60 (m, 2H), 1.55 – 1.40 (m, 2H).

*5-bromo-6-methoxymethyl-1-(2-fluoro-6-(trifluoromethyl)benzyl)pyrimidine-2,4(1H,3H)-dione* (**49**). Starting material: 1-(2-fluoro-6-(trifluoromethyl)benzyl)-6-(methoxymethyl)pyrimidine-2,4(1H,3H)-dione (**41**). White solid. Yield: 58%.  $^1\text{H NMR}$  (500 MHz,  $\text{CDCl}_3$ )  $\delta$  8.35 (brs, 1H), 7.54 (d,  $J = 7.8$  Hz, 1H), 7.40 (td,  $J = 8.1, 5.0$  Hz, 1H), 7.23 (m, 1H), 5.52 (s, 2H), 4.62 (s, 2H), 3.39 (s, 3H).

#### **General procedure for Mitsunobu reaction (d)**

To a solution of the suitable 5-bromo derivative (1.14 mmol) in tetrahydrofuran (18 mL), *N*-D- $\alpha$ -Boc-phenylglycinol (340 mg; 1.43 mmol), 40% (*w/w*) solution of diethyl azodicarboxylate in toluene (1.1 mL; 10.35 mmol), and triphenylphosphine (460 mg; 1.75 mmol) were sequentially added. The reaction mixture was stirred at room temperature until the starting material disappeared (14 h) monitoring the reaction progress by TLC analysis (hexane/ethyl acetate 6:4). The mixture was then concentrated under reduced pressure and purified by silica gel column chromatography eluting with hexane/ethyl acetate 8:2.

*tert-butyl (R)-(2-(5-bromo-4-cyclopentyl-3-(2-fluoro-6 (trifluoromethyl)benzyl)-2,6-dioxo-3,6-dihydropyrimidin-1(2H)-yl)-1 phenylethyl)carbamate (53)*. Starting material: 5-bromo-6-ethyl-1-(2-fluoro-6-(trifluoromethyl)benzyl)pyrimidine-2,4(1H,3H)-dione (**47**). White foam. Yield: 99%. Rf = 0.72 (hexane/ethyl acetate 8:2). <sup>1</sup>H NMR (500 MHz, CDCl<sub>3</sub>) δ 7.57 (d, *J* = 7.9 Hz, 1H), 7.46 – 7.31 (m, 6H), 7.31 – 7.18 (m, 1H), 5.75 – 5.30 (m, 3H), 5.16 – 5.07 (m, 1H), 4.39 (t, *J* = 12.4 Hz, 1H), 4.22 – 4.01 (m, 1H), 3.02 – 2.68 (m, 2H), 1.37 (s, 9H) (m, 3H).

*tert-butyl (R)-(2-(5-bromo-4-cyclopentyl-3-(2-fluoro-6 (trifluoromethyl)benzyl)-2,6-dioxo-3,6-dihydropyrimidin-1(2H)-yl)-1 phenylethyl)carbamate (54)*. Starting material: 5-bromo-6-cyclopentyl-1-(2-fluoro-6-(trifluoromethyl)benzyl)pyrimidine-2,4(1H,3H)-dione (**48**). White foam. Yield: 94%. Rf = 0.76 (hexane/ethyl acetate 8:2). <sup>1</sup>H NMR (500 MHz, CDCl<sub>3</sub>) δ 7.59 (d, *J* = 7.9 Hz, 1H), 7.49 – 7.39 (m, 3H), 7.37 (t, *J* = 7.5 Hz, 2H), 7.33 – 7.22 (m, 2H), 5.98 – 5.29 (m, 3H), 5.29 – 4.90 (m, 1H), 4.42 (t, *J* = 12.4 Hz, 1H), 4.13 (d, *J* = 7.1 Hz, 1H), 3.42 – 3.24 (m, 1H), 2.20 – 2.00 (m, 2H), 1.95 – 1.80 (m, 2H), 1.70 – 1.50 (m, 4H), 1.38 (s, 9H).

*tert-butyl (R)-(2-(5-bromo-3-(2-fluoro-6-(trifluoromethyl)benzyl)-4-(methoxymethyl)-2,6-dioxo-3,6-dihydropyrimidin-1(2H)-yl)-1-phenylethyl)carbamate (55)*. Starting material: 5-bromo-6-methoxymethyl-1-(2-fluoro-6-(trifluoromethyl)benzyl)pyrimidine-2,4(1H,3H)-dione (**49**). White foam. Yield: 91%. Rf = 0.72 (hexane/ethyl acetate 8:2). <sup>1</sup>H NMR (500 MHz, CDCl<sub>3</sub>) δ 7.55 (d, *J* = 7.8 Hz, 1H), 7.35 (m, 6H), 7.21 (dd, *J* = 12.0, 8.4 Hz, 1H), 5.70 – 5.43 (m, 3H), 5.20 – 5.02 (m, 1H), 4.66 (m, 2H), 4.41 – 4.33 (m, 1H), 4.11 – 4.04 (m, 1H), 3.40 (s, 3H), 1.37 (s, 9H).

### General procedure for Suzuki-Miyaura coupling reaction (*e*)

In a Schlenk tube, the suitable *N*-Boc-1-phenyl, 1-amminoethyl derivative (0.87 mmol), boronic acid (238 mg; 1.4 mmol), sodium carbonate (848 mg; 8 mmol), distilled water (1.8 mL) and dioxane (5 mL) were added and, in order to remove oxygen, argon was bubbled through this mixture for 30 minutes. Tetrakis(triphenylphosphine)palladium (162 mg; 0.14 mmol) was added and the mixture was refluxed until the starting material disappeared (11 h) monitoring the

reaction progress by TLC analysis (hexane/ethyl acetate 8:2). The mixture was then concentrated under reduced pressure and purified by chromatographic column.

*tert-butyl* (R)-(2-(4-ethyl-5-(2-fluoro-3-methoxyphenyl)-3-(2-fluoro-6-(trifluoromethyl)benzyl)-2,6-dioxo-3,6-dihydropyrimidin-1(2H)-yl)-1-phenylethyl)carbamate (**56**). Starting material: *tert-butyl* (R)-(2-(5-bromo-4-cyclopentyl-3-(2-fluoro-6-(trifluoromethyl)benzyl)-2,6-dioxo-3,6-dihydropyrimidin-1(2H)-yl)-1-phenylethyl)carbamate (**53**). White solid. Yield: 92%.  $R_f = 0.60$  (hexane/ethyl acetate 8:2).  $^1\text{H NMR}$  (500 MHz,  $\text{CDCl}_3$ )  $\delta$  7.85–7.62 (m, 1H), 7.55 (d,  $J = 7.9$  Hz, 1H), 7.45–7.20 (m, 7H), 7.13 (t,  $J = 8.1$  Hz, 1H), 7.05–6.97 (m, 1H), 6.79 (m, 1H), 5.77 (d,  $J = 7.3$  Hz, 1H), 5.63–5.25 (m, 2H), 5.08 (brs, 1H), 4.36 (dt,  $J = 34.7, 12.2$  Hz, 1H), 4.09–4.00 (m, 1H), 3.911 (s, 1.4 H), 3.905 (s, 1.6H), 2.40 (m, 2H), 1.40 (s, 9H), 1.07 (t,  $J = 7.6$  Hz, 3H). HPLC on chiral stationary phase (Phenomenex Lux Cellulose-1, *n*-hexane/*i*PrOH = 8:2, 0.5 mL/min,  $\lambda = 254$  nm)  $t_R$ (I atropisomer) = 16.35 min,  $t_R$ (II atropisomer) = 29.31 min.

*tert-butyl* (R)-(2-(4-cyclopentyl-5-(2-fluoro-3-methoxyphenyl)-3-(2-fluoro-6-(trifluoromethyl)benzyl)-2,6-dioxo-3,6-dihydropyrimidin-1(2H)-yl)-1-phenylethyl)carbamate (**57**). Starting material: *tert-butyl* (R)-(2-(5-bromo-4-cyclopentyl-3-(2-fluoro-6-(trifluoromethyl)benzyl)-2,6-dioxo-3,6-dihydropyrimidin-1(2H)-yl)-1-phenylethyl)carbamate (**54**). White solid. Yield: 94%.  $R_f = 0.62$  (hexane/ethyl acetate 8:2).  $^1\text{H NMR}$  (500 MHz,  $\text{CDCl}_3$ )  $\delta$  7.56 (d,  $J = 7.7$  Hz, 1H), 7.44–7.18 (m, 7H), 7.13 (t,  $J = 7.9$  Hz, 1H), 7.01 (td,  $J = 8.1, 1.6$  Hz, 1H), 6.79 (dt,  $J = 17.1, 7.0$  Hz, 1H), 5.83–4.78 (m, 3H), 4.42–4.16 (m, 1H), 4.04 (t,  $J = 12.6$  Hz, 1H), 3.92 (s, 1.4H), 3.91 (s,  $J = 1.6$ H), 3.16 (m, 1H), 1.97–1.42 (m, 8H), 1.40 (s, 9H). HPLC on chiral stationary phase (Phenomenex Lux Cellulose-1, *n*-hexane/*i*PrOH = 8:2, 0.5 mL/min,  $\lambda = 254$  nm)  $t_R$ (I atropisomer) = 13.4 min,  $t_R$ (II atropisomer) = 20.1 min.

*tert-butyl* (R)-(2-(5-(2-fluoro-3-methoxyphenyl)-3-(2-fluoro-6-(trifluoromethyl)benzyl)-4-(methoxymethyl)-2,6-dioxo-3,6-dihydropyrimidin-1(2H)-yl)-1-phenylethyl)carbamate (**58**). Starting material: *tert-butyl* (R)-(2-(5-bromo-3-(2-fluoro-6-(trifluoromethyl)benzyl)-4-(methoxymethyl)-2,6-dioxo-3,6-dihydropyrimidin-1(2H)-yl)-1-phenylethyl)carbamate (**55**). White solid. Yield: 95%.

$R_f = 0.55$  (hexane/ethyl acetate 8:2).  $^1\text{H NMR}$  (500 MHz,  $\text{CDCl}_3$ )  $\delta$  7.54 (d,  $J = 7.9$  Hz, 1H), 7.42 – 7.27 (m, 5H), 7.25 – 7.18 (m, 2H), 7.18 – 7.11 (m, 1H), 7.07 – 7.00 (m, 1H), 6.88 – 6.80 (m, 1H), 5.82 – 5.43 (m, 3H), 5.08 (s, 1H), 4.42 – 4.27 (m, 1H), 4.24 – 4.15 (m, 2H), 4.08 (m, 1H), 3.923 (s, 1.4H), 3.917 (s, 1.6H), 3.17 (s, 3H), 1.38 (m, 9H). HPLC on chiral stationary phase (Phenomenex Lux Cellulose-1, *n*-hexane/*i*PrOH = 8:2, 0.5 mL/min,  $\lambda = 254$  nm)  $t_R(\text{I atropisomer}) = 10.43$  min,  $t_R(\text{II atropisomer}) = 15.56$  min.

### General procedure for *N*-Boc deprotection (f)

A solution of the suitable *N*-Boc protected compound (0.58 mmol) in a mixture of trifluoroacetic acid (1.1 mL) and dichloromethane (2.1 mL) was stirred at room temperature until the starting material disappeared (2 h) monitoring the reaction progress by TLC analysis (hexane/ethyl acetate/triethylamine 60:40:1). The reaction mixture was concentrated under reduced pressure to solid residue. The residue was dissolved in ethyl acetate (5 mL) and washed with a saturated aqueous solution of  $\text{NaHCO}_3$  (5 mL). The organic phase was dried over sodium sulfate and filtered. Evaporation of the solvent under reduced pressure afforded the desired products that was used in the following step without further purification.

(*R*)-3-(2-amino-2-phenylethyl)-6-ethyl-5-(2-fluoro-3-methoxyphenyl)-1-(2-fluoro-6-(trifluoromethyl)benzyl)pyrimidine-2,4(1*H*,3*H*)-dione (**59**). Starting material: *tert*-butyl (*R*)-(2-(4-ethyl-5-(2-fluoro-3-methoxyphenyl)-3-(2-fluoro-6-(trifluoromethyl)benzyl)-2,6-dioxo-3,6-dihydropyrimidin-1(2*H*)-yl)-1-phenylethyl)carbamate (**56**). White solid. Yield: 97%.  $R_f = 0.16$  (hexane/ethyl acetate/triethylamine 60:40:1).

(*R*)-3-(2-amino-2-phenylethyl)-6-cyclopentyl-5-(2-fluoro-3-methoxyphenyl)-1-(2-fluoro-6-(trifluoromethyl)benzyl)pyrimidine-2,4(1*H*,3*H*)-dione (**60**). Starting material: *tert*-butyl (*R*)-(2-(4-cyclopentyl-5-(2-fluoro-3-methoxyphenyl)-3-(2-fluoro-6-(trifluoromethyl)benzyl)-2,6-dioxo-3,6-dihydropyrimidin-1(2*H*)-yl)-1-phenylethyl)carbamate (**57**). White solid. Yield: 89%.  $R_f = 0.21$  (hexane/ethyl acetate/triethylamine 60:40:1). This sample was further purified by column chromatography (hexane/ethyl acetate/triethylamine 1:1:0.1) in order to have the substrate for the enzyme-catalyzed *N*-acylations.  $^1\text{H NMR}$  (500 MHz,  $\text{CDCl}_3$ )  $\delta$  7.57

(d,  $J = 7.8$  Hz, 1H), 7.38 (q,  $J = 15.2, 9.7$  Hz, 6H), 7.24 (q,  $J = 11.9, 10.7$  Hz, 1H), 7.10 – 7.01 (m, 1H), 7.00 – 6.92 (m, 0.5H), 6.90 – 6.78 (m, 1H), 6.75 – 6.65 (m, 0.5H), 5.58 – 5.20 (m, 2H), 4.90 – 4.55 (m, 2H), 4.43 – 4.07 (m, 1H), 3.84 (s, 1.7H), 3.68 (s, 1.3H), 3.09 (dt,  $J = 18.5, 9.4$  Hz, 1H), 1.95 – 1.37 (m, 8H).

*(R)*-3-(2-amino-2-phenylethyl)-5-(2-fluoro-3-methoxyphenyl)-1-(2-fluoro-6-(trifluoromethyl)benzyl)-6-(methoxymethyl)pyrimidine-2,4(1H,3H)-dione (**61**).

Starting material: *tert*-butyl (*R*)-(2-(5-(2-fluoro-3-methoxyphenyl)-3-(2-fluoro-6-(trifluoromethyl)benzyl)-4-(methoxymethyl)-2,6-dioxo-3,6-dihydropyrimidin-1(2H)-yl)-1-phenylethyl)carbamate (**58**). White solid. Yield: 95%.  $R_f = 0.09$  (hexane/ethyl acetate/triethylamine 60:40:1).

#### General procedure for *N*-alkylation with ethyl-4-bromobutyrate (**g**)

To the suitable amine (0.45 mmol) dissolved in dry DMF (3.3mL), diisopropylamine (220  $\mu$ L; 1.22 mmol) and ethyl 4-bromobutyrate (94  $\mu$ L; 0.63 mmol) were added. The mixture was heated at 60°C until disappearance of the starting material (6h) monitoring the reaction progress by TLC (hexane/ethyl acetate/triethylamine 6:4:0.1). To the cooled reaction mixture, ethyl acetate (15 mL) and water (35 mL) were added. The phases were separated, and the aqueous phase was extracted with ethyl acetate (2 x 15 mL). The collected organic phases were dried over sodium sulfate, filtrated, and evaporated at reduced pressure affording a solid residue which was purified by silica gel column chromatography. Elution with hexane/ethyl acetate/triethylamine 5:5:0.25 afforded the desired product.

*Ethyl* (*R*)-4-((2-(4-ethyl-5-(2-fluoro-3-methoxyphenyl)-3-(2-fluoro-6-(trifluoromethyl)benzyl)-2,6-dioxo-3,6-dihydropyrimidin-1(2H)-yl)-1-phenylethyl)amino)butanoate (**62**). Starting material: (*R*)-3-(2-amino-2-phenylethyl)-

6-ethyl-5-(2-fluoro-3-methoxyphenyl)-1-(2-fluoro-6-

(trifluoromethyl)benzyl)pyrimidine-2,4(1H,3H)-dione (**59**). White foam. Yield: 43%.

$R_f = 0.62$  (hexane/ethyl acetate/triethylamine 6:4:0.1).  $^1\text{H NMR}$  (500 MHz,  $\text{CDCl}_3$ )  $\delta$  7.54 (d,  $J = 7.8$  Hz, 1H), 7.46 – 7.35 (m, 2H), 7.30 (td,  $J = 7.4, 3.1$  Hz, 2H), 7.26 (m, 3H), 7.15 – 7.08 (m, 1H), 6.99 (t,  $J = 8.0$  Hz, 1H), 6.80 (t,  $J = 6.7$  Hz, 0.5H), 6.76 (t,  $J = 6.9$  Hz, 0.5H), 5.45 (m, 2H), 4.25 (m, 1H), 4.18 – 4.00 (m, 4H), 3.902 (s, 1.5H), 3.899



(s, 1.5H), 2.54 – 2.32 (m, 4H), 2.29 (t,  $J=7.7$  Hz, 2H) 1.68 (brs, 2H), 1.30 – 1.14 (m, 3H), 1.07 (m, 3H).

*Ethyl* (R)-4-((2-(4-cyclopentyl-5-(2-fluoro-3-methoxyphenyl)-3-(2-fluoro-6-(trifluoromethyl)benzyl)-2,6-dioxo-3,6-dihydropyrimidin-1(2H)-yl)-1-phenylethyl)amino)butanoate (**63**). Starting material: (R)-3-(2-amino-2-phenylethyl)-6-cyclopentyl-5-(2-fluoro-3-methoxyphenyl)-1-(2-fluoro-6-(trifluoromethyl)benzyl)pyrimidine-2,4(1H,3H)-dione (**60**). White foam. Yield: 49%.  $R_f = 0.65$  (hexane/ethyl acetate/triethylamine 6:4:0.1).  $^1\text{H NMR}$  (500 MHz,  $\text{CDCl}_3$ )  $\delta$  7.54 (d,  $J = 7.8$  Hz, 1H), 7.43 – 7.28 (m, 6H), 7.11 (td,  $J = 8.0, 4.3$  Hz, 1H), 6.99 (t,  $J = 8.0$  Hz, 1H), 6.83 (m, 1H), 5.34 (m, 2H), 4.11 (m, 1H), 4.08 (m, 2H), 3.910 (s, 1.4H), 3.906 (s, 1.6H), 3.12 (m, 1H), 2.53 (brs, 2H), 2.30 (m, 2H), 1.95 – 1.38 (m, 12H), 1.21 (m, 3H). HPLC on chiral stationary phase (Phenomenex Lux Cellulose-1, *n*-hexane/*i*PrOH = 7:3, 0.75 mL/min,  $\lambda = 254$  nm)  $t_R$ (I atropisomer) = 9.4 min,  $t_R$ (II atropisomer) = 16.4 min.

*Ethyl* (R)-4-((2-(5-(2-fluoro-3-methoxyphenyl)-3-(2-fluoro-6-(trifluoromethyl)benzyl)-4-(methoxymethyl)-2,6-dioxo-3,6-dihydropyrimidin-1(2H)-yl)-1-phenylethyl)amino)butanoate (**64**). Starting material: (R)-3-(2-amino-2-phenylethyl)-5-(2-fluoro-3-methoxyphenyl)-1-(2-fluoro-6-(trifluoromethyl)benzyl)-6-(methoxymethyl)pyrimidine-2,4(1H,3H)-dione (**61**). Yellowish foam. Yield: 34%.  $R_f = 0.55$  (hexane/ethyl acetate/triethylamine 6:4:0.1).  $^1\text{H NMR}$  (500 MHz,  $\text{CDCl}_3$ )  $\delta$  7.54 (d,  $J = 7.9$ , 1H), 7.42 – 7.27 (m, 3H), 7.27- 7.18 (m, 4H), 7.12 (m, 1H), 7.02 (m, 1H), 6.83 (t,  $J = 6.8$  Hz, 0.44H), 6.76 (t,  $J = 6.8$  Hz, 0.48H), 5.53 (m, 2H), 4.30 – 4.00 (m, 5H), 3.91 (d,  $J = 1.8$  Hz, 3H), 3.16 (s, 1H), 3.15 (s, 1H), 2.40 (m, 2H), 2.27 (m, 2H), 1.67 (m, 2H), 1.28 (m, 3H), 1.22 (t,  $J = 7.1$  Hz, 3H).

#### **General procedure for sodium salt formation (f)**

To a solution of the suitable ethyl ester (0.07 mmol) in ethanol/water (240  $\mu\text{L}$ ; 205  $\mu\text{L}$ ), kept under stirring, at room temperature, NaOH (6.4 mg; 0.16 mmol) was added. The reaction progress was monitored by TLC ( $\text{CHCl}_3/\text{MeOH}/\text{H}_2\text{O}$  12.5:4:0.5) until disappearance of the starting material (16 h). Ethanol was removed at reduced pressure (40°C; 30mmHg) and to the aqueous mixture methyl isobutylketone (MIBK) (380  $\mu\text{L}$ ) was added. The mixture was kept at 55°C (1h), under vigorous stirring. The

phases were separated. The aqueous phase, after the addition of a solution of 48% NaOH *m/v* in water (80  $\mu\text{L}$ ), was extracted with MIBK (2 x 380  $\mu\text{L}$ ). The collected organic phases were washed with brine (2 mL) and concentrated (about 400  $\mu\text{L}$ ) at 50°C and at reduced pressure (30 mmHg). The obtained mixture was filtered (0.2  $\mu\text{m}$  filter) and the filtrate was added dropwise to heptane (2 mL), under vigorous stirring. After 2 h, the precipitate was recovered by suction, washed with heptane (2 x 1 mL) and dried (24h at 2mmHg; 90°C).

*6-Ethyl analogue of elagolix sodium salt (5)*. Starting material: ethyl (*R*)-4-((2-(4-ethyl-5-(2-fluoro-3-methoxyphenyl)-3-(2-fluoro-6-(trifluoromethyl)benzyl)-2,6-dioxo-3,6-dihydropyrimidin-1(2H)-yl)-1-phenylethyl)amino)butanoate (**62**). White solid. Yield: 65%. Rf = 0.65 (CHCl<sub>3</sub>/MeOH/H<sub>2</sub>O 12.5:4:0.5). <sup>1</sup>H NMR (500 MHz, CD<sub>3</sub>OD)  $\delta$  7.62 (d, *J* = 7.8 Hz, 1H), 7.53 (m, 1H), 7.44 – 7.34 (m, 6H), 7.18 – 7.10 (m, 2H), 6.78 (m, 0.5H), 6.68 (m, 0.5H), 5.41 (m, 2H), 4.55 (m, 1H), 4.43 (m, 2H), 3.89 (s, 3H), 2.84 (m, 1H), 2.76 (m, 1H), 2.50 (m, 1H), 2.45 – 2.24 (m, 3H), 1.77 (m, 2H), 1.02 (m, 3H).

*6-Cyclopentyl analogue of elagolix sodium salt (6)*. Starting material: ethyl (*R*)-4-((2-(4-cyclopentyl-5-(2-fluoro-3-methoxyphenyl)-3-(2-fluoro-6-(trifluoromethyl)benzyl)-2,6-dioxo-3,6-dihydropyrimidin-1(2H)-yl)-1-phenylethyl)amino)butanoate (**63**). White solid. Yield: 65%. Rf = 0.69 (CHCl<sub>3</sub>/MeOH/H<sub>2</sub>O 12.5:4:0.5). <sup>1</sup>H NMR (500 MHz, CD<sub>3</sub>OD)  $\delta$  7.64 (d, *J* = 8.1 Hz, 1H), 7.53 (m, 1H), 7.43 (m, 1H), 7.35 – 7.18 (m, 5H), 7.15 – 7.07 (m, 2H), 6.77 (m, 0.5H), 6.64 (m, 0.5H), 5.34 (m, 2H), 4.29 – 4.02 (m, 3H), 3.90 (s, 1.5H), 3.89 (s, 1.5H), 3.14 (m, 1H), 2.40 (m, 2H), 2.09 (m, 2H), 1.85 – 1.37 (m, 10H). (Phenomenex Lux Cellulose-1, *n*-hexane/*i*PrOH = 6:4 + 0.1% TFA, 0.3 mL/min,  $\lambda$  = 254 nm)  $t_{\text{R}}$ (I atropisomer) = 22.39 min,  $t_{\text{R}}$ (II atropisomer) = 28.92 min.

*6-Methylmethoxy analogue of elagolix sodium salt (7)*. Starting material: ethyl (*R*)-4-((2-(5-(2-fluoro-3-methoxyphenyl)-3-(2-fluoro-6-(trifluoromethyl)benzyl)-4-(methoxymethyl)-2,6-dioxo-3,6-dihydropyrimidin-1(2H)-yl)-1-phenylethyl)amino)butanoate (**64**). White solid. Yield: 60%. Rf = 0.59 (CHCl<sub>3</sub>/MeOH/H<sub>2</sub>O 12.5:4:0.5). <sup>1</sup>H NMR (500 MHz, CD<sub>3</sub>OD)  $\delta$  7.60 (dd, *J* = 7.9, 3.5 Hz, 1H), 7.50 (m, 1H), 7.40 (m, 1H), 7.35 – 7.22 (m, 5H), 7.20 – 7.04 (m, 2H), 6.78

(m, 0.45H), 6.64 (m, 0.51H), 5.45 (m, 2H), 4.44 – 4.07 (m, 5H), 3.90 (s, 3H), 3.11 (s, 1.4H), 3.10 (s, 1.5H), 2.46 (m, 2H), 2.12 (m, 2H), 1.72 (m, 2H).

#### 9.2.3.4 Synthesis of (*R*)-*N*-(2-(4-cyclopentyl-5-(2-fluoro-3-methoxyphenyl)-3-(2-fluoro-6-(trifluoromethyl)benzyl)-2,6-dioxo-3,6-dihydropyrimidin-1(2H)-yl)-1-phenylethyl)acetamide (**65**)

To a solution of **60** (100 mg, 0.17 mmol) in dichloromethane (5 mL), triethylamine (0.22 mL; 1.6 mmol) and acetic anhydride (23  $\mu$ L; 0.24 mmol) were sequentially added. The reaction progress was monitored by TLC analysis (hexane/ethyl acetate 1:1) until starting material disappearance (6h). After removal of the solvent and column chromatography (hexane/ethyl acetate 1:1), pure **65** (96 mg, 0.15 mmol, 88%) was obtained as a white foam.  $R_f$  (I atropisomer) = 0.58,  $R_f$  (II atropisomer) = 0.40 (hexane/ethyl acetate 1:1).  $^1\text{H NMR}$  (500 MHz,  $\text{CDCl}_3$ )  $\delta$  7.55 (d,  $J$  = 7.7 Hz, 1H), 7.39 (td,  $J$  = 8.1, 4.8 Hz, 1H), 7.36 – 7.16 (m, 6H), 7.13 (tt,  $J$  = 8.0, 1.8 Hz, 1H), 7.01 (td,  $J$  = 8.1, 1.6 Hz, 1H), 6.88 (d,  $J$  = 7.1 Hz, 0.43H), 6.78 (dtd,  $J$  = 7.6, 5.9, 2.8 Hz, 1H), 6.70 (ddd,  $J$  = 7.6, 5.9, 1.6 Hz, 0.43H), 5.33 – 5.15 (m, 2H), 4.51 – 4.23 (m, 1H), 4.08 (ddd,  $J$  = 13.8, 6.6, 3.5 Hz, 1H), 3.91 (s, 3H), 3.22 – 3.08 (m, 1H), 1.91 (s, 1.5H), 1.87 (s, 1.5H), 1.86 – 1.40 (m, 8H). HPLC on chiral stationary phase (Chiralpack AD-H, *n*-hexane/*i*PrOH = 8:2 + 0.1% diethylamine, 1.0 mL/min,  $\lambda$  = 254 nm)  $t_R$ (I atropisomer) = 9.00 min,  $t_R$ (II atropisomer) = 16.62 min.

#### 9.2.3.5 General Procedure for Enzyme-Catalyzed Hydrolysis

Compound **63** (5 mg; atropisomeric mixture) were suspended in di-isopropyl ether (2 mL) pre-saturated with water in a 5 mL glass vial followed by addition of the enzyme (50 mg). The mixture was shaken at 300 rpm at the room temperature. A sample of about 50  $\mu$ L was collected regularly, diluted with water, and extracted with ethyl acetate. The organic phase was concentrated under reduced pressure. The residue was dissolved in 2-propanol (about 50  $\mu$ L) and a portion (10  $\mu$ L) was injected in a HPLC system equipped with a Lux Cellulose 1 column.

## 9.2.4 Modifications at the 21-position

#### 9.2.4.1 (*R*)-*N*-(2-(4-cyclopentyl-5-(2-fluoro-3-methoxyphenyl)-3-(2-fluoro-6-(trifluoromethyl)benzyl)-2,6-dioxo-3,6-dihydropyrimidin-1(2H)-yl)-1-phenylethyl)acetamide (**14**)

Compound **14** was synthesized as reported in literature [189]: to a solution of (*R*)-3-(amino(phenyl)methyl)-5-(2-fluoro-3-methoxyphenyl)-1-(2-fluoro-6-(trifluoromethyl)benzyl)-6-methylpyrimidine 2,4(1H,3H)-dione (**20**) (286 mg; 0.52 mmol) in acetic acid (12 ml), bromine (91.0  $\mu$ l, 1.74 mmol) was added under stirring at 0°C. The reaction mixture was stirred at ambient temperature and monitored by TLC (hexane/ethyl acetate/triethylamine) until starting material disappearance (2h). The solvent was removed under reduced pressure (50°C, 30 mmHg). The oily residue was carefully poured in a saturated aqueous solution of sodium bicarbonate (20 mL) and extracted with dichloromethane (3 x 5 mL). The collected organic phases were washed with water (10 mL), dried over sodium sulfate, and filtered. Removal of the solvent resulted in a crude product that was chromatographically purified on silica gel (hexane/ethyl acetate 1:1). Pure **14** (120 mg, 0.19 mmol, 37%) was obtained as a white solid.  $R_f$  = 0.21 (hexane/ethyl acetate 1:1). The full assignment of  $^1\text{H}$  and  $^{13}\text{C}$  NMR signals is given in Section 6.1. HPLC on chiral stationary phase (Chiralpack AD-H, *n*-hexane/*i*PrOH = 7:3 + 0.1% diethylamine, 1.0 mL/min,  $\lambda$  = 254 nm)  $t_R$ (I atropisomer) = 9.72 min,  $t_R$ (II atropisomer) = 16.75 min.

#### 9.2.4.2 (*R*)-N-(2-(5-(6-bromo-2-fluoro-3-methoxyphenyl)-3-(2-fluoro-6-(trifluoromethyl)benzyl)-4-methyl-2,6-dioxo-3,6-dihydropyrimidin-1(2H)-yl)-1-phenylethyl)acetamide (**66**)

To a solution of **14** (50 mg; 0.08 mmol) in dichloromethane (4 mL), triethylamine (33  $\mu$ L; 0.24 mmol) and acetic anhydride (9.5  $\mu$ L; 0.10 mmol) were sequentially added. The reaction mixture was stirred at room temperature. The reaction progress was monitored by TLC (hexane/ethyl acetate 1:1) until starting material disappearance (1h). The solvent was removed under reduced pressure (30 mmHg, 40°C) and the residue was chromatographed over silica gel (hexane/ethyl acetate 6:4) affording pure **66** (48mg; 0.07 mmol; 88%) as a white solid.  $R_f$  = 0.65 (hexane/ethyl acetate 1:1).  $^1\text{H}$  NMR (500 MHz,  $\text{CDCl}_3$ )  $\delta$  7.56 (d,  $J$  = 7.9 Hz, 1H), 7.46 – 7.24 (m, 9H), 7.15 (d,  $J$  = 7.3 Hz, 0.5H), 7.05 – 6.97 (m, 0.5H), 6.96 – 6.89 (m, 1H), 5.83 – 5.26 (m, 3H), 4.67 – 4.41 (m, 1H), 4.14 (ddd,  $J$  = 16.8, 13.8, 3.5 Hz, 1H), 3.90 (s, 1.5H), 3.89 (s, 1.5H), 2.04 (s, 1.5H), 2.03 (s, 1.5H), 1.99 (s, 1.5H), 1.98 (s, 1.5H). HPLC on chiral stationary phase (Chiralpack AD-H, *n*-hexane/*i*PrOH = 7:3 + 0.1% diethylamine, 1.0 mL/min,  $\lambda$  = 254 nm)  $t_R$ (I atropisomer) = 11.60 min,  $t_R$ (II atropisomer) = 17.38 min.

#### 9.2.4.3 (R)-N-(2-(5-(6-bromo-2-fluoro-3-methoxyphenyl)-3-(2-fluoro-6-(trifluoromethyl)benzyl)-4-methyl-2,6-dioxo-3,6-dihydropyrimidin-1(2H)-yl)-1-phenylethyl)butyramide (67)

To a solution of **14** (50 mg; 0.08 mmol) in dichloromethane (4 mL), triethylamine (33  $\mu$ L; 0.24 mmol) and butyric anhydride (16.5  $\mu$ L; 0.10 mmol) were sequentially added. The reaction mixture was stirred at room temperature. The reaction progress was monitored by TLC (hexane/ethyl acetate 1:1) until starting material disappearance (1h). The solvent was removed under reduce pressure (30 mmHg, 40°C) and the residue was chromatographed over silica gel (hexane/ethyl acetate 6:4) affording pure **67** (51 mg; 0.07 mmol; 92%) as a white solid.  $R_f = 0.78$  (hexane/ethyl acetate 1:1).  $^1\text{H}$  NMR (500 MHz,  $\text{CDCl}_3$ )  $\delta$  7.56 (d,  $J = 7.9$  Hz, 1H), 7.46 – 7.34 (m, 4H), 7.33 – 7.28 (m, 2H), 7.24 (dd,  $J = 7.2, 2.0$  Hz, 1H), 6.92 (td,  $J = 8.8, 4.0$  Hz, 1H), 6.82 (d,  $J = 7.1$  Hz, 0H), 5.70 – 5.25 (m, 3H), 4.55 – 4.38 (m, 1H), 4.25 – 4.05 (m, 1H), 3.90 (d,  $J = 0.9$  Hz, 3H), 2.24 – 2.06 (m, 2H), 1.63 – 1.47 (m, 2H), , 0.89 (td,  $J = 7.4, 3.1$  Hz, 3H). HPLC on chiral stationary phase (Chiralpack AD-H, *n*-hexane/*i*PrOH = 7:3 + 0.1% diethylamine, 1.0 mL/min,  $\lambda = 254$  nm)  $t_{R(I \text{ atropisomer})} = 16.15$  min,  $t_{R(II \text{ atropisomer})} = 17.02$  min.

#### 9.2.4.4 General Procedure for Enzyme-Catalyzed Hydrolysis

Compounds **66** or **67** (5 mg; atropisomeric mixture) were suspended in the indicated solvent or mixture of solvents (Table 15; 2 mL) in a 5 mL glass vial followed by addition of the enzyme (50 mg). The mixture was shaken at 300 rpm and at the temperature indicated (Table 15). A sample of about 50  $\mu$ L was collected regularly, diluted with water, and extracted with ethyl acetate. The organic phase was concentrated under reduced pressure. The residue was dissolved in 2-propanol (about 50  $\mu$ L) and a portion (10  $\mu$ L) was injected in a HPLC system equipped with a Chiralpak AD-H column.

#### 9.2.4.5 General Procedure for Enzyme-Catalyzed N-acylation

Compound **14** (5 mg; atropisomeric mixture) was dissolved or suspended in the organic solvent (Table 14; 2 mL) in a 5 mL glass vial followed by addition of the enzyme (50 mg). The mixture was shaken at 300 rpm and and at the temperature indicated (Table 14). A sample of about 50  $\mu$ L was collected regularly and concentrated under reduced pressure. The residue was dissolved in 2-propanol (about

50  $\mu\text{L}$ ) and a portion (10  $\mu\text{L}$ ) was injected in a HPLC system equipped with a Chiralpak AD-H column.

### 9.3 Biological methods

The biological studies are being carried out in collaboration with Prof. Marco Bonomi and Dr. Valeria Vezzoli at “Istituto Auxologico Italiano”, Laboratory of Endocrine and Metabolic Research, Cusano Milanino in Italy.

The cDNA of GnRH1R (UniProt accession P30968) wild type (generously provided by Prof. Livio Casarini and Dr. Samantha Sperduti at the Unit of Endocrinology, Department of Biomedical, Metabolic and Neural Sciences, University of Modena and Reggio Emilia) was sub-cloned into pcDNA3.1 (+) expression vector with a HA signal and expressed in HEK293T cells. HEK293T cells were cultured in a six-well plate with Dulbecco’s modified Eagle’s medium supplemented with 10% (v/v) fetal bovine serum at a density of  $3 \times 10^5$  cells per well. Cells were collected 48 h post transfection. Cell surface expression of GnRH1R were measured by western blot using ANTI-HA antibody.

IP accumulation was determined using Cisbio IP1 assay kit according to the manufacturer’s instructions. For agonist GnRH peptide stimuli, in brief, the harvested cells were distributed in a low volume 24-well dish by adding increased concentration of agonist GnRH peptide for 1 h. For antagonist curves, cells were pre-treated with **1** ( $10^{-4}$ M) for 1 h, and then stimulated with optimized concentration ( $10^{-6}$ ,  $10^{-4}$ M) of GnRH peptide for 1 h. The optical density (OD) was read at 450 nm with BioRad microplate reader. The accumulation of IP1 was calculated according to a standard dose–response curve in GraphPad Prism 7 (GraphPad Software). Data were represented as the mean  $\pm$  SEM from three independent experiments and all experiments were repeated at least three times.

## 9.4 Crystallography

X-Ray analyses were performed on a Bruker SMART APEX II CCD Single Crystal X-ray Diffractometer, equipped with graphite-monochromated Mo-K $\alpha$  radiation ( $\lambda = 0.71073 \text{ \AA}$ ) at 298(2) K.

X-ray data were acquired in the  $\theta$  range 2–20° recording four sets of 360 bidimensional CCD frames with the following operative conditions: omega rotation axis, scan width 0.5°, acquisition time 50 s, sample-to-detector distance 50 mm, phi angle fixed at four different values (0°, 90°, 180° and 270°) for the four different sets. Omega-rotation frames were processed using the SAINT software [208] for data reduction (intensity integration, background, Lorentz, and polarization corrections) and for the determination of accurate unit-cell dimensions. Absorption effects were empirically evaluated by the SADABS software [209], applying an absorption correction to the data.

### 9.4.1 Crystal structure of 25 (Section 3.4)

The crystal structure was solved by direct methods and refined on  $F^2$  by full-matrix least-squares using Bruker's SHELXL-2018/1 [210]. Crystal data and structural parameters are summarized below:

| <b>Crystal Data</b>  |  |
|--|--|
| Chemical formula   | C <sub>20</sub> H <sub>15</sub> F <sub>5</sub> N <sub>2</sub> O <sub>3</sub> |
| $M_r$  | 426.34   |
| Crystal system, space group  | Orthorhombic, P bca  |
| $a, b, c$ (Å)  | 11.165 (2), 11.073 (2), 30.367(6)  |
| $V$ (Å <sup>3</sup> )  | 3754.2(13)   |
| $Z$  | 8  |
| $F$ (000)  | 1744   |
| Density (g/cm <sup>3</sup> )   | 1.509  |
| Temperature (K)  | 298  |
| Radiation type   | Mo-K $\alpha$ ( $\lambda = 0.71073 \text{ \AA}$ )                            |
| $\mu$ (mm <sup>-1</sup> )  | 1.135  |
| Crystal size (mm)  | 0.06 × 0.03 × 0.02   |
| <b>Data collection</b>   |  |
| Diffractometer   | Bruker-Axs Smart-Apex CCD  |
| $T_{\min}, T_{\max}$   | 0.893, 1.000   |
| No. of measured, independent and observed [ $I > 2\sigma(I)$ ] reflections | 29,138, 4175, 1715   |
| $R_{\text{int}}$   | 0.0298   |
| <b>Structure refinement</b>  |  |



|                   |   |
|-------------------|---|
| $R, wR^2, S$      | 0.0437 ( $I > 2\sigma(I)$ ) and 0.1119 (all),<br>0.0973 ( $I > 2\sigma(I)$ ) and 0.1126 (all), 0.760<br>(all) |
| No. of parameters | 271   |
| No. of restraints | 0   |

The refined structure was inspected using ORTEP-3 (v. 2020.1) [170] and analyzed by Mercury 4.0 (v. 2021.3.0) [211] and PARST [212], within the WinGX suite (v. 2021.3) [212]. Graphical representations were rendered with Mercury. Crystallographic data were deposited to the Cambridge Crystallographic Data Center under accession number CCDC 2248213.

### 9.4.2 Crystal structure of 30 (Section 4.6)

The crystal structure was solved by direct methods and refined on  $F^2$  by full-matrix least-squares using Bruker's SHELXL-2018/1 [210]. Crystal data and structural parameters are summarized below:

#### Crystal Data

|                        |  |
|------------------------|--|
| Identification code    | 30   |
| Empirical formula      | $C_{80}H_{60}F_{20}N_8O_8S_4$ (a.u.)   |
| Formula weight         | 1769.60 (a.u.)   |
| Temperature            | 150(2) K   |
| Wavelength             | 1.54184 Å  |
| Crystal system         | Triclinic  |
| Space group            | P-1  |
| Unit cell dimensions   | $a = 14.3840(3)$ Å $\alpha = 90.133(2)^\circ$ .<br>$b = 14.8334(3)$ Å $\beta = 100.079(2)^\circ$ .<br>$c = 19.4173(4)$ Å $\gamma = 103.529(2)^\circ$ . |
| Volume                 | $3961.77(15)$ Å <sup>3</sup>   |
| Z                      | 2  |
| Density (calculated)   | 1.483 Mg/m <sup>3</sup>  |
| Absorption coefficient | 2.064 mm <sup>-1</sup>   |
| F(000)                 | 1808   |
| Crystal size           | 0.05 x 0.035 x 0.02 mm <sup>3</sup>  |

#### Data collection

|   |  |
|---|--|
| $\theta$ range for data collection      | 3.067 to 65.089°   |
| Index ranges                            | $-16 \leq h \leq 13, -17 \leq k \leq 17, -22 \leq l \leq 22$ |
| Reflections collected                   | 72,884   |
| Independent reflections                 | 13491 [ $R_{int} = 0.0597$ ]                                 |
| Completeness to $\theta = 65.089^\circ$ | 99.9 %   |

#### Structure refinement

|                                      |                                    |
|--------------------------------------|------------------------------------|
| Refinement method                    | Full-matrix least-squares on $F^2$ |
| Data / restraints / parameters       | 13491 / 0 / 1101                   |
| Goodness-of-fit on $F^2$             | 1.045                              |
| Final R indices [ $I > 2\sigma(I)$ ] | $R1 = 0.0679, wR2 = 0.1853$        |

|                             |                                   |
|-----------------------------|-----------------------------------|
| R indices (all data)        | R1 = 0.0715, wR2 = 0.1893         |
| Largest diff. peak and hole | 1.381 and -0.461 eÅ <sup>-3</sup> |

---

The refined structure was inspected using ORTEP-3 (v. 2020.1) [170] and analyzed by Mercury 4.0 (v. 2021.3.0) [211] and PARST [212], within the WinGX suite (v. 2021.3) [212]. Graphical representations were rendered with Mercury.

## References

---

1. Casati, L.; Ciceri, S.; Maggi, R.; Bottai, D. Physiological and pharmacological overview of the gonadotropin releasing hormone. *Biochemical pharmacology* **2023**, *212*, 115553, doi:10.1016/j.bcp.2023.115553.
2. Schally, A.V.; Arimura, A.; Baba, Y.; Nair, R.M.; Matsuo, H.; Redding, T.W.; Debeljuk, L. Isolation and properties of the FSH and LH-releasing hormone. *Biochemical and Biophysical Research Communications* **1971**, *43*, 393–399, doi:10.1016/0006-291X(71)90766-2.
3. Maggi, R.; Cariboni, A.M.; Marelli, M.M.; Moretti, R.M.; Andrè, V.; Marzagalli, M.; Limonta, P. GnRH and GnRH receptors in the pathophysiology of the human female reproductive system. *Hum Reprod Update* **2016**, *22*, 358–381, doi:10.1093/humupd/dmv059.
4. Limonta, P.; Marelli, M.M.; Moretti, R.; Marzagalli, M.; Fontana, F.; Maggi, R. Chapter Two - GnRH in the Human Female Reproductive Axis. In *Vitamins and Hormones : Ovarian Cycle*; Litwack, G., Ed.; Academic Press, 2018; pp 27–66, ISBN 0083-6729.
5. Le Tissier, P.; Campos, P.; Lafont, C.; Romanò, N.; Hodson, D.J.; Mollard, P. An updated view of hypothalamic-vascular-pituitary unit function and plasticity. *Nat Rev Endocrinol* **2017**, *13*, 257–267, doi:10.1038/nrendo.2016.193.
6. Janes, L. Hypothalamic-Pituitary-Gonadal (HPG) Axis. *Encyclopedia of Personality and Individual Differences*; Springer, Cham, 2016; pp 1–2.
7. Ferin, M. Gonadotropin Secretion, Effects of Stress on\*. In *Encyclopedia of stress*, 2nd ed.; Fink, G., Ed.; Elsevier: San Diego, Calif, 2007-; pp 228–234, ISBN 978-0-12-373947-6.
8. Shaw, N.D.; Histed, S.N.; Srouji, S.S.; Yang, J.; Lee, H.; Hall, J.E. Estrogen negative feedback on gonadotropin secretion: evidence for a direct pituitary effect in women. *J Clin Endocrinol Metab* **2010**, *95*, 1955–1961, doi:10.1210/jc.2009-2108.
9. Tilbrook, A.J.; Clarke, I.J. Negative feedback regulation of the secretion and actions of gonadotropin-releasing hormone in males. *Biol Reprod* **2001**, *64*, 735–742, doi:10.1095/biolreprod64.3.735.
10. DePaolo, L.V.; King, R.A.; Carrillo, A.J. In vivo and in vitro examination of an autoregulatory mechanism for luteinizing hormone-releasing hormone. *Endocrinology* **1987**, *120*, 272–279, doi:10.1210/endo-120-1-272.
11. Conn, P.M.; Staley, D.D.; Yasumoto, T.; Huckle, W.R.; Janovick, J.A. Homologous desensitization with gonadotropin-releasing hormone (GnRH) also diminishes gonadotrope responsiveness to maitotoxin: a role for the GnRH receptor-regulated calcium ion channel in mediation of cellular desensitization. *Mol Endocrinol* **1987**, *1*, 154–159, doi:10.1210/mend-1-2-154.

12. Davidson, J.S.; Wakefield, I.K.; Millar, R.P. Absence of rapid desensitization of the mouse gonadotropin-releasing hormone receptor. *Biochem J* **1994**, *300* (Pt 2), 299–302, doi:10.1042/bj3000299.
13. Jennes, L.; Coy, D.; Conn, P.M. Receptor-mediated uptake of GnRH agonist and antagonists by cultured gonadotropes: evidence for differential intracellular routing. *Peptides* **1986**, *7*, 459–463, doi:10.1016/0196-9781(86)90015-X.
14. Jennes, L.; Stumpf, W.E.; Conn, P.M. Intracellular pathways of electron-opaque gonadotropin-releasing hormone derivatives bound by cultured gonadotropes. *Endocrinology* **1983**, *113*, 1683–1689, doi:10.1210/endo-113-5-1683.
15. Martin, K.; Santoro, N.; Hall, J.; Filicori, M.; Wierman, M.; Crowley, W.F. Clinical review 15: Management of ovulatory disorders with pulsatile gonadotropin-releasing hormone. *J Clin Endocrinol Metab* **1990**, *71*, 1081A-1081G, doi:10.1210/jcem-71-5-1081.
16. *Hormones, brain and behavior*; Pfaff, D.W., Ed., 2. ed.; Elsevier, Acad. Press: Amsterdam, 2009, ISBN 978-0-08-088783-8.
17. Muñoz-Cruz, S.; Togno-Pierce, C.; Morales-Montor, J. Non-reproductive effects of sex steroids: their immunoregulatory role. *Current topics in medicinal chemistry* **2011**, *11*, 1714–1727, doi:10.2174/156802611796117630.
18. Terasawa, E. The mechanism underlying the pubertal increase in pulsatile GnRH release in primates. *Journal of Neuroendocrinology* **2022**, *34*, e13119, doi:10.1111/jne.13119.
19. Bonomi, M.; Libri, D.V.; Guizzardi, F.; Guarducci, E.; Maiolo, E.; Pignatti, E.; Asci, R.; Persani, L. New understandings of the genetic basis of isolated idiopathic central hypogonadism. *Asian Journal of Andrology* **2012**, *14*, 49–56, doi:10.1038/aja.2011.68.
20. Duan, C.; Allard, J. Gonadotropin-releasing hormone neuron development in vertebrates. *General and Comparative Endocrinology* **2020**, *292*, 113465, doi:10.1016/j.ygcen.2020.113465.
21. Barran, P.E.; Roeske, R.W.; Pawson, A.J.; Sellar, R.; Bowers, M.T.; Morgan, K.; Lu, Z.-L.; Tsuda, M.; Kusakabe, T.; Millar, R.P. Evolution of constrained gonadotropin-releasing hormone ligand conformation and receptor selectivity. *J. Biol. Chem.* **2005**, *280*, 38569–38575, doi:10.1074/jbc.M503086200.
22. Millar, R.P. GnRHs and GnRH receptors. *Animal Reproduction Science* **2005**, *88*, 5–28, doi:10.1016/j.anireprosci.2005.05.032.
23. Yu, W.H.; Karanth, S.; Walczewska, A.; Sower, S.A.; McCann, S.M. A hypothalamic follicle-stimulating hormone-releasing decapeptide in the rat. *Proc. Natl. Acad. Sci. U. S. A.* **1997**, *94*, 9499–9503, doi:10.1073/pnas.94.17.9499.
24. Latimer, V.S.; Rodrigues, S.M.; Garyfallou, V.T.; Kohama, S.G.; White, R.B.; Fernald, R.D.; Urbanski, H.F. Two molecular forms of gonadotropin-releasing hormone (GnRH-I and GnRH-II) are expressed by two separate populations of cells in the rhesus macaque hypothalamus. *Molecular Brain Research* **2000**, *75*, 287–292, doi:10.1016/S0169-328X(99)00316-2.

25. Densmore, V.S.; Urbanski, H.F. Relative effect of gonadotropin-releasing hormone (GnRH)-I and GnRH-II on gonadotropin release. *J Clin Endocrinol Metab* **2003**, *88*, 2126–2134, doi:10.1210/jc.2002-021359.
26. Urbanski, H.F. Differential roles of GnRH-I and GnRH-ii neurons in the control of the primate reproductive axis. *Front. Endocrinol.* **2012**, *3*, 20, doi:10.3389/fendo.2012.00020.
27. Hong, I.-S.; Cheung, A.P.; Leung, P.C.K. Gonadotropin-releasing hormones I and II induce apoptosis in human granulosa cells. *J Clin Endocrinol Metab* **2008**, *93*, 3179–3185, doi:10.1210/jc.2008-0127.
28. Cheon, K.W.; Lee, H.S.; Parhar, I.S.; Kang, I.S. Expression of the second isoform of gonadotrophin-releasing hormone (GnRH-II) in human endometrium throughout the menstrual cycle. *Mol Hum Reprod* **2001**, *7*, 447–452, doi:10.1093/molehr/7.5.447.
29. Millar, R.P.; Pawson, A.J.; Morgan, K.; Rissman, E.F.; Lu, Z.-L. Diversity of actions of GnRHs mediated by ligand-induced selective signaling. *Frontiers in Neuroendocrinology* **2008**, *29*, 17–35, doi:10.1016/j.yfrne.2007.06.002.
30. Sower, S.A.; Chiang, Y.C.; Lovas, S.; Conlon, J.M. Primary structure and biological activity of a third gonadotropin-releasing hormone from lamprey brain. *Endocrinology* **1993**, *132*, 1125–1131, doi:10.1210/endo.132.3.8440174.
31. Deragon, K.L.; Sower, S.A. Effects of lamprey gonadotropin-releasing hormone-III on steroidogenesis and spermiation in male sea lampreys. *General and Comparative Endocrinology* **1994**, *95*, 363–367, doi:10.1006/gcen.1994.1134.
32. Kovacs, M.; Seprodi, J.; Koppan, M.; Horvath, J.E.; Vincze, B.; Teplan, I.; Flerko, B. Lamprey gonadotropin hormone-releasing hormone-III has no selective follicle-stimulating hormone-releasing effect in rats. *Journal of Neuroendocrinology* **2002**, *14*, 647–655, doi:10.1046/j.1365-2826.2002.00828.x.
33. Lin, L.S.; Roberts, V.J.; Yen, S.S. Expression of human gonadotropin-releasing hormone receptor gene in the placenta and its functional relationship to human chorionic gonadotropin secretion. *J Clin Endocrinol Metab* **1995**, *80*, 580–585, doi:10.1210/jcem.80.2.7852524.
34. Harrison, G.S.; Wierman, M.E.; Nett, T.M.; Glode, L.M. Gonadotropin-releasing hormone and its receptor in normal and malignant cells. *Endocrine-Related Cancer* **2004**, *11*, 725–748, doi:10.1677/erc.1.00777.
35. Gründker, C.; Emons, G. The Role of Gonadotropin-Releasing Hormone in Cancer Cell Proliferation and Metastasis. *Front. Endocrinol.* **2017**, *8*, 187, doi:10.3389/fendo.2017.00187.
36. Wang, L.; Chadwick, W.; Park, S.-S.; Zhou, Y.; Silver, N.; Martin, B.; Maudsley, S. Gonadotropin-releasing hormone receptor system: modulatory role in aging and neurodegeneration. *CNS & neurological disorders drug targets* **2010**, *9*, 651–660, doi:10.2174/187152710793361559.
37. Chen, Y.-M.; Qi, Q.-R.; Xie, Q.-Z.; Yang, Y.-F.; Xia, Y.; Zhou, X.-D. Effect of Progestin-primed Ovarian Stimulation Protocol on Outcomes of Aged Infertile

- Women Who Failed to Get Pregnant in the First IVF/ ICSI Cycle: A Self-controlled Study. *Current medical science* **2018**, *38*, 513–518, doi:10.1007/s11596-018-1908-z.
38. Steven J. Ory, M.D. Role of GnRH Agonists and Antagonists in Controlled Ovarian Stimulation (COS) in IVF. *Contemporary OB/GYN [Online]*, February 16, 2023. Available online: <https://www.contemporaryobgyn.net/view/role-of-gnrh-agonists-and-antagonists-in-controlled-ovarian-stimulation-cos-in-ivf> (accessed on 2 November 2023).
  39. Chandra, V.; Kim, J.J.; Benbrook, D.M.; Dwivedi, A.; Rai, R. Therapeutic options for management of endometrial hyperplasia. *Journal of gynecologic oncology* **2016**, *27*, e8, doi:10.3802/jgo.2016.27.e8.
  40. Wright, D.; Kim, J.W.; Lindsay, H.; Catherino, W.H. A Review of GnRH Antagonists as Treatment for Abnormal Uterine Bleeding-Leiomyoma (AUB-L) and Their Influence on the Readiness of Service Members. *Mil Med* **2022**, *188*, e1620-e1624, doi:10.1093/milmed/usac078.
  41. Pan, E.; McKay, R. *GNRH agonists vs antagonists in prostate cancer: How to choose*; MJH Life Sciences, 2021.
  42. Janknegt, R.; Boone, N.; Erdkamp, F.; Zambon, V. GnRH agonists and antagonists in prostate cancer. *GaBI J* **2014**, *3*, 133–142, doi:10.5639/gabij.2014.0303.031.
  43. Yan, W.; Cheng, L.; Wang, W.; Wu, C.; Yang, X.; Du, X.; Ma, L.; Qi, S.; Wei, Y.; Lu, Z.; et al. Structure of the human gonadotropin-releasing hormone receptor GnRH1R reveals an unusual ligand binding mode. *Nat Commun* **2020**, *11*, 5287, doi:10.1038/s41467-020-19109-w.
  44. Kakar, S.S.; Malik, M.; Winters, S.J.; Mazhawidza, W. Gonadotropin-Releasing Hormone Receptors: Structure, Expression, and Signaling Transduction. In *Vitamins and Hormones : Ovarian Cycle*; Litwack, G., Ed.; Academic Press, 2018; pp 151–207, ISBN 0083-6729.
  45. Millar, R.; Lowe, S.; Conklin, D.; Pawson, A.; Maudsley, S.; Troskie, B.; Ott, T.; Millar, M.; Lincoln, G.; Sellar, R.; et al. A novel mammalian receptor for the evolutionarily conserved type II GnRH. *Proc. Natl. Acad. Sci. U. S. A.* **2001**, *98*, 9636–9641, doi:10.1073/pnas.141048498.
  46. Neill, J.D.; Musgrove, L.C.; Duck, L.W. Newly recognized GnRH receptors: function and relative role. *Trends in Endocrinology & Metabolism* **2004**, *15*, 383–392, doi:10.1016/j.tem.2004.08.005.
  47. Montagnani Marelli, M.; Manea, M.; Moretti, R.M.; Marzagalli, M.; Limonta, P. Oxime bond-linked daunorubicin-GnRH-III bioconjugates exert antitumor activity in castration-resistant prostate cancer cells via the type I GnRH receptor. *International journal of oncology* **2015**, *46*, 243–253, doi:10.3892/ijo.2014.2730.
  48. Wu, H.; Li, G.; Liu, S.; Di Liu; Chen, G.; Hu, N.; Suo, Y.; You, J. Simultaneous determination of six triterpenic acids in some Chinese medicinal herbs using ultrasound-assisted dispersive liquid-liquid microextraction and high-

- performance liquid chromatography with fluorescence detection. *Journal of Pharmaceutical and Biomedical Analysis* **2015**, *107*, 98–107, doi:10.1016/j.jpba.2014.10.031.
49. Montagnani Marelli, M.; Moretti, R.M.; Mai, S.; Januszkiewicz-Caulier, J.; Motta, M.; Limonta, P. Type I gonadotropin-releasing hormone receptor mediates the antiproliferative effects of GnRH-II on prostate cancer cells. *J Clin Endocrinol Metab* **2009**, *94*, 1761–1767, doi:10.1210/jc.2008-1741.
  50. Günthert, A.R.; Gründker, C.; Hollmann, K.; Emons, G. Luteinizing hormone-releasing hormone induces JunD-DNA binding and extends cell cycle in human ovarian cancer cells. *Biochemical and Biophysical Research Communications* **2002**, *294*, 11–15, doi:10.1016/S0006-291X(02)00427-8.
  51. Kim, K.-Y.; Choi, K.-C.; Park, S.-H.; Chou, C.-S.; Auersperg, N.; Leung, P.C.K. Type II gonadotropin-releasing hormone stimulates p38 mitogen-activated protein kinase and apoptosis in ovarian cancer cells. *J Clin Endocrinol Metab* **2004**, *89*, 3020–3026, doi:10.1210/jc.2003-031871.
  52. Belchetz, P.E.; Plant, T.M.; Nakai, Y.; Keogh, E.J.; Knobil, E. Hypophysial responses to continuous and intermittent delivery of hypothalamic gonadotropin-releasing hormone. *Science* **1978**, *202*, 631–633, doi:10.1126/science.100883.
  53. PIMSTONE, B.; EPSTEIN, S.; HAMILTON, S.M.; LeROITH, D.; HENDRICKS, S. Metabolic clearance and plasma half disappearance time of exogenous gonadotropin releasing hormone in normal subjects and in patients with liver disease and chronic renal failure. *J Clin Endocrinol Metab* **1977**, *44*, 356–360, doi:10.1210/jcem-44-2-356.
  54. Jeffcoate, S.L.; Greenwood, R.H.; Holland, D.T. Blood and urine clearance of luteinizing hormone releasing hormone in man measured by radioimmunoassay. *J. Endocrinol.* **1974**, *60*, 305–314, doi:10.1677/joe.0.0600305.
  55. Barron, J.L.; Millar, R.P.; Searle, D. Metabolic clearance and plasma half-disappearance time of D-TRP6 and exogenous luteinizing hormone-releasing hormone. *J Clin Endocrinol Metab* **1982**, *54*, 1169–1173, doi:10.1210/jcem-54-6-1169.
  56. Sealfon, S.C.; Weinstein, H.; Millar, R.P. Molecular mechanisms of ligand interaction with the gonadotropin-releasing hormone receptor. *Endocr. Rev.* **1997**, *18*, 180–205, doi:10.1210/edrv.18.2.0295.
  57. Engel, J.B.; Schally, A.V. Drug Insight: clinical use of agonists and antagonists of luteinizing-hormone-releasing hormone. *Nat. Clin. Pract. Endocrinol. Metab.* **2007**, *3*, 157–167, doi:10.1038/ncpendmet0399.
  58. Kaiser, U.B. Studies of Gonadotropin-Releasing Hormone (GnRH) Action Using GnRH Receptor-Expressing Pituitary Cell Lines. *Endocr. Rev.* **1997**, *18*, 46–70, doi:10.1210/er.18.1.46.

59. Cook, T.; Sheridan, W.P. Development of GnRH antagonists for prostate cancer: new approaches to treatment. *Oncologist* **2000**, *5*, 162–168, doi:10.1634/theoncologist.5-2-162.
60. Herbst, K.L. Gonadotropin-releasing hormone antagonists. *Current Opinion in Pharmacology* **2003**, *3*, 660–666, doi:10.1016/j.coph.2003.06.009.
61. Schally, A.V. LH-RH analogues: I. Their impact on reproductive medicine. *Gynecological Endocrinology* **1999**, *13*, 401–409, doi:10.3109/09513599909167587.
62. Mezo, G.; Manea, M. Luteinizing hormone-releasing hormone antagonists. *Expert Opinion on Therapeutic Patents* **2009**, *19*, 1771–1785, doi:10.1517/13543770903410237.
63. Emons, G.; Ortmann, O.; Becker, M.; Irmer, G.; Springer, B.; Laun, R.; Hölzel, F.; Schulz, K.D.; Schally, A.V. High affinity binding and direct antiproliferative effects of LHRH analogues in human ovarian cancer cell lines. *Cancer research* **1993**, *53*, 5439–5446.
64. Kleinman, D.; Douvdevani, A.; Schally, A.V.; Levy, J.; Sharoni, Y. Direct growth inhibition of human endometrial cancer cells by the gonadotropin-releasing hormone antagonist SB-75: Role of apoptosis. *American Journal of Obstetrics and Gynecology* **1994**, *170*, 96–102, doi:10.1016/S0002-9378(13)70287-4.
65. Yano, T.; Pinski, J.; Halmos, G.; Szepeshazi, K.; Groot, K.; Schally, A.V. Inhibition of growth of OV-1063 human epithelial ovarian cancer xenografts in nude mice by treatment with luteinizing hormone-releasing hormone antagonist SB-75. *Proc. Natl. Acad. Sci. U. S. A.* **1994**, *91*, 7090–7094, doi:10.1073/pnas.91.15.7090.
66. Rama, S.; Rao, A.J. Embryo implantation and GnRH antagonists: the search for the human placental GnRH receptor. *Hum. Reprod.* **2001**, *16*, 201–205, doi:10.1093/humrep/16.2.201.
67. Yu, B.; Ruman, J.; Christman, G. The role of peripheral gonadotropin-releasing hormone receptors in female reproduction. *Fertility and Sterility* **2011**, *95*, 465–473, doi:10.1016/j.fertnstert.2010.08.045.
68. Scheiber, M.D.; Liu, J.H. The Use of Gonadotropin-Releasing Hormone to Induce Ovulation. *GLOWM* **2011**, doi:10.3843/GLOWM.10340.
69. Reid, R.L.; Leopold, G.R.; Yen, S.S. Induction of ovulation and pregnancy with pulsatile luteinizing hormone releasing factor: dosage and mode of delivery. *Fertility and Sterility* **1981**, *36*, 553–559, doi:10.1016/S0015-0282(16)45850-4.
70. Martin, K.; Santoro, N.; Hall, J.; Filicori, M.; Wierman, M.; Crowley, W.F. Clinical review 15: Management of ovulatory disorders with pulsatile gonadotropin-releasing hormone. *J Clin Endocrinol Metab* **1990**, *71*, 1081A–1081G, doi:10.1210/jcem-71-5-1081.
71. Martin, J.B. Molecular genetics in neurology. *Annals of Neurology* **1993**, *34*, 757–773, doi:10.1002/ana.410340603.



72. Casper, R.F. Introduction: Gonadotropin-releasing hormone agonist triggering of final follicular maturation for in vitro fertilization. *Fertility and Sterility* **2015**, *103*, 865–866, doi:10.1016/j.fertnstert.2015.01.012.
73. Humaidan, P.; Bredkjaer, H.E.; Bungum, L.; Bungum, M.; Grøndahl, M.L.; Westergaard, L.; Andersen, C.Y. GnRH agonist (buserelin) or hCG for ovulation induction in GnRH antagonist IVF/ICSI cycles: a prospective randomized study. *Hum Reprod* **2005**, *20*, 1213–1220, doi:10.1093/humrep/deh765.
74. Mittelman-Smith, M.A.; Wong, A.M.; Kathiresan, A.S.Q.; Micevych, P.E. Classical and membrane-initiated estrogen signaling in an in vitro model of anterior hypothalamic kisspeptin neurons. *Endocrinology* **2015**, *156*, 2162–2173, doi:10.1210/en.2014-1803.
75. Platteuw, L.; D'Hooghe, T. Novel agents for the medical treatment of endometriosis. *Curr. Opin. Obstet. Gynecol.* **2014**, *26*, 243–252, doi:10.1097/GCO.0000000000000084.
76. Zito, G.; Luppi, S.; Giolo, E.; Martinelli, M.; Venturin, I.; Di Lorenzo, G.; Ricci, G. Medical treatments for endometriosis-associated pelvic pain. *Biomed Res. Int.* **2014**, *2014*, 191967, doi:10.1155/2014/191967.
77. Eugster, E.A. Treatment of Central Precocious Puberty. *Journal of the Endocrine Society* **2019**, *3*, 965–972, doi:10.1210/js.2019-00036.
78. Schagen, S.E.E.; Cohen-Kettenis, P.T.; Delemarre-van de Waal, Henriette A.; Hannema, S.E. Efficacy and Safety of Gonadotropin-Releasing Hormone Agonist Treatment to Suppress Puberty in Gender Dysphoric Adolescents. *The Journal of Sexual Medicine* **2016**, *13*, 1125–1132, doi:10.1016/j.jsxm.2016.05.004.
79. Fontana, F.; Marzagalli, M.; Montagnani Marelli, M.; Raimondi, M.; Moretti, R.M.; Limonta, P. Gonadotropin-Releasing Hormone Receptors in Prostate Cancer: Molecular Aspects and Biological Functions. *International Journal of Molecular Sciences* **2020**, *21*, 9511, doi:10.3390/ijms21249511.
80. Huerta-Reyes, M.; Maya-Núñez, G.; Pérez-Solis, M.A.; López-Muñoz, E.; Guillén, N.; Olivo-Marin, J.-C.; Aguilar-Rojas, A. Treatment of Breast Cancer With Gonadotropin-Releasing Hormone Analogs. *Frontiers in Oncology* **2019**, *9*, 943, doi:10.3389/fonc.2019.00943.
81. Ciebiera, M.; Madueke-Laveaux, O.S.; Feduniw, S.; Ulin, M.; Spaczyński, R.; Zgliczyńska, M.; Bączkowska, M.; Zarychta, E.; Łoziński, T.; Ali, M.; et al. GnRH agonists and antagonists in therapy of symptomatic uterine fibroids - current roles and future perspectives. *Expert Opinion on Pharmacotherapy* **2023**, *24*, 1799–1809, doi:10.1080/14656566.2023.2248890.
82. Blumenfeld, Z.; Evron, A. Preserving fertility when choosing chemotherapy regimens - the role of gonadotropin-releasing hormone agonists. *Expert Opinion on Pharmacotherapy* **2015**, *16*, 1009–1020, doi:10.1517/14656566.2015.1031654.
83. Cardozo, E.R.; Thomson, A.P.; Karmon, A.E.; Dickinson, K.A.; Wright, D.L.; Sabatini, M.E. Ovarian stimulation and in-vitro fertilization outcomes of cancer

- patients undergoing fertility preservation compared to age matched controls: a 17-year experience. *J Assist Reprod Genet* **2015**, *32*, 587–596, doi:10.1007/s10815-015-0428-z.
84. Chen, H.; Xiao, L.; Li, J.; Cui, L.; Huang, W. Adjuvant gonadotropin-releasing hormone analogues for the prevention of chemotherapy-induced premature ovarian failure in premenopausal women. *Cochrane Database Syst. Rev.* **2019**, *3*, CD008018, doi:10.1002/14651858.CD008018.pub3.
  85. Mahajan, N. Fertility preservation in female cancer patients: An overview. *Journal of Human Reproductive Sciences* **2015**, *8*, 3–13, doi:10.4103/0974-1208.153119.
  86. Burnham, V.L.; Thornton, J.E. Luteinizing hormone as a key player in the cognitive decline of Alzheimer's disease. *Hormones and Behavior* **2015**, *76*, 48–56, doi:10.1016/j.yhbeh.2015.05.010.
  87. Smith, M.A.; Bowen, R.L.; Nguyen, R.Q.; Perry, G.; Atwood, C.S.; Rimm, A.A. Putative Gonadotropin-Releasing Hormone Agonist Therapy and Dementia: An Application of Medicare Hospitalization Claims Data. *Journal of Alzheimer's disease : JAD* **2018**, *63*, 1269–1277, doi:10.3233/JAD-170847.
  88. Altamira-Camacho, M.; Medina-Aguíñaga, D.; Cruz, Y.; Calderón-Vallejo, D.; Kovacs, K.; Rotondo, F.; Quintanar, J.L. Leuprolide Acetate, a GnRH Agonist, Improves the Neurogenic Bowel in Ovariectomized Rats with Spinal Cord Injury. *Dig Dis Sci* **2020**, *65*, 423–430, doi:10.1007/s10620-019-05783-4.
  89. Guzmán-Soto, I.; Salinas, E.; Hernández-Jasso, I.; Quintanar, J.L. Leuprolide acetate, a GnRH agonist, improves experimental autoimmune encephalomyelitis: a possible therapy for multiple sclerosis. *Neurochem Res* **2012**, *37*, 2190–2197, doi:10.1007/s11064-012-0842-x.
  90. Emons, G.; Gründker, C. The Role of Gonadotropin-Releasing Hormone (GnRH) in Endometrial Cancer. *Cells* **2021**, *10*, 292, doi:10.3390/cells10020292.
  91. Engel, J.; Emons, G.; Pinski, J.; Schally, A.V. AEZS-108 : a targeted cytotoxic analog of LHRH for the treatment of cancers positive for LHRH receptors. *Expert Opinion on Investigational Drugs* **2012**, *21*, 891–899, doi:10.1517/13543784.2012.685128.
  92. Gründker, C.; Emons, G. Role of Gonadotropin-Releasing Hormone (GnRH) in Ovarian Cancer. *Cells* **2021**, *10*, 437, doi:10.3390/cells10020437.
  93. Betz, S.F.; Zhu, Y.-F.; Chen, C.; Struthers, R.S. Non-peptide gonadotropin-releasing hormone receptor antagonists. *J. Med. Chem.* **2008**, *51*, 3331–3348, doi:10.1021/jm701249f.
  94. Tukun, F.-L.; Olberg, D.E.; Riss, P.J.; Haraldsen, I.; Kaass, A.; Klaveness, J. Recent Development of Non-Peptide GnRH Antagonists. *Molecules* **2017**, *22*, 2188, doi:10.3390/molecules22122188.
  95. De, B.; Plattner, J.J.; Bush, E.N.; Jae, H.S.; Diaz, G.; Johnson, E.S.; Perun, T.J. LH-RH antagonists: design and synthesis of a novel series of peptidomimetics. *J. Med. Chem.* **1989**, *32*, 2036–2038, doi:10.1021/jm00129a003.

96. Chen, C.; Wu, D.; Guo, Z.; Xie, Q.; Reinhart, G.J.; Madan, A.; Wen, J.; Chen, T.; Huang, C.Q.; Chen, M.; et al. Discovery of sodium R-(+)-4-{2-5-(2-fluoro-3-methoxyphenyl)-3-(2-fluoro-6-trifluoromethylbenzyl)-4-methyl-2,6-dioxo-3,6-dihydro-2H-pyrimidin-1-yl-1-phenylethylamino}butyrate (elagolix), a potent and orally available nonpeptide antagonist of the human gonadotropin-releasing hormone receptor. *J. Med. Chem.* **2008**, *51*, 7478–7485, doi:10.1021/jm8006454.
97. Miwa, K.; Hitaka, T.; Imada, T.; Sasaki, S.; Yoshimatsu, M.; Kusaka, M.; Tanaka, A.; Nakata, D.; Furuya, S.; Endo, S.; et al. Discovery of 1-{4-1-(2,6-difluorobenzyl)-5-(dimethylamino)methyl-3-(6-methoxy-pyridazin-3-yl)-2,4-dioxo-1,2,3,4-tetrahydrothieno[2,3-d]pyrimidin-6-ylphenyl}-3-methoxyurea (TAK-385) as a potent, orally active, non-peptide antagonist of the human gonadotropin-releasing hormone receptor. *J. Med. Chem.* **2011**, *54*, 4998–5012, doi:10.1021/jm200216q.
98. Tezuka, M.; Tamai, Y.; Kuramochi, Y.; Kobayashi, K.; Fushimi, N.; Kiguchi, S. Pharmacological characterization of linzagolix, a novel, orally active, non-peptide antagonist of gonadotropin-releasing hormone receptors. *Clinical and Experimental Pharmacology and Physiology* **2022**, *49*, 1082–1093, doi:10.1111/1440-1681.13688.
99. Shebley, M.; Polepally, A.R.; Nader, A.; Ng, J.W.; Winzenborg, I.; Klein, C.E.; Noertersheuser, P.; Gibbs, M.A.; Mostafa, N.M. Clinical Pharmacology of Elagolix: An Oral Gonadotropin-Releasing Hormone Receptor Antagonist for Endometriosis. *Clin. Pharmacokinet.* **2020**, *59*, 297–309, doi:10.1007/s40262-019-00840-7.
100. FDA. NDA Multi-Disciplinary Review and Evaluation of Elagolix (NDA 210450). Available online: [https://www.accessdata.fda.gov/drugsatfda\\_docs/nda/2018/210450Orig1s000MultiD.pdf](https://www.accessdata.fda.gov/drugsatfda_docs/nda/2018/210450Orig1s000MultiD.pdf) (accessed on 4 November 2023).
101. MacLean, D.B.; Shi, H.; Faessel, H.M.; Saad, F. Medical Castration Using the Investigational Oral GnRH Antagonist TAK-385 (Relugolix): Phase 1 Study in Healthy Males. *J Clin Endocrinol Metab* **2015**, *100*, 4579–4587, doi:10.1210/jc.2015-2770.
102. FDA. NDA/BLA Multi-disciplinary Review and Evaluation of Relugolix (NDA 214621). Available online: [https://www.accessdata.fda.gov/drugsatfda\\_docs/nda/2020/214621Orig1s000MultidisciplineR.pdf](https://www.accessdata.fda.gov/drugsatfda_docs/nda/2020/214621Orig1s000MultidisciplineR.pdf) (accessed on 4 November 2023).
103. EMA. Assessment report of linzagolix (EMA/266814/2022). Available online: [https://www.ema.europa.eu/en/documents/assessment-report/yseity-epar-public-assessment-report\\_en.pdf](https://www.ema.europa.eu/en/documents/assessment-report/yseity-epar-public-assessment-report_en.pdf) (accessed on 4 November 2023).
104. Keam, S.J. Linzagolix: First Approval. *Drugs* **2022**, *82*, 1317–1325, doi:10.1007/s40265-022-01753-9.
105. Donnez, J.; Taylor, H.S.; Taylor, R.N.; Akin, M.D.; Tatarchuk, T.F.; Wilk, K.; Gotteland, J.-P.; Lecomte, V.; Bestel, E. Treatment of endometriosis-associated

- pain with linzagolix, an oral gonadotropin-releasing hormone-antagonist: a randomized clinical trial. *Fertility and Sterility* **2020**, *114*, 44–55, doi:10.1016/j.fertnstert.2020.02.114.
106. Lamb, Y.N. Elagolix: First Global Approval. *Drugs* **2018**, *78*, 1501–1508, doi:10.1007/s40265-018-0977-4.
107. Markham, A. Relugolix: First Global Approval. *Drugs* **2019**, *79*, 675–679, doi:10.1007/s40265-019-01105-0.
108. Al-Hendy, A.; Lukes, A.S.; Poindexter, A.N.; Venturella, R.; Villarroel, C.; Critchley, H.O.D.; Li, Y.; McKain, L.; Arjona Ferreira, J.C.; Langenberg, A.G.M.; et al. Treatment of Uterine Fibroid Symptoms with Relugolix Combination Therapy. *N. Engl. J. Med.* **2021**, *384*, 630–642, doi:10.1056/NEJMoa2008283.
109. Muhammad, J.; Yusof, Y.; Ahmad, I.; Norhayati, M.N. Elagolix treatment in women with heavy menstrual bleeding associated with uterine fibroid: a systematic review and meta-analysis. *BMC Women's Health* **2022**, *22*, 14, doi:10.1186/s12905-022-01596-2.
110. Zondervan, K.T.; Becker, C.M.; Missmer, S.A. Endometriosis. *N. Engl. J. Med.* **2020**, *382*, 1244–1256, doi:10.1056/NEJMra1810764.
111. Parasar, P.; Ozcan, P.; Terry, K.L. Endometriosis: Epidemiology, Diagnosis and Clinical Management. *Curr. Obstet. Gynecol. Rep.* **2017**, *6*, 34–41, doi:10.1007/s13669-017-0187-1.
112. La Cruz, M.S.D. de; Buchanan, E.M. Uterine Fibroids: Diagnosis and Treatment. *Am. Fam. Physician* **2017**, *95*, 100–107.
113. Bergengren, O.; Pekala, K.R.; Matsoukas, K.; Fainberg, J.; Mungovan, S.F.; Bratt, O.; Bray, F.; Brawley, O.; Luckenbaugh, A.N.; Mucci, L.; et al. 2022 Update on Prostate Cancer Epidemiology and Risk Factors-A Systematic Review. *Eur. Urol.* **2023**, *84*, 191–206, doi:10.1016/j.eururo.2023.04.021.
114. Lin, W.-Y.; Chang, Y.-H.; Lin, C.-L.; Kao, C.-H.; Wu, H.-C. Erectile dysfunction and the risk of prostate cancer. *Oncotarget* **2017**, *8*, 52690–52698, doi:10.18632/oncotarget.17082.
115. Rebello, R.J.; Oing, C.; Knudsen, K.E.; Loeb, S.; Johnson, D.C.; Reiter, R.E.; Gillessen, S.; van der Kwast, T.; Bristow, R.G. Prostate cancer. *Nat. Rev. Dis. Primers* **2021**, *7*, 9, doi:10.1038/s41572-020-00243-0.
116. Becker, C.; Mehedințu, C.; Venturella, R.; Imm, S.J.; Perry, J.S.; As-Sanie, S. O-032 Effect of relugolix combination therapy in women with endometriosis-associated pain who received prior first-line hormonal treatment: SPIRIT 1 and 2. *Hum Reprod* **2023**, *38*, doi:10.1093/humrep/dead093.032.
117. Donnez, J.; Cacciottola, L.; Squifflet, J.-L.; Dolmans, M.-M. Profile of Linzagolix in the Management of Endometriosis, Including Design, Development and Potential Place in Therapy: A Narrative Review. *Drug Design, Development and Therapy* **2023**, *17*, 369–380, doi:10.2147/DDDT.S269976.

118. Han, J.; Baek, P.; Poplausky, D.; Agarwal, A.; Young, J.N.; Mubasher, A.; Niedt, G.; Patel, V.; Gulati, N. A case of lichenoid drug eruption associated with relugolix. *JAAD Case Rep.* **2023**, *33*, 33–35, doi:10.1016/j.jdcr.2023.01.003.
119. Panknin, O.; Wagenfeld, A.; Bone, W.; Bender, E.; Nowak-Reppel, K.; Fernández-Montalván, A.E.; Nubbemeyer, R.; Bäurle, S.; Ring, S.; Schmees, N.; et al. Discovery and Characterization of BAY 1214784, an Orally Available Spiroindoline Derivative Acting as a Potent and Selective Antagonist of the Human Gonadotropin-Releasing Hormone Receptor as Proven in a First-In-Human Study in Postmenopausal Women. *J. Med. Chem.* **2020**, *63*, 11854–11881, doi:10.1021/acs.jmedchem.0c01076.
120. Zou, F.; Wang, Y.; Yu, D.; Liu, C.; Lu, J.; Zhao, M.; Ma, M.; Wang, W.; Jiang, W.; Gao, Y.; et al. Discovery of the thieno2,3-dpyrimidine-2,4-dione derivative 21a: A potent and orally bioavailable gonadotropin-releasing hormone receptor antagonist. *European Journal of Medicinal Chemistry* **2022**, *242*, 114679, doi:10.1016/j.ejmech.2022.114679.
121. Li, S.; Ke, S.; Yang, C.; Chen, J.; Xiong, Y.; Zheng, L.; Liu, H.; Hong, L. A *Ligand-and-structure Dual-driven Deep Learning Method for the Discovery of Highly Potent GnRH1R Antagonist to treat Uterine Diseases*, 2022. Available online: <https://arxiv.org/pdf/2207.11547.pdf>.
122. Cui, J.; Smith, R.G.; Mount, G.R.; Lo, J.L.; Yu, J.; Walsh, T.F.; Singh, S.B.; DeVita, R.J.; Goulet, M.T.; Schaeffer, J.M.; et al. Identification of Phe313 of the gonadotropin-releasing hormone (GnRH) receptor as a site critical for the binding of nonpeptide GnRH antagonists. *Mol Endocrinol* **2000**, *14*, 671–681, doi:10.1210/mend.14.5.0464.
123. Reinhart, G.J.; Xie, Q.; Liu, X.-J.; Zhu, Y.-F.; Fan, J.; Chen, C.; Struthers, R.S. Species selectivity of nonpeptide antagonists of the gonadotropin-releasing hormone receptor is determined by residues in extracellular loops II and III and the amino terminus. *Journal of Biological Chemistry* **2004**, *279*, 34115–34122, doi:10.1074/jbc.M404474200.
124. Betz, S.F.; Reinhart, G.J.; Lio, F.M.; Chen, C.; Struthers, R.S. Overlapping, nonidentical binding sites of different classes of nonpeptide antagonists for the human gonadotropin-releasing hormone receptor. *J. Med. Chem.* **2006**, *49*, 637–647, doi:10.1021/jm0506928.
125. Sullivan, S.K.; Brown, M.S.; Gao, Y.; Loweth, C.J.; Lio, F.M.; Crowe, P.D.; Struthers, R.S.; Betz, S.F. Allosteric and orthosteric binding modes of two nonpeptide human gonadotropin-releasing hormone receptor antagonists. *Biochemistry* **2006**, *45*, 15327–15337, doi:10.1021/bi0617097.
126. Yang, X.; Lin, G.; Xia, A.; Liu, J.; Zhang, S.; Zhou, P.; Wang, Y.; Zhang, J.; Zhou, Y.; Chen, P.; et al. Discovery of Small Molecule Agonist of Gonadotropin-Releasing Hormone Receptor (GnRH1R). *Journal of Chemical Information and Modeling* **2022**, *62*, 5009–5022, doi:10.1021/acs.jcim.2c00639.
127. Kuhn, R. „*Molekulare Asymmetrie*” in *Stereochemie*, 1933.

128. Christie, G.H.; Kenner, J. LXXI.—The molecular configurations of polynuclear aromatic compounds. Part I. The resolution of  $\gamma$ -6 : 6'-dinitro- and 4 : 6 : 4' : 6'-tetranitro-diphenic acids into optically active components. *J. Chem. Soc., Trans.* **1922**, *121*, 614–620, doi:10.1039/CT9222100614.
129. Eliel, E.L.; Wilen, S.H.; Mander, L.N. *Stereochemistry of organic compounds*; Wiley: New York, 1994, ISBN 0471016705.
130. Kumarasamy, E.; Raghunathan, R.; Sibi, M.P.; Sivaguru, J. Nonbiaryl and Heterobiaryl Atropisomers: Molecular Templates with Promise for Atropselective Chemical Transformations. *Chem. Rev.* **2015**, *115*, 11239–11300, doi:10.1021/acs.chemrev.5b00136.
131. Toenjes, S.T.; Gustafson, J.L. Atropisomerism in medicinal chemistry: challenges and opportunities. *Future Med. Chem.* **2018**, *10*, 409–422, doi:10.4155/fmc-2017-0152.
132. Ōki, M. Recent Advances in Atropisomerism. In *Topics in stereochemistry*; Allinger, N.L., Ed.; Wiley: New York, 1983; pp 1–81, ISBN 9780471898580.
133. Laplante, S.R.; Edwards, P.J.; Fader, L.D.; Jakalian, A.; Hucke, O. Revealing atropisomer axial chirality in drug discovery. *ChemMedChem* **2011**, *6*, 505–513, doi:10.1002/cmdc.201000485.
134. Laplante, S.R.; D Fader, L.; Fandrick, K.R.; Fandrick, D.R.; Hucke, O.; Kemper, R.; Miller, S.P.F.; Edwards, P.J. Assessing atropisomer axial chirality in drug discovery and development. *J. Med. Chem.* **2011**, *54*, 7005–7022, doi:10.1021/jm200584g.
135. Pecorari, D.; Mazzanti, A.; Mancinelli, M. Atropostatin: Design and Total Synthesis of an Atropisomeric Lactone-Atorvastatin Prodrug. *Molecules* **2023**, *28*, doi:10.3390/molecules28073176.
136. Zask, A.; Murphy, J.; Ellestad, G.A. Biological stereoselectivity of atropisomeric natural products and drugs. *Chirality* **2013**, *25*, 265–274, doi:10.1002/chir.22145.
137. Glunz, P.W. Recent encounters with atropisomerism in drug discovery. *Bioorg. Med. Chem. Lett.* **2018**, *28*, 53–60, doi:10.1016/j.bmcl.2017.11.050.
138. Donohoe, C.; Schaberle, F.A.; Rodrigues, F.M.S.; Gonçalves, N.P.F.; Kingsbury, C.J.; Pereira, M.M.; Senge, M.O.; Gomes-da-Silva, L.C.; Arnaut, L.G. Unraveling the Pivotal Role of Atropisomerism for Cellular Internalization. *Journal of the American Chemical Society* **2022**, *144*, 15252–15265, doi:10.1021/jacs.2c05844.
139. Lanman, B.A.; Allen, J.R.; Allen, J.G.; Amegadzie, A.K.; Ashton, K.S.; Booker, S.K.; Chen, J.J.; Chen, N.; Frohn, M.J.; Goodman, G.; et al. Discovery of a Covalent Inhibitor of KRASG12C (AMG 510) for the Treatment of Solid Tumors. *J. Med. Chem.* **2020**, *63*, 52–65, doi:10.1021/acs.jmedchem.9b01180.
140. Lanman, B.A.; Parsons, A.T.; Zech, S.G. Addressing Atropisomerism in the Development of Sotorasib, a Covalent Inhibitor of KRAS G12C: Structural, Analytical, and Synthetic Considerations. *Acc. Chem. Res.* **2022**, *55*, 2892–2903, doi:10.1021/acs.accounts.2c00479.

141. Mancinelli, M.; Bencivenni, G.; Pecorari, D.; Mazzanti, A. Stereochemistry and Recent Applications of Axially Chiral Organic Molecules. *Eur J Org Chem* **2020**, *2020*, 4070–4086, doi:10.1002/ejoc.201901918.
142. Heeb, J.-P.; Clayden, J.; Smith, M.D.; Armstrong, R.J. Interrogating the configurational stability of atropisomers. *Nat. Protoc.* **2023**, *18*, 2745–2771, doi:10.1038/s41596-023-00859-y.
143. Rickhaus, M.; Jundt, L.; Mayor, M. Determining Inversion Barriers in Atropisomers - A Tutorial for Organic Chemists. *Chimia (Aarau)* **2016**, *70*, 192–202, doi:10.2533/chimia.2016.192.
144. Miner, J.N.; Tan, P.K.; Hyndman, D.; Liu, S.; Iverson, C.; Nanavati, P.; Hagerty, D.T.; Manhard, K.; Shen, Z.; Girardet, J.-L.; et al. Lesinurad, a novel, oral compound for gout, acts to decrease serum uric acid through inhibition of urate transporters in the kidney. *Arthritis Res. Ther.* **2016**, *18*, 214, doi:10.1186/s13075-016-1107-x.
145. Wang, J.; Zeng, W.; Li, S.; Shen, L.; Gu, Z.; Zhang, Y.; Li, J.; Chen, S.; Jia, X. Discovery and Assessment of Atropisomers of ( $\pm$ )-Lesinurad. *ACS Med. Chem. Lett.* **2017**, *8*, 299–303, doi:10.1021/acsmchemlett.6b00465.
146. Basilaia, M.; Chen, M.H.; Secka, J.; Gustafson, J.L. Atropisomerism in the Pharmaceutically Relevant Realm. *Acc. Chem. Res.* **2022**, *55*, 2904–2919, doi:10.1021/acs.accounts.2c00500.
147. Patel, S.; Sandha, K.; Waingankar, A.; Jain, P.; Abhyankar, A. Atropisomerism transforming anti-cancer drug discovery. *Chem. Biol. Drug Des.* **2023**, *101*, 138–157, doi:10.1111/cbdd.14155.
148. Perreault, S.; Chandrasekhar, J.; Patel, L. Atropisomerism in Drug Discovery: A Medicinal Chemistry Perspective Inspired by Atropisomeric Class I PI3K Inhibitors. *Acc. Chem. Res.* **2022**, *55*, 2581–2593, doi:10.1021/acs.accounts.2c00485.
149. Nalbandian, C.; Hecht, D.; Gustafson, J. The Preorganization of Atropisomers to Increase Target Selectivity. *Synlett* **2016**, *27*, 977–983, doi:10.1055/s-0035-1561314.
150. Ciceri, S.; Colombo, D.; Fassi, E.M.A.; Ferraboschi, P.; Grazioso, G.; Grisenti, P.; Iannone, M.; Castellano, C.; Meneghetti, F. Elagolix Sodium Salt and Its Synthetic Intermediates: A Spectroscopic, Crystallographic, and Conformational Study. *Molecules* **2023**, *28*, doi:10.3390/molecules28093861.
151. Tucci, F.C.; Hu, T.; Mesleh, M.F.; Bokser, A.; Allsopp, E.; Gross, T.D.; Guo, Z.; Zhu, Y.-F.; Struthers, R.S.; Ling, N.; et al. Atropisomeric property of 1-(2,6-difluorobenzyl)-3-(2R)-amino-2-phenethyl-5-(2-fluoro-3-methoxyphenyl)-6-methyluracil. *Chirality* **2005**, *17*, 559–564, doi:10.1002/chir.20198.
152. Guo, Z.; Chen, Y.; Huang, C.Q.; Gross, T.D.; Pontillo, J.; Rowbottom, M.W.; Saunders, J.; Struthers, S.; Tucci, F.C.; Xie, Q.; et al. Uracils as potent antagonists of the human gonadotropin-releasing hormone receptor without atropisomers. *Bioorg. Med. Chem. Lett.* **2005**, *15*, 2519–2522, doi:10.1016/j.bmcl.2005.03.057.

153. Zhao, L.; Guo, Z.; Chen, Y.; Hu, T.; Wu, D.; Zhu, Y.-F.; Rowbottom, M.; Gross, T.D.; Tucci, F.C.; Struthers, R.S.; et al. 5-Aryluracils as potent GnRH antagonists-Characterization of atropisomers. *Bioorg. Med. Chem. Lett.* **2008**, *18*, 3344–3349, doi:10.1016/j.bmcl.2008.04.029.
154. Guo, Z.; Chen, Y.; Wu, D.; Chen, C.; Wade, W.; Dwight, W.J.; Huang, C.Q.; Tucci, F.C. Preparation of pyrimidine-2,4(1H,3H)-dione derivatives as gonadotropin-releasing hormone receptor antagonists.
155. Lewis, R.J.; Sax, N.I. *Sax's dangerous properties of industrial materials*, 11th ed.; Wiley-Interscience: Hoboken, N.J., 2004-, ISBN 9780471476627.
156. Larrañaga, M.D.; Lewis, R.J.; Lewis, R.A.; Hawley, G.G. *Hawley's condensed chemical dictionary*, Sixteenth edition; John Wiley & Sons, Inc: Hoboken, New Jersey, 2016, ISBN 1119312469.
157. Sulake, R.S.; Shinde, S.R.; Siyan, R.S.; Bhise, N.B.; Singh, G.P. Process for the preparation of elagolix and pharmaceutically acceptable salts thereof.
158. Bader, A.R.; Cummings, L.O.; Vogel, H.A. Transesterification. I.  $\beta$ -Keto Esters. *J. Am. Chem. Soc.* **1951**, *73*, 4195–4197, doi:10.1021/ja01153a045.
159. Gallagher, D.; Treiber, L.; Hughes, R.; Campopiano, O.; Wang, P.; Zhao, Y.; Chou, S.; Ouellette, M.; Hettinger, D. Processes for the preparation of uracil derivatives.
160. Silverstein, R.M.; Webster, F.X.; Kiemle, D.J.; Bryce, D.L. *Spectrometric identification of organic compounds*, Eighth edition; Wiley: Hoboken, NJ, 2015, ISBN 9780470616376.
161. Gotor, V. Non-conventional hydrolase chemistry: amide and carbamate bond formation catalyzed by lipases. *Bioorg. Med. Chem.* **1999**, *7*, 2189–2197, doi:10.1016/s0968-0896(99)00150-9.
162. N. Borse, B.; Borude, V.S.; Shukla, S.R. Synthesis of novel dihydropyrimidin-2(1h)-ones derivatives using lipase and their antimicrobial activity. *ccl* **2012**, *1*, 59–68, doi:10.5267/j.ccl.2012.3.001.
163. Puertas, S.; Brieva, R.; Robledo, F.; Gotor, V. Lipase catalyzed aminolysis of ethyl propiolate and acrylic esters. Synthesis of chiral acrylamides. *Tetrahedron* **1993**, *49*, 4007–4014, doi:10.1016/S0040-4020(01)89914-2.
164. Zhong, X.; Lv, Q.; Yong, Q.; Hu, W.; Li, D.; Ji, S.; Zhan, L.; Chen, W.; Li, M.; Lin, J.; et al. Forced degradation studies of elagolix sodium with the implementation of high resolution LC-UV-PDA-MSn (n = 1,2,3...) and NMR structural elucidation. *Journal of Pharmaceutical and Biomedical Analysis* **2023**, *224*, 115198, doi:10.1016/j.jpba.2022.115198.
165. Pretsch, E.; Biemann, K.; Clerc, T.; Seibl, J.; Simon, W. *Tables of Spectral Data for Structure Determination of Organic Compounds*; Springer Berlin / Heidelberg: Berlin, Heidelberg, 2014, ISBN 9783662224557.
166. Radex Marek; Antonin Lycka. <sup>15</sup>N NMR Spectroscopy in Structural Analysis. *Current Organic Chemistry*, *6*, 35–66.



167. Sepsey, A.; Németh, D.R.; Németh, G.; Felinger, A. Rate constant determination of interconverting enantiomers by chiral chromatography using a stochastic model. *J. Chromatogr. A* **2018**, *1564*, 155–162, doi:10.1016/j.chroma.2018.06.014.
168. Sabia, R.; Ciogli, A.; Pierini, M.; Gasparri, F.; Villani, C. Dynamic high performance liquid chromatography on chiral stationary phases. Low temperature separation of the interconverting enantiomers of diazepam, flunitrazepam, prazepam and tetrazepam. *J. Chromatogr. A* **2014**, *1363*, 144–149, doi:10.1016/j.chroma.2014.07.097.
169. Derdour, L.; Skliar, D. A review of the effect of multiple conformers on crystallization from solution and strategies for crystallizing slow inter-converting conformers. *Chemical Engineering Science* **2014**, *106*, 275–292, doi:10.1016/j.ces.2013.11.025.
170. Farrugia, L.J. WinGX and ORTEP for Windows : an update. *J Appl Cryst* **2012**, *45*, 849–854, doi:10.1107/S0021889812029111.
171. Becke, A.D. Density-functional exchange-energy approximation with correct asymptotic behavior. *Phys. Rev. A Gen. Phys.* **1988**, *38*, 3098–3100, doi:10.1103/PhysRevA.38.3098.
172. Becke, A.D. Density-functional thermochemistry. III. The role of exact exchange. *J. Chem. Phys.* **1993**, *98*, 5648–5652, doi:10.1063/1.464913.
173. Mennucci, B.; Tomasi, J.; Cammi, R.; Cheeseman, J.R.; Frisch, M.J.; Devlin, F.J.; Gabriel, S.; Stephens, P.J. Polarizable Continuum Model (PCM) Calculations of Solvent Effects on Optical Rotations of Chiral Molecules. *J. Phys. Chem. A* **2002**, *106*, 6102–6113, doi:10.1021/jp020124t.
174. Khatoon, H.; Abdulmalek, E. A Focused Review of Synthetic Applications of Lawesson's Reagent in Organic Synthesis. *Molecules* **2021**, *26*, doi:10.3390/molecules26226937.
175. Felczak, K.; Bretner, M.; Kulikowski, T.; Shugar, D. High-Yield Regioselective Thiation of Biologically Important Pyrimidinones, Dihydropyrimidinones and Their Ribo, 2'-Deoxyribo and 2', 3'-Dideoxyribo Nucleosides. *Nucleosides and Nucleotides* **1993**, *12*, 245–261, doi:10.1080/07328319308021210.
176. Łapucha, A.R. A Rapid and Efficient Synthesis of Sulfur Analogues of Pyrimidine Bases. *Synthesis* **1987**, *1987*, 256–258, doi:10.1055/s-1987-27906.
177. Les, A.; Adamowicz, L. Tautomerism of 2- and 4-thiouracil. Ab initio theoretical study. *J. Am. Chem. Soc.* **1990**, *112*, 1504–1509, doi:10.1021/ja00160a032.
178. YAMANE, A.; INOUE, H.; UEDA, T. Introduction of carbon substituents into pyrimidine and purine nucleosides by sulfur extrusion (Nucleosides and nucleotides. XXX). *Chem. Pharm. Bull.* **1980**, *28*, 157–162, doi:10.1248/cpb.28.157.
179. Dorokhov, V.A.; Gordeev, M.F.; Komkov, A.V.; Bogdanov, V.S. Synthesis of derivatives of 4-alkylthiouracil, cytosine, pyrido[2,3-d]pyrimidine, and

- pyrimido[4,5-d]pyrimidine from the N,S- and N,N-acetals of diacetylketene and isocyanates. *Russ Chem Bull* **1991**, *40*, 2267–2273, doi:10.1007/BF00961050.
180. Reist, M.; Testa, B.; Carrupt, P.-A.; Jung, M.; Schurig, V. Racemization, enantiomerization, diastereomerization, and epimerization: Their meaning and pharmacological significance. *Chirality* **1995**, *7*, 396–400, doi:10.1002/chir.530070603.
181. Oikawa, Y.; Sugano, K.; Yonemitsu, O. Meldrum's acid in organic synthesis. 2. A general and versatile synthesis of .beta.-keto esters. *J. Org. Chem.* **1978**, *43*, 2087–2088, doi:10.1021/jo00404a066.
182. Rossino, G.; Robescu, M.S.; Licastro, E.; Tedesco, C.; Martello, I.; Maffei, L.; Vincenti, G.; Bavaro, T.; Collina, S. Biocatalysis: A smart and green tool for the preparation of chiral drugs. *Chirality* **2022**, *34*, 1403–1418, doi:10.1002/chir.23498.
183. Patel, R.N. Synthesis of chiral pharmaceutical intermediates by biocatalysis. *Coordination Chemistry Reviews* **2008**, *252*, 659–701, doi:10.1016/j.ccr.2007.10.031.
184. Bornscheuer, U.T.; Kazlauskas, R.J. *Hydrolases in organic synthesis: Regio- and stereoselective biotransformations*, 2nd ed.; Wiley-VCH; John Wiley: Weinheim, Chichester, 2006, ISBN 3527607129.
185. Méndez-Sánchez, D.; López-Iglesias, M.; Gotor-Fernández, V. Hydrolases in Organic Chemistry. Recent Achievements in the Synthesis of Pharmaceuticals. *COC* **2016**, *20*, 1186–1203, doi:10.2174/1385272819666150819190956.
186. Watts, O.F.B.; Berreur, J.; Collins, B.S.L.; Clayden, J. Biocatalytic Enantioselective Synthesis of Atropisomers. *Acc. Chem. Res.* **2022**, *55*, 3362–3375, doi:10.1021/acs.accounts.2c00572.
187. Dukeshereer, D.; Mao, M.; Vonder Embse, R.; Yalamanchili, G.; Vaidyanathan, R.; Chekal, B.; Klemm, G.; Vanderroest, R.; Geurink, R. Processes for the preparation of 3-[4-(2,4-difluorobenzyloxy)-3-bromo-6-methyl-2-oxopyridin-1(2H)-yl]-N,4-dimethylbenzamide and related compounds.
188. Xing, L.; Devadas, B.; Devraj, R.V.; Selness, S.R.; Shieh, H.; Walker, J.K.; Mao, M.; Messing, D.; Samas, B.; Yang, J.Z.; et al. Discovery and characterization of atropisomer PH-797804, a p38 MAP kinase inhibitor, as a clinical drug candidate. *ChemMedChem* **2012**, *7*, 273–280, doi:10.1002/cmdc.201100439.
189. Soli, E.D.; Surber, B.W.; Reed, A.D. Synthesis of H-3- and C-14-labeled elagolix. *Journal of labelled compounds & radiopharmaceuticals* **2021**, *64*, 254–261, doi:10.1002/jlcr.3908.
190. Trinquet, E.; Bouhelal, R.; Dietz, M. Monitoring Gq-coupled receptor response through inositol phosphate quantification with the IP-One assay. *Expert Opin. Drug Discov.* **2011**, *6*, 981–994, doi:10.1517/17460441.2011.608658.
191. Bordoli, L.; Kiefer, F.; Arnold, K.; Benkert, P.; Battey, J.; Schwede, T. Protein structure homology modeling using SWISS-MODEL workspace. *Nat. Protoc.* **2009**, *4*, 1–13, doi:10.1038/nprot.2008.197.

192. Waterhouse, A.; Bertoni, M.; Bienert, S.; Studer, G.; Tauriello, G.; Gumienny, R.; Heer, F.T.; Beer, T.A.P. de; Rempfer, C.; Bordoli, L.; et al. SWISS-MODEL: homology modelling of protein structures and complexes. *Nucleic Acids Res.* **2018**, *46*, W296-W303, doi:10.1093/nar/gky427.
193. Waltenspühl, Y.; Schöppe, J.; Ehrenmann, J.; Kummer, L.; Plückthun, A. Crystal structure of the human oxytocin receptor. *Sci. Adv.* **2020**, *6*, eabb5419, doi:10.1126/sciadv.abb5419.
194. Lu, C.; Wu, C.; Ghoreishi, D.; Chen, W.; Wang, L.; Damm, W.; Ross, G.A.; Dahlgren, M.K.; Russell, E.; Bargaen, C.D. von; et al. OPLS4: Improving Force Field Accuracy on Challenging Regimes of Chemical Space. *J. Chem. Theory Comput.* **2021**, *17*, 4291–4300, doi:10.1021/acs.jctc.1c00302.
195. Friesner, R.A.; Banks, J.L.; Murphy, R.B.; Halgren, T.A.; Klicic, J.J.; Mainz, D.T.; Repasky, M.P.; Knoll, E.H.; Shelley, M.; Perry, J.K.; et al. Glide: a new approach for rapid, accurate docking and scoring. 1. Method and assessment of docking accuracy. *J. Med. Chem.* **2004**, *47*, 1739–1749, doi:10.1021/jm0306430.
196. Mao, Y.; Zhang, Y. Thermal conductivity, shear viscosity and specific heat of rigid water models. *Chemical Physics Letters* **2012**, *542*, 37–41, doi:10.1016/j.cplett.2012.05.044.
197. Beard, H.; Cholleti, A.; Pearlman, D.; Sherman, W.; Loving, K.A. Applying physics-based scoring to calculate free energies of binding for single amino acid mutations in protein-protein complexes. *PLOS ONE* **2013**, *8*, e82849, doi:10.1371/journal.pone.0082849.
198. Genheden, S.; Ryde, U. The MM/PBSA and MM/GBSA methods to estimate ligand-binding affinities. *Expert Opin. Drug Discov.* **2015**, *10*, 449–461, doi:10.1517/17460441.2015.1032936.
199. Lan, C.B.; Auclair, K. Ammonium Chloride-Promoted Rapid Synthesis of Monosubstituted Ureas under Microwave Irradiation. *Eur J Org Chem* **2021**, *2021*, 5135–5146, doi:10.1002/ejoc.202101059.
200. O'Brien, P.M.; Sliskovic, D.R.; Blankley, C.J.; Roth, B.D.; Wilson, M.W.; Hamelhele, K.L.; Krause, B.R.; Stanfield, R.L. Inhibitors of acyl-CoA:cholesterol O-acyl transferase (ACAT) as hypocholesterolemic agents. 8. Incorporation of amide or amine functionalities into a series of disubstituted ureas and carbamates. Effects on ACAT inhibition in vitro and efficacy in vivo. *J. Med. Chem.* **1994**, *37*, 1810–1822, doi:10.1021/jm00038a010.
201. Zhang, F.; Wang, Y.; Wang, Y.; Pan, Y. Electrochemical Deoxygenative Thiolation of Preactivated Alcohols and Ketones. *Organic Letters* **2021**, *23*, 7524–7528, doi:10.1021/acs.orglett.1c02738.
202. Liu, Y.; Hao, Q.; Lin, K.; Zhou, W.; Pan, J.; Chen, L.; Zhou, T. Preparation of elagolix intermediate.
203. So, G.K.-M.; Cheng, G.; Wang, J.; Chang, X.; Kwok, C.-C.; Zhang, H.; Che, C.-M. Efficient Color-Tunable Copper(I) Complexes and Their Applications in

- Solution-Processed Organic Light-Emitting Diodes. *Chem. Asian J.* **2017**, *12*, 1490–1498, doi:10.1002/asia.201700081.
204. Jerca, V.V.; Lava, K.; Verbraeken, B.; Hoogenboom, R. Poly(2-cycloalkyl-2-oxazoline)s: high melting temperature polymers solely based on Debye and Keesom van der Waals interactions. *Polym. Chem.* **2016**, *7*, 1309–1322, doi:10.1039/C5PY01755F.
205. Bradshaw, B.; Parra, C.; Bonjoch, J. Organocatalyzed asymmetric synthesis of morphans. *Organic Letters* **2013**, *15*, 2458–2461, doi:10.1021/ol400926p.
206. Xu, G.; Jia, S.; Li, W.; Mao, L.; Jiang, Y.; Dong, W.; Shen, J.; Jiang, T. Preparation of piperidine-connected 1,2,3-triazole compounds and their application as antibacterial agents.
207. Schirmer, E.; Shanab, K.; Datterl, B.; Neudorfer, C.; Mitterhauser, M.; Wadsak, W.; Philippe, C.; Spreitzer, H. Syntheses of precursors and reference compounds of the melanin-concentrating hormone receptor 1 (MCHR1) tracers <sup>11</sup>C SNAP-7941 and <sup>18</sup>F FE@SNAP for positron emission tomography. *Molecules* **2013**, *18*, 12119–12143, doi:10.3390/molecules181012119.
208. *SMART & SAINT Software Reference Manual, Version 6.45; Bruker Analytical X-Ray Systems, Inc.: Madison, WI, USA, 2003.*
209. Sheldrick, G.M. *SADABS, Version 2008/1; Bruker AXS Inc.: Karlsruhe, Germany, 2008.*
210. Sheldrick, G.M. *SHELXL-2018; Universität Göttingen: Göttingen, Germany, 2018.*
211. Macrae, C.F.; Sovago, I.; Cottrell, S.J.; Galek, P.T.A.; McCabe, P.; Pidcock, E.; Platings, M.; Shields, G.P.; Stevens, J.S.; Towler, M.; et al. Mercury 4.0: from visualization to analysis, design and prediction. *J Appl Cryst* **2020**, *53*, 226–235, doi:10.1107/s1600576719014092.
212. Nardelli, M. Parst: A system of fortran routines for calculating molecular structure parameters from results of crystal structure analyses. *Computers & Chemistry* **1983**, *7*, 95–98, doi:10.1016/0097-8485(83)85001-3.

# Scientific CV

---

Author ID: ORCID: 0000-0003-1202-941X; Scopus Author ID: 55817060000

## Publications

1. CICERI, S.; COLOMBO, C.; FASSI, E.M.A.; FERRABOSCHI, P.; GRAZIOSO, G.; GRISENTI, P.; IANNONE, M.; CASTELLANO, C.; MENEGHETTI, F. Elagolix Sodium Salt and Its Synthetic Intermediates: A Spectroscopic, Crystallographic, and Conformational Study. *Molecules* **2023**, *28*, 3861.
2. CASATI, L.; CICERI, S.; MAGGI, R.; BOTTAI, D. Physiological and pharmacological overview of the gonadotropin releasing hormone. *Biochem. Pharmacol.* **2023**, *212*, 115553.
3. DELBUE, S.; PARIANI, E.; PARAPINI, S.; GALLI, C.; BASILICO, N.; D'ALESSANDRO, S.; PELLEGRINO, S.; PINI, E.; CICERI, S.; FERRABOSCHI, P.; GRISENTI, P. Heat-Treated Lysozyme Hydrochloride: A Study on Its Structural Modifications and Anti-SARS-CoV-2 Activity. *Molecules* **2023**, *28*, 2848.
4. CAZZANIGA, G.; MORI, M.; MENEGHETTI, F.; CHIARELLI, L.R.; STELITANO, G.; CALIGIURI, I.; RIZZOLIO, F.; CICERI, S.; POLI, G.; STAVIER, D.; ORTORE, G.; TUCCINARDI, T.; VILLA, S. Virtual screening and crystallographic studies reveal an unexpected  $\gamma$ -lactone derivative active against MptpB as a potential antitubercular agent. *Eur. J. Med. Chem* **2022**, *234*, 114235.
5. IANNONE, M. N.; STUCCHI, S.; TUROLLO, E. A.; BERETTA, C.; CICERI, S.; CHINELLO, C.; PAGANI, L.; TODDE, S.; FERRABOSCHI, P. Synthesis and automated fluorine-18 radiolabeling of new PSMA-617 derivatives with a CuAAC radiosynthetic approach. *J. Label. Compd. Radiopharm.* **2022**, *65*, 48-62.
6. FERRABOSCHI, P.; CICERI, S.; GRISENTI, P. Applications of Lysozyme, an Innate Immune Defense Factor, as an Alternative Antibiotic. *Antibiotics* **2021**, *10*(12), 1534.
7. CICERI, S.; COLOMBO, D.; FERRABOSCHI, P.; GRISENTI, P.; IANNONE, M.; MORI, M.; MENEGHETTI, F. Vecuronium bromide and its advanced intermediates: a crystallographic and spectroscopic study. *Steroids* **2021**, *176*, 108928.
8. MORI, M.; VILLA, S.; CICERI, S.; COLOMBO, D.; FERRABOSCHI, P.; MENEGHETTI, F. An Outline of the Latest Crystallographic Studies on Inhibitor-Enzyme Complexes for the Design and Development of New

Therapeutics against Tuberculosis. *Molecules* **2021**, *26*(23), 7082.

9. CICERI, S.; FERRABOSCHI, P.; GRISENTI, P.; REZA ELAHI, S.; CASTELLANO, C.; MORI, M.; MENEGHETTI, F. (*S*)-Pramipexole and Its Enantiomer, Dexpramipexole: A New Chemoenzymatic Synthesis and Crystallographic Investigation of Key Enantiomeric Intermediates. *Catalysts* **2020**, *10*, 941.
10. MENEGHETTI, F.; FERRABOSCHI, P.; GRISENTI, P.; REZA ELAHI, S.; MORI, M.; CICERI, S. Crystallographic and NMR Investigation of Ergometrine and Methylegometrine, Two Alkaloids from *Claviceps purpurea*. *Molecules* **2020**, *25*, 331.
11. CICERI, S.; GRISENTI, P.; REZA ELAHI, S.; FERRABOSCHI, P. A New Chemoenzymatic Synthesis of the Chiral Key Intermediate of the Antiepileptic Brivaracetam. *Molecules* **2018**, *23*, 2206.
12. LUGATO, B.; STUCCHI, S.; CICERI, S.; IANNONE, M. N.; TUROLLA, E. A.; GIULIANO, L.; CHINELLO, C.; TODDE, S.; FERRABOSCHI, P. A novel versatile precursor suitable for <sup>18</sup>F-radiolabeling via “click chemistry”. *J. Label. Compd. Radiopharm.* **2017**, *60*(10), 466-480.
13. FERRABOSCHI, P.; CICERI, S.; GRISENTI, P. Synthesis of antitumor fluorinated pyrimidine nucleosides. *Org. Prep. Proced. Int.* **2017**, *49*(2), 69-154.
14. FERRABOSCHI, P.; CIUFFREDA, P.; CICERI, S.; GRISENTI, P.; CASTELLANO, C.; MENEGHETTI, F. Crystallographic and spectroscopic study on a known orally active progestin. *Steroids* **2015**, *104*, 137-144.
15. CICERI, S.; CIUFFREDA, P.; GRISENTI, P.; FERRABOSCHI, P. Synthesis of the antitumoral nucleoside capecitabine through a chemo-enzymatic approach. *Tetrahedron Lett.* **2015**, *56*(43), 5909-5913.
16. FERRABOSCHI, P.; CICERI, S.; CIUFFREDA, P.; DE MIERI, M.; ROMANO, D.; GRISENTI, P. Baker’s yeast catalyzed preparation of a new enantiomerically pure synthon of (*S*)-pramipexole and its enantiomer (dexpramipexole). *Tetrahedron: Asymmetry* **2014**, *25*(16-17), 1239-1245.
17. BASSETTI, M.; CICERI, S.; LANCIA, F.; PASQUINI, C. Hydration of aromatic terminal alkynes catalyzed by iron(III) sulfate hydrate under chlorine-free conditions. *Tetrahedron Lett.* **2014**, *55*(9), 1608-1612.
18. FERRABOSCHI, P.; CICERI, S.; GRISENTI, P. Chemoenzymatic synthesis of the enantiomerically pure 1,2,3,4-tetrahydroquinoline moiety of the antithrombotic (2*R*)- and (2*S*)-argatroban. *Tetrahedron: Asymmetry* **2013**, *24*(18), 1142-1147.

## Oral presentations

1. CICERI, S. Elagolix and its derivatives: analytical and theoretical investigations of their atropisomeric properties. Summer School on Pharmaceutical Analysis (SSPA) 2023, Rimini, 11-13 September **2023**. Book of abstracts pag 358.
2. CICERI, S.; GRISENTI, P.; MENEGHETTI, M.; MORI, M.; REZA ELAHI, S.; FERRABOSCHI, P. Biocatalysts for the synthesis of pharmacologically active compounds. *1<sup>st</sup> Virtual Symposium for Young Organic Chemists of Società Chimica Italiana*, online, November 3-6<sup>th</sup>, **2020**. Book of abstracts O41, pag 51.
3. CICERI, S.; COLOMBO, D.; COMPOSTELLA, F.; REZA ELAHI, S.; FERRABOSCHI, P. The sad story of an enzymatic reaction in the fridge. The COVID-19 papers, Department of Medical Biotechnology and Translational Medicine, Online, September 28<sup>th</sup>, **2020**.
4. FERRABOSCHI, P.; CICERI, S.; GUIDI, B.; REZA ELAHI, S.; GRISENTI, P. Biocatalytic Approach to the Synthesis of Pharmacologically Active Compounds. *XXXVIII National Congress of the Organic Chemistry Division of the Italian Chemical Society*, Milan, September 9-13<sup>th</sup>, **2018**. Book of abstracts OC11, pag 61.

## Posters

1. CICERI, S.; COLOMBO, D.; FASSI, E. M.A.; FERRABOSCHI, P.; GRAZIOSO, G.; GRISENTI, P.; MENEGHETTI, F. Insights on the atropisomeric properties of elagolix and its derivatives. Poster presentation, *Chirality 2023*, Rome, 24-27 July **2023**. Book of abstract PC-18, pag. 116.
2. CICERI, S.; COLOMBO, D.; FASSI, E.; FERRABOSCHI, P.; GRAZIOSO, G.; GRISENTI, P.; MENEGHETTI, F. Elagolix analogues as potential new GnRH antagonists: design, synthesis and characterization. *Ischia Advanced School of Organic Chemistry (IASOC)*, Ischia, September 23-26<sup>th</sup>, **2022**. Book of abstracts P23, pag 26.
3. CICERI, S.; COLOMBO, D.; FASSI, E.; FERRABOSCHI, P.; GRAZIOSO, G.; GRISENTI, P.; MENEGHETTI, F. Elagolix analogues as potential new GnRH antagonists. *6<sup>th</sup> BioMeTra Workshop*, Aula Magna, LITA Building – Segrate (MI), September 20<sup>th</sup>, **2022**. Book of abstracts pag 36.
4. CICERI, S.; COLOMBO, D.; FERRABOSCHI, P.; GRISENTI, P.; SFORNA, S. V.; MENEGHETTI, F. Design, synthesis, characterization, and biological activity of new derivatives of elagolix, a potent GnRH antagonist. *European*

*School of Medicinal Chemistry ESMEC*, online, June 28th – July 1st, **2021**.  
Book of abstracts pag. 67.

5. CICERI, S.; FERRABOSCHI, P.; GRISENTI, P.; MORI, M.; MENEGHETTI, F. Biocatalytic synthesis of two pharmacologically active compounds: (*S*)-pramipexole and its enantiomer, dexpramipexole. *Italian Young Medicinal Chemistry Virtual Meeting*, July 22-24<sup>th</sup>, **2020**. Book of abstracts P56.
6. CICERI, S.; GUIDI, B.; REZA ELAHI, S.; FERRABOSCHI, P. A biocatalytic approach to the synthesis of pharmacologically active compounds. *Workshop BIOMETRA 2018*, Segrate (MI), September 24<sup>th</sup>, 2018. Book of abstracts P10, pag 28.
7. CICERI, S.; GRISENTI, P.; FERRABOSCHI, P. Use of biocatalysts for selective transformations in the synthesis of pharmacologically active molecules. *XXV National Congress of the Italian Chemical Society*, Arcavacata di Rende, September 07-12<sup>th</sup>, **2014**. Book of abstracts IND-P14, pag 541.
8. FERRABOSCHI, P.; VANDONI, V.; CICERI, S. Biocatalyzed preparation of biologically active compounds. 1<sup>o</sup> conference of the Department “BIOMETRA” “*Meet together*”, Milan, July 1<sup>st</sup>, **2013**. PC 21.

## Grants

1. Scholarship provided by Divisione di Chimica Organica (Società Chimica Italiana) for the participation to the Congress “Chirality **2023**”, Rome.
2. Scholarship provided by Divisione di Chimica Organica (Società Chimica Italiana) for the participation to the Summer School “IASOC **2022**”, Ischia.
3. Scholarship provided by Italfarmaco for the participation to the Summer School “ESMEC **2021**”, online.
4. Scholarship provided by the Organic Chemistry Division of the Italian Chemical Society for the participation to the XXXVIII National Congress of the Organic Chemistry Division of the Italian Chemical Society, Milan, **2018**.
5. Scholarship provided by the Industrial Chemistry Division of the Italian Chemical Society molecules for the participation to the XXV National Congress of the Italian Chemical Society, Arcavacata di Rende, **2014**.



## Acknowledgement

---

I would like to express my deepest gratitude to Prof. Fiorella Meneghetti and Dr. Paride Grisenti, my supervisors, for their unwavering guidance, invaluable insights, and continuous support throughout the entire research process. Their mentorship has been instrumental in shaping the trajectory of this thesis.

A special thanks goes to Prof. Patrizia Ferraboschi (Department of Medical Biotechnology and Translational Medicine, University of Milan), the person who passed on to me the love of research and with whom I filled sheets and sheets with new ideas and chemical reactions.

I thank all the people that have been contributed and enriched my research work: Prof. Diego Colombo (Department of Medical Biotechnology and Translational Medicine, University of Milan) for turning me into a little NMR expert; Prof. Giovanni Grazioso and Dr. Enrico Fassi (Department of Pharmaceutical Sciences, University of Milan) for their crucial computational support; Prof. Roberto Maggi (Department of Pharmaceutical Sciences, University of Milan) for insightful discussions on GnRHR and possible ways to biologically assays the new molecules; Prof. Marco Bonomi and Dr. Valeria Vezzoli (Istituto Auxologico Italiano), who have faced several difficulties in developing the biological method on such a complex receptor, but now are about to proceed to assay the newly synthesized molecules; Prof. Livio Casarini and Dr. Samantha Sperduti (Unit of Endocrinology, Department of Biomedical, Metabolic and Neural Sciences, University of Modena and Reggio Emilia) for generously providing the plasmid encoding the human GnRH1R.

My sincerest thanks go to my PhD colleagues and to Prof. Pietro Allevi, Prof. Federica Compostella, Dr. Laura Morelli, Dr. Paola Rota, Dr. Paolo La Rocca, and Dr. Marco Iannone, whose shared experiences, accompanied by a few relaxing drinks, were a source of inspiration and motivation.

I am grateful to my family for their unwavering support, encouragement, and understanding during the challenging phases of this academic journey. A special thanks to Sophy, my love, for being my muse, supporting me in times of despair and teaching me to see things from other points of view as well.

I would like to express my deepest appreciation to my friends for their encouragement, understanding, and pleasant distractions that provided me with

renewed energy during the demanding periods of research.

Last but not least, I would like to thank Prof. Riccardo Stradi, whose memory and teachings are always alive in me.

This thesis would never have been possible without all the above-mentioned people. I am grateful for the collaborative, enriching environment which has helped shape my doctoral journey. Both the positive and successful moments, as well as the negative and unsuccessful ones, have given me new motivation to find new and sometimes better solutions.